# A general subtraction scheme for next-to-next-to-leading order computations in perturbative Quantum Chromodynamics

Von der Fakultät für Mathematik, Informatik und Naturwissenschaften der RWTH Aachen University zur Erlangung des akademischen Grades eines Doktors der Naturwissenschaften genehmigte Dissertation.

vorgelegt von

David Heymes, M.Sc.

aus Mönchengladbach-Neuwerk.

Berichter: Universitätsprofessor Dr. rer. nat. Michal Czakon
Universitätsprofessor Dr. rer. nat. Werner Bernreuther

Tag der mündlichen Prüfung: 23. September 2015

David Heymes

PhD thesis

# A general subtraction scheme for next-to-next-to-leading order computations in perturbative Quantum Chromodynamics

Institute for Theoretical Particle Physics and Cosmology
RWTH Aachen University

Aachen (Germany), September 2015

# Kurzfassung

Ein allgemeines Subtraktionsschema zur störungstheoretischen Berechnung von Quantenkorrekturen zur zweiten Ordnung in der Quantenchromodynamik

David Heymes

Die verlässliche Interpretation von Messergebnissen am Large Hadron Collider (LHC) is nur möglich, wenn genaue Vorhersagen im Rahmen des Standardmodels der Teilchenphysik existieren. Ein wichtiges theoretisches Werkzeug für diese Vorhersagen ist die störungstheoretische Behandlung der Quantenchromodynamik (QCD). Dieses erlaubt präzise Abschätzungen von Wechselwirkungsquerschnitten von stark wechselwirkenden Teilchen.
Die Koeffizienten der störungstheoretischen Reihe nach der führenden Ordnung besitzen infrarote Singularitäten in verschiedenen Beiträgen. Zwei Ursachen dieser Singularitäten können unterschieden werden. Entweder gehen masselose, virtuelle Teilchen in Schleifenbeiträgen auf ihre Massenschale oder zusätzliche, masselose Teilchen im Endzustand werden weich oder kollinear zu weiteren masselosen Teilchen. In der Summe der einzelnen Beiträge heben sich die Singularitäten auf, wenn in der Rechnung ein entsprechendes Regulierungsschema verwendet wird.
Für die erste Ordnung der störungstheoretischen Reihe existieren allgemeine Subtraktionsschemata, die es erlauben den physikalischen Wechselwirkungsquerschnitt zu berechnen. Singularitäten, die dimensional reguliert werden, heben sich vor der Phasenraumintegration analytisch auf. Die Integration kann schließlich mit Monte Carlo Methoden ausgeführt werden.
In der zweiten Ordnung der störungstheoretischen Reihe ist die Struktur der infraroten Singularitäten weitaus komplizierter. Verschiedene Schemata wurden vorgeschlagen, um physikalische Vorhersagen zu dieser Ordnung für einzelne Prozesse zu machen.
In der vorliegenden Dissertation wird die allgemeine Formulierung des Subtraktionsschemas Stripper (SecToR Improved Phase sPacE for Real radiation) im Detail behandelt. Dieses Schema basiert auf einer numerischen Aufhebug der infraroten Divergenzen. Im Rahmen von Stripper ist eine prozessunabhängige Berechnung der zweiten Ordnung möglich.
Im Weiteren wird die Implementierung des Schemas diskutiert, die es erlaubt Prozesse am LHC zu der gegebenen Ordnung zu simulieren. Der Leitgedanke hinter der Implementierung ist die prozessunabhängige Subtraktion von der Berechnung der prozessabhängigen Matrixelemente zu trennen. Baumniveau Matrixelemente sind in der Software implementiert. Ein- und Zweischleifen Matrixelemente können einfach hinzugefügt werden. Erste Tests der Implementierung werden diskutiert.

## Abstract

A general subtraction scheme for next-to-next-to-leading order computations in perturbative Quantum Chromodynamics

David Heymes

Accurate and robust theoretical predictions are essential in order to perform a reliable interpretation of measurements at the Large Hadron Collider with respect to the Standard Model of Particle Physics. A major theoretical tool to provide precise predictions for scattering cross sections of strongly interacting particles is perturbative Quantum Chromodynamics (QCD). Starting at next-to-leading order in the perturbative series the calculation suffers from infrared singularities in different parts of the calculation. There are two origins of these singularities. Either massless virtual particles in loop contributions go on-shell or additional massless particles in the final state become soft or collinear. Using an appropriate regularization method singularities cancel in the sum of different contributions. At next-to-leading order subtraction methods are established, that allow to calculate the physical cross section in dimensional regularization using Monte Carlo methods. Singularities cancel analytically before the integration is performed.
At next-to-next-to-leading order in the perturbative series the infrared singular structure is more involved and different schemes have been proposed to provide physical predictions for individual processes.
In this thesis, the general formulation of the sector improved residue subtraction scheme is presented, a framework to compute next-to-next-to-leading order corrections in perturbative QCD. This approach, named Stripper (SecToR Improved Phase sPacE for Real radiation), relies on the numerical cancellation of regularized infrared singularities and provide a process independent framework to calculate physical cross sections.
In a second step, the explicit implementation of the subtraction scheme in a Monte Carlo event generator is outlined. The main idea of the implementation is to separate the process independent subtraction scheme from the process dependent evaluation of matrix elements. While tree-level matrix elements are already available, one- and two-loop matrix elements can be included easily.
Finally, first partial tests of the software for top-pair production in hadron collisions are presented.

## List of publications

### Articles

[1] Czakon, Michal and Heymes, David
"Four-dimensional formulation of the sector-improved residue subtraction scheme",
*Nuclear Physics B* **890** (2015) 152-227, arXiv:1408.2500 [hep-ph]

### Proceedings

[2] Heymes, David
"General formulation of the sector-improved residue subtraction",
*J.Phys.Conf.Ser.* **608** (2015), arXiv:1410.2696 [hep-ph]

[3] Heymes, David
"Four-dimensional formulation of the sector improved residue subtraction",
*PoS* **LL2014** (2014), arXiv:1408.2679 [hep-ph]

# Contents

# CHAPTER 1

## Introduction

The main task of the particle physics community in the era of the Large Hadron Collider (LHC) is the reliable interpretation of measurements with respect to the Standard Model of particle physics. The LHC has been built as a discovery machine for the Higgs boson and new physics. The discovery of the Higgs boson in 2012 [4, 5] has completed the list of Standard Model particles that are observed in nature. However, no traces for physics beyond the Standard Model have been observed so far. The main focus of the physics program for the LHC Run II, from 2015 to 2018, is therefore [6, 7]:

- Precision measurements of the properties of the Higgs boson
- Searches for physics beyond the Standard Model

For both programs, precision predictions within the Standard Model play an essential role, but not in the *traditional* sense of precision particle physics.

Traditionally, precision physics is related to lepton colliders and precision measurements of electroweak parameters. In contrast to hadron colliders, the center-of-mass energy at lepton colliders can be fine tuned to study specific observables or processes. For example, the most precise measurement of the $Z$ boson mass, $m_Z = (91.1875 \pm 0.0021)$ GeV, has been obtained by the experiments at LEP[1] and SLC[2] [8]. It is improbable that a hadron collider like the LHC can compete in this context in the near future. Due to the large pile-up of events at different energy scales in a hadronic environment, precision studies of a single observable at a specific energy scale are challenging. In contrast, the high number of possible events at different energy scales, free a lot of space for new discoveries. In conclusion, Hadron colliders are built as discovery machines.

As already mentioned, no new particle has been observed during Run I, apart from the Higgs boson. New phenomena will be possibly detected as small deviations from the Standard Model predictions. This demands a new form of precision particle physics at hadron colliders, which is complementary to the traditional form: *Discovery* precision particle physics. Models that try to describe physics beyond the Standard Model can only be excluded, if the Standard Model background is precisely known. (An example can be found in [9].) In this sense, a precise knowledge of the Standard Model is essential to discriminate between Standard Model events and signals that originate possibly from *new* physics.

1 Large Electron Positron Collider
2 Stanford Linear Collider

Precision physics at hadron colliders requires a considerable effort from the experimental collaborations as well as the theoretical community. In order to offer predictions for hadrons collisions, perturbative Quantum Chromodynamics (QCD) is a reliable tool in order to estimate theoretical uncertainties for a specific class of processes. QCD is the fundamental Quantum field theory that describes the strong dynamics of colored particles, namely quarks and gluons. They build the constituents of the proton. In the high energy regime, which will be quantified later in this work, the strong coupling $\alpha_s \ll 1$ and a perturbative treatment of the theory is possible. In this regime, the hadronic cross section to produce a specific final state factorizes into parton distribution functions, that describe the probability of finding a quark or a gluon inside the proton, and a partonic cross section, that describes the hard scattering of quarks and gluons.
The theoretical uncertainty of a prediction for hadron colliders depends on several ingredients. It depends on the error on the parameters that are needed for the process under consideration. By parameters the free parameters of the Standard Model are meant, *e.g.* masses and coupling constants. They are usually measured in separate experiments, like the mass of the $Z$ boson in the above example, or in the same experiment using different processes.
The second source of uncertainty are the parton distribution functions. They describe the dynamics of quarks and gluons inside the proton at low energies. In this regime, a perturbative treatment of QCD is not possible and a direct calculation of these functions is in general not viable. The parton distribution functions are extracted from different experimental results using precise QCD predictions. In this regard, two cases have to be distinguished: Either parton distribution functions serve as an ingredient of the hadronic cross section in order to predict its theoretical value, or the experimental measurement of a cross section and the calculation of the partonic cross section are used in order to determine the parton distribution functions [10–13].
The remaining source of uncertainty is the perturbative expansion of the partonic cross section in $\alpha_s$. The knowledge of the number of coefficients in the perturbative series determines the value and the theoretical uncertainty of the prediction. This topic is addressed in the present work.
The computation of the leading-order contribution to processes relevant for the LHC is completely automated and neither conceptual nor computational problems for the evaluation of high multiplicity processes exist. Predictions are provided in form of general purpose event generators (see for example [14, 15]).
Starting at next-to-leading order the calculation suffers from soft and collinear (infrared) divergences, which appear in different parts of the calculation. They arise either in the one-loop matrix element of the virtual contribution or in the real contribution as one additional final state parton becomes unresolved. However, using an appropriate regularization, the singularities cancel in the final result. An automation of this calculation is much more involved compared to the leading order case, since one-loop matrix elements have to be evaluated and the singular structure has to be handled in a general manner. A general framework to handle phase space singularities is provided by subtraction methods [16, 17]. They provide a process independent recipe to evaluate cross sections at next-to-leading order in the strong coupling $\alpha_s$. Nowadays, all ingredients can be evaluated automatically and multi-purpose computer programs have been used to calculate the next-to-leading order cross sections for most of the processes that are relevant at the LHC (see for example [14, 18]).
The complexity of the next-to-next-to-leading order correction of the cross section increases tremendously with respect to the next-to-leading order correction. On the one hand, two-loop matrix elements have to be evaluated. While the general structure of arbitrary one-loop matrix elements is known, two-loop matrix elements have to be evaluated on a case by case basis. Up to now, only matrix elements for $2 \to 2$ processes have been evaluated. On the other hand, the complexity also

increases due to the involved infrared singular structure. Singularities appear in all ingredients, that have to be evaluated.
Initial state collinear singularities have to be treated by appropriated collinear renormalization terms. In the double-virtual contribution explicit infrared singularities arise in the two-loop matrix element. The real-virtual contribution contains a one-loop matrix element and an additional parton in the final state, which can become soft or collinear. The one-loop corrections can be calculated using tools that have been developed for next-to-leading order calculations. Singularities, due to the additional final state parton, have to be regulated by an appropriate subtraction method.
The final ingredient is the double-real contribution, which contains tree-level matrix elements that contain up to two unresolved partons in the final state. This contribution requires the development of a subtraction scheme that regularizes up to two unresolved partons.
In this work, the whole structure of higher order QCD corrections up to next-to-next-to-leading order will be addressed. In particular, the subtraction scheme Stripper[1] is presented. It fulfills all requirements necessary to calculate cross sections up to next-to-next-to-leading order in perturbative QCD. It is implemented as a general framework to calculate fully differential cross sections for arbitrary processes, if the matrix elements are provided. The implementation of the scheme is an important step towards fully automated computations at next-to-next-to-leading order in perturbative QCD.
The first idea has been developed in [19] and has been successfully applied for the first time to the calculation of the total cross section of top quark pair production [20]. The four-dimensional formulation of the scheme has been first outlined in [1] and will be presented in detail in this work.
The present work is organized as follows. In chapter 2 precision measurements at the LHC are discussed. Three examples are given in which next-to-next-to-leading order corrections have been necessary in order to interpret the data correctly. These examples provide a general motivation for precision calculations beyond next-to-leading order.
In chapter 3 the foundations of fixed order calculations in perturbative QCD are reviewed. The main focus lies on perturbative predictions at next-to-next-to-leading order. Techniques to evaluate one- and two-loop matrix elements are summarized. Finally, an overview of subtraction and slicing methods at next-to-next-to-leading order is given. Their limitations and differences are discussed in the end of the chapter.
Chapter 4 contains the main part of the work. The four dimensional formulation of the subtraction scheme Stripper is fully outlined. In this formulation the subtraction scheme can be used as a general framework to calculate cross sections at next-to-next-to-leading order in the strong coupling. The numerical verification of the scheme is presented at the end of the chapter.
In chapter 5, the realization of the subtraction scheme in a C++-program is discussed. The relation between physical concepts and C++-classes is described. Topics related to the implementation of the subtraction framework that go beyond its first theoretical description are discussed afterwards. First partial contributions for differential cross sections in $t\bar{t}$-production in proton collisions at next-to-next-to-leading order verify the functionality of the software at the end of the chapter. A full phenomenological study of processes using the presented implementation is beyond the main scope of this work and is left for the future.

Several aspects of precision QCD are not covered in the present work. For example matching parton showers to fixed order calculations or analytic resummation techniques provide additional

1 SecToR ImProved phase sPacE for Real-radiation

important tools to understand LHC measurements. Nevertheless, they are beyond the scope of this work and are not discussed.
It should be mentioned that at the discussed level of precision next-to-leading order electroweak corrections can become as important as next-to-next-to-leading order QCD corrections. A recent calculation and further references can be found in [21]. The discussion of electroweak corrections is however not directly related to the main topic of this work.

# CHAPTER 2

## Precision measurements at the Large Hadron Collider (LHC)

The Large Hadron Collider (LHC) has just started its Run 2 and collects data at a center-of-mass energy of 13 TeV since April 2015. During Run I, which started in early 2010 and continued until end of 2012, the two main experimental collaborations, ATLAS[1] and CMS[2], collected around $25\,\mathrm{fb}^{-1}$ of proton-proton data for a center-of-mass energy $\sqrt{s} = 8$ TeV. The luminosity at the CMS experiment was about [6]

$$\mathcal{L} = \frac{1}{\sigma}\frac{\mathrm{d}N}{\mathrm{d}t} \simeq 7 \cdot 10^{33}\,\mathrm{cm}^{-2}s^{-1}\,, \tag{2.1}$$

and of similar order for the ATLAS experiment [7]. The integrated luminosity over the whole first run at 7 and 8 TeV is depicted in the left plot of Fig. 2.1. The right plot shows the predicted total cross sections for some Standard Model benchmark processes as well as the total cross section for proton proton collisions. For a center-of-mass energy $\sqrt{s} < 4$ TeV, cross sections are also given for proton antiproton collisions, in order to compare the number events at the Tevatron to the number of events at the LHC. The number of events per second for different center-of-mass energies can be extracted directly from the plot. For example, the number of events for the production of a top quark pair is considered. At the Tevatron, with a peak luminosity of circa $10^{32}\mathrm{cm}^{-2}s^{-1}$, $10^{-3}$ top pairs have been produced per second. Hence, in one year $10^4$ events could be recorded. At the LHC at 8 TeV, about 0.1 pairs have been produced per second. During the run in 2012, about $10^6$ top quark pairs have been produced. A upgrade to 14 TeV will produce one $t\bar{t}$-pair per second and in one year $10^7$ events could be produced.
Similarly for the production of a Higgs boson via gluon fusion $\sigma_{ggH}$. The cross section at 8 TeV is about 19 pb [23]. Hence, more than half a million Higgs bosons have been produced in 2012 in this channel, and led to its discovery. Since, the total cross section at 14 TeV is more than twice as big as at 8 TeV [23], the number of events that will be counted during Run II will be more than one million per year.
The given numbers exemplify that the LHC is also a precision experiment for testing the Standard Model. Due to the large number of events, the experimental statistical error for benchmark processes lies in the percent regime or even below.
In the following, examples of measurements from Run I at the LHC are considered. It will be shown that in those cases predictions at next-to-next-to-leading order in perturbative QCD have been necessary to match the experimental precision.

1 A Toroidal LHC ApparatuS
2 Compact Muon Solenoid

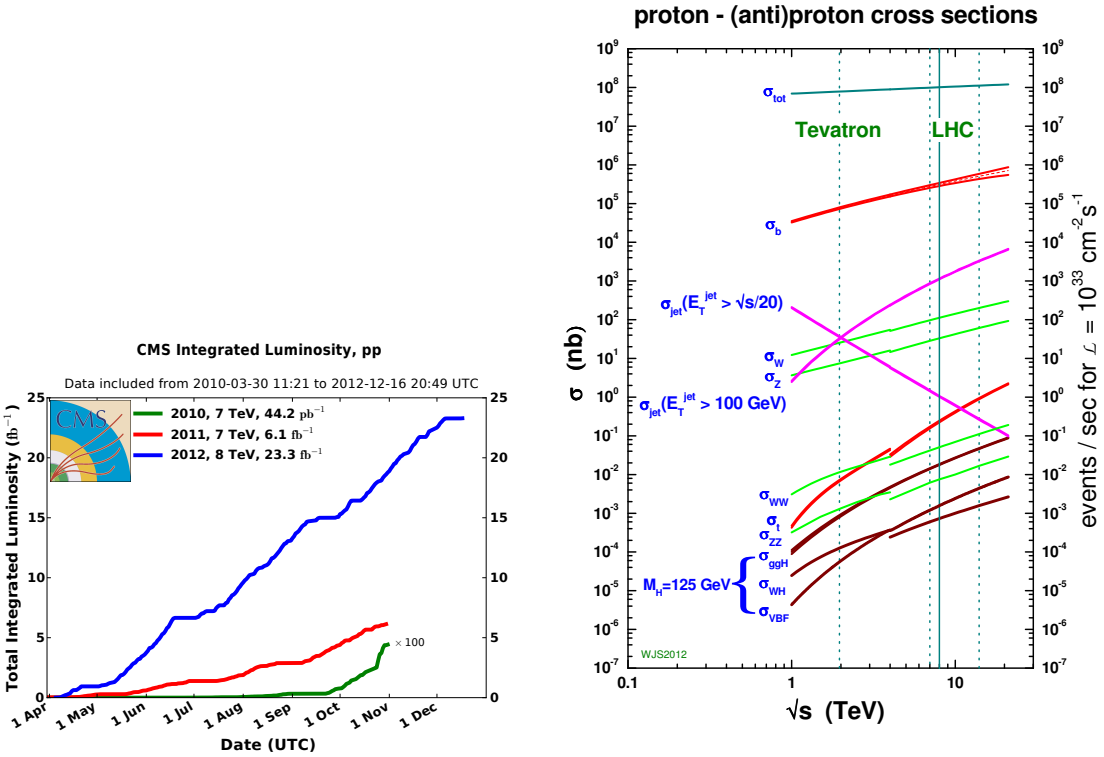


**Figure 2.1:** **Left** [6]: The integrated luminosity of the LHC taken at the CMS experiment during the three years 2010 (green), 2011(red) and 2012 (blue) of Run I. **Right** [22]: Total predicted cross sections for several benchmark processes at proton-(anti)proton colliders as a functions of the center-of-mass energy $\sqrt{s}$. The discontinuity for some of the cross sections is due to the switch from a proton-antiproton cross section below 4 TeV to a proton-proton cross section above 4 TeV. The total cross sections for $t\bar{t}$ and $b\bar{b}$ are denoted by $\sigma_t$ and $\sigma_b$ respectively.

In particular the total cross sections for the productions of two vector bosons is a prime example. The comparison with fixed order theory predictions is shown in the left plot of Fig. 2.2. Focusing on the production of a $W$-pair helps to understand specific features that can occur in higher order predictions. The cross section for the production is measured to be [26]

$$\sigma_{WW}^{\text{exp}}(7\text{TeV}) = 52.4 \pm 2.0(\text{stat}) \pm 4.5(\text{syst.}) \pm 1.2(\text{lum.})\,\text{pb}\,, \tag{2.2}$$

at 7 TeV using an integrated luminosity of 4.92 fb$^{-1}$. The measured value at 8 TeV for a dataset of integrated luminosity of 19.4 fb$^{-1}$ is [27]

$$\sigma_{WW}^{\text{exp}}(8\text{TeV}) = 60.1 \pm 0.9(\text{stat}) \pm 3.2(\text{syst.}) \pm 1.6(\text{lum.})\,\text{pb}\,. \tag{2.3}$$

The increase of luminosity lowers the statistical error by more than a factor of 2. The theoretical prediction at 7 TeV at next-to-leading order slightly underestimates the experimental result, if only the statistical error is considered. This behavior is understood if the theoretical prediction at different perturbative orders is examined. The plot on the right hand side of Fig. 2.2 shows the prediction for the total cross section at leading order, next-to-leading-order and next-to-next-to-leading order as a function of the center-of-mass energy of the protons. The diagram is taken from [25], in which the behavior of the perturbative expansion is explained. The leading order prediction completely fails to

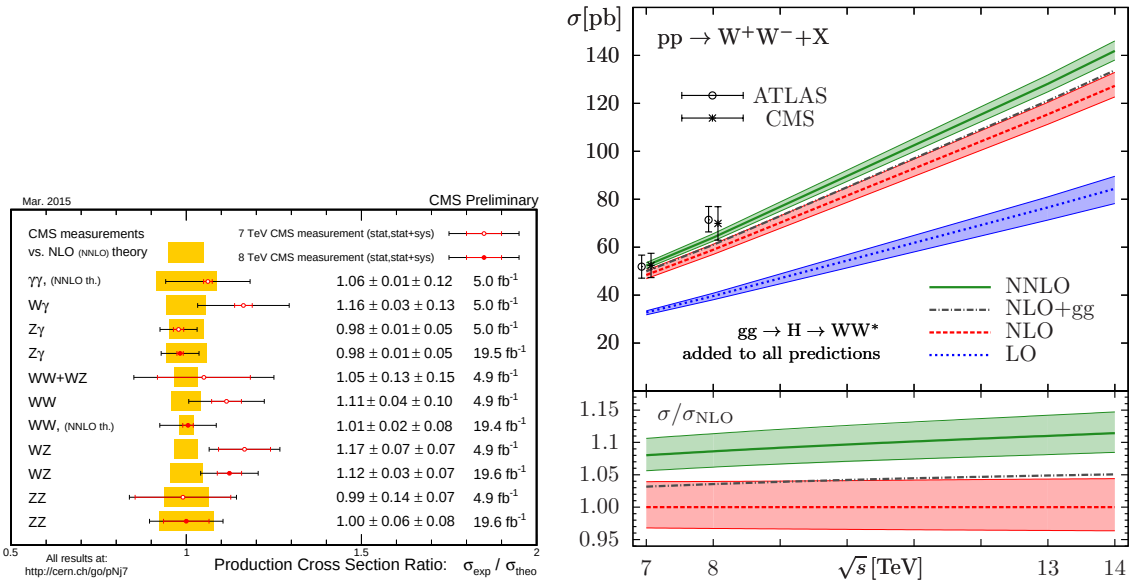


**Figure 2.2:** **Left** [24]: Summary plot of the CMS measurement of the total cross section for vector boson pair production in comparison with (next-to-)next-to-leading order QCD predictions. The used data set is specified in the last column. The theory uncertainty is depicted by the yellow band. An overall agreement is observed. **Right** [25]: The theoretical prediction for the total $W^+W^-$ cross section as a function of the hadronic center-of-mass energy. Results of the leading-order (blue), the next-to-leading order (red) and next-to-next-to-leading order (green) calculation are shown. The error band is due to the variation of factorization and renormalization scale.

describe the data at both energies of the colliding protons. The next-to-leading order contribution enlarges the cross section by $50\% - 60\%$ with respect to the leading order contribution, while the theoretical uncertainty stays unchanged at the order of $2\% - 5\%$. The next-to-next-to-leading order introduces another correction of about 10% and a first slight decrease of the theoretical uncertainty is observed. Owing to the fact that the higher order corrections do not lie within the error band of the previous order, the scale uncertainties at leading and next-to-leading order do not represent the correct theoretical error due to missing higher order contributions. This is a characteristic feature of this process. New partonic channels emerge at next-to-leading order and at next-to-next-to-leading order of the perturbative series. They contribute significantly to the total cross section and shift the prediction towards the measured value. Beyond next-to-next-to-leading order no additional channels arise and the given theoretical error estimate can be taken as the first reliable uncertainty of the final prediction and is in good agreement with the measured value.

An observable, that has been measured with incredible precision at the CMS and ATLAS experiments, is the total cross section for top quark pair production. The combined value measured for leptonic decay channels of the top quark reads [30–33]

$$\sigma_{t\bar{t}}^{\text{exp}}(8\text{TeV}) = 240.6 \pm 1.4(\text{stat}) \pm 5.7(\text{syst.}) \pm 6.2(\text{lum.})\,\text{pb}\,, \tag{2.4}$$

where data sets of $5.3 - 20.3$ fb$^{-1}$ have been included. The statistical error is of the order 0.5% and the uncertainty is dominated by the systematical error and the error on the luminosity. In the left plot of Fig. 2.3, the recent measurement of the total cross section at the LHC and the Tevatron are compared to the next-to-next-to-leading order prediction [34]. It can be observed that the Standard Model prediction agrees very well with the measured value. For this observable, a next-to-next-to-leading order prediction is required in order to keep up with the experimental

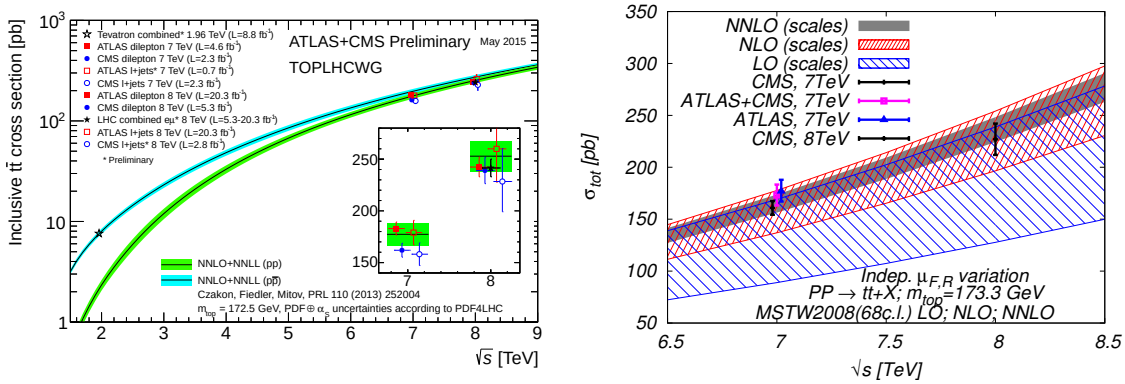


**Figure 2.3: Left** [28]: The theoretical prediction for total production cross section of $t\bar{t}$ for proton-proton collisions (green) and proton-antiproton collisions (blue) at next-to-next-to-leading order, including next-to-next-to-leading logarithmic soft gluon effects. The prediction is compared to measurements at the LHC and Tevatron. **Right** [29]: Factorization and renormalization scale dependence of the total cross section at leading order (blue), next-to-leading order (red) and next-to-next-to-leading order (gray).

precision. This can be seen in the right plot of Fig. 2.3, which is taken from [29]. It shows the theoretical uncertainty due to variation of the factorization and renormalization scale for each order in perturbation theory. In contrast to the previous example, the scale uncertainty significantly reduces, if higher orders of the perturbative series are included. Additionally, the central value of the theory prediction lies within the error band of the previous order. This indicates a good convergence of the series and a reliable estimation of the theoretical error. The scale uncertainty of the final prediction has been estimated to be about 5%, an inclusion of soft gluon effects through next-to-next-to-leading logarithmic resummation reduces this uncertainty to about 3%. Additional theoretical uncertainties, due to the top quark mass, the strong coupling and the used parton distribution functions are of the same order [29].

In addition to the inclusive observables discussed so far, higher order corrections can have an impact on the shape of differential distributions. As an example, the differential cross section measurement for the Drell-Yan process $pp \to Z/\gamma^* \to ll$ is considered [35], where the final state leptons $l$ are either electrons or muons. The measurement, which is differential in the invariant mass of the lepton pair $m_{ll}$ below 66 GeV, is shown in Fig. 2.4. This measurement includes data from the early 2011 7 TeV run of integrated luminosity of 1.6 fb$^{-1}$ in the region $m_{ll} = 26 - 66$ GeV (left plot), the statistical error is determined to lie below 1%. An even lower region could be probed using 2010 LHC data of integrated luminosity of 35 pb$^{-1}$ (right plot). The data is compared to three different theoretical predictions, where all of them include higher order electroweak corrections (HOEW) and photon induced contributions (PI). The next-to-leading order QCD prediction does not describe the measured data in both cases in the low $m_{ll}$ region. The inclusion of additional radiation to the next-to-leading order prediction in terms of a parton shower matched to the next-to-leading order prediction [37, 38] describes the data already more accurately. Nevertheless, the theoretical error in this case is still of the order $10\% - 20\%$ in the low $m_{ll}$ region. The next-to-next-to-leading order prediction [39–42] provides the first satisfactorily description of the data, while the theoretical uncertainty, which is of the order $5\% - 10\%$ in the first bin, remains larger than the overall experimental error.

The three given examples show that higher order QCD prediction up to next-to-next-to-leading order are required. Next-to-leading order predictions in perturbative QCD are nowadays standard. Highly elaborated automated tools exist for a automated calculation (see also section 3.3.1), including several massive particles and processes of high multiplicity.

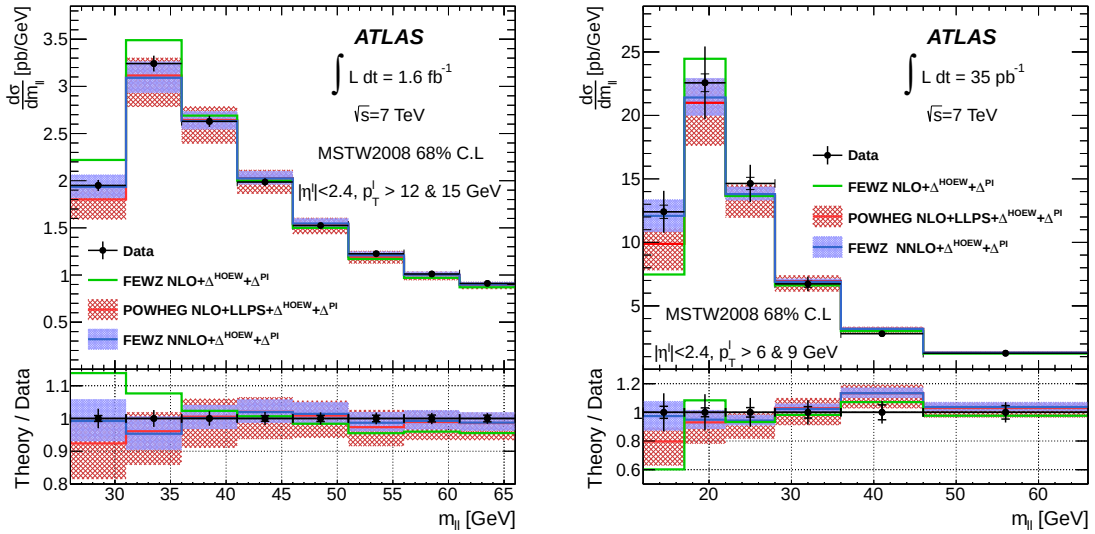


**Figure 2.4:** [35] Measured differential cross section $\frac{d\sigma}{dm_{ll}}$ in two regions below the $Z$ mass peak: $26\,\text{GeV} < m_{ll} < 66\,\text{GeV}$ (left) and $12\,\text{GeV} < m_{ll} < 66\,\text{GeV}$ (right). The data is compared with theory predictions at next-to-leading-order and next-to-next-to-leading order, which were obtained using the software FEWZ [36], and a next-to-leading order prediction matched to parton showers using POWHEG[37]. Electroweak effects ($\Delta^{\text{HOEW}}$) and photon induced contributions ($\Delta^{\text{PI}}$) are included.

The list of known corrections at next-to-next-to-leading order for hadron collisions is rather short. The production of a Higgs boson can be calculated differentially and dedicated software exists [41, 43–46]. Recently the total cross sections for single Higgs production via gluon fusion has been calculated at next-to-next-to-next-to-leading order accuracy [23]. The Drell-Yan cross section and single vector boson production has been calculated and is available differentially [40, 41, 47]. The first calculation of a next-to-next-to-leading order cross section including colored particles in the final state, has been the total cross section for $t\bar{t}$-production [34]. The first differential distributions have been presented in [48]. Partial results for dijet productions in hadron collisions have been presented in [49, 50], where currently only the purely gluonic contributions have been fully computed. The calculations of vector boson pairs at next-to-next-to-leading order accuracy can be found in [25, 51–53]. All channels for the differential cross section of Higgs+jet and W+jet productions have been presented [54–56].

The mentioned examples, represent only a tiny part of Standard Model physics that can be tested at the LHC. Completely differential next-to-next-to-leading order calculations for several additional processes are demanded. For example, calculating the cross section for dijet production at this order of accuracy could be used to constrain the gluon parton distribution function. The list of known next-to-next-to-leading order prediction includes only up to two particles in the final state. This is due to the lack of two-loop amplitudes for $2 \to 3$ processes and efficient tools to compute real corrections.

Another important issue is, how results can be made accessible for the experimental community. The tools and theoretical frameworks that have been applied to most of the precision predictions mentioned in this chapter will be summarized in the next chapter. Up to now no general tool exists that allows to compute differential next-to-next-to-leading order corrections on a process independent basis. In this work, the theoretical basis of the subtraction scheme STRIPPER is explained and its implementation discussed. This implementation serves as a general framework to calculate

differential cross sections, in principle, for arbitrary processes.

# CHAPTER 3

## Precision predictions in perturbative QCD

## 3.1 Foundations of perturbative QCD

### 3.1.1 The strong coupling

QCD is a renormalizable Yang-Mills quantum field theory with gauge group SU($N_c$), where $N_c = 3$ is the number of quark color charges observed in nature. The corresponding Lagrangian is

$$\begin{aligned}\mathcal{L}_{\text{QCD}} = &-\frac{1}{4}F^a_{\mu\nu}F^{\mu\nu,a} - \frac{1}{2\xi^0}\left(\partial_\mu A^{\mu,a}\right)^2 + \left(\partial^\mu \bar{c}^a\right)\left(\delta^{ac}\partial_\mu + g_s^0 f^{abc}A^b_\mu\right)c^c \\ &+ \sum_f \bar{\psi}_{f,i}\left(\delta_{ij}i\partial\!\!\!/ + g_s^0 A\!\!\!/^a t^a_{ij} - \delta_{ij}m_f^0\right)\psi_{f,j}\,,\end{aligned} \tag{3.1}$$

where the gauge is fixed covariantly. The last sum includes all quark flavors $f \in \{u,d,c,s,b,t\}$, where the number of quark flavors is $n_f = 6$. The fields $c^a$ and $\bar{c}^a$ are Faddev-Popov ghost and anti-ghost fields respectively [57]. The indices $\{a,b,c\}$ are color charge indices in the adjoint representation, running from 1 to $N_c^2 - 1$, and $\{i,j\}$ the color charge indices in the fundamental representation, running from 1 to $N_c$. The QCD field strength tensor is defined as

$$F^a_{\mu\nu} = \partial_\mu A^a_\nu - \partial_\nu A^a_\mu + g_s^0 f^{abc}A^b_\mu A^c_\nu\,. \tag{3.2}$$

The above Lagrangian is expressed through bare fields $A^a, \psi_{f,i}$, bare mass parameters $m_f^0$ and the bare strong coupling constant $g_s^0$, which is conventionally replaced by the QCD fine structure constant

$$\alpha_s^0 = \frac{(g_s^0)^2}{4\pi}\,. \tag{3.3}$$

The theory needs to be renormalized, in order to be predictive. If physical quantities are calculated in perturbation theory in the strong coupling $\alpha_s^0$, integrals will be divergent as internal momenta become large. They are ultraviolet(UV)-divergent. This is not a conceptual problem, since it reflects the fact that the theory is an effective field theory which is applicable only up to an unknown energy scale $\Lambda$. Introducing $\Lambda$ as a cutoff renders the theory finite and predictive. However, predictions at some energy scale $E \ll \Lambda$ should not depend on the cutoff scale. In order to achieve this the bare parameters of the theory have to depend on this energy scale $\Lambda$ and are infinite as $\Lambda \to \infty$. Renormalizing the theory at an arbitrary scale $\mu_R^2 \sim E^2$, the renormalization scale, means to replace these divergent parameters by the physical parameters at this scale, which are measured. Consequently, the physical parameters depend on the energy scale $\mu_R^2$, whereas a final prediction

should be independent of the renormalization scale.
In practical applications of perturbative QCD, it is more convenient to use dimensional regularization [58] rather than introducing a UV-cutoff $\Lambda$. In dimensional regularization the theory is formulated in $d = 4 - 2\varepsilon$ space time dimensions and UV-divergences appear as poles in the regulator $\varepsilon$. The UV-limit, $\Lambda \to \infty$ corresponds to $\varepsilon \to 0$.
The relation between renormalized and bare parameters can be formulated order by order in perturbation theory and is given by multiplicative renormalization constants $Z(\alpha_s)$. For the coupling it reads explicitly

$$\alpha_s^0 = \mu_\mathrm{R}^{2\varepsilon} Z_{\alpha_s} \alpha_s(\mu_\mathrm{R}^2)\,, \tag{3.4}$$

where the introduction of the renormalization scale $\mu_\mathrm{R}^2$ ensures that $\alpha_s$ is dimensionless in $d = 4 - 2\varepsilon$. The scheme that defines the particular form of $Z_{\alpha_s}$ beyond the singular term, is called renormalization scheme. Different schemes define different renormalization scales. The modified minimal subtraction scheme $\overline{\mathrm{MS}}$ is widely used in applications and will be exclusively used in this thesis. At leading order the renormalization constant for the strong coupling reads

$$Z_{\alpha_s} = 1 - \frac{\alpha_s}{4\pi}\frac{\beta_0}{\varepsilon} + \mathcal{O}(\alpha_s^2), \tag{3.5}$$

where $\beta_0 = \frac{11}{3}C_A - \frac{4}{3}n_f T_F$. We can use the renormalization group (RG) equation for the strong coupling to obtain the dependence of the coupling constant on the scale. The RG equation is a consequence of the fact that the bare coupling cannot depend on $\mu_\mathrm{R}^2$

$$0 = \frac{\mathrm{d}}{\mathrm{d}\log\mu_\mathrm{R}^2}\alpha_s^0 \quad \Rightarrow \quad \frac{\mathrm{d}}{\mathrm{d}\log\mu_\mathrm{R}^2}\alpha_s = \beta(\alpha_s) = -\alpha_s\left(\left(\frac{\alpha_s}{4\pi}\right)\beta_0 + \left(\frac{\alpha_s}{4\pi}\right)^2\beta_1 + \left(\frac{\alpha_s}{4\pi}\right)^3\beta_2 + \cdots\right), \tag{3.6}$$

where the QCD $\beta$-function can be calculated using $Z_{\alpha_s}$ and taking the limit $\varepsilon \to 0$.
This function is negative which implies that the strong coupling strength decreases for high energies. This effect is known as asymptotic freedom and was discovered by Gross, Wilczek and Politzer [59–61]. The coefficients up to $\beta_3$ can be found in [62, 63]. If the coupling constant at some scale $\mu_0$ is known the RG equation is used to obtain the coupling at some arbitrary scale $\mu$. The first order solution is

$$\alpha_s(\mu) = \frac{\alpha_s(\mu_0)}{1 + \frac{\beta_0}{2\pi}\log\left(\frac{\mu}{\mu_0}\right)} = \frac{2\pi}{\beta_0}\frac{1}{\log\left(\frac{\mu}{\Lambda_\mathrm{QCD}}\right)}\,. \tag{3.7}$$

The energy scale parameter $\Lambda_\mathrm{QCD}$ indicates the pole of the function, known as the Landau pole. A perturbative treatment of QCD is only valid if $\mu > \Lambda_\mathrm{QCD}$. Fig. 3.1 depicts the world average of the value of $\alpha_s(Q)$, extracted from different measurements at different energy scales $Q$. The line depicts the theory prediction in Eq. (3.7) of the running. Using the RG equation, the different values are combined at $Q = m_Z = 91.1876 \pm 0.0021$ GeV, the mass of the $Z$ boson. It is used to fix $\Lambda_\mathrm{QCD} \simeq 213\,\mathrm{MeV}$.
At low energies quarks and gluons are strongly coupled and only appear as colorless bound states, the hadrons. In the following quarks and gluons are denoted as partons. Possible treatments of QCD in the low energy regime are direct numerical computations on a space-time lattice or effective field theory treatments of the bound states, e.g. chiral perturbation theory.
Only when the energy scale is large with respect to $\Lambda_\mathrm{QCD}$, partons can be treated as free asymptotic states and a perturbative treatment of the theory in $\alpha_s \ll 1$ is possible.

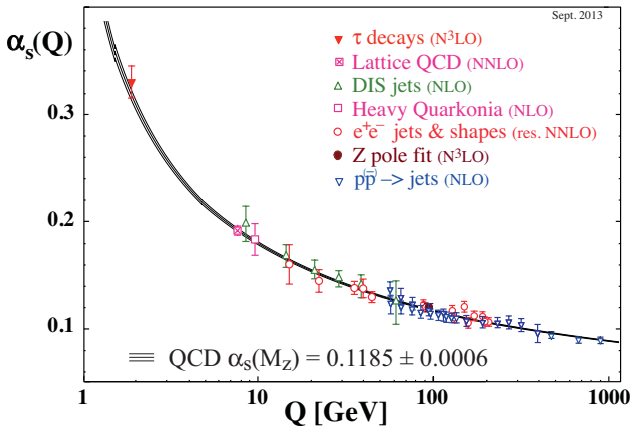


**Figure 3.1:** The measured value of $\alpha_s$ in comparison with the theoretical prediction of the running. The values are extracted at different energies $Q$ and subsequently evolved to the scale of the $Z$ boson mass. The averaged value at this scale includes all the measurements [64]

### 3.1.2 Massless QCD and decoupling of heavy quarks

The renormalized masses $m_f(\mu)$ of quarks are scale dependant and can be defined in the $\overline{\text{MS}}$ scheme. As they do not exist as asymptotic free states a direct measurement of light quark masses is not possible. However, it is possible to estimate the renormalized mass parameter by comparing experimental results to theoretical predictions. The quark masses are given in Tab. 3.1. The typical

| | | |
|---|---|---|
| $m_u$ | $(2.3 \pm 0.7)$ MeV | $\overline{\text{MS}}$ |
| $m_d$ | $(4.8 \pm 0.5)$ MeV | $\overline{\text{MS}}$ |
| $m_s$ | $(95 \pm 5)$ MeV | $\overline{\text{MS}}$ |
| $m_c$ | $(1.275 \pm 0.025)$ GeV | $\overline{\text{MS}}$ |
| $m_b$ | $(4.18 \pm 0.03)$ GeV | $\overline{\text{MS}}$ |
| $m_t$ | $(173.21 \pm 0.51 \pm 0.71)$ GeV | measurement |

**Table 3.1:** The light quarks masses $\{u,d,c,s,b\}$ are $\overline{\text{MS}}$ - mass estimates. The top-quark mass is directly measurable [64].

energy scales of hard processes at hadron colliders are much larger than light quark masses, where we denote the number of light quark flavors by $n_l$ and the number of heavy quark flavors by $n_h$. For the LHC, typically $n_l = 5$ quark masses are negligible and only the top quark is considered as massive. The QCD Lagrangian is replaced, by an effective massless QCD Lagrangian, where the number of active flavours is $n_l$. The top quark decouples from the theory, if the typical scales are smaller than $m_t$. If the scales are comparable to $m_t$, the top quark is kept as a massive fermion. Consequently, we eventually deal with two different Lagrangians, the first one contains $n_l$ active massless quark flavours and the other contains $n_l + 1$ active quark flavors. The renormalized coupling $\alpha_s^{(n_l)}$ in the $n_l$ - flavor theory, can be related to the coupling of the theory containing one massive

quark $\alpha_s^{(n_l+1)}$. The relation reads [65]

$$\alpha_s^{(n_l)}(\mu) = \zeta_{\alpha_s}(\mu,\alpha_s^{(n_l+1)},m_t)\,\alpha_s^{(n_l+1)}(\alpha_s)\,, \tag{3.8}$$

where $\zeta_{\alpha_s}$ is the heavy quark decoupling constant and is known up to four loops [66, 67].

### 3.1.3 Perturbative QCD at hadron colliders

The hadronic cross section in high energy collisions factorizes in a long distance contribution, the parton distribution functions (PDFs), and a short distance contribution, the partonic cross section

$$\begin{aligned}\sigma_{h_1h_2}(P_1,P_2) = &\sum_{ab}\iint_0^1 \mathrm{d}x_1\mathrm{d}x_2\, f_{a/h_1}(x_1,\mu_\mathrm{F}^2)\, f_{b/h_2}(x_2,\mu_\mathrm{F}^2)\,\hat{\sigma}_{ab}(x_1P_1,x_2P_2;\,\alpha_s(\mu_\mathrm{R}^2),\,\mu_\mathrm{R}^2,\,\mu_\mathrm{F}^2)\\ &+\mathcal{O}(\frac{\Lambda_\mathrm{QCD}}{Q})\,.\end{aligned} \tag{3.9}$$

The PDFs $f_{a|h}$, are non-perturbative objects. They describe the dynamics of the parton $a$ inside a hadron $h$. In a first approximation, they are the probability distribution of finding a parton of flavor $a$ and momentum fraction $p_i = x_iP_j$ inside the hadron, where $P_j$ is the hadronic momentum. These functions are extracted experimentally.

The partonic cross section $\hat{\sigma}_{ab}$ describes the hard interaction of free gluons and quarks at a hard scale $Q$. The cross section is collinearly renormalized, such that initial state collinear singularities are absorbed into the parton distribution functions.

It is worth to notice that the factorization formula (3.9) has not been demonstrated for general hadronic cross sections. General proofs exist for Deep Inelastic Scattering (DIS) and Drell-Yan processes. A summary can be found in [68]. As the formula suggests, factorization is only applicable when $Q > \Lambda_\mathrm{QCD}$, in other words, when the soft and the hard scale describing the process are well separated.

On a partonic level, we can calculate cross sections directly using QCD perturbatively. The partonic cross section for a generic inclusive scattering process with $n$ partons in the final state $a+b \to n+X$ is defined through

$$\hat{\sigma}_{ab} = \sum_{m=n}\frac{1}{2\hat{s}}\frac{1}{N_{ab}}\int \mathrm{d}\Phi_m\langle\mathcal{M}_m|\mathcal{M}_m\rangle F_m\,, \tag{3.10}$$

where $a$ and $b$ are incoming massless partons, $n$ denotes the number of outgoing colored particles for the specific observable and $N_{ab}$ is the average factor for color and spin of the incoming partons. Even though the work mainly focuses on $n$ partons in the final state, non-QCD particles can be included into the final state without changing the content of this work. The partonic center-of-mass energy is $\hat{s} = (p_1+p_2)^2$, where $p_1$ and $p_2$ are the momenta of the incoming partons. $F_n$ is a measurement function that defines a specific observable under consideration and is a function of the final state momenta. The only requirement on this function is that it has to describe an infrared safe observable, i.e. it has to be insensitive to collinear and soft final state partons

$$F_n \to F_{n-1},\ \text{if}\quad p_i \to 0 \tag{3.11}$$

$$F_n \to F_{n-1},\ \text{if}\quad p_i||p_j\,, \tag{3.12}$$

where $p_i$ and $p_j$ are final state parton momenta. The precise definition of renormalized matrix elements $|\mathcal{M}_m\rangle$ and the phase space measure $\mathrm{d}\Phi_m$ is given in Appendix A.

The expansion of the partonic cross section in $\alpha_s(\mu_\mathrm{R}^2)$ reads

$$\hat{\sigma}_{ab} = \hat{\sigma}_{ab}^{(0)} + \hat{\sigma}_{ab}^{(1)} + \hat{\sigma}_{ab}^{(2)} + \cdots \,. \tag{3.13}$$

The partonic cross section, which is not directly accessible experimentally, can be used to calculate the hadronic cross section using the factorization formula (3.9). Even though the PDFs are non-perturbative objects, their dependence on the factorization scale $\mu_\mathrm{F}^2$ can be extracted using perturbative QCD

$$\mu_\mathrm{F}^2 \frac{\mathrm{d}}{\mathrm{d}\mu_\mathrm{F}^2} f_{a|h}\left(x,\mu_\mathrm{F}^2\right) = \frac{\alpha_s}{\pi} \int_x^1 \frac{\mathrm{d}\xi}{\xi} f_{b|h}(\xi,\mu_\mathrm{F}^2) P_{ba}\left(\frac{x}{\xi}\right) \,. \tag{3.14}$$

This equation, so called DGLAP equation, allows to resum large logarithms in the PDFs.

## 3.2 Fixed order calculations

The partonic cross section can be written as an expansion in $\alpha_s$ (3.13). Each contribution of this expansion can be decomposed according to the multiplicity of the final state. At leading order in $\alpha_s$ the cross section reads

$$\hat{\sigma}_{ab}^{(0)} = \hat{\sigma}_{ab}^{\mathrm{B}} = \frac{1}{2\hat{s}} \frac{1}{N_{ab}} \int \mathrm{d}\boldsymbol{\Phi}_n \, \langle \mathcal{M}_n^{(0)} | \mathcal{M}_n^{(0)} \rangle \, \mathrm{F}_n \,, \tag{3.15}$$

where the tree-level contribution of the matrix element is $|\mathcal{M}_n^{(0)}\rangle$. The leading order contribution is called the Born approximation. At this order the phase space integral is completely finite and can be evaluated using Monte Carlo methods directly. The measurement function $\mathrm{F}_n$ ensures that no final state parton becomes soft and no final state parton becomes collinear to another parton.
At next-to-leading order (NLO) three ingredients contribute to the partonic cross section

$$\hat{\sigma}_{ab}^{(1)} = \hat{\sigma}_{ab}^{\mathrm{R}} + \hat{\sigma}_{ab}^{\mathrm{V}} + \hat{\sigma}_{ab}^{\mathrm{C}} \,, \tag{3.16}$$

where

$$\hat{\sigma}_{ab}^{\mathrm{R}} = \frac{1}{2\hat{s}} \frac{1}{N_{ab}} \int \mathrm{d}\boldsymbol{\Phi}_{n+1} \, \langle \mathcal{M}_{n+1}^{(0)} | \mathcal{M}_{n+1}^{(0)} \rangle \, \mathrm{F}_{n+1} \,, \tag{3.17}$$

$$\hat{\sigma}_{ab}^{\mathrm{V}} = \frac{1}{2\hat{s}} \frac{1}{N_{ab}} \int \mathrm{d}\boldsymbol{\Phi}_n \, 2\mathrm{Re} \, \langle \mathcal{M}_n^{(0)} | \mathcal{M}_n^{(1)} \rangle \, \mathrm{F}_n \,, \tag{3.18}$$

$$\hat{\sigma}_{ab}^{\mathrm{C}}(p_1,p_2) = \frac{\alpha_s}{2\pi} \frac{1}{\varepsilon} \left(\frac{\mu_\mathrm{R}^2}{\mu_\mathrm{F}^2}\right)^{\varepsilon} \sum_c \int_0^1 \mathrm{d}z \left[ P_{ca}^{(0)}(z) \, \hat{\sigma}_{cb}^{\mathrm{B}}(zp_1,p_2) + P_{cb}^{(0)}(z) \, \hat{\sigma}_{ac}^{\mathrm{B}}(p_1,zp_2) \right] \,. \tag{3.19}$$

The real radiation contribution $\hat{\sigma}_{ab}^{\mathrm{R}}$ contains one additional particle in the final state. The measurement function $F_{n+1}$ allows this massless particle to become unresolved, *i.e.* soft or collinear. This results in a logarithmic singularity of the phase space integral. Using dimensional regularization, the phase space integral can, in principle, be solved. The infrared-singularities appear as poles in the dimensional regulator $\varepsilon = (4-d)/2$.
The virtual contribution, $\hat{\sigma}_{ab}^{\mathrm{V}}$, consists of the $n$-particle phase space integration of the interference term of the tree-level matrix element and the one-loop matrix element $|\mathcal{M}_n^{(1)}\rangle$. In dimensional regularization the one-loop matrix element contains explicit poles in the dimensional regulator, the infrared-singularities of the loop integral.
The collinear factorization contribution $\hat{\sigma}_{ab}^{\mathrm{C}}$ is the convolution of the Born cross section with the

leading order splitting functions. It ensures that the partonic cross section $\hat{\sigma}_{ab}$ is collinearly renormalized at the factorization scale $\mu_{\mathrm{F}}^2$. It contains an explicit collinear infrared-pole in the dimensional regulator $\varepsilon$.
Each of the three contributions diverges separately as $\varepsilon \to 0$, but the sum is finite. As stated by the Kinoshita-Lee-Nauenberg (KLN) theorem [69, 70], virtual poles cancel the soft and final state collinear poles of the real radiation. Initial state collinear singularities in the real contribution are absorbed in the parton distribution functions by collinear renormalization.
At next-to-next-to-leading order (NNLO) the partonic cross section can be separated into five contributions

$$\hat{\sigma}_{ab}^{(2)} = \hat{\sigma}_{ab}^{\mathrm{RR}} + \hat{\sigma}_{ab}^{\mathrm{RV}} + \hat{\sigma}_{ab}^{\mathrm{VV}} + \hat{\sigma}_{ab}^{\mathrm{C1}} + \hat{\sigma}_{ab}^{\mathrm{C2}} \,. \tag{3.20}$$

The first three terms read explicitly

$$\hat{\sigma}_{ab}^{\mathrm{RR}} = \frac{1}{2\hat{s}} \frac{1}{N_{ab}} \int \mathrm{d}\boldsymbol{\Phi}_{n+2} \, \langle \mathcal{M}_{n+2}^{(0)} | \mathcal{M}_{n+2}^{(0)} \rangle \, \mathrm{F}_{n+2} \,, \tag{3.21}$$

$$\hat{\sigma}_{ab}^{\mathrm{RV}} = \frac{1}{2\hat{s}} \frac{1}{N_{ab}} \int \mathrm{d}\boldsymbol{\Phi}_{n+1} \, 2\mathrm{Re} \, \langle \mathcal{M}_{n+1}^{(0)} | \mathcal{M}_{n+1}^{(1)} \rangle \, \mathrm{F}_{n+1} \,, \tag{3.22}$$

$$\hat{\sigma}_{ab}^{\mathrm{VV}} = \frac{1}{2\hat{s}} \frac{1}{N_{ab}} \int \mathrm{d}\boldsymbol{\Phi}_{n} \left( 2\mathrm{Re} \, \langle \mathcal{M}_{n}^{(0)} | \mathcal{M}_{n}^{(2)} \rangle + \langle \mathcal{M}_{n}^{(1)} | \mathcal{M}_{n}^{(1)} \rangle \right) \mathrm{F}_{n} \,. \tag{3.23}$$

The double-real radiation contribution, $\hat{\sigma}_{ab}^{\mathrm{RR}}$, contains two additional partons in the final state, that can generate soft and collinear poles in the dimensional regulator $\varepsilon$ after integration over the phase space. The real-virtual contribution, $\hat{\sigma}_{ab}^{\mathrm{RV}}$, contains explicit poles of the one-loop matrix element and additional real poles are obtained after integrating the phase space of the additional unresolved parton in the final state.
The double-virtual contribution, $\hat{\sigma}_{ab}^{\mathrm{VV}}$, contains the square of the one-loop matrix element and the interference of the tree-level matrix element and the two-loop matrix element. Just explicit infrared-poles of the loop integrals in dimensional regularization are present.
At this order, two contributions of the collinear renormalization of different final state multiplicity are present. They read in terms of factorization $\mu_{\mathrm{F}}^2$ and renormalization scale $\mu_{\mathrm{R}}^2$

$$\hat{\sigma}_{ab}^{\mathrm{C1}}(p_1,p_2) = \frac{\alpha_s}{2\pi} \frac{1}{\varepsilon} \left( \frac{\mu_{\mathrm{R}}^2}{\mu_{\mathrm{F}}^2} \right)^{\varepsilon} \sum_c \int_0^1 \mathrm{d}z \left[ P_{ca}^{(0)}(z) \, \hat{\sigma}_{cb}^{\mathrm{R}}(zp_1,p_2) + P_{cb}^{(0)}(z) \, \hat{\sigma}_{ac}^{\mathrm{R}}(p_1,zp_2) \right] \,, \tag{3.24}$$

$$\begin{aligned}
\hat{\sigma}_{ab}^{\mathrm{C2}}(p_1,p_2) &= \frac{\alpha_s}{2\pi} \frac{1}{\varepsilon} \left( \frac{\mu_{\mathrm{R}}^2}{\mu_{\mathrm{F}}^2} \right)^{\varepsilon} \sum_c \int_0^1 \mathrm{d}z \left[ P_{ca}^{(0)}(z) \, \hat{\sigma}_{cb}^{\mathrm{V}}(zp_1,p_2) + P_{cb}^{(0)}(z) \, \hat{\sigma}_{ac}^{\mathrm{V}}(p_1,zp_2) \right] \\
&+ \left( \frac{\alpha_s}{2\pi} \right)^2 \frac{1}{2\varepsilon} \left( \frac{\mu_{\mathrm{R}}^2}{\mu_{\mathrm{F}}^2} \right)^{2\varepsilon} \sum_c \int_0^1 \mathrm{d}z \left[ P_{ca}^{(1)}(z) \, \hat{\sigma}_{cb}^{\mathrm{B}}(zp_1,p_2) + P_{cb}^{(1)}(z) \, \hat{\sigma}_{ac}^{\mathrm{B}}(p_1,zp_2) \right] \\
&+ \left( \frac{\alpha_s}{2\pi} \right)^2 \frac{\beta_0}{4\varepsilon^2} \left[ \left( \frac{\mu_{\mathrm{R}}^2}{\mu_{\mathrm{F}}^2} \right)^{2\varepsilon} - 2 \left( \frac{\mu_{\mathrm{R}}^2}{\mu_{\mathrm{F}}^2} \right)^{\varepsilon} \right] \sum_c \int_0^1 \mathrm{d}z \left[ P_{ca}^{(0)}(z) \, \hat{\sigma}_{cb}^{\mathrm{B}}(zp_1,p_2) + P_{cb}^{(0)}(z) \, \hat{\sigma}_{ac}^{\mathrm{B}}(p_1,zp_2) \right] \\
&+ \left( \frac{\alpha_s}{2\pi} \right)^2 \frac{1}{2\varepsilon^2} \left( \frac{\mu_{\mathrm{R}}^2}{\mu_{\mathrm{F}}^2} \right)^{2\varepsilon} \sum_{cd} \int_0^1 \mathrm{d}z \left[ \left( P_{cd}^{(0)} \otimes P_{da}^{(0)} \right)(z) \, \hat{\sigma}_{cb}^{\mathrm{B}}(zp_1,p_2) + \left( P_{cd}^{(0)} \otimes P_{db}^{(0)} \right)(z) \, \hat{\sigma}_{ac}^{\mathrm{B}}(p_1,zp_2) \right] \\
&+ \left( \frac{\alpha_s}{2\pi} \right)^2 \frac{1}{\varepsilon^2} \left( \frac{\mu_{\mathrm{R}}^2}{\mu_{\mathrm{F}}^2} \right)^{2\varepsilon} \sum_{cd} \iint_0^1 \mathrm{d}z \, \mathrm{d}\bar{z} \left[ P_{ca}^{(0)}(z) \, P_{db}^{(0)}(\bar{z}) \, \hat{\sigma}_{cd}^{\mathrm{B}}(zp_1,\bar{z}p_2) \right] \,,
\end{aligned} \tag{3.25}$$

where

$$(f \otimes g)(x) = \iint_0^1 \mathrm{d}y\, \mathrm{d}z\, f(y) g(z)\, \delta(x - yz) \,. \tag{3.26}$$

The explicit form of the splitting functions is given in [71]. The finiteness of the sum of the five contributions is ensured by the KLN theorem.
As the discussion above suggests, the complexity of fixed order calculations raises significantly at each order of perturbation theory. On the one hand, this is due to the increasing number of loops in the matrix elements of the virtual contributions. On the other hand, phase space integrals for high multiplicities can only be performed using Monte Carlo integration techniques. Increasing the number of unresolved partons in the final state, the number of singular phase space configurations increases as well. Hence, methods to extract phase space singularities before any numerical integration is performed are required.
In the following section, techniques to calculate one-loop and two-loop matrix elements are summarized.
Section 3.4 discusses methods to regulate the real radiation contributions at next-to-leading and next-to-next-to-leading order. These subtraction and slicing methods allow a numerical integration over the phase space. Subsequently, a summary of the properties of the discussed methods is presented.

## 3.3 Virtual contribution

In this section, techniques to calculate virtual contributions to the cross section are discussed. First the evaluation of one-loop integrals is summarized, as they appear in the virtual contribution of the next-to-leading order cross section, as well as in the real-virtual and double-virtual part of the next-to-next-to-leading order cross section. While the general problem of evaluating arbitrary one-loop integrals is solved theoretically for arbitrary numbers of final state particles, a numerical stable and efficient implementation of one-loop matrix elements is challenging for high multiplicities. A more detailed review on this topic can be found in [72].
Afterwards, the calculation of two-loop amplitudes is discussed. In contrast to the one-loop case, no general solution has been found yet to calculate two-loop integrals for arbitrary processes. In the past years a lot of effort has been devoted to develop new ideas. Some virtual contributions for processes that are phenomenologically relevant for the LHC can be calculated.

### 3.3.1 One-loop matrix elements

A general one-loop integral contributing to $|\mathcal{M}_n^{(1)}\rangle$ in a renormalizable Quantum field theory has the following form

$$I_N = \int \frac{\mathrm{d}^d l}{(4\pi)^d} \frac{\mathcal{N}(l)}{D_0 D_1 \cdots D_{N-1}} \,, \tag{3.27}$$

where $N$ denotes the number of external particles attached to the loop. The integral is said to be the $N$-point integral. The number of propagator denominators $D_i$ is equal to the number of external legs attached to the loop. The denominators are defined as

$$D_i = ((l + q_i)^2 - m_i^2 + i\epsilon) \,, \tag{3.28}$$

where $m_i$ is the mass of the corresponding particle in the loop, where for massless quarks and gluons $m_i = 0$. External momenta $p_k$ are ordered and fulfill momentum conservation, $\sum_{i=1}^{N} p_i = 0$. Hence, the momenta in the denominators are $q_i = \sum_{j=1}^{i} p_k,$.

The numerator $\mathcal{N}(l)$ is in general a function of the loop-momentum contracted with external vectors. Therefore, the integral is in general a tensor integral of rank $r$. The integral of rank $r = 0$ is said to be a scalar integral. For an arbitrary process the highest rank of a contributing integral, comes from a diagram, where all external momenta $p_i$ are the actual external momenta of the particles in the process. Such a diagram is called ring diagram.

Given the Feynman rules for a non-abelian gauge theory, the highest rank of such an integral can be determined. If it is assumed that the diagram contains only gluons, each three-gluon vertex contributes at most one power of the loop momentum to the integral. Hence, the highest rank of such an integral is $r_{\max} = N$. Allowing fermions as well, the result is the same, since each fermion propagator will contribute one power of the loop momentum, while the fermion-vector boson vertex does not. Scalars in the theory do not change this counting likewise.

A loop integral is ultraviolet-divergent, if $r \geq 2N - 4$. Hence, integrals with $N \geq 5$ are ultraviolet finite.

In theories with massless particles one-loop integrals are infrared-divergent, when internal massless propagator go on shell. Both forms of singularities are logarithmic and generate poles in the $\varepsilon$, when the integral in $d = 4 - 2\varepsilon$ dimensions is evaluated.

It was proven that any tensor integral $I_N$ can be written in a minimal basis of scalar integrals as [73]

$$I_N = c_{4;i} I_{4;i} + c_{3;i} I_{3;i} + c_{2;i} I_{2;i} + c_{1;i} I_{1;i} + \mathcal{R} + \mathcal{O}(\varepsilon) \,, \tag{3.29}$$

where $I_{N;i}$ are scalar $N$-point functions of some configuration $i$ of external momenta, where the scalar integrals are normally referred to as tadpoles ($N = 1$), bubbles ($N = 2$), triangles ($N = 3$) and boxes ($N = 4$).

The reduction of tensor integrals of any order $N$ to scalar integrals of $N \leq 4$ is possible because of the dimensionality of space-time $d = 4$. Four external linear independent vectors build up a basis in four dimensions. Because of energy momentum conservation, at least five external momenta are needed to obtain such a basis. All remaining vectors and the loop momentum can be expressed in such a basis. It has been shown that scalar $N$ point integrals, with $N \geq 5$, can be reduced to the mentioned minimal basis of scalar integrals [73–75].

If no singularities are present and regularization is not needed, the expansion is true with $\mathcal{R} = 0$. But since the calculation is performed $d = 4 - 2\varepsilon$ dimensions, a so called rational term $\mathcal{R}$ remains. Hence, the problem of calculating one-loop matrix elements or integrals is reduced to the problem of reducing the tensor integrals to the above basis of master integrals and subsequently finding the coefficients $c_{N;i}$ and the rational part $\mathcal{R}$.

Traditionally, the reduction of integrals can be performed by the Passarino-Veltman method [76]. The key idea is to expand the tensor integral into form factors of all possible tensor structures of external momenta that are allowed by Lorentz covariance. Contracting this expansion with the different tensor structures results in a system of linear equations for the form factors. In each step of the reduction the form factors corresponding to a rank $r$ tensor integral are related to form factors corresponding to lower rank tensors and eventually lower number of external legs. Inverting the system of linear equations leads therefore ultimately to the result for the integral.

However, numerical instabilities, due to vanishing Gram determinants arise, when using this method

naively. Improved techniques for tensor reduction have been developed and have proven their applicability to multiparticle processes [77, 78]. Even though these techniques lead to fast and stable numerical codes [79, 80], large algebraic expressions have to be handled and limits the applicability of these techniques.
A different approach to reduce one-loop integrals and to get the coefficients and the rational part in Eq. (3.29) is the OPP (Ossola-Papadopoulos-Pittau) method [81]:
The integrand numerator of any $N$-point one-loop amplitude (3.27) can be parameterized as

$$\begin{aligned}\mathcal{N}(l) = &\sum_{i_0<i_1<i_2<i_3}^{N-1} \left[d(i_0,i_1,i_2,i_3) + \tilde{d}(l;i_0,i_1,i_2,i_3)\right] \prod_{i\neq i_0,i_1,i_2,i_3}^{N-1} D_i \\ &+ \sum_{i_0<i_1<i_2}^{N-1} \left[c(i_0,i_1,i_2) + \tilde{c}(l;i_0,i_1,i_2)\right] \prod_{i\neq i_0,i_1,i_2}^{N-1} D_i \\ &+ \sum_{i_0<i_1}^{N-1} \left[b(i_0,i_1) + \tilde{b}(l;i_0,i_1)\right] \prod_{i\neq i_0,i_1}^{N-1} D_i \\ &+ \sum_{i_0}^{N-1} \left[a(i_0) + \tilde{a}(l;i_0)\right] \prod_{i\neq i_0}^{N-1} D_i \\ &+ \tilde{P}(l) \prod_{i}^{N-1} D_i \ .\end{aligned} \tag{3.30}$$

This is only a rewriting of Eq. (3.29), where the coefficients $d$, $c$, $b$ and $a$ correspond to the coefficients of the box, triangle, bubble and tadpole diagrams respectively. The rational term $\mathcal{R}$ contains all coefficients that still depend explicitly on the loop momentum, which are $\tilde{d}$, $\tilde{c}$, $\tilde{b}$, $\tilde{a}$ and $\tilde{P}$. The dependence on the loop momentum of the rational terms can be explicitly determined [81, 82].
The above formula can be applied to the full one-loop matrix element, rather than to individual Feynman diagrams. Then, the values of the constant coefficients can be determined by evaluating the amplitude integrand, i.e. both sides of Eq. (3.30), at specific values of $l$. This leads to a system of linear equations for the coefficients. The OPP procedure selects the loop momenta in such a way that 4, 3 , 2 or 1 of the possible denominators $D_i$ vanish. In this way the linear system is triangular and can be solved recursively.
At this point it becomes clear that the OPP procedure is related to unitarity. The vanishing of a propagator effectively sets the virtual particle on-shell. In the language of diagrammatic unitarity the specific propagator is cut and Cutkosky rules are applied for the cut propagator [83]

$$\frac{i}{p^2 - m^2 + i\epsilon} \to 2\pi\delta^{(+)}\left(p^2 - m^2\right) \ . \tag{3.31}$$

Applying this procedure to both sides of the one-loop matrix element of the form (3.27) in the OPP expansion Eq. (3.30). The l.h.s. can be calculated by just tree level diagrams, since at least one propagator is cut. Selecting the cuts in such a way that on the r.h.s. only one of the master integrals in Eq. (3.29) survives, it is possible to determine the coefficients. This is particularly easy for the box-integral coefficients: Correspondingly four propagators are cut, that results in a product of tree-level amplitudes on the l.h.s. and the box coefficient $d(i_0,i_1,i_2,i_3)$. The loop momentum is completely fixed by four $\delta$-functions. Recursively, the coefficients $d$, $c$, $b$ and $a$ can be determined

using four-dimensional loop momenta. This part of the amplitude is therefore called *cut-constructible*. The whole procedure is called *generalized unitarity*.
Using unitarity to reconstruct one-loop amplitudes from tree-level amplitudes was first considered in [84]. For numerical programs an efficient way to calculate tree-level amplitudes for on-shell complex momenta in d-dimensions is needed. This is widely done using recursion relations between amplitudes of different number of external legs based on [85].
Different automated tools exist to compute one-loop amplitudes, the virtual contribution to a NLO cross section, using either traditional tensor reduction methods [86–89] or generalized unitarity in combination with the OPP method [18, 89–94] or a complete numerical approach[95].

### 3.3.2 Two-loop matrix elements

Two-loop matrix elements are notoriously more difficult to calculate than one-loop matrix elements. New and different methods have to be applied. This section focuses on techniques that have been employed to calculate two-loop four-point matrix elements contributing to cross sections in hadron collisions at next-to-next-to-leading order QCD.
A general two-loop integral contributing to $|\mathcal{M}_n^{(2)}\rangle$ can be written as

$$I = \int \frac{\mathrm{d}^d k}{(2\pi)^d} \frac{\mathrm{d}^d l}{(2\pi)^d} \frac{\mathcal{N}(k,l)}{D_1 D_2 \cdots D_N} \,, \tag{3.32}$$

where the propagator denominators $D_i$ and the numerator $\mathcal{N}(l,k)$ depend in general on the loop momenta $l$ and $k$, the external momenta $p_i$ and the masses $m_i$, with $i = 1...N$. As in the one-loop case, $I$ is in principle a complicated tensor integral of the loop momenta.
A software for the numerical evaluation of dimensional regularized multi-loop integrals based on sector decomposition exists [96]. There are attempts to find a common basis for arbitrary two-loop integrands by applying generalized unitarity in multi-loop calculations [97, 98], but finding such a $d$-dimensional representation as in the one-loop case is not yet in sight.
The approach is therefore on a case by case basis. First the tensor integral is converted into scalar integrals of the form

$$I \propto \int \frac{\mathrm{d}^d k}{(2\pi)^d} \frac{\mathrm{d}^d l}{(2\pi)^d} \frac{\mathcal{S}(k,l)}{D_1^{a_1} D_2^{a_2} \cdots D_t^{a_t}} \,, \tag{3.33}$$

where in this case *scalar* means that the numerator $\mathcal{S}$ in Eq. (3.33) only depends on scalar products of external momenta and loop momenta.
One method to achieve this, is to project directly on the tree-level matrix element and sum over spin and color degrees of freedom $\langle \mathcal{M}_n^{(0)} | \mathcal{M}_n^{(2)} \rangle$ of the external particles, *e.g.* [99–104] or expand the integrand in all possible Lorentz covariant structures, that respect the symmetries of the considered process. Corresponding projection operators return the coefficients of the expansions containing the scalar integrals, *e.g.* [105]. A different method is to insert specific helicity states for the external particles to obtain scalar integrals [106, 107].
The set of denominators $\{D_1 \cdots D_t\}$ defines a topology of an integral. Relations among integrals of the form (3.33) can be found using *integration-by-parts* (IBP) [108]:

$$\int \frac{\mathrm{d}^d k}{(2\pi)^d} \frac{\mathrm{d}^d l}{(2\pi)^d} \frac{\partial}{\partial k^\mu} v^\mu f(k,l,\{p_i\}) = 0 \,, \tag{3.34}$$

$$\int \frac{\mathrm{d}^d k}{(2\pi)^d} \frac{\mathrm{d}^d l}{(2\pi)^d} \frac{\partial}{\partial l^\mu} v^\mu f(k,l,\{p_i\}) = 0 \,, \tag{3.35}$$

where the vector $v^\mu$ can be any of the vectors in the integral and $f(l,k,\{p_i\})$ is a generic integrand of the form (3.33). Equations (3.34) and (3.35) represent non-trivial linear relations among different scalar integrals. The IBP relations are just the consequence of the vanishing of the integral of a total derivative with respect to a loop momentum. On top on the IBP relations additional relations among different types of integrals can be obtained using Lorentz invariance (LI) [109]

$$I(p_1 + \delta p_1, \ldots, p_N + \delta p_N) = I(p_1, \ldots, p_N) \,, \tag{3.36}$$

where $\delta$ defines an infinitesimal Lorentz-transformation for the external momenta

$$p_1 \to p_1 + \delta p_1 = p_1^\mu + \delta^\mu_\nu p_1^\nu \,, \text{ with } \quad \delta^\mu_\nu = -\delta^\nu_\mu \,. \tag{3.37}$$

After performing a Taylor-expansion in the infinitesimal parameter $\delta$, the antisymmetric form of the relation between different integrals reads

$$\left( p_1^\nu \frac{\partial}{\partial p_{1\mu}} - p_1^\mu \frac{\partial}{\partial p_{1\nu}} + \cdots + p_1^\nu \frac{\partial}{\partial p_{1\mu}} - p_1^\mu \frac{\partial}{\partial p_{1\nu}} \right) I(p_1 + \delta p_1, \ldots, p_N + \delta p_N) = 0 \,. \tag{3.38}$$

This results in non-trivial relations only when the derivatives act on the integrand rather then the full integral itself. The IBP and LI relations do not yet provide any information about the integrals themselves, but can be used as a starting point to reduce the set of integrals to a limited number of master integrals. This reduction can be automated in terms of the *Laporta algorithm* [110]. Automated tools that perform this reduction are publicly available, *e.g.* [111, 112]. However, depending on the number of integrals and the number of parameters, which are independent kinematic invariants and particle masses, the reduction demands high computational resources. Besides, the set of master integrals is not unique and not are priory known.
In the following, the set of $N$ master integrals is denoted by the $N$-dimensional vector $\boldsymbol{I}$ for convenience. After the reduction has been performed, the main task is to solve the master integrals. Since all remaining integrals are linearly related to the master integrals, the full two-loop amplitude is known, if the master integrals are known.
Different approaches exist to get analytic results for loop integrals and a summary of methods can be found in [113]. The mathematical structure of multi-loop integrals is summarized in [114]. Here, one method is outlined that led to results for some benchmark processes at the LHC. The method of differential equations has been first discussed in [115–117] and extended to $2 \to 2$ processes in [109]. In contrast to other methods, the Feynman integral is not calculated directly, but differential equations in the available independent parameters are derived. The parameters are particle masses and invariants, which are built from the external momenta. The set of these momenta and masses is denoted by $\{x_i\}$. The derivative of a master integral, with respect to one of the parameter results again in a scalar Feynman integral that can be related to the set of master integrals using the IBP and LI relations. The result is a system of coupled first order differential equations in each variable

$$\frac{\partial \boldsymbol{I}(\varepsilon,\{x_i\})}{\partial x_j} = \boldsymbol{A}_j(\varepsilon,\{x_i\})\, \boldsymbol{I}(\varepsilon,\{x_i\}) \,, \tag{3.39}$$

where $\boldsymbol{A}_j$ is a $N \times N$ matrix. In order find a solution to the differential equation, a boundary condition has to be provided. Usually this condition is obtained in a kinematic regime of the invariants, where the integral can be solved exactly. The result is required as a Laurent expansion in $\varepsilon$. Hence, the differential equations are expanded in $\varepsilon$ and coupled differential equations order by

order in $\varepsilon$ are obtained.
In [103, 104] the differential equations for the two-loop master integrals to top quark pair production were solved using a numerical approach. In this case, two parameters are independent, the Mandelstam invariant $x_1 = t$ and the top quark mass $x_2 = m_t$. The center-of-mass energy has been set to one and could be recovered in the final result. This amounts to a general rescaling of the integrals. First, boundary conditions in the high energy limit were derived in a semi-numerical approach. The boundary conditions serve as starting points to integrate numerically the differential equation along a chosen path in the plane of parameters $(m_t^2,t)$ to obtain the result for a given master integral for each point on a grid representing the domain of the function.
In order to solve the differential equation analytically, the basis of special function needs to be determined, in which the result can be represented. For $2 \to 2$ processes with one mass scale, like top pair production and vector boson pair production with only massless propagators a major progress has been made in the past few years and analytic results for master integrals have become available. It has been shown [118], that an appropriate choice of the basis integrals, directly returns the solution of the integrals in terms of an appropriate representation of the special functions. This basis of master integrals, called the canonical basis, is defined such that the differential Eq. (3.39) has the following form

$$\frac{\partial \boldsymbol{I}(\varepsilon,\{x_i\})}{\partial x_j} = \varepsilon\, \boldsymbol{A}_j(\{x_i\})\, \boldsymbol{I}(\varepsilon,\{x_i\})\,. \tag{3.40}$$

Its solution can be written formally as

$$\boldsymbol{I}(\varepsilon,\{x_i\}) = \left[P e^{\varepsilon \int_0^{x_j} \mathrm{d}x_j\, \boldsymbol{A}_j(\{x_i\})}\right] \boldsymbol{I}(\varepsilon,\{x_i\}|_{x_j=0})\,, \tag{3.41}$$

where $P$ denotes the path ordering and a boundary condition at $x_j = 0$ has been assumed. If additionally the differential of matrix is logarithmic

$$\mathrm{d}\boldsymbol{A}_j(\{x_i\}) = \sum_k \boldsymbol{A}_{jk} \mathrm{d}\log(r_k)\,, \tag{3.42}$$

where $r$ is a rational function of the invariants $\{x_i\}$ and $\boldsymbol{A}_{jk}$ is a constant matrix, the result contains only generalized polylogarithms. This can be immediately seen by expanding the general result in $\varepsilon$ and comparing it to the definition of generalized polylogarithms [119]

$$G(a_1,\ldots,a_n;x) = \int_0^x \frac{\mathrm{d}t}{t-a_1}\, G(a_2,\ldots,a_n;t)\,, \tag{3.43}$$

where $G(x) = 1$ and $G(0) = 0$, and $G(a_1,x) = \log(1 - \frac{x}{a_1})$. Each next order in the $\varepsilon$ expansion, generates an additional integral over the logarithm. The solution is a sum of contributions of *uniform degree of transcendentality* [118]. The result is particularly compact and reduces the complexity of the final result in contrast to solving the differential equation in a different basis.
Even though, the result is notably easy in the canonical basis, a recipe how to find the canonical basis of master integrals, if it exists, is an open question. In general, heuristic methods to find the canonical basis on a case by case basis have been used (see e.g. [120]).
Analytic results for master integrals for $2 \to 2$ processes using differential equations have been presented in the last years. The two-loop integrals for $q\overline{q} \to VV$, where $VV$ represent two vector bosons of equal masses, have been calculated in [119, 120]. The contributions to $q\overline{q} \to V_1V_2$, $q\overline{q}' \to V_1V_2$ and $gg \to V_1V_2$, where $V_1$ and $V_2$ are two off-shell vector bosons of different masses, are

given in [105, 121–125]. These amplitudes are necessary, if the decay of the final state electroweak bosons is taken into account at next-to-next-to-leading order.
As already mentioned the full two-loop corrections to $pp \to t\bar{t}$ are available numerically. The bulk of the analytic two-loop contribution has become available in the meantime [126–129].
The complexity of these calculations is due to multiple scales appearing in the two-loop master integrals: the independent invariants, external masses and massive propagators.
Two-loop integrals, for purely massless $2 \to 2$ processes have been calculated already several years before. For dijet production in hadron collisions all necessary two-loop amplitudes are available [99–102, 106, 107, 130].

## 3.4 Subtraction methods and phase space slicing

In section 3.3 methods to evaluate virtual contributions of the cross section have been discussed. For the purpose of calculating the full cross section beyond leading order the evaluation of phase space integrals, that contain one or two unresolved partons, is necessary. At next-to-leading order the real contribution in Eq. (3.17) contains one unresolved parton. A direct numerical integration is not possible. There are two possible solutions to this problem.
The first method is phase space slicing [131–134]. The main idea is to split the phase space into two regions. The first region contains the singular limits of the matrix elements. The second region is finite and can therefore be integrated numerically. In the singular region the matrix element can be approximated and the integration is carried out analytically.
The second solution to this problem is subtraction. A subtraction term, that mimics the behavior of the matrix element in all singular limits, is added to the real radiation contribution in order to render the integral finite. A widely used method has been introduced by Catani and Seymour in [16] and its massive extension can be found in [135]. To clarify this method a short description is given in the following. The next-to-leading order contribution of the partonic cross section is written as

$$\hat{\sigma}^{(1)} = \int_{n+1} \left[ \mathrm{d}\hat{\sigma}^{\mathrm{R}} - \mathrm{d}\hat{\sigma}^{\mathrm{S}} \right] + \int_{n+1} \mathrm{d}\hat{\sigma}^{\mathrm{S}} + \int_{n} \mathrm{d}\hat{\sigma}^{\mathrm{V}} \,, \tag{3.44}$$

where the collinear factorization contribution has been omitted for simplicity. The subtraction term $\mathrm{d}\hat{\sigma}^{\mathrm{S}}$ fulfills the requirement that it has the same pointwise singular behavior as the real contribution itself, if calculated in $d$ dimensions. This allows to set $\varepsilon \to 0$ for the term in the square brackets and the phase space integral over $n+1$ final state partons can be evaluated using Monte-Carlo integration methods. All singularities are gathered in the last two terms. The subtraction term should be such that the singular behavior due to one unresolved parton can be integrated explicitly over the unresolved one particle phase space. In this integration explicit poles in $\varepsilon$ appear that cancel the explicit poles of the virtual contribution. Finally, a generic next-to-leading order calculation can be evaluated as follows

$$\hat{\sigma}^{(1)} = \int_{n+1} \left[ \mathrm{d}\hat{\sigma}^{\mathrm{R}} - \mathrm{d}\hat{\sigma}^{\mathrm{S}} \right]_{\varepsilon=0} + \int_{n} \left[ \mathrm{d}\hat{\sigma}^{\mathrm{V}} + \int_{1} \mathrm{d}\hat{\sigma}^{\mathrm{S}} \right]_{\varepsilon=0} . \tag{3.45}$$

The method is universal, which means it does not depend on the specific hard process. This follows from the fact, that QCD matrix elements factorize in the soft and collinear limits into a universal function that contains the traces of the unresolved parton and a reduced matrix element, that contains only the remaining hard particles. The specific factorization formulas are outlined in section 3.4.1. Using these limits a process independent form of the subtraction term as a sum of dipole

contributions can be constructed

$$\mathrm{d}\hat{\sigma}^{\mathrm{S}} = \sum_{\text{dipoles}} \mathrm{d}\hat{\sigma}^{\mathrm{B}} \otimes \mathrm{d}V_{\text{dipole}} \,, \tag{3.46}$$

where each dipole mimics the singular behavior of a pair of two partons out of the $n+1$ partons. In order to obtain the factorized form in Eq. (3.46) a factorization of the $n+1$ parton phase into a $n$ parton phase space and a one parton phase space is needed. This allows for an explicit integration of the dipole term

$$\int_{n+1} \mathrm{d}\hat{\sigma}^{\mathrm{S}} = \sum_{\text{dipoles}} \int_{n} \mathrm{d}\hat{\sigma}^{\mathrm{B}} \otimes \int_{1} \mathrm{d}V_{\text{dipole}} = \int_{n} \mathrm{d}\hat{\sigma}^{\mathrm{B}} \otimes \boldsymbol{I}^{(1)} \,. \tag{3.47}$$

The $\boldsymbol{I}^{(1)}$-operator has the same pole structure as the virtual contribution, which is given by $\mathbf{Z}^{(1)}$, as will outlined in in Eq. (4.108) and appendix B.1. Explicit expressions for the dipole and the integrated dipole terms as well as the phase space factorizations have been worked out explicitly in [16, 135]. This next-to-leading order subtraction scheme can be implemented directly in next-to-leading order event generators.

Another subtraction scheme for next-to-leading order calculations has been introduced for the calculation of $e^+e^- \to 3\,\text{jets}$ in [17] and named after the authors Frixione-Kunszt-Signer (FKS) scheme. The general idea, in contrast to the dipole subtraction scheme, is that the $n+1$ parton phase space is separated into regions that allow only one specific pair of partons to become collinear. A parametrization in angles and energies allows to obtain subtraction terms for each region and a numerical evaluation in $d = 4$ dimensions is possible. The form of the subtraction terms is such that they can be analytically integrated over the unresolved particle's phase space, after a remapping to the reduced kinematics is applied. As in the dipole formalism poles cancel analytically, before any numerical integration is performed.

Several comparisons between phase space slicing and Dipole subtraction methods can be found in [136, 137]. The general conclusion that has been drawn from these comparisons is that the subtraction method is superior to phase space slicing in efficiency and accuracy of the numerical evaluation by an order of magnitude [136].

The infrared singular phase space structure of a next-to-next-to-leading order cross section is much more involved than that of the next-to-leading order cross section. First, $n+1$ parton phase space integrations over the one-loop matrix element in $\mathrm{d}\hat{\sigma}^{\mathrm{RV}}$ are present. A construction of subtraction terms requires factorization formulas of one-loop matrix elements in soft and collinear limits. Following the next-to-leading order approach an analytic integration of splitting and soft functions over the one particle phase space has to be still possible. Second, the double-real contribution $\mathrm{d}\hat{\sigma}^{\mathrm{RR}}$ contains up to two unresolved partons in the allowed phase space region. A multitude of subtraction terms has to be constructed, that ensure the convergence of the integration as one or two partons become unresolved. The general factorization properties of the matrix elements can be used to obtain a process independent scheme. However, if a analytic cancellation between real and virtual poles is demanded, the subtraction terms should be analytically integrable over the one or two particle phase space. Since, the splitting and soft functions are more complicated, this task is non-trivial and has been the main drawback for analytic subtraction schemes at next-to-next-to-leading order.

In the first part of this section, soft and collinear limits of matrix elements are discussed, that are, in general, needed to construct local subtraction terms at next-to-next-to-leading order. Subsequently, different proposals for next-to-next-to-leading order subtraction schemes and slicing methods are

discussed and their applications are summarized. Finally, the different approaches are compared. In chapter 4, the construction of the subtraction scheme STRIPPER is outlined in great detail. In contrast to analytic subtraction schemes, the requirement of an analytic cancellation of poles is dropped and, apart from trivial integrals, only numerical integrations have to be performed.

### 3.4.1 Soft and collinear limits of matrix elements

The basis of each local subtraction scheme is the behavior of matrix elements in the infrared limit of external partons. The matrix element factorizes into a reduced matrix element, which contains all information about the hard process, and a process independent function that encodes all traces of unresolved partons. To setup a next-to-next-to-leading order subtraction scheme several limits of matrix elements need to be known, as up to two final state partons are unresolved. They are listed in the following.

*Single-collinear limit of tree-level amplitudes*

The collinear limit of two final state partons of momentum $p_1$ and $p_2$ is defined as the limit $k_\perp^\mu \to 0$ in the Sudakov parameterization

$$\begin{aligned} p_1^\mu &= zp^\mu + k_\perp^\mu - \frac{k_\perp^2}{z}\frac{n^\mu}{2p\cdot n}\,, \quad p_2^\mu = (1-z)p^\mu - k_\perp^\mu - \frac{k_\perp^2}{1-z}\frac{n^\mu}{2p\cdot n}\,, \\ s_{12} &= 2p_1\cdot p_2 = -\frac{k_\perp^2}{z(1-z)}\,, \quad p^2 = n^2 = p\cdot k_\perp = n\cdot k_\perp = 0\,. \end{aligned} \tag{3.48}$$

The matrix element factorizes into a spin-correlated reduced matrix element and a splitting function [138]

$$|\mathcal{M}^{(0)}_{a_1,a_2,\ldots}(p_1,p_2,\ldots)|^2 \simeq 4\pi\alpha_s \frac{2}{s_{12}} \langle \mathcal{M}^{(0)}_{a,\ldots}(p,\ldots)|\hat{\mathbf{P}}^{(0)}_{a_1a_2}(z,k_\perp;\varepsilon)|\mathcal{M}^{(0)}_{a,\ldots}(p,\ldots)\rangle\,. \tag{3.49}$$

The splitting function $\hat{\mathbf{P}}^{(0)}_{a_1a_2}(z,k_\perp;\varepsilon)$ describes the splitting of a parton of flavor $a$ into two partons of flavor $a_1$ and $a_2$. The splitting functions are given in appendix B.2.1.

*Single-soft limit of tree-level amplitudes*

The singular limit of one gluon with momentum $q \to 0$ leads to the factorization formula [138]

$$|\mathcal{M}^{(0)}_{g,a_1,\ldots}(q,p_1,\ldots)|^2 \simeq -4\pi\alpha_s \sum_{(i,j)} \Big(\mathcal{S}_{ij}(q) - \mathcal{S}_{ii}(q)\Big) \langle \mathcal{M}^{(0)}_{a_1,\ldots}(p_1,\ldots)|\mathbf{T}_i\cdot\mathbf{T}_j|\mathcal{M}^{(0)}_{a_1,\ldots}(p_1,\ldots)\rangle\,, \tag{3.50}$$

where the soft function, governing the leading singular behavior, is

$$\mathcal{S}_{ij}(q) = \frac{p_i\cdot p_j}{(p_i\cdot q)\,(p_j\cdot q)}\,. \tag{3.51}$$

In the soft limit, the matrix element reduces to the sum of double color correlated matrix elements, without the soft parton.

*Triple-collinear limit of tree-level amplitudes*

The collinear limit of three partons of momentum $p_1$, $p_2$ and $p_3$ in the Sudakov parameterization

$$p_i^\mu = z_i p^\mu + k_{\perp i}^\mu - \frac{k_{\perp i}^2}{z_i}\frac{n^\mu}{2p\cdot n}\,, \quad i = 1,2,3\,, \tag{3.52}$$

as $k_{\perp i} \to 0$ results in a factorization of the matrix element [138]

$$|\mathcal{M}^{(0)}_{a_1,a_2,a_3,\dots}(p_1,p_2,p_3,\dots)|^2 \simeq \left(\frac{8\pi\alpha_s}{s_{123}}\right)^2 \langle \mathcal{M}^{(0)}_{a,\dots}(p,\dots)|\hat{\mathbf{P}}^{(0)}_{a_1a_2a_3}(z_i,k_{\perp i};\varepsilon)|\mathcal{M}^{(0)}_{a,\dots}(p,\dots)\rangle \,. \tag{3.53}$$

The reduced matrix elements can contain up to two spin correlations, if the splitting parton is a gluon. The leading collinear behavior is governed by the invariant $s^2_{123}$ in the prefactor. The splitting function describes the correct behavior also in the iterated collinear limit, where first parton $a_1$ and $a_2$ become collinear and subsequently the parton $a_{12}$ becomes collinear to parton $a_3$. Apart from that, if up to two of the three collinear partons become soft, the behavior of the matrix element is correctly mimicked by the very same factorization formula.

*Double-soft limit of tree-level amplitudes*

There are two cases to distinguish for the double-soft limit. Either two gluons of momentum $q_1$ and $q_2$ become soft or a massless quark-antiquark pair of momentum $q_1$ and $q_2$ radiated by a single gluon becomes soft. The factorization formula for the former case reads [20, 138]

$$\begin{aligned}|\mathcal{M}^{(0)}&{}_{g,g,a_1,\dots}(q_1,q_2,p_1,\dots)|^2 \simeq \\ &(4\pi\alpha_s)^2 \left[\frac{1}{2}\sum_{ijkl} \mathcal{S}_{ij}(q_1)\mathcal{S}_{kl}(q_2)\, \langle \mathcal{M}^{(0)}_{a_1,\dots}(p_1,\dots)|\, \{\mathbf{T}_i\cdot\mathbf{T}_j, \mathbf{T}_k\cdot\mathbf{T}_l\}\, |\mathcal{M}^{(0)}_{a_1,\dots}(p_1,\dots)\rangle \right. \\ &\left. - C_A \sum_{ij} \mathcal{S}_{ij}(q_1,q_2)\, \langle \mathcal{M}^{(0)}_{a_1,\dots}(p_1,\dots)|\mathbf{T}_i\cdot\mathbf{T}_j|\mathcal{M}^{(0)}_{a_1,\dots}(p_1,\dots)\rangle\right] ,\end{aligned} \tag{3.54}$$

while for the latter case it is

$$|\mathcal{M}^{(0)}_{q,\bar{q},a_1,\dots}(q_1,q_2,p_1,\dots)|^2 \simeq (4\pi\alpha_s)^2\, T_F \sum_{ij} \mathcal{I}_{ij}(q_1,q_2)\, \langle \mathcal{M}^{(0)}_{a_1,\dots}(p_1,\dots)|\mathbf{T}_i\cdot\mathbf{T}_j|\mathcal{M}^{(0)}_{a_1,\dots}(p_1,\dots)\rangle \,. \tag{3.55}$$

In this limit, quadruple color correlators for the reduced matrix element appear. The leading soft behavior is factorized in the soft functions $\mathcal{S}_{ij}(q)$, $\mathcal{S}_{ij}(q_1,q_2)$ and $\mathcal{I}_{ij}(q_1,q_2)$, given in appendix B.2.2.

*Soft-collinear limit of tree level amplitudes*

Soft-collinear limits of the same parton pair are directly obtained by taking the soft limit of the splitting function describing the collinear limit. However, there is one case which needs a bit more investigation and is not completely covered by the above formulas. The limit where two partons of momentum $q_1$ and $q_2$ become collinear and both of them soft. This limit can be described by first taking the collinear limit of the two partons and subsequently taking the soft limit of a gluon, that is the product of the collinear partons. The factorization formula is

$$\begin{aligned}|\mathcal{M}^{(0)}&{}_{a_1,a_2,a_3\dots}(q_1,q_2,\dots)|^2 \simeq \\ &\left(4\pi\alpha_s\right)^2 \frac{2}{s_{12}} \hat{P}^{(0)\,\mu\nu}_{a_1a_2}(z_{12},k_\perp;\varepsilon)\, \langle \mathcal{M}^{(0)}_{a_3,\dots}(p,\dots)|\mathbf{J}_\mu(u_1+u_2)\mathbf{J}_\nu(u_1+u_2)|\mathcal{M}^{(0)}_{a_3,\dots}(p,\dots)\rangle \,,\end{aligned} \tag{3.56}$$

where the soft current is defined as

$$\mathbf{J}^{\mu}(q) = \sum_i \mathbf{T}_i \frac{p_i^{\mu}}{p_i \cdot q} \,. \tag{3.57}$$

*Single-collinear limit of one-loop amplitudes*

To derive soft and collinear subtraction terms for the $\hat{\sigma}^{RV}$ contribution of the next-to-next-to-leading order cross section, infrared limits of one-loop matrix elements need to be known. The collinear limit, as defined in Eq. (3.48), lead to the following factorization [139–144]

$$\begin{aligned} 2\mathrm{Re}\,\langle \mathcal{M}^{(0)}_{a_1,a_2,\ldots}(p_1,p_2,\ldots)|\mathcal{M}^{(1)}_{a_1,a_2,\ldots}(p_1,p_2,\ldots)\rangle \simeq \\ 4\pi\alpha_s \frac{2}{s_{12}} \Bigg[ 2\mathrm{Re}\,\langle \mathcal{M}^{(0)}_{a,\ldots}(p,\ldots)|\hat{\mathbf{P}}^{(0)}_{a_1a_2}(z,k_\perp;\varepsilon)|\mathcal{M}^{(1)}_{a,\ldots}(p,\ldots)\rangle \\ + \frac{\alpha_s}{4\pi}\langle \mathcal{M}^{(0)}_{a,\ldots}(p,\ldots)|\hat{\mathbf{P}}^{(1)}_{a_1a_2}(z,k_\perp;\varepsilon)|\mathcal{M}^{(0)}_{a,\ldots}(p,\ldots)\rangle \Bigg] \,. \end{aligned} \tag{3.58}$$

At this order the one-loop splitting function $\hat{\mathbf{P}}^{(1)}_{a_1a_2}$ is needed as well as the spin-correlated one-loop matrix element with one parton less.

*Single-soft limit of one-loop amplitudes*

The last limit to study is the single soft gluon limit of the one-loop matrix element. In this limit the matrix element behaves as [145, 146]

$$\begin{aligned} 2\mathrm{Re}\,\langle \mathcal{M}^{(0)}_{g,a_1,\ldots}(q,p_1,\ldots)|\mathcal{M}^{(1)}_{g,a_1,\ldots}(q,p_1,\ldots)\rangle \simeq \\ -4\pi\alpha_s \Bigg\{ \sum_{(i,j)} \Big( \mathcal{S}_{ij}(q) - \mathcal{S}_{ii}(q) \Big) \, 2\mathrm{Re}\,\langle \mathcal{M}^{(0)}_{a_1,\ldots}(p_1,\ldots)|\mathbf{T}_i \cdot \mathbf{T}_j|\mathcal{M}^{(1)}_{a_1,\ldots}(p_1,\ldots)\rangle \\ + \frac{\alpha_s}{4\pi} \Bigg[ \sum_{(i,j)} \left( \mathcal{S}_{ij}(q) - \mathcal{S}_{ii}(q) \right) R_{ij} \, \langle \mathcal{M}^{(0)}_{a_1,\ldots}(p_1,\ldots)|\mathbf{T}_i \cdot \mathbf{T}_j|\mathcal{M}^{(0)}_{a_1,\ldots}(p_1,\ldots)\rangle \\ -4\pi \sum_{(i,j,k)} \mathcal{S}_{ik}(q) \, I_{ij} \, \langle \mathcal{M}^{(0)}_{a_1,\ldots}(p_1,\ldots)|f^{abc}T_i^a T_j^b T_k^c|\mathcal{M}^{(0)}_{a_1,\ldots}(p_1,\ldots)\rangle \Bigg] \Bigg\} \,. \end{aligned} \tag{3.59}$$

The explicit form of splitting and soft functions that appear in this section are partially collected in appendix B. The full set of functions can be found in [1].

In the following several subtraction and slicing methods are discussed. Some of them use the explicit factorization formulas outlined in the present section, while others use variations of this formulas. The subtraction scheme STRIPPER, that will be discussed afterwards, uses the full information of the factorization formulas.

### 3.4.2 Antenna subtraction

The antenna subtraction scheme has been introduced for next-to-leading order calculations in [147, 148]. The main difference to the dipole formalism is that color-ordered amplitudes are considered

(see appendix A.1). The soft and collinear limits of color-ordered amplitudes are especially easy and QED like, since color is treated separately. It is instructive to understand the next-to-leading order subtraction first and afterwards the generalization to next-to-next-to-leading order. The detailed description of the subtraction scheme is given in [149] and this discussion provides a short summary. Here only leading color contributions are discussed. A generalization to subleading color contributions is in general possible, but non-trivial. It has been presented in the purely gluonic case in [150].
The real radiation contribution to the cross section in the leading color approximation is written as

$$\hat{\sigma}^{\mathrm{R}} = \mathcal{N} \sum_{I_{n+1}} \int \mathrm{d}\boldsymbol{\Phi}_{n+1} \, |\mathcal{M}^{(0)}_{I_{n+1}}(p_1, \ldots, p_{n+1})|^2 \, \mathrm{F}_{n+1} \, , \tag{3.60}$$

where for simplicity only final state colored partons are considered and all partons are massless. The factor $\mathcal{N}$ contains all remaining factors that are irrelevant for the further discussion. $|\mathcal{M}^{(0)}_{I_{n+1}}|^2$ denotes the color-ordered, squared and spin summed matrix element, where the leading color factors are included in contrast to Eq. A.24. The color ordering is such that particle 1 is color connected to particle 2 and particle 2 is color connected to particle 3 and so on. The sum runs over all color ordered matrix elements $I_{n+1}$ for $n+1$ particles. The subtraction term in Eq. (3.45) is constructed in terms of antennae and reads

$$\mathrm{d}\hat{\sigma}^{\mathrm{S}} = \mathcal{N} \sum_{I_{n+1}} \mathrm{d}\boldsymbol{\Phi}_{n+1} \sum_{j} X^0_{ijk} |\mathcal{M}^{(0)}_{I_n}(p_1, \ldots, \tilde{p}_I, \tilde{p}_K, \ldots, p_{n+1})|^2 \, \mathrm{F}_n \, . \tag{3.61}$$

This term contains a reduced matrix element of $n$ partons that depends on new momenta $\tilde{p}_I$ and $\tilde{p}_k$ which are linear combinations of the three momenta $p_i$, $p_j$ and $p_k$. The leading order antenna function $X^0_{ijk}$ depends only on the three momenta $p_i$, $p_j$ and $p_k$ and mimics the singular behavior of the matrix element as parton $j$ becomes unresolved. For example in the soft limit the color ordered amplitude factorizes as follows

$$|\mathcal{M}^{(0)}_{I_{n+1}}(p_1, \ldots, p_i, p_j, p_k, \ldots, p_{n+1})|^2 \simeq \frac{2 s_{ij}}{s_{ij} s_{jk}} |\mathcal{M}^{(0)}_{I_{n+1}}(p_1, \ldots, \tilde{p}_I, \tilde{p}_K, \ldots, p_{n+1})|^2 \, , \tag{3.62}$$

where in this case $\tilde{p}_I = p_i$ and $\tilde{p}_k = p_k$. The singular limit of the color ordered amplitude only affects partons that are color connected to the unresolved parton. Therefore, the factorization formula is considerably easier than the soft factorization of the full matrix element, which is given in Eq. (3.50). To be able to integrate the antennae explicitly over the unresolved phase space, the phase space has to be factorized into a $n$ particle phase space and an antenna phase space

$$\mathrm{d}\boldsymbol{\Phi}_{n+1}(p_1, \ldots, p_{n+1}) = \mathrm{d}\boldsymbol{\Phi}_n(p_1, \ldots, \tilde{p}_I, \tilde{p}_K, \ldots, p_{n+1}) \cdot \mathrm{d}\boldsymbol{\Phi}_{X_{ijk}}(p_i, p_j, p_k; \tilde{p}_I + \tilde{p}_K) \, . \tag{3.63}$$

The antenna function is analytically integrated over the antenna phase space to obtain explicit poles in $\varepsilon$

$$\mathcal{X}^0_{ijk} \propto \int \mathrm{d}\boldsymbol{\Phi}_{X_{ijk}} X^0_{ijk} \, . \tag{3.64}$$

The antenna subtraction method can be generalized to cross section calculations at next-to-next-to-leading order. Considering only colored particles in the final state, subtraction terms for the double-real contribution and the real-virtual contribution have to be provided. The next-to-next-to-

leading order cross section at leading color is written as

$$\hat{\sigma}^{(2)} = \int_{n+2} \left[ \mathrm{d}\hat{\sigma}^{\mathrm{RR}} - \mathrm{d}\hat{\sigma}^{\mathrm{S,RR}} \right] + \int_{n+2} \mathrm{d}\hat{\sigma}^{\mathrm{S,RR}} + \int_{n+1} \left[ \mathrm{d}\hat{\sigma}^{\mathrm{RV}} - \mathrm{d}\hat{\sigma}^{\mathrm{S,RV}} \right] + \int_{n+1} \mathrm{d}\hat{\sigma}^{\mathrm{S,RV}} + \int_{n} \mathrm{d}\hat{\sigma}^{\mathrm{VV}} \,, \tag{3.65}$$

which is essentially a generalization of formula (3.45). The subtraction term $\mathrm{d}\hat{\sigma}^{\mathrm{S,RR}}$ mimics the behavior of the double real contribution in soft and collinear limits. The double-real contribution in leading color approximation reads

$$\hat{\sigma}^{\mathrm{RR}} = \mathcal{N} \sum_{I_{n+2}} \int \mathrm{d}\boldsymbol{\Phi}_{n+2} \, |\mathcal{M}^{(0)}_{I_{n+2}}(p_1, \ldots, p_{n+2})|^2 \, \mathrm{F}_{n+2} \,. \tag{3.66}$$

For the construction of appropriate subtraction terms different cases have to be distinguished:
If only one of the final state partons becomes unresolved, the antenna function of the next-to-leading order case can be used and the contribution to the subtraction term reads

$$\mathrm{d}\hat{\sigma}^{\mathrm{S,RR,1}} = \mathcal{N} \sum_{I_{n+2}} \mathrm{d}\boldsymbol{\Phi}_{n+2} \sum_{j} X^0_{ijk} |\mathcal{M}^{(0)}_{I_{n+1}}(p_1, \ldots, \tilde{p}_I, \tilde{p}_K, \ldots, p_{n+1})|^2 \, \mathrm{F}_{n+1} \,. \tag{3.67}$$

If two partons $j$ and $k$ become unresolved, that are adjacent in the color ordered amplitude, the subtraction term is obtained from an antenna function that contains all double unresolved limits of the matrix element that are color connected to parton $j$ and $k$, $X^0_{ijkl}$. However, this function is singular in limits, when only one of the partons becomes unresolved and this singularities are not present in the matrix elements. Hence, appropriate iterated single unresolved antenna functions have to be subtracted. This contribution to the subtraction term reads

$$\mathrm{d}\hat{\sigma}^{\mathrm{S,RR,2}} =$$
$$\mathcal{N} \sum_{I_{n+2}} \mathrm{d}\boldsymbol{\Phi}_{n+2} \left[ \sum_{jk} \left( X^0_{ijkl} - X^0_{ijk} X^0_{IKl} - X^0_{jkl} X^0_{iJL} \right) |\mathcal{M}^{(0)}_{I_{n+1}}(p_1, \ldots, \tilde{p}_I, \tilde{p}_L, \ldots, p_{n+1})|^2 \, \mathrm{F}_n \right] \,, \tag{3.68}$$

the sum inside the bracket selects only color adjacent pairs $j$,$k$ and the adjacent hard momenta $i$,$l$. An integration of the antenna functions over the unresolved phase space is possible after factorizing the phase space using an appropriate mapping [151]

$$\mathrm{d}\boldsymbol{\Phi}_{n+2}(p_1, \ldots, p_{n+2}) = \mathrm{d}\boldsymbol{\Phi}_n(p_1, \ldots, \tilde{p}_I, \tilde{p}_L, \ldots, p_{n+2}) \cdot \mathrm{d}\boldsymbol{\Phi}_{X_{ijkl}}(p_i, p_j, p_k, p_l; \tilde{p}_I + \tilde{p}_L) \,. \tag{3.69}$$

The integral over the unresolved contribution can be performed analytically

$$\mathcal{X}^0_{ijkl} \propto \int \mathrm{d}\boldsymbol{\Phi}_{X_{ijkl}} X^0_{ijkl} \,. \tag{3.70}$$

The next case to consider is, when the unresolved partons $i$ and $j$ are completely disconnected. The subtraction term is obtained by independently using a next-to-leading order antenna function for each of the disconnected triple separately [149]. The remaining case is the almost color unconnected case. In this configuration the two unresolved partons are separated by one hard parton. Using iteratively the next-to-leading order antenna function the appropriate subtraction term can be constructed.
The subtraction term $\mathrm{d}\hat{\sigma}^{\mathrm{S,RV}}$ for the real virtual contribution can be constructed in a similar way.

For example, the subtraction term for the single-unresolved case of the one-loop matrix element reads

$$\begin{aligned} \mathrm{d}\hat{\sigma}^{\mathrm{S,RV,1}} =& \mathcal{N} \sum_{I_{n+1}} \mathrm{d}\boldsymbol{\Phi}_{n+1} \sum_{j} \Big[ X^0_{ijk} |\mathcal{M}^{(1)}_{I_{n+1}}(p_1,\dots,\tilde{p}_I,\tilde{p}_K,\dots,p_{n+1})|^2 \mathrm{F}_n \\ &+ X^1_{ijk} |\mathcal{M}^{(0)}_{I_{n+1}}(p_1,\dots,\tilde{p}_I,\tilde{p}_K,\dots,p_{n+1})|^2 \, \mathrm{F}_n \Big] \ , \end{aligned} \tag{3.71}$$

where the one-loop three parton antenna function has been introduced. The structure of the factorization formula can be compared to the factorization formula of the full one-loop matrix element in the soft or collinear limits given in Eqs. (3.58) and (3.59). To obtain the integrated subtraction terms the antenna functions are analytically integrated over the three parton antenna phase space.

The specific form of the antenna functions is given by the ratio of color ordered matrix elements. The tree-level antenna functions are

$$X^0_{ijk} \propto \frac{|\mathcal{M}^{(0)}_{ijk}|^2}{|\mathcal{M}^{(0)}_{IK}|^2} \ , \qquad X^0_{ijkl} \propto \frac{|\mathcal{M}^{(0)}_{ijkl}|^2}{|\mathcal{M}^{(0)}_{IL}|^2} \ , \tag{3.72}$$

and the one-loop three parton antenna reads

$$X^1_{ijk} = S \frac{|\mathcal{M}^{(1)}_{ijk}|^2}{|\mathcal{M}^{(0)}_{IK}|^2} - X^0_{ijk} \frac{|\mathcal{M}^{(1)}_{IK}|^2}{|\mathcal{M}^{(0)}_{IK}|^2} \ , \tag{3.73}$$

where $S$ is a symmetry factor. The three parton matrix elements $\mathcal{M}_{ijk}$ implies that the partons $i$,$j$,$k$ are ordered.

It should be noted that the antenna subtraction terms are not pointwise convergent, since spin correlations in the collinear limits are not considered. Nevertheless, a recipe to obtain stable and integrable integrands anyhow is presented in [152]. The antenna subtraction method has been originally introduced to calculate $e^+e^- \to 3$ jets at next-to-next-to-leading order [152–160]. It has been generalized to hadrons in the initial state in [161–165]. This allowed for the calculation of the gluonic channel for dijet production at leading color in gluon fusion [50] and the quark annihilation channel [166]. The generalization to full color in the pure gluonic channel has been presented in [49]. The antenna formalism has been generalized to massive partons in the final state [167–171]. First contributions to differential distributions in $pp \to t\bar{t}$ in the quark annihilation channel have been calculated [172, 173] at leading color.

Additionally, the subtraction method has been successfully applied to Higgs boson production in association with one jet at next-to-next-to-leading order in gluon fusion [174].

### 3.4.3 Colorful subtraction

The colorful subtraction scheme has been worked out in several publications [144, 175–184], while it is still limited to colorless initial states. In contrast to the antenna approach the full squared amplitude is considered and subtraction terms are constructed using the explicit limits given in section 3.4.1. The next-to-next-to-leading order cross section and subtraction terms are arranged with respect to the multiplicity of the phase space integral [144]

$$\mathrm{d}\hat{\sigma}^{(2)}_{n+2} = \Big\{ \mathrm{d}\hat{\sigma}^{\mathrm{RR}}_{n+2} \, F_{n+2} - \mathrm{d}\hat{\sigma}^{\mathrm{RR,S_2}}_{n+2} \, F_n - \Big[ \mathrm{d}\hat{\sigma}^{\mathrm{RR,S_1}}_{n+1} \, F_{n+1} - \mathrm{d}\hat{\sigma}^{\mathrm{RR,S_{12}}}_{n+2} \, F_n \Big] \Big\}_{\varepsilon=0} \ , \tag{3.74}$$

$$\mathrm{d}\hat{\sigma}^{(2)}_{n+1} = \left\{ \left[ \mathrm{d}\hat{\sigma}^{\mathrm{RV}}_{n+1} + \int_1 \mathrm{d}\hat{\sigma}^{\mathrm{RR,S_1}}_{n+2} \right] F_{n+1} - \left[ \mathrm{d}\hat{\sigma}^{\mathrm{RV,S_1}}_{n+1} + \left( \int_1 \mathrm{d}\hat{\sigma}^{\mathrm{RR,S_1}}_{n+2} \right)^{S_1} \right] F_n \right\}_{\varepsilon=0} , \tag{3.75}$$

$$\mathrm{d}\hat{\sigma}^{(2)}_{n} = \left\{ \mathrm{d}\hat{\sigma}^{\mathrm{VV}}_{n} + \int_2 \left[ \mathrm{d}\hat{\sigma}^{\mathrm{RR,S_2}}_{n+1} - \mathrm{d}\hat{\sigma}^{\mathrm{RR,S_{12}}}_{n+2} \right] + \int_1 \left[ \mathrm{d}\hat{\sigma}^{\mathrm{RV,S_1}}_{n+1} + \left( \int_1 \mathrm{d}\hat{\sigma}^{\mathrm{RR,S_1}}_{n+2} \right)^{S_1} \right] \right\}_{\varepsilon=0} F_n , \tag{3.76}$$

where the measurement function is written explicitly to highlight the number of resolved particles entering the matrix element in the related cross section. The construction is such that each contribution is integrable and finite in four dimensions. The double-real cross section is regularized by pointwise subtraction terms $\mathrm{d}\hat{\sigma}^{\mathrm{RR,S_2}}_{n+2}$ and $\mathrm{d}\hat{\sigma}^{\mathrm{RR,S_1}}_{n+1}$, where the former contains all limits as two partons are unresolved, while the latter behaves as the matrix element in the limit as one parton becomes unresolved. The additional subtraction term $\mathrm{d}\hat{\sigma}^{\mathrm{RR,S_{12}}}_{n+2}$ regularize remaining phase space singularities in $\mathrm{d}\hat{\sigma}^{\mathrm{RR,S_1}}_{n+1}$, since one of the remaining $n+1$ partons can become soft or collinear. The real-virtual contribution contains explicit virtual poles. These poles cancel analytically with the integrated subtraction term $\int_1 \mathrm{d}\hat{\sigma}^{\mathrm{RR,S_1}}_{n+1}$. This can be directly observed by comparison to the next-to-leading order formula (3.45), which is recovered by setting $F_n = 0$. In this limit, the above calculation corresponds to a next-to-leading order calculation of a $n+1$ jet observable, where the real-virtual cross section plays the role of the virtual contribution. The double-real contribution plays the role of the real radiation and the subtraction term $\mathrm{d}\hat{\sigma}^{\mathrm{RR,S_1}}_{n+1}$ is equal to $\mathrm{d}\hat{\sigma}^{\mathrm{S}}$. However, at next-to-next-to-leading order one of the $n+1$ partons in both terms in the first bracket of Eq. (3.75) leads to phase space singularities. They are regularized respectively by the subtraction terms in the second bracket of Eq. (3.75). The last equation contains the double-virtual contribution, which exhibits only explicit poles. These poles cancel ultimately with all remaining integrated subtraction terms. The first bracket in Eq. (3.76) contains the explicit integration over two unresolved partons while the second bracket is integrated over one unresolved parton.
The subtraction terms as well as the analytic integrations have been worked out in the before mentioned publications. The colorful subtraction scheme has been applied to the Higgs boson decay into a $b\bar{b}$-pair in [185].

### 3.4.4 $q_T$-subtraction and $q_T$-slicing

The $q_T$-subtraction approach, in the form presented here, is exclusively defined for hadronic scattering into a colorless final state $F(Q)$

$$h_1 + h_2 \to F(Q) + X , \tag{3.77}$$

where Q is the invariant mass of the final state, which in general consists of one or more particles (leptons, Higgs bosons, vector bosons,...), with $Q^2 = (\sum_i q_i)^2$. The subtraction method has been presented in [41]. The partonic initial state at leading order is either gluon fusion or quark pair annihilation to retain a colorless final state. This subtraction scheme is equally formulated for the next-to-leading order and next-to-next-to-leading order cross section. The basic observation used for setting up the scheme is that at leading order the transverse momentum $\boldsymbol{q}_T = \sum_i \boldsymbol{q}_{T,i}$ of the final state $F$ is zero, since no partons are available that can recoil against the transverse momentum. Contributions with $\boldsymbol{q}_T \neq 0$ at higher orders are thence given by the lower order contribution of the same process in association with one additional jet

$$\mathrm{d}\sigma^{F}_{(\mathrm{N})\mathrm{NLO}}|_{\boldsymbol{q}_T \neq 0} = \mathrm{d}\sigma^{F+\mathrm{jet}}_{(\mathrm{N})\mathrm{LO}} . \tag{3.78}$$

In this kinematic configuration the infrared divergences of the next-to-next-to-leading order singularities are the same as in the next-to-leading order cross section and available subtraction methods, like the dipole subtraction formalism can be used. If $\boldsymbol{q}_T \to 0$ is taken into account, additional singularities occur on the right hand side, due to the infrared limits of the additional massless partons, forming the jets. These singularities are regulated by subtracting a counterterm $\mathrm{d}\sigma^{\mathrm{CT}}_{\mathrm{(N)LO}}$. Since this counterterm mimics the behaviour of the right hand side in the limit $\boldsymbol{q}_T \to 0$, the phase space is integrable. The precise form of the counterterm can be determined from transverse momentum resummation (see [186, 187] and references therein). For a hard scattering process, as given in (3.77), enhancements due to large logarithms of the form $\log^n\left(Q^2/\boldsymbol{q}_T^2\right)$ appear in the limit $\boldsymbol{q}_T \to 0$. These logarithms can be resummed to all orders in $\alpha_s$. Since the resummation formula provides a description of the cross section in the low $\boldsymbol{q}_T$ limit, it can be used as a subtraction term, after it is expanded to the order needed for the fixed order calculation. Since only the limit of the counterterm is uniquely defined, there is an arbitrariness in its explicit choice with respect to terms that do not depend on $\boldsymbol{q}_T$. The full integrable cross section can finally be written as

$$\mathrm{d}\sigma^{F}_{\mathrm{(N)NLO}} = \mathcal{H}^{F}_{\mathrm{(N)NLO}} \otimes \mathrm{d}\sigma^{F}_{\mathrm{LO}} + \left[\mathrm{d}\sigma^{F+\mathrm{jets}}_{\mathrm{(N)LO}} - \mathrm{d}\sigma^{\mathrm{CT}}_{\mathrm{(N)LO}}\right] , \tag{3.79}$$

where the hard function $\mathcal{H}^F$ is independent of $\boldsymbol{q}_T$. After the precise form of the counterterm is fixed, $\mathcal{H}^F$ can be fixed such that the integral over the whole phase space returns the total cross section at the given order. The hard function contains the physical content of the one-loop contribution at next-to-leading order and that of the two-loop contribution at next-to-next-to-leading order. Therefore, its precise form at next-to-next-to-leading order can be fixed if the corresponding two-loop matrix elements are known. The cross section $\mathrm{d}\sigma^{F+\mathrm{jets}}_{\mathrm{NLO}}$ contains the real-virtual and double-real contribution. Since the counterterm subtracts singularities as $\boldsymbol{q}_T \to 0$, the kinematics of the counterterm are always the kinematics of the Born contribution. However, the counterterm is non-local, since all possible soft and collinear singularities are summarized in only one variable. Thus, the subtraction is not pointwise.

Even though the scheme is formulated as a subtraction that can be integrated over the full phase space, the actual implementation is rather inspired by the traditional slicing methods. The integral over the phase space is divided in a low $\boldsymbol{q}_T$ and high $\boldsymbol{q}_T$ region. In the low $\boldsymbol{q}_T$ region the cross section can be replaced by the resummation formula, while in the high $\boldsymbol{q}_T$ region the integration can be performed without necessarily introducing a counterterm.

The $q_T$-subtraction/slicing method has been applied to a multitude of processes at next-to-next-to-leading order: First it has been used to calculate Higgs boson production in hadron collisions [41, 45] and subsequently to single vector boson production [40]. Higgs boson in association with a $W$-boson has been considered in [188] and the production of two photons is outlined in [189]. After the two-loop matrix elements for more involved $2 \to 2$ processes have become available, results for the following processes in proton proton collisions were presented: $Z\gamma$ and $W\gamma$ in [51, 52], $ZZ$ in [53] and $WW$ in [25].

The extension of the $q_T$-subtraction method to colored final states has also be investigated. In particular, first steps towards an all order resummation formula of the transverse momentum of a $t\bar{t}$-pair were presented in [190–192].

### 3.4.5 $N$-jettiness slicing

The $q_T$-subtraction is built on the observation that only one kinematic parameter, the transverse momentum of the final state $F$, separates two phase space regions. In the first region, $\boldsymbol{q}_T \neq 0$, the next-to-next-to-leading order cross section can be calculated using a next-to-leading order calculation

of the same process with one additional jet. The contribution of the second region, $\boldsymbol{q}_T \to 0$ could be recovered by using the behavior of the cross section in this particular limit, which is given by an all order resummation formula.
This approach is not restricted to the transverse momentum variable, but can in principle be generalized to each kinematic variable of the given process, that separates the phase space into a infrared singular region and a infrared finite region. Nevertheless, the behavior of the cross section in the infrared singular region has to be known.
Another variable, that fulfills this requirement is $N$-jettiness [193] and the slicing procedure according to this variable has been presented in [194–196]. The global event shape variable $N$-jettiness is defined as

$$\mathcal{T}_N = \sum_k \min_i \left\{ \frac{p_i \cdot q_k}{Q_i} \right\} , \tag{3.80}$$

where the sum runs over all final state momenta $q_k$. The momenta $p_i$, for $i = a,b,1,\dots N$, specify the momenta of the $N$ final state jets after a jet clustering algorithm has been applied. The partonic initial state momenta are $p_a$ and $p_b$, they are denoted as beam jets. The energies $Q_i$ can be chosen to be twice the energy of the considered jet. Hence, the momenta $\frac{p_i}{Q_i}$ define the $N$ axes to which particles are clustered in the case of $N$ jets. At leading order in the perturbative series, each of the $n$ final state partons is associated with one jet, therefore $\mathcal{T}_N = 0$. For higher orders in the perturbative series more partons will be clustered into one jet and $\mathcal{T}_N \geq 0$. A cut $\mathcal{T}_N^{\text{cut}}$ is introduced to split the phase space into two regions, which allows to write the cross section schematically as

$$\sigma_X = \int_0^{\mathcal{T}_N^{\text{cut}}} \mathrm{d}\mathcal{T}_N \frac{\mathrm{d}\sigma_X}{\mathrm{d}\mathcal{T}_N} + \int_{\mathcal{T}_N^{\text{cut}}} \mathrm{d}\mathcal{T}_N \frac{\mathrm{d}\sigma_X}{\mathrm{d}\mathcal{T}_N} . \tag{3.81}$$

The region $\mathcal{T}_N \geq \mathcal{T}_N^{\text{cut}}$ contains an additional resolved jet. Therefore, the contribution in this region can be obtained by a next-to-leading order calculation of the same observable with N+1 jets. If the $\mathcal{T}_{\text{cut}}$ is small enough the first contribution can be calculated using the resummation formula that approximates the matrix element correctly in the small $N$-jettiness region. A factorization theorem has been derived in the framework of the soft-collinear effective field theory (SCET) and a resummation in the small jettiness limit has been performed [197]. In the factorized form the cross section in the small $N$-jettiness limit reads

$$\sigma_X^{\text{sing}}(\mathcal{T}_N^{\text{cut}}) \equiv \int_0^{\mathcal{T}_N^{\text{cut}}} \mathrm{d}\mathcal{T}_N \frac{\mathrm{d}\sigma_X}{\mathrm{d}\mathcal{T}_N} = \int H \otimes B \otimes B \otimes S \otimes \left[ \prod_{i=1}^{N} J_i \right] + \mathcal{O}\left( \frac{\mathcal{T}_N^{\text{cut}}}{\min\{Q_i\}} \right) , \tag{3.82}$$

where $H$ is the hard function that contains the virtual contributions. The beam functions $B$ describe collinear radiation along the beam axis, while the jet functions $J_i$ describe collinear radiation along the jet directions. The formula is expanded to next-to-next-to leading order to reproduce the fixed order contribution in the low $\mathcal{T}_N$ regime. The hard function contains the physical contribution of the two-loop matrix element. The jet and beam functions are known to the required accuracy [198–201]. The soft function $S$ describes soft radiation and can be evaluated numerically at next-to-next-to leading order [196]. If the cut is too small the numerical evaluation of the second term in Eq. (3.81) still suffers from infrared enhanced terms, that need to be subtracted and a final formula can be

rewritten as

$$\sigma_X = \sigma_X^{\text{sing}}(\mathcal{T}_N^{\text{off}}) + \int_{\mathcal{T}_N^{\text{cut}}} \mathrm{d}\mathcal{T}_N \left[ \frac{\mathrm{d}\sigma_X}{\mathrm{d}\mathcal{T}_N} - \frac{\mathrm{d}\sigma_X^{\text{sing}}}{\mathrm{d}\mathcal{T}_N} \theta\left(\mathcal{T}_N < \mathcal{T}_N^{\text{off}}\right) \right] + \mathcal{O}\left( \frac{\mathcal{T}_N^{\text{cut}}}{\min\{Q_i\}} \right) , \tag{3.83}$$

where another cut $\mathcal{T}_N^{\text{off}}$ has been introduced. This formula can be directly compared to the $q_T$-subtraction/slicing formula in Eq. (3.79), where corresponding terms are easily identified. The counterterm term, the second term in the square bracket, is a non-local subtraction term that regularizes the cross section at next-to-leading order in all the infrared limits of the additional parton in the final state. As discussed in [194] the cutoff $\mathcal{T}_N^{\text{cut}}$ can be made smaller than the numerical precision of the final result.
A advantage with respect to $q_T$ subtraction/slicing is that the $N$-jettiness slicing can be applied to processes including colored particles in the final state. However, currently it is limited to massless partons. An extension to massive partons in the final state is theoretically possible. The slicing method in the form without any counterterm Eq. (3.81) has been applied to $W$ boson production in association with one jet [56] and Higgs boson production in association with one jet [195].

### 3.4.6 Comparison of different schemes

The discussed subtraction and slicing schemes are in a certain sense process independent. This means that they can be applied to several different processes. Only matrix elements, that depend on the kinematics of the hard process have to be adapted. In the following discussion, the characteristics of the subtraction scheme Stripper are anticipated and compared to the properties of the schemes discussed previously. The verification, that the subtraction scheme has indeed these properties, will be given in chapter 4 and chapter 5.
The discussion starts with the class of processes to which the schemes can be applied at present. Thereby, only the conceptual possibility is discussed for the current formulation of the scheme, by neglecting the fact that the two-loop amplitude has to be available, too. The colorful subtraction scheme is applicable to processes with uncolored particles in the initial state. A proposal to extend the method to colored initial states has been presented in [180], but not yet applied to a physical process. The $q_T$-subtraction/slicing method is currently only applicable to colorless final states, since only for this class of processes a resummation formula in the low $q_T$ region is available. Attempts to extend the formulation to a final state heavy quark pair exist [190–192], and would allow to apply the scheme also to $t\bar{t}$ production in hadron collisions. The $N$-jettiness slicing scheme is in principle generally applicable to processes including colored particles in the final state. In its present version, it is however only formulated and tested for massless partons. An extension to massive partons should be possible and is explained in [194]. The subtraction schemes that are not restricted in the class of processes that they can handle at next-to-next-to-leading order are antenna subtraction and Stripper. The difference between these two schemes is that Stripper treats the full color dependence of the process implicitly, while antenna subtraction terms for leading and subleading color contributions have to be provided separately. The full formulation of the antenna subtraction scheme for subleading color terms is not yet available.
Another criterion to distinguish the different subtraction approaches is the locality of the subtraction terms. This criterion is fulfilled, if the subtraction terms are constructed in terms of the explicit limits of the matrix elements in all infrared singular regions, which were discussed in section 3.4.1. Hence, the colorful subtraction scheme and Stripper are local. Antenna subtraction also uses explicit limits of the color ordered amplitudes. However, spin correlation in the case of gluon splittings are not taken into account explicitly, which results in a non-local subtraction term. Nevertheless, the

convergence of the numerical integral can be made pointwise, as has been explained in [152]. The $q_T$ and $N$-jettiness schemes are non-local, since all infrared singular phase space points are indicated by only one variable $\boldsymbol{q}_T$ or $\mathcal{T}_N$. The subtraction terms, if present in the implementation, correctly approximates the next-to-leading order cross section with one additional jet only if already some phase space is integrated out.
The locality of the subtraction scheme has an impact on the numerical convergence of the integral. While a local subtraction is expected to converge much faster, for a non-local subtraction much more integration points are needed for convergence. In this sense, the calculation of only a next-to-leading order cross section in the $q_T$ and $N$-jettiness method is traded for a slower convergence of the integral. A explicit comparison between a slicing method and a subtraction scheme regarding accuracy and efficiency as it has been performed at next-to-leading order would be instructive.
The last criterion in order to compare the schemes is related to the cancellation of poles between virtual and real contributions to the cross section. In all schemes, that were discussed in this section, the poles cancel analytically. This analytic cancellation relies on the explicit analytic evaluation of integrated subtraction terms in the antenna subtraction and the colorful subtraction scheme. The integration of these terms beyond next-to-leading order is highly non-trivial and a multitude of different cases has to be considered. For $q_T$-subtraction/slicing and $N$-jettiness slicing all ingredient of the resummation formula need to be known analytically to the required order. The soft function in Eq. (3.82) is currently not known analytically.
The subtraction scheme Stripper is constructed in such a way that also pole terms arising from real contributions are calculated numerically, such that finally a numerical cancellation of poles between virtual and real contributions is achieved. Since the major part of the phase space integration is already performed using Monte-Carlo integration methods, the insistence on an analytic cancellation is not necessary and will not change the physical prediction. The correctness of the numerical cancellation relies on the KLN theorem and the explicit construction of the subtraction terms. The full construction of the scheme is outlined in the next chapter.

# CHAPTER 4

## Sector improved residue subtraction scheme

This chapter provides a detailed explanation of the subtraction scheme STRIPPER. The main content of this chapter has been published in [1]. The acronym STRIPPER stands for SecToR Improved Phase sPacE for Real radiation and already summarizes the main idea behind the subtraction scheme: The phase space for a real radiation contribution of a cross section is divided into sectors. This allows for a straightforward generation of subtraction and integrated subtraction terms up to next-to-next-to-leading order in QCD. Contrary to subtraction schemes discussed in section 3.4, no analytic integration of the integrated subtraction terms is needed. All non-trivial integrations can be done simultaneously using Monte Carlo methods.
The subtraction scheme has been firstly presented in [19] and allowed to calculate the next-to-next-to-leading order corrections to the total top-quark pair production cross section in hadron collisions [20, 34, 202–204]. The top-quark forward backward asymmetry at Tevatron has been determined by means of the same framework [48]. Additionally, the subtraction scheme has proven its applicability to next-to-next-to-leading order corrections besides top-quark pair production. Results for the following list of processes were obtained using an independent STRIPPER subtraction framework: $Z$-boson decay into a massless lepton pair at next-to-next-to-leading order QED [205], fully differential top-quark decays [206], inclusive semileptonic charmless b-quark decays [207], Higgs-boson production in association with a jet [54, 55], the spin asymmetry in muon decays [208] and single-top production in the t-channel [209].
The original idea of the subtraction scheme was to avoid complicated analytic integrations completely, since those integrations seemed to be the bottleneck of other subtraction schemes applied at next-to-next-to-leading order. The scheme merges ideas of the subtraction scheme by Frixione, Kunszt and Signer [17] and sector decomposition by Binoth and Heinrich [210]. It focused on the numerical calculation of the double-real cross section in Eq. (3.20) as a Laurent-expansion in the dimensional regulator $\varepsilon$. Concerning the IR-structure of the phase space, this contribution is the most complicated part, since two of the external partons can become soft and/or collinear. This ultimately results in poles up to order $\varepsilon^{-4}$. The remaining contributions in Eq. (3.20) contain at most one additional real radiated, potentially unresolved particle and were calculated with next-to-leading order-like subtraction tools. A finite result has been obtained by summing all contributions of the cross section. The poles canceled numerically as predicted by the KLN theorem.
In this way, the result can only be finite, when all contributions are consistently treated in $d = 4 - 2\varepsilon$ space-time dimensions. It means that, to avoid any complications in the calculation, resolved and unresolved particles are treated in $d$ dimensions, which is known as the conventional dimensional regularization scheme (CDR). This treatment keeps the scheme safe and makes sure that the final

result is free of IR poles. However, it is also the main weakness when formulating the scheme for general $2 \to 2$ processes and beyond.
The first reason is that Born level matrix elements containing just resolved particles are needed as an expansion in $\varepsilon$. Even though, there are lots of automated tools that provide matrix elements for arbitrary Standard Model processes, all of them only provide the physical coefficient at $\mathcal{O}(\varepsilon^0)$. For each new process, the matrix element has to be recalculated from the very beginning to obtain higher orders in the $\varepsilon$ expansion.
The second reason is even more obstructive, if cross sections of high multiplicity are concerned. The subtraction scheme relies on a physical parameterization of particle momenta in the final state. The beam axis is chosen to be the $z$-direction, which is treated as the first explicit parameterized space dimension. Each extra particle added to the phase space effectively increases the explicit space dimension by one. Energy-momentum conservation only constraints the momentum of one final state particle, since it is given by the sum of all other particles. Hence, when working in CDR the space-time dimension can grow beyond four for two and more particles in the final state at Born level.
For example, a Born level $2 \to 2$ process will have at most four external particles at next-to-next-to-leading order. This means that during a calculation five dimensions have to be treated exactly [20]. It is therefore questionable, if the subtraction scheme in the original form is applicable to processes of even higher multiplicities.
On the other hand, it should not be necessary to treat resolved particles in more than four dimensions, since they are observable objects. From general considerations about the full next-to-next-to-leading order cross section [211] and the analytic properties of matrix elements it is indeed not necessary to treat resolved particles in unphysical dimensions, as will be outlined in this chapter.
This, however, requires a reformulation of the subtraction scheme STRIPPER in the 't Hooft-Veltmann regularization (HV) scheme. In 't Hooft-Veltman regularization only momenta and polarization vectors of unresolved particles are $d$-dimensional. In Tab. 4.1 the difference between the HV and CDR subtraction scheme is summarized. In this chapter, the theory of the four dimensional formu-

| | CDR | 't Hooft-Veltman |
|---|---|---|
| Resolved particle | $d$-dimensions | 4-dimensions |
| Unresolved particle | $d$-dimensions | $d$-dimensions |

**Table 4.1:** Dimensions of momenta and spin degrees of freedom in 't Hooft-Veltman dimensional regularization scheme and the conventional dimensional regularization scheme (CDR).

lation of the sector improved residue subtraction scheme is presented. This formulation requires a detailed study of the infrared structure of all contributions to an arbitrary next-to-next-to-leading order cross section. Only four dimensional external momenta and polarizations for the evaluation of matrix elements are finally required.
The factorizing behavior of matrix elements outlined in section 3.4.1 dictates the appropriate set up of the subtraction scheme. First, the decomposition due to the singular phase space structure is discussed in section 4.1. The phase space parameterization, outlined in section 4.2, is the essential starting point to obtain subtraction terms using factorization properties of QCD matrix elements in infrared singular regions. The generation of subtraction and integrated subtraction term is discussed in section 4.3. The next step is to identify contributions that are separately finite (section 4.5). Corrections terms in the double-real subtraction contribution have to be added to render the

final result correct. The finite contributions are subsequently reexpressed in the 't Hooft-Veltman regularization scheme by modifying the measurement function in such a way that it restricts resolved momenta to four dimensions (section 4.6).
In this formulation, all matrix elements can be calculated in four dimensions and all momenta of resolved particles are four dimensional. Unresolved momenta are still higher dimensional, but they appear only in splitting and soft functions and not in the matrix elements themselves. It is explained that at most six-dimensional momenta are needed for arbitrary multiplicities.
While this chapter outlines the theory of the scheme, the next chapter describes its actual implementation as a general framework to calculate next-to-next-to-leading order QCD corrections.

## 4.1 Phase space decomposition

In general, a QCD process at higher orders contains a multitude of massless partons that can become potentially unresolved. However, the measurement functions $F_{n+1}$, in $\hat{\sigma}^{\mathrm{R}}$ at next-to-leading order and $\hat{\sigma}^{\mathrm{RV}}$ at next-to-next-to-leading order, and the measurement function $F_{n+2}$, in $\hat{\sigma}^{\mathrm{RR}}$, exclude phase space points, where more than one particle, respectively two particles, are unresolved. A major conceptional simplification of the problem is provided by decomposing the phase space into sectors, where only specified partons can become unresolved. This has been the main idea of the Frixione-Kunszt-Signer next-to-leading order subtraction method [17]. It could be achieved by using $\theta$-functions and cutting the phase space into disjunct pieces. Though, hard cuts on the phase space will artificially worsen the convergence of the phase space Monte Carlo integration. To avoid this, smooth functions were introduced in [212] for the next-to-leading order subtraction. These *selector functions* [19], should satisfy two requirements. First, summing all functions should return unity to provide a decomposition of the phase space and second, in the collinear and soft limits of the remaining partons, that are not selected by the functions, the function vanishes. This regulates other singularities in a given sector.
In the case of one unresolved parton in the phase space, at most two particles are chosen to specify the single-collinear pair: The *unresolved* parton $i$ that can become soft and a *reference* parton $k$. The selector function has the form $\mathcal{S}_{i,k}$ and the sector is called a *single-collinear* sector.
In case of two unresolved partons, two types of sectors have to be distinguished. The *triple-collinear* sector allows three partons to become collinear to each other and is described by a function $\mathcal{S}_{ij,k}$, where partons $i$ and $j$ are the unresolved partons that are allowed to become soft. The reference parton $k$ specifies the triple-collinear direction, as will be demonstrated in section 4.2. The *double-collinear* sector selects two pairs of partons to become collinear and is specified by a function $\mathcal{S}_{i,k;j,l}$. In this case two reference partons $\{k,l\}$ are needed to indicate the collinear directions. The unresolved partons $\{i,j\}$ can approach the soft limit.
The function $\mathcal{S}_{i,k}$ in the single-collinear sector can be written as

$$\mathcal{S}_{i,k} = \frac{1}{D_1\, d_{i,k}} \text{ , with} \qquad D_1 = \sum_{ik} \frac{1}{d_{i,k}} \text{ ,} \tag{4.1}$$

where the auxiliary functions are similar to the ones given in [212]

$$d_{i,k} = \left(\frac{E_i}{\sqrt{\hat{s}}}\right)^{\alpha} (1-\cos\theta_{ik})^{\beta} \text{ .} \tag{4.2}$$

The required properties are readily satisfied by choosing $\alpha = \gamma$ for a gluon $i$ and $\alpha = 0$ for a quark $i$, while $\beta$,$\gamma > 0$. The decomposition of unity is easily verified

$$\sum_{ik} \mathcal{S}_{i,k} = 1 \; . \tag{4.3}$$

The above definition can be generalized to the triple- and double-collinear sectors by introducing another auxiliary function

$$d_{ij,k} = \left(\frac{E_i}{\sqrt{\hat{s}}}\right)^{\alpha_i} \left(\frac{E_j}{\sqrt{\hat{s}}}\right)^{\alpha_j} \left[(1-\cos\theta_{ij})(1-\cos\theta_{ik})(1-\cos\theta_{jk})\right]^{\beta} \; , \tag{4.4}$$

where $\alpha_{i,j} = \gamma$ for gluons, $\alpha_i = \alpha_j = \gamma$ for a quark anti-quark pair and $\alpha_{i,j} = 0$ otherwise. The selector functions are defined by

$$\mathcal{S}_{ij,k} = \frac{1}{D_2\, d_{ij,k}} \; , \quad \mathcal{S}_{i,k;j,l} = \frac{1}{D_2\, d_{i,k} d_{j,l}} \; , \quad D_2 = \sum_{ij} \Big[ \sum_k \frac{1}{d_{ij,k}} + \sum_{kl} \frac{1}{d_{i,k} d_{j,l}} \Big] \tag{4.5}$$

and are a decomposition of unity

$$\sum_{ij} \Big[ \sum_k \mathcal{S}_{ij,k} + \sum_{kl} \mathcal{S}_{i,k;j,l} \Big] = 1 \; . \tag{4.6}$$

A little subtlety for $\mathcal{S}_{i,k;j,l}$ has to be taken into account to regulate all double-soft limits correctly. In contrast to the next-to-leading order case, $\alpha$ is set to $\gamma$ in $d_{i,k}$ and $d_{j,l}$, if $(i,j)$ is a quark anti-quark pair.
In order to keep the number of sectors, that are actually computed, to a minimum, it is necessary to investigate the set of flavors that describe the same sector. First of all, unresolved partons $(i,j)$ can only occur in the final state, while reference partons $(k,l)$ are in the initial or in the final state. Of course, all indices in all cases have to be different. A single-collinear sector, where the reference parton $i$ is in the initial state the possible flavor pairs $(a_i,a_k)$ are

$$(g,g),\ (g,q),\ (g,\bar{q}),\ (q,g),\ (\bar{q},g),\ (q,q),\ (\bar{q},\bar{q}) \; . \tag{4.7}$$

Is the reference parton a final state particle the possible flavor structures are

$$(g,g),\ (g,q),\ (g,\bar{q}),\ (q,\bar{q}) \; . \tag{4.8}$$

In the triple-collinear sector the set of flavors that lead to a triple collinear singularity are

$$\{g,g,g\},\ \{g,g,q\},\ \{g,g,\bar{q}\}\ \{g,q,\bar{q}\}, \{q,\bar{q},q^{(\prime)}\} \; , \tag{4.9}$$

where all flavor assignments are chosen to be in the final state. The flavor $q'$ specifies a quark of different flavor. Relying on this list, the set of possible flavor assignments $(a_i,a_j,a_k)$ appearing in $\mathcal{S}_{i,j;k}$ is

$$(g,g,g),\ (g,g,q),\ (g,g,\bar{q}),\ (g,q,g),\ (g,\bar{q},g),\ (g,q,q),\ (g,\bar{q},\bar{q}),\ (q,\bar{q},g),\ (q,\bar{q},q'),\ (q',q,q),\ (q',\bar{q},\bar{q}) \; , \tag{4.10}$$

if $a_k$ is in the initial state, and

$$(g,g,g),\ (g,g,q),\ (g,g,\bar{q}),\ (g,q,\bar{q}),\ (q,\bar{q},g),\ (q,\bar{q},q')\ , \tag{4.11}$$

if $a_k$ is in the final state.
The number of sectors that are finally computed can be reduced for multiparton amplitudes. If the flavor assignments of two sectors is equal the contribution to the full cross section will necessarily be equal. Thus, only one of the contributions has to be evaluated. For a multigluon amplitude, this means that at most three sectors have to be considered.

## 4.2 Phase space parameterization

The decomposition of the phase space into single-collinear, double-collinear and triple-collinear sectors in section 4.1 is followed by an appropriate parameterization of each of the sectors. The phase space is split into a part containing the unresolved partons of momentum $u_i$ and the reference parton with momentum $r_i$, if the reference parton is in the final state, and a part containing all remaining final state partons of momentum $q_i$

$$\int \mathrm{d}\boldsymbol{\Phi}_{n+n_u} = \int \mathrm{d}\boldsymbol{\Phi}_{\substack{\text{reference}\\\text{unresolved}}} \int \mathrm{d}\boldsymbol{\Phi}_{n-n_{fr}}(Q)\ , \quad n \geq 2\ , \quad n_u \in \{1,2\}\ , \quad 0 \leq n_{fr} \leq n_u\ , \tag{4.12}$$

where $n$ is the number of final state partons of the leading order contribution, $n_u$ is the number of unresolved momenta, while $n_{fr}$ is the number of reference momenta in the final state.
The formula (4.12) should not be understood as a complete factorization of the phase space into two independent parts. The resolved part of the phase space $\mathrm{d}\boldsymbol{\Phi}_{n-n_{fr}}(Q)$ depends on momenta and energies of the unresolved part $\mathrm{d}\boldsymbol{\Phi}_{\substack{\text{reference}\\\text{unresolved}}}$, through $Q$. Therefore, the order of the integrations is important, as the integration boundaries of a given momentum integral depends in general on the parameters of other momentum integrals. The momentum $Q$ can be seen as the total available momentum for the remaining final state particles

$$Q \to q_1 + \ldots + q_{n-n_{fr}}\ . \tag{4.13}$$

The minimal invariant mass of $Q$ is given by the sum of masses of final state particles

$$Q_{\min} = \sum_{i=1}^{n} m_i\ . \tag{4.14}$$

The maximal energy of a final state massless parton can be derived using energy momentum conservation and requiring that all massive states are at rest. This energy is denoted by

$$E_{\max} = \frac{\sqrt{\hat{s}}}{2}\left(1 - \frac{Q_{\min}^2}{\hat{s}}\right)\ , \tag{4.15}$$

where $\sqrt{\hat{s}}$ is the partonic center-of-mass energy. The important guideline to choose a parameterization in the different sectors for $\mathrm{d}\boldsymbol{\Phi}_{\substack{\text{reference}\\\text{unresolved}}}$ is to find parameters that indicate directly the appearance of a soft or collinear singularities as they approach zero. A convenient set of parameters is directly related to the energies of the unresolved partons, denoted by $\xi_i$, to indicate soft limits, and to the angles between the reference particle(s) and the unresolved particles, denoted by $\eta_i$, to indicate

collinear limits. The single unresolved phase space thence contains

$$\iint_0^1 \mathrm{d}\eta\,\mathrm{d}\xi\,\eta^{a_1-b_1\varepsilon}\,\xi^{a_2-b_2\varepsilon}\,, \tag{4.16}$$

while the phase space of two unresolved partons contains

$$\iiiint_0^1 \mathrm{d}\eta_1\mathrm{d}\eta_2\mathrm{d}\xi_1\mathrm{d}\xi_2\,\eta_1^{a_1-b_1\varepsilon}\,\eta_2^{a_2-b_2\varepsilon}\,\xi_1^{a_3-b_3\varepsilon}\,\xi_2^{a_4-b_4\varepsilon}\,, \tag{4.17}$$

in dimensional regularization. IR-divergences are regulated as $\varepsilon < 0$. Because of the selector functions, no other divergences are present, apart form those as $x \to 0$, where $x \in \{\eta,\xi\}$ or $x \in \{\eta_1,\eta_2,\xi_1,\xi_2\}$.
To obtain such a parameterization in each sector, the invariance under rotations of the single particle measure can be used. The unresolved partons are thereby rotated into the frame, in which the reference parton propagates in $z$-direction. This allows for a simple parameterization in $d$-dimensional spherical coordinates. The notation for rotation matrices and unit vectors is fixed in appendix A.2. All parameterizations are given as if all particles have $d$-dimensional momenta. The step to four dimensions will be discussed later in this chapter.

### 4.2.1 Single-collinear sector parameterization

In the single-collinear sector the number of unresolved partons is $n_u = 1$. The reference parton is either in the initial state or in the final state. The momenta are parameterized as

$$r^\mu = r^0\,\hat{r}^\mu = r^0\begin{pmatrix}1\\ \hat{\boldsymbol{r}}\end{pmatrix}\,, \quad u^\mu = u^0\,\hat{u}^\mu = u^0\begin{pmatrix}1\\ \hat{\boldsymbol{u}}\end{pmatrix}\,, \tag{4.18}$$

where unit vectors are given by

$$\begin{aligned}\hat{\boldsymbol{r}} &= \hat{\boldsymbol{n}}^{(3-2\varepsilon)}(\alpha_1,\alpha_2,\ldots)\,,\\ \hat{\boldsymbol{u}} &= \boldsymbol{R}_1^{(3-2\varepsilon)}(\alpha_1,\alpha_2,\ldots)\hat{\boldsymbol{n}}^{(3-2\varepsilon)}(\theta,\phi,\rho_1,\rho_2,\ldots)\,.\end{aligned} \tag{4.19}$$

For a reference momentum in the initial state the phase space reads

$$\int \mathrm{d}\boldsymbol{\Phi}_{n+1} = \int \mathrm{d}\boldsymbol{\Phi}_{\text{unresolved}} \int \mathrm{d}\boldsymbol{\Phi}_n(zp_1+p_2-u)\,. \tag{4.20}$$

A final state reference momentum leads to the phase space parameterization

$$\begin{aligned}\int \mathrm{d}\boldsymbol{\Phi}_{n+1} = \left(\frac{\mu_R^2 e^{\gamma_\mathrm{E}}}{4\pi}\right)^\varepsilon &\int_{\mathbb{S}_1^{2-2\varepsilon}} \mathrm{d}\boldsymbol{\Omega}(\alpha_1,\alpha_2,\ldots)\\ &\times \int \mathrm{d}\boldsymbol{\Phi}_{\text{unresolved}} \int_0^{r^0_{\max}} \frac{\mathrm{d}r^0\,(r^0)^{1-2\varepsilon}}{2(2\pi)^{3-2\varepsilon}} \int \mathrm{d}\boldsymbol{\Phi}_{n-1}(zp_1+p_2-r-u)\,,\end{aligned} \tag{4.21}$$

where in both cases the initial state can be boosted along the beam axis. This is denoted by the energy fraction parameter $z$. This will be important for the formulation of the subtraction scheme in four dimensions, as the contribution $\hat{\sigma}^{\mathrm{C1}}$, that relies on the above parameterization, needs to be

evaluated in a boosted reference frame. The maximal energy of the reference parton is given by

$$r^0_{\max} = \frac{2\sqrt{\hat{s}}\,\big(E_{\max} - u^0\big) - \big(s - 2p_1\cdot u)(1-z)}{2\left[\sqrt{\hat{s}} - \hat{r}\cdot\big(u + p_1(1-z)\big)\right]}\,. \tag{4.22}$$

In the special case $n = 2$ the resolved phase space is completely fixed by energy momentum conservation and reads

$$\int_0^{r^0_{\max}} \frac{\mathrm{d}r^0\,(r^0)^{1-2\varepsilon}}{2(2\pi)^{3-2\varepsilon}} \int \mathrm{d}\boldsymbol{\Phi}_1(zp_1 + p_2 - r - u) = \frac{(r^0_{\max})^{1-2\varepsilon}}{4(2\pi)^{2-2\varepsilon}} \frac{1}{\sqrt{\hat{s}} - \hat{r}\cdot\big(u + p_1(1-z)\big)}\,. \tag{4.23}$$

As anticipated in (4.16), the phase space of the unresolved parton is

$$\begin{aligned}\int \mathrm{d}\boldsymbol{\Phi}_{\text{unresolved}} = \left(\frac{\mu_R^2 e^{\gamma_{\mathrm{E}}}}{4\pi}\right)^{\varepsilon} \int_{\mathbb{S}_1^{2-2\varepsilon}} \mathrm{d}\boldsymbol{\Omega}(\theta,\phi,\rho_1,\ldots) \int_0^{u^0_{\max}} \frac{\mathrm{d}u^0\,(u^0)^{1-2\varepsilon}}{2(2\pi)^{3-2\varepsilon}} = \\ \frac{E^2_{\max}}{(2\pi)^3}\left(\frac{\pi\mu_R^2 e^{\gamma_{\mathrm{E}}}}{4E^2_{\max}}\right)^{\varepsilon} \int_{\mathbb{S}_1^{1-2\varepsilon}} \mathrm{d}\boldsymbol{\Omega}(\phi,\rho_1,\ldots) \iint_0^1 \mathrm{d}\eta\,\mathrm{d}\xi\,\eta^{-\varepsilon}\,\xi^{1-2\varepsilon}\big(1-\eta\big)^{-\varepsilon}\xi_{\max}^{2-2\varepsilon}\,.\end{aligned} \tag{4.24}$$

Energy and angular parameters are linearly related to the integration variables that indicate the soft and collinear limit

$$u^0 = E_{\max}\,\xi\,\xi_{\max}\,, \quad \cos\theta = 1 - 2\eta\,, \quad \xi_{\max} = \frac{1 - \frac{\sqrt{\hat{s}}}{2E_{\max}}(1-z)}{1 - \frac{1}{\sqrt{\hat{s}}}(p_1\cdot\hat{u})(1-z)}\,. \tag{4.25}$$

In the collinear factorization formula of the matrix element (3.49) the collinear limit was characterized by a transverse momentum, leading to spin correlations in the case of a gluon splitting. In the given parameterization the normalized transverse direction is given by

$$u^\mu_\perp = \begin{pmatrix} 0 \\ \hat{\boldsymbol{u}}_\perp \end{pmatrix}\,, \quad \hat{\boldsymbol{u}}_\perp = \lim_{\theta\to 0}\frac{\hat{\boldsymbol{u}} - \hat{\boldsymbol{r}}}{\|\hat{\boldsymbol{u}} - \hat{\boldsymbol{r}}\|} = \left.\frac{\partial\hat{\boldsymbol{u}}}{\partial\theta}\right|_{\theta=0} = \hat{\boldsymbol{R}}_1^{(3-2\varepsilon)}(\alpha_1,\alpha_2,\ldots)\hat{\boldsymbol{n}}^{(3-2\varepsilon)}\left(\frac{\pi}{2},\phi,\rho_1,\rho_2,\ldots\right)\,. \tag{4.26}$$

### 4.2.2 Triple-collinear sector parameterization

In this sector, two unresolved momenta have to be considered. Singular limits occur as the unresolved momenta become collinear to each other and/or to a single reference momentum. A suitable parameterization of the three relevant momenta is given by

$$r^\mu = r^0\,\hat{r}^\mu = r^0\begin{pmatrix}1\\ \hat{\boldsymbol{r}}\end{pmatrix}\,, \quad u_1^\mu = u_1^0\,\hat{u}_1^\mu = u_1^0\begin{pmatrix}1\\ \hat{\boldsymbol{u}}_{\boldsymbol{1}}\end{pmatrix}\,, \quad u_2^\mu = u_2^0\,\hat{u}_2^\mu = u_2^0\begin{pmatrix}1\\ \hat{\boldsymbol{u}}_{\boldsymbol{2}}\end{pmatrix}\,, \tag{4.27}$$

where the angular vectors are parameterized as

$$\begin{aligned}\hat{\boldsymbol{r}} &= \hat{\boldsymbol{n}}^{(3-2\varepsilon)}(\alpha_1,\alpha_2,\ldots)\,,\\ \hat{\boldsymbol{u}}_{\boldsymbol{1}} &= \boldsymbol{R}_1^{(3-2\varepsilon)}(\alpha_1,\alpha_2,\ldots)\hat{\boldsymbol{n}}^{(3-2\varepsilon)}(\theta_1,\phi_1,\rho_1,\rho_2,\ldots)\,,\\ \hat{\boldsymbol{u}}_{\boldsymbol{2}} &= \boldsymbol{R}_1^{(3-2\varepsilon)}(\alpha_1,\alpha_2,\ldots)\boldsymbol{R}_2^{(3-2\varepsilon)}(\phi_1,\rho_1,\rho_2,\ldots)\hat{\boldsymbol{n}}^{(3-2\varepsilon)}(\theta_2,\phi_2,\sigma_1,\sigma_2,\ldots)\,.\end{aligned} \tag{4.28}$$

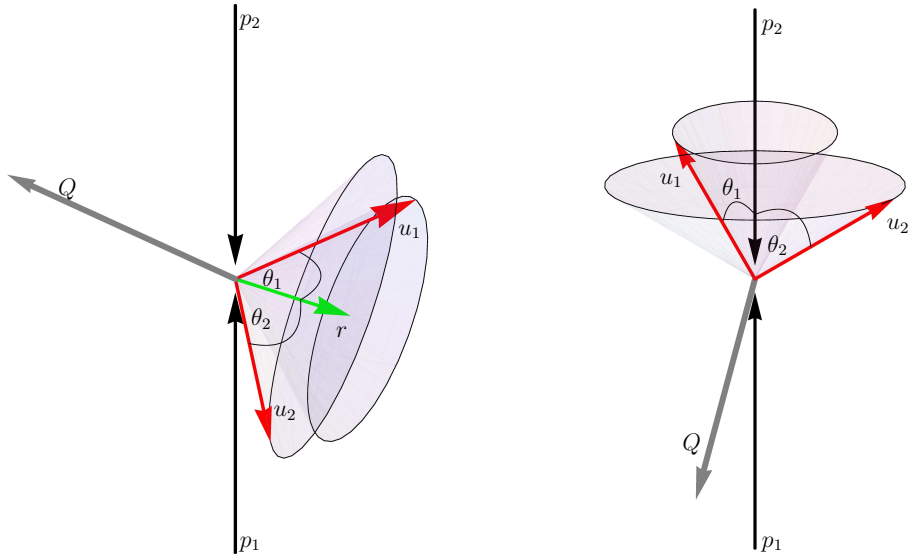


**Figure 4.1:** Parameterization of the triple-collinear sector for the reference momentum $r$ in the final state (left) and the reference momentum in the initial state $r = p_1$ (right). $Q$ is the momentum of all additional particles in the final state, $p_1$ and $p_2$ are initial state momenta [1].

The given parameterization is essentially a generalization of the parameterization in the single-collinear sector. The first rotation $\boldsymbol{R}_1^{(3-2\varepsilon)}(\alpha_1, \alpha_2, \ldots)$, illustrated for two distinct cases in Fig. 4.1, allows for direct parameterization of the angles between the reference momentum and the unresolved momenta

$$\hat{\boldsymbol{r}} \cdot \hat{\boldsymbol{u}}_{\boldsymbol{1}} = \cos\theta_1 \ , \quad \hat{\boldsymbol{r}} \cdot \hat{\boldsymbol{u}}_{\boldsymbol{2}} = \cos\theta_2 \ . \tag{4.29}$$

The additional rotation of the second unresolved momentum $\boldsymbol{R}_2^{(3-2\varepsilon)}(\phi_1, \rho_1, \rho_2, \ldots)$ ensures the simplest parameterization of the angle between the unresolved momenta which is still possible by rotational invariance

$$\hat{\boldsymbol{u}}_{\boldsymbol{1}} \cdot \hat{\boldsymbol{u}}_{\boldsymbol{2}} = \cos(\theta_1 - \theta_2) + (1 - \cos\phi_2)\sin\theta_1 \sin\theta_2 \ . \tag{4.30}$$

The phase space for an initial state reference momentum reads

$$\int \mathrm{d}\boldsymbol{\Phi}_{n+2} = \int \mathrm{d}\boldsymbol{\Phi}_{\text{unresolved}} \int \mathrm{d}\boldsymbol{\Phi}_n(p_1 + p_2 - u_1 - u_2) \ , \tag{4.31}$$

whereas for $r$ in the final state it is

$$\begin{aligned} \int \mathrm{d}\boldsymbol{\Phi}_{n+2} = &\left(\frac{\mu_R^2 e^{\gamma_\mathrm{E}}}{4\pi}\right)^{\varepsilon} \int_{S_1^{2-2\varepsilon}} \mathrm{d}\boldsymbol{\Omega}(\alpha_1, \alpha_2, \ldots) \\ &\times \int \mathrm{d}\boldsymbol{\Phi}_{\text{unresolved}} \int_0^{r^0_{\max}} \frac{\mathrm{d}r^0\,(r^0)^{1-2\varepsilon}}{2(2\pi)^{3-2\varepsilon}} \int \mathrm{d}\boldsymbol{\Phi}_{n-1}(p_1 + p_2 - r - u_1 - u_2) \ . \end{aligned} \tag{4.32}$$

For $n = 2$ the phase space can be evaluated explicitly

$$\int_0^{r^0_{\max}} \frac{\mathrm{d}r^0\,(r^0)^{1-2\varepsilon}}{2(2\pi)^{3-2\varepsilon}} \int \mathrm{d}\boldsymbol{\Phi}_1(p_1+p_2-r-u_1-u_2) = \frac{(r^0_{\max})^{1-2\varepsilon}}{4(2\pi)^{2-2\varepsilon}} \frac{1}{\sqrt{\hat{s}}-\hat{r}\cdot(u_1+u_2)}\,, \tag{4.33}$$

where

$$r^0_{\max} = \frac{\sqrt{\hat{s}}\left(E_{\max}-u_1^0-u_2^0\right)+u_1\cdot u_2}{\sqrt{\hat{s}}-\hat{r}\cdot(u_1+u_2)}\,. \tag{4.34}$$

The parameters are replaced by the physical variables $\hat{\xi}_{1,2}, \hat{\eta}_{1,2}$ related to soft and collinear limits

$$\begin{gathered} u_1^0 = E_{\max}\,\hat{\xi}_1\,, \quad u_2^0 = E_{\max}\,\hat{\xi}_2\,, \\ \cos\theta_1 = 1-2\hat{\eta}_1\,, \quad \cos\theta_2 = 1-2\hat{\eta}_2\,, \quad \cos\phi_2 = \frac{1-2\eta_3-(1-2\hat{\eta}_1)(1-2\hat{\eta}_2)}{4\sqrt{(1-\hat{\eta}_1)\hat{\eta}_1(1-\hat{\eta}_2)\hat{\eta}_2}}\,, \\ \eta_3 = \frac{\hat{u}_1\cdot\hat{u}_2}{2} = \frac{1-\cos\theta_{12}}{2} = \frac{(\hat{\eta}_1-\hat{\eta}_2)^2}{\hat{\eta}_1+\hat{\eta}_2-2\hat{\eta}_1\hat{\eta}_2-2(1-2\zeta)\sqrt{\hat{\eta}_1(1-\hat{\eta}_1)\hat{\eta}_2(1-\hat{\eta}_2)}}\,. \end{gathered} \tag{4.35}$$

This parameterization is not yet sufficient to factorize all singular limits as two particles become unresolved. Overlapping singularities in the double-soft, triple-collinear or soft-collinear limit can be factorized by a method based on sector decomposition [210]. This idea was developed for two unresolved particles in the phase space integral in [20]. A complete factorization is achieved by splitting the phase space further to disentangle overlapping soft singularities

$$\int \mathrm{d}\boldsymbol{\Phi}_{\text{unresolved}} = \int \mathrm{d}\boldsymbol{\Phi}_{\text{unresolved}} \left(\theta(\hat{\xi}_1-\hat{\xi}_2)+\theta(\hat{\xi}_2-\hat{\xi}_1)\right), \tag{4.36}$$

and subsequently to disentangle overlapping collinear and soft-collinear singularities. In this way, each of the two parts in Eq. (4.36) is further decomposed into five sectors, which is illustrated in Fig. 4.2. The unresolved phase space measure written as a sum of the five sectors reads

$$\begin{aligned} &\int \mathrm{d}\boldsymbol{\Phi}_{\text{unresolved}}\,\theta(u_1^0-u_2^0) = \\ &\left(\frac{\mu_R^2 e^{\gamma_{\mathrm{E}}}}{4\pi}\right)^{2\varepsilon} \int_{\mathcal{S}_1^{2-2\varepsilon}} \mathrm{d}\boldsymbol{\Omega}(\theta_1,\phi_1,\rho_1,\ldots) \int_{\mathcal{S}_1^{2-2\varepsilon}} \mathrm{d}\boldsymbol{\Omega}(\theta_2,\phi_2,\sigma_1,\sigma_2,\ldots) \\ &\times \int_0^{u^0_{\max}} \frac{\mathrm{d}u_1^0\,(u_1^0)^{1-2\varepsilon}}{2(2\pi)^{3-2\varepsilon}} \int_0^{u^0_{2\,\max}} \frac{\mathrm{d}u_2^0\,(u_2^0)^{1-2\varepsilon}}{2(2\pi)^{3-2\varepsilon}}\,\theta\big(u_1^0-u_2^0\big) = \\ &\frac{E^4_{\max}}{(2\pi)^6}\left(\frac{\pi\mu_R^2 e^{\gamma_{\mathrm{E}}}}{8E^2_{\max}}\right)^{2\varepsilon} \int_{\mathcal{S}_1^{1-2\varepsilon}} \mathrm{d}\boldsymbol{\Omega}(\phi_1,\rho_1,\ldots) \int_{\mathcal{S}_1^{-2\varepsilon}} \mathrm{d}\boldsymbol{\Omega}(\sigma_1,\sigma_2,\ldots) \int_0^1 \mathrm{d}\zeta \left(\zeta\big(1-\zeta\big)\right)^{-\frac{1}{2}-\varepsilon} \\ &\times \iiiint_0^1 \mathrm{d}\eta_1\mathrm{d}\eta_2\mathrm{d}\xi_1\mathrm{d}\xi_2 \sum_{i=1}^{5} \mu_{\mathcal{S}_i}\,, \end{aligned} \tag{4.37}$$

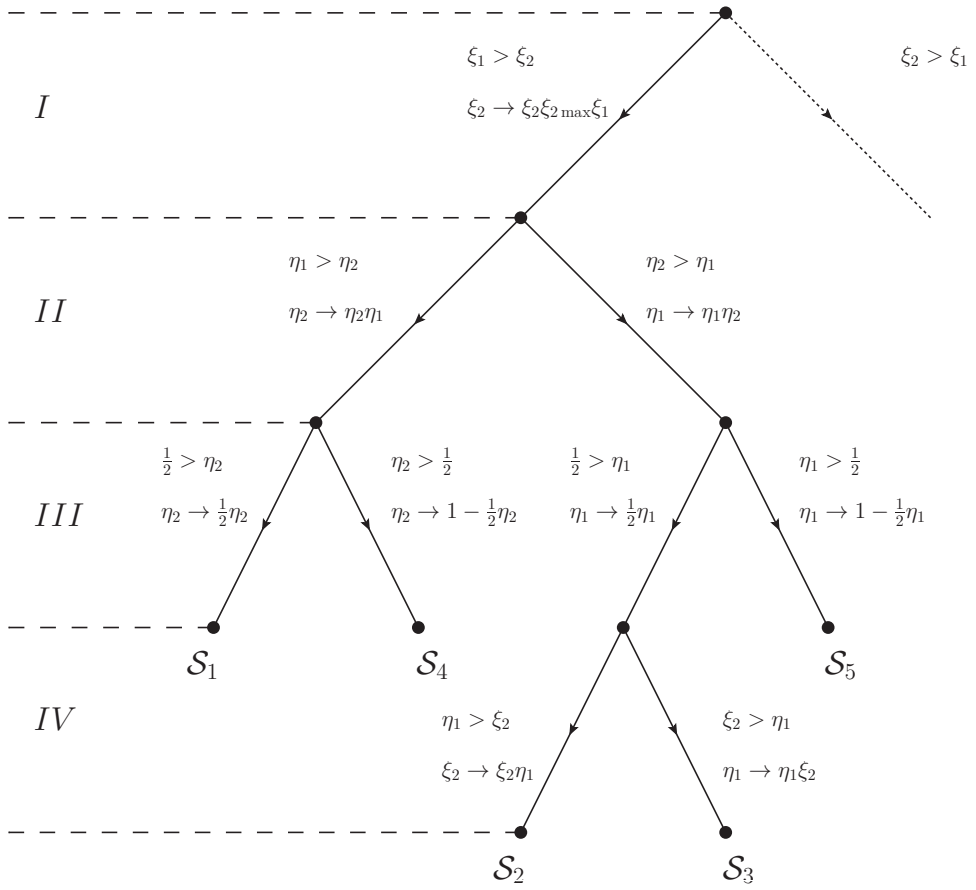


**Figure 4.2:** Decomposition tree of the triple-collinear sector phase space. Starting at the root with the physical parameters $\eta_i = \hat{\eta}_i$, $\xi_i = \hat{\xi}_i$, decompositions are performed at four levels corresponding to the factorization of the soft (I), collinear (II and III) and soft-collinear (IV) limits. The omitted right branch of the tree corresponds to a different ordering of the energies of the unresolved partons, and can be obtained by renaming the indices of the variables, $1 \leftrightarrow 2$ [20].

where

$$\xi_{2\,\max} = \min\left[1,\ \frac{1}{\hat{\xi}_1}\frac{1-\hat{\xi}_1}{1-\frac{2E_{\max}}{\sqrt{\hat{s}}}\hat{\xi}_1\,\eta_3}\right],$$

$$\eta_{31}(\eta_1,\eta_2) = \left.\frac{\eta_3}{\eta_1}\right|_{\substack{\hat{\eta}_1=\eta_1\\ \hat{\eta}_2=\eta_1\eta_2/2}} = \frac{(2-\eta_2)^2}{2\left(2+\eta_2(1-2\eta_1)-2(1-2\zeta)\sqrt{\eta_2(1-\eta_1)(2-\eta_1\eta_2)}\right)}, \tag{4.38}$$

$$\eta_{32}(\eta_1,\eta_2) = \left.\frac{\eta_3}{\eta_1\eta_2^2}\right|_{\substack{\hat{\eta}_1=\eta_1\\ \hat{\eta}_2=\eta_1(2-\eta_2)/2}} = \frac{1}{2\left(2+(1-2\eta_1)(2-\eta_2)-2(1-2\zeta)\sqrt{(1-\eta_1)(2-\eta_2)(2-\eta_1(2-\eta_2))}\right)}.$$

The relation between the original physical variables and the variables after sector decomposition is given in Tab. 4.2. The sector specific part of the measure is given in Tab. 4.3.

For the single-collinear and triple-collinear factorization formula in Eqs. (3.49) and (3.53) transverse momenta are defined. The normalized vectors read

$$u_{i\perp}^{\mu} = \begin{pmatrix} 0 \\ \hat{\boldsymbol{u}}_{\boldsymbol{i}\perp} \end{pmatrix} , \quad i = 1,2,3 , \tag{4.39}$$

where

$$\hat{\boldsymbol{u}}_{\mathbf{1}\perp} = \lim_{\theta_1\to 0} \frac{\hat{\boldsymbol{u}}_{\mathbf{1}} - \hat{\boldsymbol{r}}}{\|\hat{\boldsymbol{u}}_{\mathbf{1}} - \hat{\boldsymbol{r}}\|} = \left.\frac{\partial \hat{\boldsymbol{u}}_{\mathbf{1}}}{\partial\theta_1}\right|_{\theta_1=0} = \hat{\boldsymbol{R}}_1^{(3-2\varepsilon)}(\alpha_1,\alpha_2,\ldots)\hat{\boldsymbol{n}}^{(3-2\varepsilon)}\left(\frac{\pi}{2},\phi_1,\rho_1,\rho_2,\ldots\right) , \tag{4.40}$$

$$\hat{\boldsymbol{u}}_{\mathbf{2}\perp} = \lim_{\theta_2\to 0} \frac{\hat{\boldsymbol{u}}_{\mathbf{2}} - \hat{\boldsymbol{r}}}{\|\hat{\boldsymbol{u}}_{\mathbf{2}} - \hat{\boldsymbol{r}}\|} = \left.\frac{\partial \hat{\boldsymbol{u}}_{\mathbf{2}}}{\partial\theta_2}\right|_{\theta_2=0} = \hat{\boldsymbol{R}}_1^{(3-2\varepsilon)}(\alpha_1,\alpha_2,\ldots)\hat{\boldsymbol{R}}_2^{(3-2\varepsilon)}(\phi_1,\rho_1,\rho_2,\ldots)\hat{\boldsymbol{n}}^{(3-2\varepsilon)}\left(\frac{\pi}{2},\phi_2,\sigma_1,\sigma_2,\ldots\right) . \tag{4.41}$$

The third transverse vector $\hat{\boldsymbol{u}}_{\mathbf{3}\perp}^{\pm}$ characterizes the collinear limit of the unresolved momenta $u_1$ and $u_2$. This limit can only occur in sector $\mathcal{S}_4$, as $\eta_2 \to 0$, and sector $\mathcal{S}_5$, as $\eta_1 \to 0$. However, in the triple-collinear limit, $\eta_1 \to 0$ in sector $\mathcal{S}_4$ and $\eta_2 \to 0$ in sector $\mathcal{S}_5$, the subtraction term depends on $\hat{\boldsymbol{u}}_{\mathbf{3}\perp}^{\pm}$. This vector can be defined through

$$\hat{\boldsymbol{u}}_{\mathbf{3}\perp}^{\pm} = \hat{\boldsymbol{R}}_1^{(3-2\varepsilon)}(\alpha_1,\alpha_2,\ldots)\hat{\boldsymbol{R}}_1^{(3-2\varepsilon)}(\theta_1,\phi_1,\rho_1,\rho_2,\ldots)\hat{\boldsymbol{n}}^{(3-2\varepsilon)}\left(\frac{\pi}{2},\tilde{\phi}_2^{\pm},\sigma_1,\sigma_2,\ldots\right) , \tag{4.42}$$

where an auxiliary angle $\tilde{\phi}_2^{\pm}$ has been defined

$$\tan\tilde{\phi}_2^{\pm}(\theta_1,\zeta) = \pm\sin\theta_1\,\partial_{\theta_2}^{+}\phi_2(\theta_1,\zeta) , \quad \tilde{\phi}_2^{+} \in \left[0,\frac{\pi}{2}\right[ , \quad \tilde{\phi}_2^{-} \in \left[\frac{\pi}{2},\pi\right[ . \tag{4.43}$$

In the given parameterization, $\tilde{\phi}_2^{\pm}$ can be explicitly derived in terms of the integration variables $\eta_1, \eta_2$, and $\zeta$. In sector $\mathcal{S}_4$ it reads

$$\cos\tilde{\phi}_2^{-} = -\frac{1+\sqrt{(1-\frac{1}{2}\eta_2)}(2\zeta-1)}{\sqrt{2-\frac{1}{2}\eta_2+2\sqrt{(1-\frac{1}{2}\eta_2)}(2\zeta-1)}} \xrightarrow{\eta_2\to 0} -\sqrt{\zeta} , \tag{4.44}$$

$$\sin\tilde{\phi}_2^{-} = \frac{\sqrt{(1-\frac{1}{2}\eta_2)4\zeta(1-\zeta)}}{\sqrt{2-\frac{1}{2}\eta_2+2\sqrt{(1-\frac{1}{2}\eta_2)}(2\zeta-1)}} \xrightarrow{\eta_2\to 0} \sqrt{1-\zeta} . \tag{4.45}$$

In sector $\mathcal{S}_5$ it is

$$\cos\tilde{\phi}_2^{+} = \frac{\sqrt{(1-\frac{1}{2}\eta_1)}+(2\zeta-1)}{\sqrt{2-\frac{1}{2}\eta_1+2\sqrt{(1-\frac{1}{2}\eta_1)}(2\zeta-1)}} \xrightarrow{\eta_1\to 0} \sqrt{\zeta} , \tag{4.46}$$

| | $\mathcal{S}_1$ | $\mathcal{S}_2$ | $\mathcal{S}_3$ | $\mathcal{S}_4$ | $\mathcal{S}_5$ |
|---|---|---|---|---|---|
| $\hat{\eta}_1$ | $\eta_1$ | $\frac{1}{2}\eta_1\eta_2$ | $\frac{1}{2}\eta_1\eta_2\xi_2$ | $\eta_1$ | $\frac{1}{2}(2-\eta_1)\eta_2$ |
| $\hat{\eta}_2$ | $\frac{1}{2}\eta_1\eta_2$ | $\eta_2$ | $\eta_2$ | $\frac{1}{2}\eta_1(2-\eta_2)$ | $\eta_2$ |
| $\hat{\xi}_1$ | $\xi_1$ | $\xi_1$ | $\xi_1$ | $\xi_1$ | $\xi_1$ |
| $\hat{\xi}_2$ | $\xi_1\xi_2\xi_{2\,\max}$ | $\eta_1\xi_1\xi_2\xi_{2\,\max}$ | $\xi_1\xi_2\xi_{2\,\max}$ | $\xi_1\xi_2\xi_{2\,\max}$ | $\xi_1\xi_2\xi_{2\,\max}$ |

**Table 4.2:** The physical variables $\hat{\eta}_1$,$\hat{\eta}_2$, $\hat{\xi}_1$, $\hat{\xi}_2$, expressed through the sector variables, $\eta_1, \eta_2, \xi_1, \xi_2$ in the five sectors after sector decomposition, depicted in Fig. 4.2.

| | $\mu_{\mathcal{S}_i}$ |
|---|---|
| $\mathcal{S}_1$ | $\eta_1^{1-2\varepsilon}\eta_2^{-\varepsilon}\xi_1^{3-4\varepsilon}\xi_2^{1-2\varepsilon}\left((1-\eta_1)(2-\eta_1\eta_2)\right)^{-\varepsilon}\left(\frac{\eta_{31}(\eta_1,\eta_2)}{2-\eta_2}\right)^{1-2\varepsilon}\xi_{2\,\max}^{2-2\varepsilon}$ |
| $\mathcal{S}_2$ | $\eta_1^{2-3\varepsilon}\eta_2^{1-2\varepsilon}\xi_1^{3-4\varepsilon}\xi_2^{1-2\varepsilon}\left((1-\eta_2)(2-\eta_1\eta_2)\right)^{-\varepsilon}\left(\frac{\eta_{31}(\eta_2,\eta_1)}{2-\eta_1}\right)^{1-2\varepsilon}\xi_{2\,\max}^{2-2\varepsilon}$ |
| $\mathcal{S}_3$ | $\eta_1^{-\varepsilon}\eta_2^{1-2\varepsilon}\xi_1^{3-4\varepsilon}\xi_2^{2-3\varepsilon}\left((1-\eta_2)(2-\eta_1\eta_2\xi_2)\right)^{-\varepsilon}\left(\frac{\eta_{31}(\eta_2,\eta_1\xi_2)}{2-\eta_1\xi_2}\right)^{1-2\varepsilon}\xi_{2\,\max}^{2-2\varepsilon}$ |
| $\mathcal{S}_4$ | $\eta_1^{1-2\varepsilon}\eta_2^{1-2\varepsilon}\xi_1^{3-4\varepsilon}\xi_2^{1-2\varepsilon}\left((1-\eta_1)(2-\eta_2)(2-\eta_1(2-\eta_2))\right)^{-\varepsilon}\eta_{32}^{1-2\varepsilon}(\eta_1,\eta_2)\,\xi_{2\,\max}^{2-2\varepsilon}$ |
| $\mathcal{S}_5$ | $\eta_1^{1-2\varepsilon}\eta_2^{1-2\varepsilon}\xi_1^{3-4\varepsilon}\xi_2^{1-2\varepsilon}\left((1-\eta_2)(2-\eta_1)(2-\eta_2(2-\eta_1))\right)^{-\varepsilon}\eta_{32}^{1-2\varepsilon}(\eta_2,\eta_1)\,\xi_{2\,\max}^{2-2\varepsilon}$ |

**Table 4.3:** Integration measures, $\mu_{\mathcal{S}_i}$ as it appears in the full phase space measure (4.37).

$$\sin\tilde{\phi}_2^+ = \frac{\sqrt{4\zeta(1-\zeta)}}{\sqrt{2-\frac{1}{2}\eta_1+2\sqrt{(1-\frac{1}{2}\eta_1)}(2\zeta-1)}} \xrightarrow{\eta_1\to 0} \sqrt{1-\zeta}\,. \tag{4.47}$$

### 4.2.3 Double-collinear sector parameterization

The parameterization of the double-collinear sector can be regarded as applying the parameterization of the single-collinear sector to two pairs of reference and unresolved momenta $(r_1,u_1)$ and $(r_2,u_2)$. This is however only possible as long as $n > n_{fr}$. In the case $n = n_u = n_{fr} = 2$, there is no freedom of rotating the second unresolved momentum, since one reference momentum is fixed by energy-momentum conservation. This case will be treated separately after the more general case is discussed.

#### General case $n > n_{fr}$

The four relevant momenta read

$$\begin{aligned} r_1^\mu &= r_1^0\,\hat{r}_1^\mu = r_1^0\begin{pmatrix}1\\ \hat{\boldsymbol{r}}_{\boldsymbol{1}}\end{pmatrix}\,, \quad r_2^\mu = r_2^0\,\hat{r}_2^\mu = r_2^0\begin{pmatrix}1\\ \hat{\boldsymbol{r}}_{\boldsymbol{2}}\end{pmatrix}\,, \\ u_1^\mu &= u_1^0\,\hat{u}_1^\mu = u_1^0\begin{pmatrix}1\\ \hat{\boldsymbol{u}}_{\boldsymbol{1}}\end{pmatrix}\,, \quad u_2^\mu = u_2^0\,\hat{u}_2^\mu = u_2^0\begin{pmatrix}1\\ \hat{\boldsymbol{u}}_{\boldsymbol{2}}\end{pmatrix}\,, \end{aligned} \tag{4.48}$$

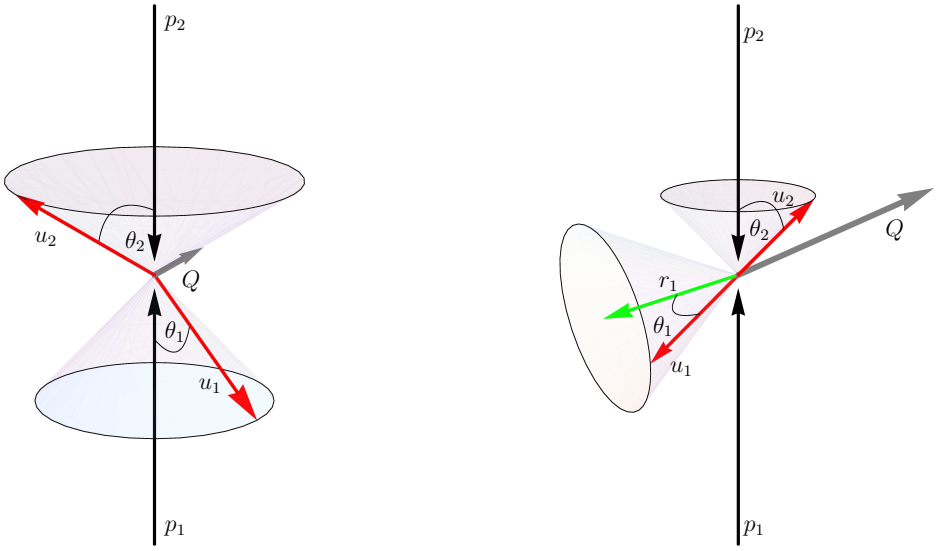


**Figure 4.3:** Parameterization of the double-unresolved sector with two unresolved momenta denoted by $u_1$ and $u_2$. The left example shows the case of two initial state reference momenta with $r_1 = p_2$ and $r_2 = p_1$. The right picture shows a case with one final state reference momentum, $r_1$, and one initial state reference momentum, $r_2 = p_1$ [1].

where the angular parameterizations are illustrated in Fig. 4.3

$$\begin{aligned}
\hat{\boldsymbol{r}}_{\mathbf{1}} &= \hat{\boldsymbol{n}}^{(3-2\varepsilon)}(\alpha_1, \alpha_2, \ldots) \,, \\
\hat{\boldsymbol{r}}_{\mathbf{2}} &= \hat{\boldsymbol{n}}^{(3-2\varepsilon)}(\beta_1, \beta_2, \ldots) \,, \\
\hat{\boldsymbol{u}}_{\mathbf{1}} &= \boldsymbol{R}_1^{(3-2\varepsilon)}(\alpha_1, \alpha_2, \ldots)\hat{\boldsymbol{n}}^{(3-2\varepsilon)}(\theta_1, \phi_1, \rho_1, \rho_2, \ldots) \,, \\
\hat{\boldsymbol{u}}_{\mathbf{2}} &= \boldsymbol{R}_1^{(3-2\varepsilon)}(\beta_1, \beta_2, \ldots)\boldsymbol{R}_4^{(3-2\varepsilon)}(\rho_2, \rho_3, \ldots)\hat{\boldsymbol{n}}^{(3-2\varepsilon)}(\theta_2, \phi_2, \sigma_1, \sigma_2, \ldots) \,.
\end{aligned} \tag{4.49}$$

It is important to notice the additional rotation of the second unresolved momentum $\boldsymbol{R}_4^{(3-2\varepsilon)}(\rho_2, \rho_3, \ldots)$. It makes sure that starting at dimension six, all angles that parameterize the direction of $u_2$ are defined relative to the direction of $u_1$. This limits the number of extra dimensions that are needed for $u_1$ to five and for $u_2$ to six, after reformulating the subtraction scheme in the 't Hooft-Veltman regularization scheme (see section 4.6).
If both reference momenta are in the initial state, the phase space integral is split as

$$\int \mathrm{d}\boldsymbol{\Phi}_{n+2} = \int \mathrm{d}\boldsymbol{\Phi}_{\text{unresolved}} \int \mathrm{d}\boldsymbol{\Phi}_n(p_1 + p_2 - u_1 - u_2) \,. \tag{4.50}$$

If $r_1$ is in the final state and $r_2$ in the initial state, the phase space is split accordingly

$$\begin{aligned}
\int \mathrm{d}\boldsymbol{\Phi}_{n+2} = &\left(\frac{\mu_R^2 e^{\gamma_\mathrm{E}}}{4\pi}\right)^{\varepsilon} \int_{S_1^{2-2\varepsilon}} \mathrm{d}\boldsymbol{\Omega}(\alpha_1, \alpha_2, \ldots) \int \mathrm{d}\boldsymbol{\Phi}_{\text{unresolved}} \\
&\times \int_0^{r_{\max}^0} \frac{\mathrm{d}r_1^0 \, (r_1^0)^{1-2\varepsilon}}{2(2\pi)^{3-2\varepsilon}} \int \mathrm{d}\boldsymbol{\Phi}_{n-1}(p_1 + p_2 - r_1 - u_1 - u_2) \,,
\end{aligned} \tag{4.51}$$

and Eq. (4.33) can be applied, if $n = 2$. If both particles are in the final state, the phase space can be written as

$$\int \mathrm{d}\boldsymbol{\Phi}_{n+2} = \left(\frac{\mu_R^2 e^{\gamma_\mathrm{E}}}{4\pi}\right)^{2\varepsilon} \int_{\mathbb{S}_1^{2-2\varepsilon}} \mathrm{d}\boldsymbol{\Omega}(\alpha_1, \alpha_2, \ldots) \int_{\mathbb{S}_1^{2-2\varepsilon}} \mathrm{d}\boldsymbol{\Omega}(\beta_1, \beta_2, \ldots) \int \mathrm{d}\boldsymbol{\Phi}_\mathrm{unresolved}$$
$$\times \int_0^{r_{\max}^0} \frac{\mathrm{d}r_1^0\,(r_1^0)^{1-2\varepsilon}}{2(2\pi)^{3-2\varepsilon}} \int_0^{r_{2\max}^0} \frac{\mathrm{d}r_2^0\,(r_2^0)^{1-2\varepsilon}}{2(2\pi)^{3-2\varepsilon}} \int \mathrm{d}\boldsymbol{\Phi}_{n-2}(p_1 + p_2 - r_1 - r_2 - u_1 - u_2)\,. \quad (4.52)$$

The energy maximum for $r_2$ is given by

$$r_{2\,\max}^0 = \frac{\sqrt{\hat{s}}\,\big(E_{\max} - u_1^0 - u_2^0 - r_1^0\big) + r_1 \cdot (u_1 + u_2) + u_1 \cdot u_2}{\sqrt{\hat{s}} - \hat{r}_2 \cdot (u_1 + u_2 + r_1)}\,, \quad (4.53)$$

while the maximum of $r_1$ is given in Eq. (4.34). The resolved part of the measure in Eq. (4.52) can be completely integrated using energy-momentum conservation, if $n = 3$. The result reads

$$\int_0^{r_{2\,\max}^0} \frac{\mathrm{d}r_2^0\,(r_2^0)^{1-2\varepsilon}}{2(2\pi)^{3-2\varepsilon}} \int \mathrm{d}\boldsymbol{\Phi}_1(p_1 + p_2 - u_1 - u_2) = \frac{(r_{2\,\max}^0)^{1-2\varepsilon}}{4(2\pi)^{2-2\varepsilon}} \frac{1}{\sqrt{\hat{s}} - \hat{r}_2 \cdot (u_1 + u_2 + r_1)}\,. \quad (4.54)$$

In contrast to the triple-collinear sector, only overlapping soft singularities can occur in the double-collinear sector. The unresolved part of the phase space is therefore split to disentangle those singularities.

$$\int \mathrm{d}\boldsymbol{\Phi}_\mathrm{unresolved} = \int \mathrm{d}\boldsymbol{\Phi}_\mathrm{unresolved} \Big(\theta(u_1^0 - u_2^0) + \theta(u_2^0 - u_1^0)\Big)\,. \quad (4.55)$$

The first contribution, which is be denoted by sector $\mathcal{S}_6$ in the following, is given by

$$\int \mathrm{d}\boldsymbol{\Phi}_\mathrm{unresolved}\,\theta(u_1^0 - u_2^0) =$$
$$\left(\frac{\mu_R^2 e^{\gamma_\mathrm{E}}}{4\pi}\right)^{2\varepsilon} \int_{\mathbb{S}_1^{2-2\varepsilon}} \mathrm{d}\boldsymbol{\Omega}(\theta_1, \phi_1, \rho_1, \ldots) \int_{\mathbb{S}_1^{2-2\varepsilon}} \mathrm{d}\boldsymbol{\Omega}(\theta_2, \phi_2, \sigma_1, \sigma_2, \ldots)$$
$$\times \int_0^{u_{\max}^0} \frac{\mathrm{d}u_1^0\,(u_1^0)^{1-2\varepsilon}}{2(2\pi)^{3-2\varepsilon}} \int_0^{u_{2\,\max}^0} \frac{\mathrm{d}u_2^0\,(u_2^0)^{1-2\varepsilon}}{2(2\pi)^{3-2\varepsilon}}\,\theta\big(u_1^0 - u_2^0\big) =$$
$$\frac{E_{\max}^4}{(2\pi)^6} \left(\frac{\pi\mu_R^2 e^{\gamma_\mathrm{E}}}{4E_{\max}^2}\right)^{2\varepsilon} \int_{\mathbb{S}_1^{1-2\varepsilon}} \mathrm{d}\boldsymbol{\Omega}(\phi_1, \rho_1, \ldots) \int_{\mathbb{S}_1^{1-2\varepsilon}} \mathrm{d}\boldsymbol{\Omega}(\phi_2, \sigma_1, \sigma_2, \ldots)$$
$$\times \iiiiint_0^1 \mathrm{d}\eta_1 \mathrm{d}\eta_2 \mathrm{d}\xi_1 \mathrm{d}\xi_2\, \eta_1^{-\varepsilon} \eta_2^{-\varepsilon} \xi_1^{3-4\varepsilon} \xi_2^{1-2\varepsilon} \Big(\big(1-\eta_1\big)\big(1-\eta_2\big)\Big)^{-\varepsilon} \xi_{2\,\max}^{2-2\varepsilon}\,, \quad (4.56)$$

where the physical parameters are expressed in terms of the integration variables

$$u_1^0 = E_{\max}\,\xi_1\,, \quad u_2^0 = E_{\max}\,\xi_1\xi_2\xi_{2\,\max}\,, \quad \xi_{2\,\max} = \min\left[1,\, \frac{1}{\xi_1} \frac{1-\xi_1}{1 - \frac{E_{\max}}{\sqrt{\hat{s}}}\,\xi_1\,\hat{u}_1 \cdot \hat{u}_2}\right]\,,$$
$$\cos\theta_1 = 1 - 2\eta_1\,, \quad \cos\theta_2 = 1 - 2\eta_2\,. \quad (4.57)$$

Transverse momenta for the two collinear pairs are

$$u_{i\perp}^{\mu} = \begin{pmatrix} 0 \\ \hat{\boldsymbol{u}}_{\boldsymbol{i}\perp} \end{pmatrix} , \quad i = 1{,}2 , \tag{4.58}$$

with

$$\hat{\boldsymbol{u}}_{\mathbf{1}\perp} = \lim_{\theta_1 \to 0} \frac{\hat{\boldsymbol{u}}_{\mathbf{1}} - \hat{\boldsymbol{r}}_{\mathbf{1}}}{\|\hat{\boldsymbol{u}}_{\mathbf{1}} - \hat{\boldsymbol{r}}_{\mathbf{1}}\|} = \left.\frac{\partial \hat{\boldsymbol{u}}_{\mathbf{1}}}{\partial \theta_1}\right|_{\theta_1 = 0} = \hat{\boldsymbol{R}}_1^{(3-2\varepsilon)}(\alpha_1, \alpha_2, \ldots) \hat{\boldsymbol{n}}^{(3-2\varepsilon)} \left(\frac{\pi}{2}, \phi_1, \rho_1, \rho_2, \ldots\right) , \tag{4.59}$$

$$\begin{aligned} \hat{\boldsymbol{u}}_{\mathbf{2}\perp} = \lim_{\theta_2 \to 0} \frac{\hat{\boldsymbol{u}}_{\mathbf{2}} - \hat{\boldsymbol{r}}_{\mathbf{2}}}{\|\hat{\boldsymbol{u}}_{\mathbf{2}} - \hat{\boldsymbol{r}}_{\mathbf{2}}\|} = \left.\frac{\partial \hat{\boldsymbol{u}}_{\mathbf{2}}}{\partial \theta_2}\right|_{\theta_2 = 0} = \\ \hat{\boldsymbol{R}}_1^{(3-2\varepsilon)}(\beta_1, \beta_2, \ldots) \hat{\boldsymbol{R}}_4^{(3-2\varepsilon)}(\rho_2, \rho_3, \ldots) \hat{\boldsymbol{n}}^{(3-2\varepsilon)} \left(\frac{\pi}{2}, \phi_2, \sigma_1, \sigma_2, \ldots\right) . \end{aligned} \tag{4.60}$$

Special case, $n = n_u = n_{fr} = 2$

This parameterization has been the main result of [213]. However, even though it is outlined there, the explicit formulas are given here for completeness. In this case, the phase space contains only the four final state vectors given in Eq. (4.48). The angular parameterization is shown in Fig. 4.4. It is defined using an auxiliary vector that specifies the collinear directions

$$\boldsymbol{r} = r_1^0 \, \hat{\boldsymbol{r}}_{\mathbf{1}} + u_1^0 \, \hat{\boldsymbol{u}}_{\mathbf{1}} = -r_2^0 \, \hat{\boldsymbol{r}}_{\mathbf{2}} - u_2^0 \, \hat{\boldsymbol{u}}_{\mathbf{2}} , \quad r = \|\boldsymbol{r}\| , \quad \hat{\boldsymbol{r}} = \frac{\boldsymbol{r}}{r} . \tag{4.61}$$

The unresolved momenta are parameterized with respect to the auxiliary vector

$$\begin{aligned} \hat{\boldsymbol{r}} &= \hat{\boldsymbol{n}}^{(3-2\varepsilon)}(\alpha_1, \alpha_2, \ldots) , \\ \hat{\boldsymbol{u}}_{\mathbf{1}} &= \boldsymbol{R}_1^{(3-2\varepsilon)}(\alpha_1, \alpha_2, \ldots) \hat{\boldsymbol{n}}^{(3-2\varepsilon)}(\tilde{\theta}_1, \phi_1, \rho_1, \rho_2, \ldots) , \\ \hat{\boldsymbol{u}}_{\mathbf{2}} &= -\boldsymbol{R}_1^{(3-2\varepsilon)}(\alpha_1, \alpha_2, \ldots) \boldsymbol{R}_4^{(3-2\varepsilon)}(\rho_2, \rho_3, \ldots) \hat{\boldsymbol{n}}^{(3-2\varepsilon)}(\tilde{\theta}_2, \phi_2, \sigma_1, \sigma_2, \ldots) . \end{aligned} \tag{4.62}$$

The full phase space is

$$\begin{aligned} \int \mathrm{d}\boldsymbol{\Phi}_4 = \left(\frac{\mu_R^2 e^{\gamma_\mathrm{E}}}{4\pi}\right)^{3\varepsilon} \int_{\mathbb{S}_1^{2-2\varepsilon}} \mathrm{d}\boldsymbol{\Omega}(\alpha_1, \alpha_2, \ldots) \\ \times \int_{\mathbb{S}_1^{1-2\varepsilon}} \mathrm{d}\boldsymbol{\Omega}(\phi_1, \rho_1, \ldots) \int_{\mathbb{S}_1^{1-2\varepsilon}} \mathrm{d}\boldsymbol{\Omega}(\phi_2, \sigma_1, \sigma_2, \ldots) \\ \times \int_0^\infty \frac{\mathrm{d}u_1^0 \, (u_1^0)^{1-2\varepsilon}}{2(2\pi)^{3-2\varepsilon}} \int_{-1}^1 \mathrm{d}\cos\theta_1 \, \left(1 - \cos^2\theta_1\right)^{-\varepsilon} \int_0^\infty \frac{\mathrm{d}u_2^0 (u_2^0)^{1-2\varepsilon}}{2(2\pi)^{3-2\varepsilon}} \int_{-1}^1 \mathrm{d}\cos\theta_2 \, \left(1 - \cos^2\theta_2\right)^{-\varepsilon} \\ \times \left(\frac{1 - \cos^2\tilde{\theta}_1}{1 - \cos^2\theta_1}\right)^{-\varepsilon} \left(\frac{1 - \cos^2\tilde{\theta}_2}{1 - \cos^2\theta_2}\right)^{-\varepsilon} \frac{r_1^0 \, r_2^0}{4 \, (2\pi)^{2-2\varepsilon} \, r^{1+2\varepsilon} \left|r_1^0 + r_2^0 + u_1^0 \cos\theta_1 + u_2^0 \cos\theta_2\right|} , \end{aligned} \tag{4.63}$$

where the parameters are

$$\cos\tilde{\theta}_i = \frac{r_i^0 \cos\theta_i + u_i^0}{r} , \tag{4.64}$$

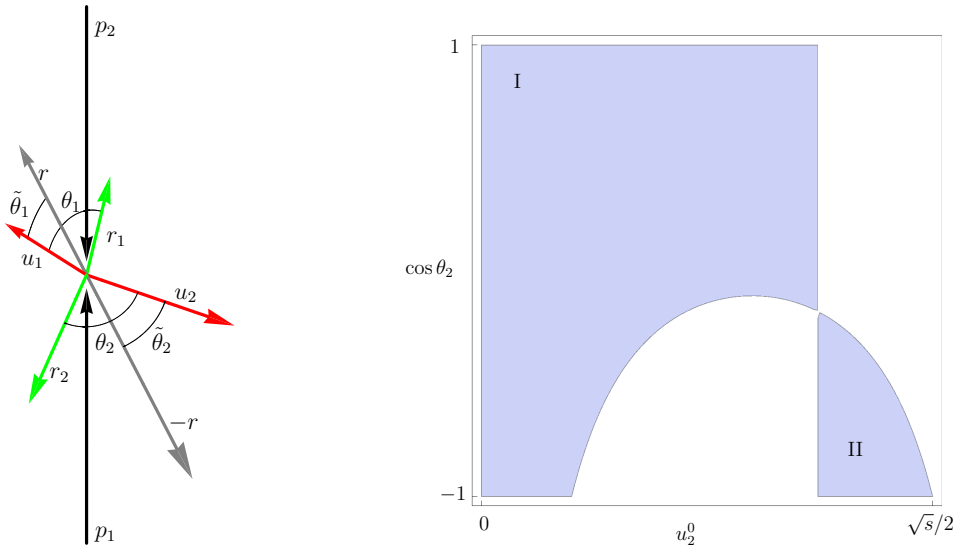


**Figure 4.4:** **Left:** Double-collinear sector parameterization for a four particle massless phase space, where the reference momenta $r_1$ and $r_2$ are in the final state. The auxiliary reference vector $r = r_1 + u_1$ is defined in order parameterize the phase space using the angles $\tilde{\theta}_1$ and $\tilde{\theta}_2$.
**Right:** The parameters of the unresolved momentum $u_1$ are fixed. The parameters of the momentum $u_2$ split the phase space in two disjunct regions [1].

$$
\begin{aligned}
r_1^0 &= \frac{\hat{s} - 2\sqrt{\hat{s}}\left(u_1^0 + u_2^0\right) + 2u_2^0\left(u_1^0 + u_2^0\right) + 2\left(\sqrt{\hat{s}} - u_1^0 - u_2^0\right)u_2^0\cos\theta_2}{2\left(\sqrt{\hat{s}} - u_1^0\left(1-\cos\theta_1\right) - u_2^0\left(1-\cos\theta_2\right)\right)}\,, \\
r_2^0 &= \frac{\hat{s} - 2\sqrt{\hat{s}}\left(u_1^0 + u_2^0\right) + 2u_1^0\left(u_1^0 + u_2^0\right) + 2\left(\sqrt{\hat{s}} - u_1^0 - u_2^0\right)u_1^0\cos\theta_1}{2\left(\sqrt{\hat{s}} - u_1^0\left(1-\cos\theta_1\right) - u_2^0\left(1-\cos\theta_2\right)\right)}\,, \\
r &= \sqrt{\left(u_1^0\right)^2 + \left(r_1^0\right)^2 + 2u_1^0 r_1^0\cos\theta_1} = \sqrt{\left(u_2^0\right)^2 + \left(r_2^0\right)^2 + 2u_2^0 r_2^0\cos\theta_2}\,.
\end{aligned}
\tag{4.65}
$$

In order to cover the full phase space using the above parameters, two integration regions are identified as depicted in the right plot of Fig. 4.4. Region I is limited by

$$
\begin{aligned}
0 \;\leq\; u_2^0 \;&<\; \frac{\hat{s} - 2u_1^0\left(\sqrt{\hat{s}} - u_1^0\right)\left(1-\cos\theta_1\right)}{2\left(\sqrt{\hat{s}} - u_1^0\left(1-\cos\theta_1\right)\right)}\,, \\
-\min\left[1, \frac{\hat{s} - 2\sqrt{\hat{s}}\left(u_1^0 + u_2^0\right) + 2u_2^0\left(u_1^0 + u_2^0\right)}{2u_2^0\left(\sqrt{\hat{s}} - u_1^0 - u_2^0\right)}\right] \;&\leq\; \cos\theta_2 \;\leq\; 1\,,
\end{aligned}
\tag{4.66}
$$

where

$$
r_1^0 + r_2^0 + u_1^0\cos\theta_1 + u_2^0\cos\theta_2 \;>\; 0\,. \tag{4.67}
$$

Region II is defined as

$$\frac{\hat{s}-2u_1^0\left(\sqrt{\hat{s}}-u_1^0\right)(1-\cos\theta_1)}{2\left(\sqrt{\hat{s}}-u_1^0\,(1-\cos\theta_1)\right)} \;\leq\; u_2^0 \;\leq\; \frac{\sqrt{\hat{s}}}{2}\,,$$

$$-1 \;\leq\; \cos\theta_2 \;\leq\; -\frac{\hat{s}-2\sqrt{\hat{s}}\left(u_1^0+u_2^0\right)+2u_2^0\left(u_1^0+u_2^0\right)}{2u_2^0\left(\sqrt{\hat{s}}-u_1^0-u_2^0\right)}\,, \tag{4.68}$$

with

$$r_1^0+r_2^0+u_1^0\cos\theta_1+u_2^0\cos\theta_2 \;\leq\; 0\,. \tag{4.69}$$

In both regions the parameters of the first momentum are unrestricted and read

$$0\leq u_1^0\leq\frac{\sqrt{\hat{s}}}{2}\,,\quad -1\leq\cos\theta_1\leq 1\,. \tag{4.70}$$

It is noticeable, that region II does not contain any singularities. Since it vanishes in the soft or collinear limit. Hence, it can be integrated directly in four dimensions. The contribution in region I is again split due to overlapping soft singularities. The whole phase space reads

$$\begin{aligned}\int \mathrm{d}\boldsymbol{\Phi}_4 = \int \mathrm{d}\boldsymbol{\Phi}_4 \Big[\Big(\theta(u_1^0-u_2^0)+\theta(u_2^0-u_1^0)\Big)\,\theta\big(r_1^0+r_2^0+u_1^0\cos\theta_1+u_2^0\cos\theta_2\big)\\ +\theta\big(-r_1^0-r_2^0-u_1^0\cos\theta_1-u_2^0\cos\theta_2\big)\Big]\,,\end{aligned} \tag{4.71}$$

where the first contribution reads explicitly

$$\begin{aligned}\int \mathrm{d}\boldsymbol{\Phi}_4\,\theta(u_1^0-u_2^0)\,\theta\big(r_1^0+r_2^0+u_1^0\cos\theta_1+u_2^0\cos\theta_2\big) &= \int_{\mathbb{S}_1^{2-2\varepsilon}}\mathrm{d}\boldsymbol{\Omega}(\alpha_1,\alpha_2,\ldots)\\ &\times\frac{E_{\max}^4}{4(2\pi)^8}\left(\frac{\pi\mu_R^2e^{\gamma_\mathrm{E}}}{E_{\max}^2}\right)^{3\varepsilon}\int_{\mathbb{S}_1^{1-2\varepsilon}}\mathrm{d}\boldsymbol{\Omega}(\phi_1,\rho_1,\ldots)\int_{\mathbb{S}_1^{1-2\varepsilon}}\mathrm{d}\boldsymbol{\Omega}(\phi_2,\sigma_1,\sigma_2,\ldots)\\ &\times\iiiint_0^1\mathrm{d}\eta_1\mathrm{d}\eta_2\mathrm{d}\xi_1\mathrm{d}\xi_2\,\eta_1^{-\varepsilon}\eta_2^{-\varepsilon}\xi_1^{3-4\varepsilon}\xi_2^{1-2\varepsilon}\\ &\times\eta_{2\,\max}^{1-\varepsilon}\,\xi_{2\,\max}^{2-2\varepsilon}\left(\frac{1}{\eta_1}\left(1-\cos^2\tilde{\theta}_1\right)\right)^{-\varepsilon}\left(\frac{1}{\eta_2}\left(1-\cos^2\tilde{\theta}_2\right)\right)^{-\varepsilon}\\ &\times\left(\frac{E_{\max}}{r}\right)^{2\varepsilon}\frac{r_1^0\,r_2^0}{r\left(r_1^0+r_2^0+u_1^0\cos\theta_1+u_2^0\cos\theta_2\right)}\,.\end{aligned} \tag{4.72}$$

The physical parameters are defined as

$$\begin{gathered}u_1^0=E_{\max}\,\xi_1\,,\quad u_2^0=E_{\max}\,\xi_1\xi_2\xi_{2\,\max}\,,\\ \cos\theta_1=1-2\eta_1\,,\quad \cos\theta_2=1-2\eta_2\eta_{2\,\max}\,,\\ \eta_{2\,\max}=\min\left[1,\frac{1}{\xi_1}\frac{1-\xi_1}{\xi_2\xi_{2\,\max}\big(2-\xi_1(1+\xi_2\xi_{2\,\max})\big)}\right]\,,\xi_{2\,\max}=\min\left[1,\frac{1}{\xi_1}\frac{1-\eta_1\xi_1(2-\xi_1)}{1-\eta_1\xi_1}\right]\,.\end{gathered} \tag{4.73}$$

Finally, the transverse vectors for this case read

$$u_{i\perp}^{\mu} = \begin{pmatrix} 0 \\ \hat{\boldsymbol{u}}_{\boldsymbol{i}\perp} \end{pmatrix} , \quad i = 1,2 , \tag{4.74}$$

where

$$\hat{\boldsymbol{u}}_{\mathbf{1}\perp} = \lim_{\theta_1 \to 0} \frac{\hat{\boldsymbol{u}}_{\mathbf{1}} - \hat{\boldsymbol{r}}_{\mathbf{1}}}{\|\hat{\boldsymbol{u}}_{\mathbf{1}} - \hat{\boldsymbol{r}}_{\mathbf{1}}\|} = \left. \frac{\partial \hat{\boldsymbol{u}}_{\mathbf{1}}}{\partial \tilde{\theta}_1} \right|_{\tilde{\theta}_1 = 0} = \hat{\boldsymbol{R}}_1^{(3-2\varepsilon)}(\alpha_1, \alpha_2, \ldots) \hat{\boldsymbol{n}}^{(3-2\varepsilon)} \left( \frac{\pi}{2}, \phi_1, \rho_1, \rho_2, \ldots \right) , \tag{4.75}$$

$$\begin{aligned} \hat{\boldsymbol{u}}_{\mathbf{2}\perp} = \lim_{\theta_2 \to 0} \frac{\hat{\boldsymbol{u}}_{\mathbf{2}} - \hat{\boldsymbol{r}}_{\mathbf{2}}}{\|\hat{\boldsymbol{u}}_{\mathbf{2}} - \hat{\boldsymbol{r}}_{\mathbf{2}}\|} = \left. \frac{\partial \hat{\boldsymbol{u}}_{\mathbf{2}}}{\partial \tilde{\theta}_2} \right|_{\tilde{\theta}_2 = 0} = \\ - \hat{\boldsymbol{R}}_1^{(3-2\varepsilon)}(\alpha_1, \alpha_2, \ldots) \hat{\boldsymbol{R}}_4^{(3-2\varepsilon)}(\rho_2, \rho_3, \ldots) \hat{\boldsymbol{n}}^{(3-2\varepsilon)} \left( \frac{\pi}{2}, \phi_2, \sigma_1, \sigma_2, \ldots \right) . \end{aligned} \tag{4.76}$$

## 4.3 Generation of subtraction terms

The parameterization given in the previous section allows for a very simple construction of subtraction terms and an extraction of poles in $\varepsilon$ before any integration is performed. The main purpose has been to find integration parameters, $\{\eta,\xi\}$ or $\{\eta_1,\eta_2,\xi_1,\xi_2\}$, that indicate unambiguously soft and collinear limits in each sector as they approach zero.
In the single-collinear parameterization the relevant contribution to the phase space integral is (see Eq. (4.24))

$$\iint_0^1 \mathrm{d}\eta \, \mathrm{d}\xi \, \eta^{-\varepsilon} \, \xi^{1-2\varepsilon} . \tag{4.77}$$

This parameterization is used if there is one additional parton in the phase space. The relevant contributions are $\hat{\sigma}^{\mathrm{R}}$, $\hat{\sigma}^{\mathrm{C1}}$ and $\sigma^{\mathrm{RV}}$ . The limit $\eta \to 0$ indicates the collinear limit of $u$ and $r$. The soft limit of the unresolved momentum is approached as $\xi \to 0$. In these limits subtraction terms for the matrix elements are necessary, that are constructed using the singular limits of matrix elements discussed in section 3.4.1. If the contribution that contains only tree-level matrix elements, $\hat{\sigma}^{\mathrm{R}}$, is considered, the relevant limits are given in Eq. (3.49), for the collinear and soft-collinear limit, and in Eq. (3.50), for the soft limit. The leading singular behavior of these functions can be factorized and reads

$$\frac{1}{\eta} \frac{1}{\xi^2} . \tag{4.78}$$

The full real radiation cross section $\hat{\sigma}^{\mathrm{R}}$ is written in the following form [1]

$$\hat{\sigma}^{\mathrm{R}} = \sum_{ik} \iint_0^1 \frac{\mathrm{d}\eta}{\eta^{1+\varepsilon}} \frac{\mathrm{d}\xi}{\xi^{1+2\varepsilon}} f_{i,k}(\eta,\xi) , \tag{4.79}$$

where the sum contains all single-collinear sectors, as discussed in section 4.1. An important observation is that the function $f_{i,k}(\eta,\xi)$ is regular in the soft and collinear limit $x \to 0$, where

1 The collinear factorization contribution $\hat{\sigma}^{\mathrm{C1}}$ is treated similarly.

$x \in \{\eta,\xi\}$. For an initial state reference momentum it reads explicitly

$$\begin{aligned} f_{i,k}(\eta,\xi) =& \frac{E_{\max}^2}{16\pi^3 \hat{s} N_{ab}} \left( \frac{\pi \mu_{\mathrm{R}}^2 e^{\gamma_{\mathrm{E}}}}{4E_{\max}^2(1-\eta)} \right)^{\varepsilon} \\ & \times \int_{\mathbb{S}_1^{1-2\varepsilon}} \mathrm{d}\boldsymbol{\Omega}(\phi,\rho_1,\ldots) \int \mathrm{d}\boldsymbol{\Phi}_n\big(p_1+p_2-u\big)\, \mathcal{S}_{i,k} \left[ \eta\, \xi^2 \langle \mathcal{M}_{n+1}^{(0)} | \mathcal{M}_{n+1}^{(0)} \rangle \right] \mathrm{F}_{n+1} \,, \end{aligned} \tag{4.80}$$

where the phase space parameterization in (4.20) and (4.24) has been used for $z = 1$. At this point, poles can be extracted by using the following formula iteratively for the two variables

$$\frac{1}{x^{1+a\varepsilon}} = -\frac{1}{a\varepsilon}\delta(x) + \left[ \frac{1}{x^{1+a\varepsilon}} \right]_+ \,, \tag{4.81}$$

where the plus-distribution is defined by

$$\int_0^1 \mathrm{d}x \, \left[ \frac{1}{x^{1+a\varepsilon}} \right]_+ f(x) = \int_0^1 \mathrm{d}x \, \frac{f(x)-f(0)}{x^{1+a\varepsilon}} \,. \tag{4.82}$$

Two kinds of subtraction terms are generated in this way. Terms containing explicit poles are called *integrated subtraction terms*, while endpoint subtractions are *subtraction terms*. Three different limits need to be evaluated, namely $f_{i,k}(\eta,0)$, $f_{i,k}(0,\xi)$ and $f_{i,k}(0,0)$. For the selector function $\mathcal{S}_{i,k}$, the measurement function $F_{n+1}$ and the remaining phase space measure it amounts to setting the appropriate variable to zero. For the matrix element the appropriate limits of the factorization formulas are used. The final result for the real radiation cross section can be written as a Laurent series

$$\hat{\sigma}^{\mathrm{R}} = \hat{\sigma}^{\mathrm{R},0} + \frac{\hat{\sigma}^{\mathrm{R},1}}{\varepsilon} + \frac{\hat{\sigma}^{\mathrm{R},2}}{\varepsilon^2} \,, \tag{4.83}$$

where each coefficient is integrated using Monte Carlo methods.
The real-virtual contribution $\hat{\sigma}^{\mathrm{RV}}$ is treated in a similar way, since again only one parton is unresolved. The conceptual difference to the previous case is, that soft and collinear limits of one-loop matrix elements are involved. The explicit limits are given in Eqs. (3.58) and (3.59). Each limit consists of two terms. The collinear limit contains the tree-level splitting function and the one-loop splitting function. Likewise, the soft limit: It contains the tree-level soft function and the one-loop soft function. It turns out that the different terms scale differently with respect to the variables $\eta$ and $\xi$. The two different scalings are

$$\frac{1}{\eta}\frac{1}{\xi^2} \quad \text{and} \quad \frac{1}{\eta^{1+\varepsilon}}\frac{1}{\xi^{2+2\varepsilon}} \,. \tag{4.84}$$

The formula (4.81) is modified in order to account for this behavior

$$\int_0^1 \frac{\mathrm{d}x}{x^{1+a\varepsilon}} f(x) = -\frac{1}{a\varepsilon} f_0 - \frac{1}{(a+b)\varepsilon} f_\varepsilon + \int_0^1 \frac{\mathrm{d}x}{x^{1+a\varepsilon}} \big( f(x) - f_0 - x^{-b\varepsilon} f_\varepsilon \big) \,, \tag{4.85}$$

where the function $f(x)$ behaves as

$$f(x) \xrightarrow[x\to 0]{} f_0 + x^{-b\varepsilon} f_\varepsilon \,. \tag{4.86}$$

Again, the formula can be applied to $\eta$ and $\xi$ independently and the limits of the one-loop matrix elements have to be considered to obtain a Laurent expansion for the real-virtual cross section, i.e.

subtraction and integrated subtraction terms.
The construction of subtraction and integrated subtraction terms for the double-real contribution to the cross section $\hat{\sigma}^{\mathrm{RR}}$ is performed in the same manner as it has been explained for $\hat{\sigma}^{\mathrm{R}}$ previously. At first, the cross section is decomposed into triple-collinear and double-collinear sectors as explained in section 4.1

$$\hat{\sigma}^{\mathrm{RR}} = \sum_{ijk} \hat{\sigma}^{\mathrm{RR}}_{ij,k} + \sum_{ijkl} \hat{\sigma}^{\mathrm{RR}}_{ik,jl} \,. \tag{4.87}$$

Each triple-collinear sector is further decomposed into five subsectors using the appropriate parameterization Eq. (4.37) for the unresolved momenta

$$\hat{\sigma}^{\mathrm{RR}}_{ij,k} = \sum_{\mathcal{S}=\mathcal{S}_1}^{\mathcal{S}_5} \hat{\sigma}^{\mathrm{RR},\mathcal{S}}_{ij,k} \,. \tag{4.88}$$

This decomposition ensures that each term in the above sum contains a regulating measure of the form

$$\iiiint_0^1 \mathrm{d}\eta_1 \mathrm{d}\eta_2 \mathrm{d}\xi_1 \mathrm{d}\xi_2 \, \eta_1^{a_1-b_1\varepsilon} \, \eta_2^{a_2-b_2\varepsilon} \, \xi_1^{a_3-b_3\varepsilon} \, \xi_2^{a_4-b_4\varepsilon} \,, \tag{4.89}$$

where the variables $a_i$ and $b_i$ for the triple-collinear sectors can be determined from Tab. 4.3. In the double-collinear sectors they are given by

$$\begin{aligned} a_1 &= 0 \,, \quad a_2 = 0 \,, \quad a_3 = 3 \,, \quad a_4 = 1 \,, \\ b_1 &= 1 \,, \quad b_2 = 1 \,, \quad b_3 = 4 \,, \quad b_4 = 2 \,. \end{aligned} \tag{4.90}$$

The limit of one of the variables $x \to 0$, where $x \in \{\eta_1,\eta_2,\xi_1,\xi_2\}$, corresponds to a soft and/or collinear limit. *Single unresolved* limits and *double unresolved* limits can be distinguished. While in a single unresolved limit one parton vanishes, two final state partons vanish in the double unresolved case. Table 4.4 specifies the physical limits as one of the variables $x$ goes to zero. It is emphasized that the limit of a single variable $x \to 0$ can indicate either a single or a double unresolved limit.

| | $\eta_1$ | $\eta_2$ | $\xi_1$ | $\xi_2$ |
|---|---|---|---|---|
| $\mathcal{S}_1$ | $u_1 \| \| u_2 \| \| r$ (DU) | $u_2 \| \| r$ (SU) | $u_1 \to 0$, $u_2 \to 0$ (DU) | $u_2 \to 0$ (SU) |
| $\mathcal{S}_2$ | $u_1 \| \| r$, $u_2 \to 0$ (DU) | $u_1 \| \| u_2 \| \| r$ (DU) | $u_1 \to 0$, $u_2 \to 0$ (DU) | $u_2 \to 0$ (SU) |
| $\mathcal{S}_3$ | $u_1 \| \| r$ (SU) | $u_1 \| \| u_2 \| \| r$ (DU) | $u_1 \to 0$, $u_2 \to 0$ (DU) | $u_2 \to 0$, $u_1 \| \| r$ (DU) |
| $\mathcal{S}_4$ | $u_1 \| \| u_2 \| \| r$ (DU) | $u_1 \| \| u_2$ (SU) | $u_1 \to 0$, $u_2 \to 0$ (DU) | $u_2 \to 0$ (SU) |
| $\mathcal{S}_5$ | $u_1 \| \| u_2$ (SU) | $u_1 \| \| u_2 \| \| r$ (DU) | $u_1 \to 0$, $u_2 \to 0$ (DU) | $u_2 \to 0$ (SU) |
| $\mathcal{S}_6$ | $u_1 \| \| r_1$ (SU) | $u_2 \| \| r_2$ (SU) | $u_1 \to 0$, $u_2 \to 0$ (SU) | $u_2 \to 0$ (SU) |

**Table 4.4:** The limits as indicated by the variable $x \in \{\eta_1,\eta_2,\xi_1,\xi_2\}$, as $x \to 0$. Single-unresolved limits (SU) descrbe the vanishing of one final state partcle, whereas double-unresolved limits (DU) describe the vanishing of two final state particles.

Each contribution to $\hat{\sigma}^{\mathrm{RR}}$ is recast into a form appropriate to generate subtraction and integrated

subtraction terms

$$\iiiint_0^1 \frac{\mathrm{d}\eta_1}{\eta_1^{1+b_1\varepsilon}} \frac{\mathrm{d}\eta_2}{\eta_2^{1+b_2\varepsilon}} \frac{\mathrm{d}\xi_1}{\xi_1^{1+b_3\varepsilon}} \frac{\mathrm{d}\xi_2}{\xi_2^{1+b_4\varepsilon}} f(\eta_1,\eta_2,\xi_1,\xi_2) \,. \tag{4.91}$$

The formula (4.81) can be applied iteratively in each variable. The sum of all sectors is given as a Laurent series

$$\hat{\sigma}^{\mathrm{RR}} = \hat{\sigma}^{\mathrm{R},0} + \frac{\hat{\sigma}^{\mathrm{RR},1}}{\varepsilon} + \frac{\hat{\sigma}^{\mathrm{RR},2}}{\varepsilon^2} + \frac{\hat{\sigma}^{\mathrm{RR},3}}{\varepsilon^3} + \frac{\hat{\sigma}^{\mathrm{RR},4}}{\varepsilon^4} \,. \tag{4.92}$$

In each sector there are fifteen different limits for the function $f(\eta_1,\eta_2,\xi_1,\xi_2)$ to consider. This function always contains, the selector function, either $\mathcal{S}_{ij,k}$ or $\mathcal{S}_{ik,jl}$, the measurement function $F_{n+2}$, the phase space measure and a regulated matrix element

$$\eta_1^{1+a_1}\eta_2^{1+a_2}\xi_1^{1+a_3}\xi_2^{1+a_4}\langle \mathcal{M}^{(0)}_{n+2}|\mathcal{M}^{(0)}_{n+2}\rangle \,. \tag{4.93}$$

The limit of the matrix element can be obtained by using all factorization formulas for tree-level amplitudes, discussed in section 3.4.1. The pattern for choosing the correct formula for a given limit is as follows. If only one variable vanishes, the corresponding limit can be taken from Tab. 4.4. If an unresolved momentum is soft and collinear, in the corresponding collinear limit the soft variable $\xi_i$ is set to zero. For example, to construct the function $f(0,\eta_2,0,\xi_2)$ in sector $\mathcal{S}_1$, the triple-collinear limit is taken, *i.e.* Eq. (3.53), and the variable $\xi_1$ is set to zero. If two independent single-unresolved limits are encountered, the corresponding factorization formulas are used iteratively. For example, to construct the function $f(0,0,\xi_1,\xi_2)$ in sector $\mathcal{S}_6$ the formula for the collinear limit (3.49) is applied independently to the two collinear pairs.

The procedure outlined above is in general sufficient to obtain finite results for each contribution of a next-to-next-to leading order cross section. However, the procedure has been described completely for $d$-dimensional external momenta and polarization states, which also means that all matrix elements that appear in subtraction terms are needed in $d$ dimensions to have a finite and correct result. The above scheme can be improved, if the structure of the infrared-singularities of real and virtual contributions is investigated and separately finite parts are identified.

## 4.4 Azimuthal average and iterated limits

In the previous section subtraction and integrated subtraction terms have been generated for collinear and soft limits. The collinear subtraction terms contain in general spin correlated matrix elements of the form

$$\langle \mathcal{M}| \frac{u_\perp^\mu u_\perp^\nu}{u_\perp^2} |\mathcal{M}\rangle \,. \tag{4.94}$$

This is necessary to ensure pointwise convergence of the formula in the collinear limit. However, if an explicit collinear pole term is considered, an integrated collinear subtraction term, spin correlations are not necessary and may be integrated over the azimuthal directions. Additionally, virtual poles are known to only contain color correlations, but are free of spin correlations, a cancellation of poles between real and virtual contributions will take place among uncorrelated matrix elements. In principle spin correlated matrix elements can be replaced directly by their averaged counterparts using the formula

$$\left[\int_{\mathbb{S}_1^{1-2\varepsilon}} \mathrm{d}\boldsymbol{\Omega}\, 1\right]^{-1} \int_{\mathbb{S}_1^{1-2\varepsilon}} \mathrm{d}\boldsymbol{\Omega}(\phi,\rho_1,\rho_2,\ldots)\, \frac{u_\perp^\mu u_\perp^\nu}{u_\perp^2} = \frac{1}{2(1-\varepsilon)} \left( g^{\mu\nu} - \frac{r^\mu \bar{r}^\nu + r^\nu \bar{r}^\mu}{r\cdot\bar{r}} \right) \,, \tag{4.95}$$

where the transverse vector $u_\perp$ is the only object that depends on the azimuthal angles $\phi, \rho_1, \rho_2, \ldots$, that parameterize the direction transverse to the collinear direction. The collinear direction is defined by the reference momenta $r$ and $\bar{r}$, where $\bar{r}^\mu = r_\mu$. By transversality of the matrix elements the longitudinal part, proportional to $r$, vanishes. The above formula is directly applicable in the single-collinear sector, section 4.2.1, and the double-collinear sector, section 4.2.3, where $u_\perp$ and $r$ have to be replaced by $u_{\perp,i}$ and $r_i$ accordingly. In these cases the phase space integral contains the integration over azimuthal angles explicitly.
In the triple-collinear sector, section 4.2.2, the above formula can directly applied for a pole related to the collinearity of $u_1$ and $r$. In this case the measure exhibits the aziumuthal integration directly, as can be seen in Eq. (4.37). In the case of $u_2||r$, in principle the same argument holds. Only the second rotation in $u_{\perp,2}$ with respect to $u_1$, Eq. (4.41), has to be made undone, which is always possible using the invariance of the measure under rotations. The nonlinear mapping, $\phi_2(\theta_1,\theta_2,\zeta)$ does not spoil the argument, since the $u_{\perp,2}$ depends correctly on the angle $\phi_2$ and is therefore correctly averaged. In the triple-collinear limit, $u_1||u_2||r$, the average is performed straightfowardly using the same reasoning.
The only case that needs more investigation appears in the triple-collinear parameterization as $u_1||u_2$ become collinear. Due to the parameterization in this sector the transverse vector $u^\pm_{\perp,3}$ depends on the azimuthal angle $\tilde{\phi}_2^\pm$ (4.42), but the angle that is explicitly integrated is $\phi_2(\theta_1,\theta_2,\zeta)$. The remaining azimuthal angles $\sigma_1,\sigma_2,\ldots$ are correctly integrated. In order to investigate the impact on the average, the integration measure including $\mathrm{d}\phi_2$ should be compared to the measure in terms of $\mathrm{d}\tilde{\phi}_2$ in the collinear limit $\theta_1 \approx \theta_2 \neq 0$. It can be shown that in this limit the integration measure is

$$\int_0^\pi \mathrm{d}\tilde{\phi}_2 \, |\tan\tilde{\phi}_2|^{-2\varepsilon} \,, \tag{4.96}$$

while it should be

$$\int_0^\pi \mathrm{d}\tilde{\phi}_2 \, \sin^{-2\varepsilon}\tilde{\phi}_2 \,, \tag{4.97}$$

to average the function correctly. The difference is obviously of order $\varepsilon$. It means that the contribution to the pole term will be averaged properly, while the finite contribution will get a correction. This correction can be calculated by explicitly performing the integral

$$\left[\int_0^\pi \mathrm{d}\tilde{\phi}_2 \, |\tan\tilde{\phi}_2|^{-2\varepsilon} \int_{\mathcal{S}_1^{-2\varepsilon}} \mathrm{d}\boldsymbol{\Omega}\, 1\right]^{-1} \int_0^\pi \mathrm{d}\tilde{\phi}_2 \, |\tan\tilde{\phi}_2|^{-2\varepsilon} \int_{\mathcal{S}_1^{-2\varepsilon}} \mathrm{d}\boldsymbol{\Omega}(\sigma_1,\sigma_2,\ldots)\, \frac{u^\mu_{3\perp} u^\nu_{3\perp}}{u^2_{3\perp}} = \frac{1}{2}\left(g^{\mu\nu} - \frac{u_1^\mu \bar{u}_1^\nu + u_1^\nu \bar{u}_1^\mu}{u_1\cdot\bar{u}_1}\right) - \varepsilon\, u^\mu_{3\perp}(\tilde{\phi}_2 = 0)\, u^\nu_{3\perp}(\tilde{\phi}_2 = 0) \,, \tag{4.98}$$

The first term on the right hand side is the correct average in four dimensions, where the longitudinal (collinear) direction in this case is set by $u_1$, where $\bar{u}_1^\mu = u_{1\,\mu}$. The second term takes into account the error made due to the different measure in the first azimuthal angle.
The above formula is only relevant in sector $\mathcal{S}_4$ as a pole is taken in $\eta_2$ and sector $\mathcal{S}_5$ as a pole is taken in $\eta_1$, as can be verified in Tab. 4.4. Spin correlations only appear in splitting functions if the splitting particle is a gluon. Applying formula (4.98) to these cases amounts to the following replacements

$$\hat{P}^{(0)\,\mu\nu}_{gg}(z,u_{3\perp};\varepsilon) \longrightarrow -\, g^{\mu\nu}\left[2C_A\left(\frac{z}{1-z} + \frac{1-z}{z} + (1-\varepsilon)z(1-z)\right)\right] \tag{4.99}$$

$$
\begin{aligned}
&+ 4C_A\varepsilon(1-\varepsilon)z(1-z)\,u_{3\perp}^{\mu}(\tilde{\phi}_2=0)\,u_{3\perp}^{\nu}(\tilde{\phi}_2=0)\,,\\
\hat{P}_{q\bar{q}}^{(0)\,\mu\nu}(z,u_{3\perp};\varepsilon) \;\longrightarrow\; &- g^{\mu\nu}\Big[T_F\big(1-2z(1-z)\big)\Big] - 4T_F\varepsilon z(1-z)\,u_{3\perp}^{\mu}(\tilde{\phi}_2=0)\,u_{3\perp}^{\nu}(\tilde{\phi}_2=0)\,,
\end{aligned}
\tag{4.100}
$$

where the terms of order $\varepsilon^0$ are exactly the spin averaged functions in $d=4$ dimensions, given in Eqs. (B.21) and (B.22).

Using the spin averaged splitting functions for the single unresolved collinear poles has additionally an impact on the choice of functions used for collinear subtraction terms for the same pole term in the double-real contribution. For example, if the single-collinear pole $\eta_2=0$ in sector $\mathcal{S}_1$ is considered, the pole contains a subtraction term due to the remaining collinear limit $\eta_1=0$. This subtraction term cannot be constructed using the triple splitting function, since it allows spin correlations for both limits, while the first limit is described by an averaged splitting function. The integral would not be pointwise convergent anymore. The appropriate subtraction formula is given by the iterated collinear limit, where spin correlations only in the *second* limit arise. For the example in sector $\mathcal{S}_1$ the limit is given by

$$
\begin{aligned}
&\overline{|\mathcal{M}^{(0)}_{a_r,a_1,a_2,\dots}(r,u_1,u_2,\dots)|^2} \simeq\\
&\qquad\frac{\big(8\pi\alpha_s\big)^2}{s_{r2}\,s_{1r2}}\,\langle\hat{\mathbf{P}}^{(0)}_{a_r a_2}(z_{r2};\varepsilon)\rangle\,\langle\mathcal{M}^{(0)}_{a,\dots}(p,\dots)|\hat{\mathbf{P}}^{(0)}_{a_1 a_{r2}}(z_{1r2},u_{1\perp};\varepsilon)|\mathcal{M}^{(0)}_{a,\dots}(p,\dots)\rangle\,,
\end{aligned}
\tag{4.101}
$$

where the invariant $s_{r2}=2r\cdot u_2$ describes the collinear limit $r||u_2$, for which the pole has been taken. The invariant $s_{1r2}=2u_1\cdot(r+u_2)$ describes the subsequent collinear limit. All iterated cases can be found in Tab. 4.4 and the construction of the subtraction term follows the given example. If the splitting functions for the first splitting are in sector $\mathcal{S}_4$ and $\mathcal{S}_5$, where residual spin correlation are present (Eq. (4.98)), the iterated limits are given by

$$
\begin{aligned}
&\overline{|\mathcal{M}^{(0)}_{a_r,g,g,\dots}(r,u_1,u_2,\dots)|^2} \simeq\\
&\qquad\frac{\big(8\pi\alpha_s\big)^2}{s_{12}\,s_{r12}}\Bigg[2C_A\left(\frac{z_{12}}{1-z_{12}}+\frac{1-z_{12}}{z_{12}}+(1-\varepsilon)z_{12}(1-z_{12})\right)\\
&\qquad\qquad\times\,\langle\mathcal{M}^{(0)}_{a_r,\dots}(p,\dots)|\hat{\mathbf{P}}^{(0)}_{a_r g}(z_{r12},u_{1\perp};\varepsilon)|\mathcal{M}^{(0)}_{a_r,\dots}(p,\dots)\rangle\\
&+ 4C_A\varepsilon(1-\varepsilon)z_{12}(1-z_{12})\,\langle\mathcal{M}^{(0)}_{a_r,\dots}(p,\dots)|\hat{\mathbf{P}}^{(0)}_{Pa_r g}\big(z_{r12},u_{1\perp},u_{3\perp}^{\mu}(\tilde{\phi}_2=0)\big)|\mathcal{M}^{(0)}_{a_r,\dots}(p,\dots)\rangle\Bigg]\,,
\end{aligned}
\tag{4.102}
$$

for gluons, and

$$
\begin{aligned}
&\overline{|\mathcal{M}^{(0)}_{a_r,q,\bar{q},\dots}(r,u_1,u_2,\dots)|^2} \simeq\\
&\qquad\frac{\big(8\pi\alpha_s\big)^2}{s_{12}\,s_{r12}}\Bigg[T_F\Big(1-2z_{12}(1-z_{12})\Big)\,\langle\mathcal{M}^{(0)}_{a_r,\dots}(p,\dots)|\hat{\mathbf{P}}^{(0)}_{q\bar{q}}(z_{r12},u_{1\perp};\varepsilon)|\mathcal{M}^{(0)}_{a_r,\dots}(p,\dots)\rangle\\
&\qquad- 4T_F\varepsilon z_{12}(1-z_{12})\,\langle\mathcal{M}^{(0)}_{a_r,\dots}(p,\dots)|\hat{\mathbf{P}}^{(0)}_{Pa_r g}\big(z_{r12},u_{1\perp},u_{3\perp}^{\mu}(\tilde{\phi}_2=0)\big)|\mathcal{M}^{(0)}_{a_r,\dots}(p,\dots)\rangle\Bigg]\,,
\end{aligned}
\tag{4.103}
$$

for quarks. In this case, splitting functions with a polarized reference gluon are needed $\hat{\mathbf{P}}^{(0)}_{Pa_rg}$. They read

$$\hat{P}^{(0),\,\mu\nu}_{Pgg}\left(z,k_\perp,\epsilon_1^\mu\right) = 2C_A\left[g^{\mu\nu}\frac{(\epsilon_1\cdot k_\perp)^2}{k_\perp^2}\left(\frac{1-z}{z}\right)+\left(\frac{z}{1-z}\right)\epsilon_1^\mu\epsilon_1^\nu - z(1-z)\frac{k_\perp^\mu k_\perp^\nu}{k_\perp^2}\right] , \tag{4.104}$$

$$\hat{P}^{(0),\,ss'}_{Pgq}\left(z,k_\perp,\epsilon_1^\mu\right) = \delta^{ss'}C_F\left[-2\frac{(\epsilon_1\cdot k_\perp)^2}{k_\perp^2}\left(\frac{1-z}{z}\right)+\frac{1}{2}z\right] , \tag{4.105}$$

where $\epsilon_1^\mu$ is a real polarization vector of the reference gluon.

## 4.5 Separation of finite contributions

In this section, the infrared structure of contributions to a next-to-next-to-leading order cross section is analyzed. In this discussion subtraction terms are included, that were obtained with the methods discussed so far in this chapter. Thus, all contributions are in principle integrable using Monte Carlo methods. Nevertheless, the contributions are separately divergent in the limit $\varepsilon \to 0$, since each part is given as a Laurent series having explicit poles up to order $\varepsilon^{-4}$. In order to understand how poles cancel among different parts, the pole structure of virtual contributions has to be discussed as well as the pole structure of integrated subtraction terms. The goal is to group contributions, that are independently finite. This separation is the main step to confine resolved momenta to four physical dimensions, which will be explained in section 4.6.
The infrared singular structure of a virtual renormalized amplitude factorizes into an operator acting on a vector in color space

$$|\mathcal{M}_n\rangle = \mathbf{Z}(\varepsilon,\{p_i\},\{m_i\},\mu_R)\,|\mathcal{F}_n\rangle\ . \tag{4.106}$$

The infrared renormalization constant $\mathbf{Z}$ contains all virtual poles in $\varepsilon$ and is given as a expansion in the strong coupling $\alpha_s$ (see appendix B.1). Expanding the above equation up to next-to-next-to-leading order accuracy, the virtual amplitudes are

$$|\mathcal{M}_n^{(0)}\rangle = |\mathcal{F}_n^{(0)}\rangle\ , \tag{4.107}$$

$$|\mathcal{M}_n^{(1)}\rangle = \mathbf{Z}^{(1)}|\mathcal{M}_n^{(0)}\rangle + |\mathcal{F}_n^{(1)}\rangle\ , \tag{4.108}$$

$$|\mathcal{M}_n^{(2)}\rangle = \left(\mathbf{Z}^{(2)} - \mathbf{Z}^{(1)}\mathbf{Z}^{(1)}\right)|\mathcal{M}_n^{(0)}\rangle + \mathbf{Z}^{(1)}|\mathcal{M}_n^{(1)}\rangle + |\mathcal{F}_n^{(2)}\rangle\ , \tag{4.109}$$

where the amplitudes $|\mathcal{F}_n^{(i)}\rangle$ are called finite remainders, as they are regular in the limit $\varepsilon \to 0$. The renormalization constants are uniquely defined, if they contain only poles in $\varepsilon$ and no finite contribution.

The different contributions to the cross section were discussed in section 3.2 and serve as a starting point to separate finite ingredients. The Born contribution to the cross section is finite by itself, since neither virtual poles nor phase space singularities occur. At next-to-leading order the real and virtual contributions are separated as

$$\hat{\sigma}^{\mathrm{R}} = \hat{\sigma}^{\mathrm{R}}_{\mathrm{F}} + \hat{\sigma}^{\mathrm{R}}_{\mathrm{U}}\ , \quad \hat{\sigma}^{\mathrm{V}} = \hat{\sigma}^{\mathrm{V}}_{\mathrm{F}} + \hat{\sigma}^{\mathrm{V}}_{\mathrm{U}}\ . \tag{4.110}$$

The subscript “F” stands for finite and describes contributions that are finite as $\varepsilon \to 0$. The subscript “U” indicates unresolved contributions that contain explicit poles. The finite contribution to the

real-radiation cross section is

$$\hat{\sigma}_{\mathrm{F}}^{\mathrm{R}} = \frac{1}{2\hat{s}}\frac{1}{N}\int \mathrm{d}\boldsymbol{\Phi}_{n+1}\left[\langle \mathcal{M}_{n+1}^{(0)}|\mathcal{M}_{n+1}^{(0)}\rangle\,\mathrm{F}_{n+1} + \text{subtraction terms}\right], \tag{4.111}$$

where the subtraction terms are obtained as discussed previously. The integrated subtraction terms are isolated into $\hat{\sigma}_{\mathrm{U}}^{\mathrm{R}}$. The virtual contribution is decomposed according to expansion (4.108)

$$\hat{\sigma}_{\mathrm{F}}^{\mathrm{V}} = \frac{1}{2\hat{s}}\frac{1}{N}\int \mathrm{d}\boldsymbol{\Phi}_{n}\,2\mathrm{Re}\,\langle \mathcal{M}_{n}^{(0)}|\mathcal{F}_{n}^{(1)}\rangle\,\mathrm{F}_{n}\,, \quad \hat{\sigma}_{\mathrm{U}}^{\mathrm{V}} = \frac{1}{2\hat{s}}\frac{1}{N}\int \mathrm{d}\boldsymbol{\Phi}_{n}\,2\mathrm{Re}\,\langle \mathcal{M}_{n}^{(0)}|\mathbf{Z}^{(1)}|\mathcal{M}_{n}^{(0)}\rangle\,\mathrm{F}_{n}\,. \tag{4.112}$$

Finite contributions are separated

$$\hat{\sigma}_{\mathrm{F}}^{\mathrm{R}}\,, \quad \hat{\sigma}_{\mathrm{F}}^{\mathrm{V}}\,, \quad \hat{\sigma}_{\mathrm{U}} = \hat{\sigma}_{\mathrm{U}}^{\mathrm{R}} + \hat{\sigma}_{\mathrm{U}}^{\mathrm{V}} + \hat{\sigma}^{\mathrm{C}}\,. \tag{4.113}$$

It is important to notice that the contribution $\hat{\sigma}_{\mathrm{U}}$ only contains matrix elements with $n$ partons. $n+1$ parton matrix elements are only present in $\hat{\sigma}_{\mathrm{F}}^{\mathrm{R}}$ which can be readily evaluated putting $\varepsilon \to 0$ before the integration is performed. At next-to-next-to-leading order the separation is more involved and matrix elements of different multiplicity and analytic structure are separated. The double-virtual contribution can be decomposed using formula (4.109)

$$\hat{\sigma}^{\mathrm{VV}} = \hat{\sigma}_{\mathrm{F}}^{\mathrm{VV}} + \hat{\sigma}_{\mathrm{FR}}^{\mathrm{VV}} + \hat{\sigma}_{\mathrm{DU}}^{\mathrm{VV}}\,, \tag{4.114}$$

where

$$\hat{\sigma}_{\mathrm{F}}^{\mathrm{VV}} = \frac{1}{2\hat{s}}\frac{1}{N}\int \mathrm{d}\boldsymbol{\Phi}_{n}\left[2\mathrm{Re}\,\langle \mathcal{M}_{n}^{(0)}|\mathcal{F}_{n}^{(2)}\rangle + \langle \mathcal{F}_{n}^{(1)}|\mathcal{F}_{n}^{(1)}\rangle\right]\mathrm{F}_{n}\,, \tag{4.115}$$

$$\hat{\sigma}_{\mathrm{FR}}^{\mathrm{VV}} = \frac{1}{2\hat{s}}\frac{1}{N}\int \mathrm{d}\boldsymbol{\Phi}_{n}\,2\mathrm{Re}\,\langle \mathcal{M}_{n}^{(0)}|\left(\mathbf{Z}^{(1)\,\dagger} + \mathbf{Z}^{(1)}\right)|\mathcal{F}_{n}^{(1)}\rangle\,\mathrm{F}_{n}\,, \tag{4.116}$$

$$\hat{\sigma}_{\mathrm{DU}}^{\mathrm{VV}} = \frac{1}{2\hat{s}}\frac{1}{N}\int \mathrm{d}\boldsymbol{\Phi}_{n}\left[2\mathrm{Re}\,\langle \mathcal{M}_{n}^{(0)}|\mathbf{Z}^{(2)}|\mathcal{M}_{n}^{(0)}\rangle + \langle \mathcal{M}_{n}^{(0)}|\mathbf{Z}^{(1)\,\dagger}\mathbf{Z}^{(1)}|\mathcal{M}_{n}^{(0)}\rangle\right]\mathrm{F}_{n}\,. \tag{4.117}$$

The subscript "FR" summarizes contributions that are proportional to the real part of the one-loop finite remainder, whereas the subscript "DU" means double-unresolved and states that poles are due to two unresolved partons, in this case these are two virtual partons. The real-virtual contribution is separated as follows

$$\hat{\sigma}^{\mathrm{RV}} = \hat{\sigma}_{\mathrm{F}}^{\mathrm{RV}} + \hat{\sigma}_{\mathrm{SU}}^{\mathrm{RV}} + \hat{\sigma}_{\mathrm{FR}}^{\mathrm{RV}} + \hat{\sigma}_{\mathrm{DU}}^{\mathrm{RV}}\,, \tag{4.118}$$

where the single contributions read

$$\hat{\sigma}_{\mathrm{F}}^{\mathrm{RV}} = \frac{1}{2\hat{s}}\frac{1}{N}\int \mathrm{d}\boldsymbol{\Phi}_{n+1}\left[2\mathrm{Re}\,\langle \mathcal{M}_{n+1}^{(0)}|\mathcal{F}_{n+1}^{(1)}\rangle\,\mathrm{F}_{n+1} + \text{subtraction terms}\right], \tag{4.119}$$

$$\hat{\sigma}_{\mathrm{SU}}^{\mathrm{RV}} = \frac{1}{2\hat{s}}\frac{1}{N}\int \mathrm{d}\boldsymbol{\Phi}_{n+1}\left[2\mathrm{Re}\,\langle \mathcal{M}_{n+1}^{(0)}|\mathbf{Z}^{(1)}|\mathcal{M}_{n+1}^{(0)}\rangle\,\mathrm{F}_{n+1} + \text{subtraction terms}\right]. \tag{4.120}$$

The subscript "SU" stands for single unresolved and in this case contain only virtual poles of the $n+1$ amplitude. The subtraction terms for the two contributions above can be derived explicitly and are given in appendix B.3.1 and B.3.2. Integrated subtraction terms containing real poles are merged into $\hat{\sigma}_{\mathrm{FR}}^{\mathrm{RV}}$ and $\hat{\sigma}_{\mathrm{DU}}^{\mathrm{RV}}$. Where in the former all contributions proportional to the $n$ particle one-loop finite reminder are gathered, while in the double-unresolved part all contributions proportional to

the $n$ particle tree-level amplitude are put together.
The double-real radiation contribution is separated into parts of similar origin

$$\hat{\sigma}^{\mathrm{RR}} = \hat{\sigma}^{\mathrm{RR}}_{\mathrm{F}} + \hat{\sigma}^{\mathrm{RR}}_{\mathrm{SU}} + \hat{\sigma}^{\mathrm{RR}}_{\mathrm{DU}} \,. \tag{4.121}$$

The finite part just contains the $n+2$ particle matrix element and all subtraction terms

$$\hat{\sigma}^{\mathrm{RR}}_{\mathrm{F}} = \frac{1}{2\hat{s}}\frac{1}{N}\int \mathrm{d}\boldsymbol{\Phi}_{n+2}\left[\langle \mathcal{M}^{(0)}_{n+2}|\mathcal{M}^{(0)}_{n+2}\rangle\,\mathrm{F}_{n+2} + \text{subtraction terms}\right] . \tag{4.122}$$

This contribution can be evaluated in four dimensions already. The integrated subtraction terms are arranged into two classes. The single-unresolved (SU) class contains poles that are due to limits as one parton vanishes. It contains therefore $n+1$ particle matrix elements as well as subtraction terms for the remaining unresolved parton. The pole terms can be read from Tab. 4.4 and are listed in Tab. 4.5. The double unresolved contribution contains all poles terms, due to both unresolved particles vanishing. Only $n$ parton matrix elements are present.

Finally, collinear subtraction contributions are decomposed according to matrix elements, that appear in different parts of these contributions. The cross section $\hat{\sigma}^{\mathrm{C1}}$ in Eq. (3.24) is the convolution of the leading order splitting function and the real radiation cross section in a next-to-leading order cross section. Hence, it can be decomposed as shown in Eq. (4.110). The finite contribution $\hat{\sigma}^{\mathrm{R}}_{\mathrm{F}}$ corresponds to a single unresolved contribution $\hat{\sigma}^{\mathrm{C1}}_{\mathrm{SU}}$, since an explicit pole is already present in the collinear factorization formula. This is interpreted as arising in the collinear limit of the first unresolved parton. Similarly, the unresolved contribution $\hat{\sigma}^{\mathrm{R}}_{\mathrm{U}}$ containing integrated subtraction terms leads to a double unresolved contribution $\hat{\sigma}^{\mathrm{C1}}_{\mathrm{DU}}$. The cross section $\hat{\sigma}^{\mathrm{C2}}$ in (3.24) contains the virtual contribution of the next-to-leading order cross section $\hat{\sigma}^{\mathrm{V}}$ which can be separated into the finite remainder contribution and the pole term. The latter is a double unresolved contribution, taking into account the convolution with a splitting function. The other parts in $\hat{\sigma}^{\mathrm{C2}}$ contain only convolutions of Born level cross sections and splitting functions, each contribution is therefore also interpreted as double-unresolved. The decomposition of the collinear factorization is finally

$$\hat{\sigma}^{\mathrm{C1}} = \hat{\sigma}^{\mathrm{C1}}_{\mathrm{SU}} + \hat{\sigma}^{\mathrm{C1}}_{\mathrm{DU}} \,, \quad \hat{\sigma}^{\mathrm{C2}} = \hat{\sigma}^{\mathrm{C2}}_{\mathrm{FR}} + \hat{\sigma}^{\mathrm{C2}}_{\mathrm{DU}} \,. \tag{4.123}$$

By merging similar parts, the following cross sections are defined

$$\begin{aligned} \hat{\sigma}_{\mathrm{FR}} &= \hat{\sigma}^{\mathrm{RV}}_{\mathrm{FR}} + \hat{\sigma}^{\mathrm{VV}}_{\mathrm{FR}} + \hat{\sigma}^{\mathrm{C2}}_{\mathrm{FR}} \,, \quad \hat{\sigma}_{\mathrm{SU}} = \hat{\sigma}^{\mathrm{RR}}_{\mathrm{SU}} + \hat{\sigma}^{\mathrm{RV}}_{\mathrm{SU}} + \hat{\sigma}^{\mathrm{C1}}_{\mathrm{SU}} \,, \\ \hat{\sigma}_{\mathrm{DU}} &= \hat{\sigma}^{\mathrm{RR}}_{\mathrm{DU}} + \hat{\sigma}^{\mathrm{RV}}_{\mathrm{DU}} + \hat{\sigma}^{\mathrm{VV}}_{\mathrm{DU}} + \hat{\sigma}^{\mathrm{C1}}_{\mathrm{DU}} + \hat{\sigma}^{\mathrm{C2}}_{\mathrm{DU}} \,. \end{aligned} \tag{4.124}$$

At this point it is instructive to discuss which contributions are finite separately. Obviously, $\hat{\sigma}^{\mathrm{RR}}_{\mathrm{F}}$, $\hat{\sigma}^{\mathrm{RV}}_{\mathrm{F}}$ and $\hat{\sigma}^{\mathrm{VV}}_{\mathrm{F}}$ are finite. By the KLN theorem, the full next-to-next-to-leading order cross section is finite and therefore the sum $\hat{\sigma}_{\mathrm{FR}} + \hat{\sigma}_{\mathrm{SU}} + \hat{\sigma}_{\mathrm{DU}}$ must be finite. In [211] it has been proven that $\hat{\sigma}_{\mathrm{FR}}$ is independently finite, which can be understood directly: The integrated subtraction terms only contain leading order splitting and soft functions, while virtual poles are only due to $\mathbf{Z}^{(1)}$. This is the same pattern that occurs in the next-to-leading order cross section, which is certainly finite. In conclusion, since $\hat{\sigma}_{\mathrm{FR}}$ is finite, $\hat{\sigma}_{\mathrm{SU}} + \hat{\sigma}_{\mathrm{DU}}$ has to be finite.
Unfortunately, this separation is not sufficient to formulate the subtraction scheme in 't Hooft-Veltman regularization, since in $\hat{\sigma}_{\mathrm{SU}}$ only one parton is unresolved and in $\hat{\sigma}_{\mathrm{DU}}$ two partons are unresolved. Parameterizing the two contributions differently will spoil the cancellation of infrared poles. It is thus necessary to render the two contributions separately finite, such that the full

| | $\mathcal{S}_1$ | $\mathcal{S}_2$ | $\mathcal{S}_3$ | $\mathcal{S}_4$ | $\mathcal{S}_5$ | $\mathcal{S}_6$ |
|---|---|---|---|---|---|---|
| double-pole | $(\eta_2,\xi_2)$ | | | $(\eta_2,\xi_2)$ | $(\eta_1,\xi_2)$ | $(\eta_2,\xi_2)$ |
| single-pole | $\eta_2,\xi_2$ | $\xi_2$ | $\eta_1$ | $\eta_2,\xi_2$ | $\eta_1,\xi_2$ | $\eta_1,\eta_2,\xi_2$ |

**Table 4.5:** Poles taken in the sector variables that contribute to $\hat{\sigma}^{\mathrm{RR}}_{\mathrm{SU}}$. The the remaining poles contribute to $\hat{\sigma}^{\mathrm{RR}}_{\mathrm{DU}}$.

next-to-next-to-leading order cross section contains the finite parts summarized in Tab. 4.6.

| | |
|---|---|
| LO | $\hat{\sigma}^{B}$ |
| NLO | $\hat{\sigma}^{\mathrm{R}}_{\mathrm{F}}\,,\quad \hat{\sigma}^{\mathrm{V}}_{\mathrm{F}}\,,\quad \hat{\sigma}_{\mathrm{U}}=\hat{\sigma}^{\mathrm{R}}_{\mathrm{U}}+\hat{\sigma}^{\mathrm{V}}_{\mathrm{U}}+\hat{\sigma}^{\mathrm{C}}$ |
| NNLO | $\hat{\sigma}^{\mathrm{RR}}_{\mathrm{F}}\,,\quad \hat{\sigma}^{\mathrm{RV}}_{\mathrm{F}}\,,\quad \hat{\sigma}^{\mathrm{VV}}_{\mathrm{F}}\,,\quad \hat{\sigma}_{\mathrm{FR}}=\hat{\sigma}^{\mathrm{RV}}_{\mathrm{FR}}+\hat{\sigma}^{\mathrm{VV}}_{\mathrm{FR}}+\hat{\sigma}^{\mathrm{C2}}_{\mathrm{FR}}\,,$ |
| | $\hat{\sigma}_{\mathrm{SU}}=\hat{\sigma}^{\mathrm{RR}}_{\mathrm{SU}}+\hat{\sigma}^{\mathrm{RV}}_{\mathrm{SU}}+\hat{\sigma}^{\mathrm{C1}}_{\mathrm{SU}}\,,\quad \hat{\sigma}_{\mathrm{DU}}=\hat{\sigma}^{\mathrm{RR}}_{\mathrm{DU}}+\hat{\sigma}^{\mathrm{RV}}_{\mathrm{DU}}+\hat{\sigma}^{\mathrm{VV}}_{\mathrm{DU}}+\hat{\sigma}^{\mathrm{C1}}_{\mathrm{DU}}+\hat{\sigma}^{\mathrm{C2}}_{\mathrm{DU}}$ |

**Table 4.6:** Separately finite contributions to a next-to-next-to-leading order cross section calculation. The definitions for the contributions can be found in the main text.

### 4.5.1 Separation of single- and double-unresolved contributions

In order to obtain a finite result for the single-unresolved and double-unresolved contribution independently the structure of pole cancellation has to be examined. It is sufficient to find suitable counterterms to the single-unresolved contribution and make it finite, since the same counterterms will provide a finite result for the double-unresolved contribution. Therefore, the three contributions of $\hat{\sigma}^{\mathrm{RR}}_{\mathrm{SU}}$, $\hat{\sigma}^{\mathrm{RV}}_{\mathrm{SU}}$ and $\hat{\sigma}^{\mathrm{C1}}_{\mathrm{SU}}$ are investigated. Each contribution consists of a main term that contains the $n+1$ particle matrix element and suitable subtraction terms that provide subtractions due to the additional parton becoming soft or collinear. If the next-to-next-to-leading order measurement function for the observable containing $n$ partons in the final state is replaced by a next-to-leading order measurement function for $n+1$ partons in each of the three contributions, only the main term will remain. The subtraction terms vanish, since they describe two unresolved partons, which is not allowed by the measurement function. In the sum of all contributions to $\hat{\sigma}_{\mathrm{SU}}$ the poles will cancel, since effectively it is a next-to-leading order calculation. The single unresolved cross section corresponds to the unresolved cross section $\hat{\sigma}_U$.

Hence, going back to the next-to-next-to-leading order case, poles among the unsubtracted term cancel, whereas poles among subtraction terms do not cancel. This is because of the different parameterizations used in $\hat{\sigma}^{\mathrm{RV}}_{\mathrm{SU}}$ and $\hat{\sigma}^{\mathrm{RR}}_{\mathrm{SU}}$ [1]. The real-virtual contribution is given in the single-collinear parameterization described in section 4.2.1. In general it can be written in form of the two relevant parameters

$$\iint_0^1 \frac{\mathrm{d}\eta}{\eta^{1+a\varepsilon}}\frac{\mathrm{d}\xi}{\xi^{1+b\varepsilon}}\Big(f(\eta,\xi)-f(0,\xi)-f(\eta,0)+f(0,0)\Big)\,. \tag{4.125}$$

1 The poles due to final state limits are discussed first. The discussion of initial state poles, including $\hat{\sigma}^{\mathrm{C1}}_{\mathrm{SU}}$, will be provided afterwards.

The main term $f(\eta,\xi)$, which is the unsubtracted contribution, contains the operator $\mathbf{Z}^{(1)}$ and the corresponding matrix element. The remaining terms in Eq. (4.125) are subtraction terms in the two physical variables $\xi$ and $\eta$, which are integrated over the full unit square. The double-real contribution is either given in the triple-collinear parameterization (section 4.2.2) or the double collinear parameterization (section 4.2.3). It contains double pole and single pole terms as summarized in Tab. 4.5. The double pole terms are of the form

$$\iint_0^1 \frac{\mathrm{d}\eta_1}{\eta_1^{1+a\varepsilon}} \frac{\mathrm{d}\xi_1}{\xi_1^{1+b\varepsilon}} \Big( g(\eta_1,\xi_1) - g(0,\xi_1) - g(\eta_1,0) + g(0,0) \Big) \,. \tag{4.126}$$

The sector variables $\eta_1$ and $\xi_1$ in this case, correspond directly to the physical variables as can be verified in Tab. 4.2. Therefore, they correspond directly to the variables $\eta$ and $\xi$ in the real-virtual contribution and are also integrated over the full unit square. Thus, not only the double pole in $g(\eta_1,\xi_2)$ will cancel the double pole in $f(\eta,\xi)$ but also the double poles of the subtraction terms of $g$ will cancel the the double poles of the subtraction terms of $f$, since they are generated in the same variables integrated over the full integration region.
The single pole contributions turn out to be the bottleneck in this discussion. In general the single pole contribution of $\hat{\sigma}_{\mathrm{SU}}^{\mathrm{RR}}$ has the following form

$$\begin{aligned}\iiint_0^1 \frac{\mathrm{d}y}{y^{1+a\varepsilon}} \frac{\mathrm{d}x_1}{x_1^{1+b_1\varepsilon}} \frac{\mathrm{d}x_2}{x_2^{1+b_2\varepsilon}} \Bigg\{ \Bigg[ \Big( g(y,x_1,x_2) - g(y,x_1,0) \Big) - \Big( g(0,x_1,x_2) - g(0,x_1,0) \Big) \Bigg] \\ - \Bigg[ \Big( g(y,0,x_2) - g(0,0,x_2) \Big) - \Big( g(y,0,0) - g(0,0,0) \Big) \Bigg] \Bigg\} \,.\end{aligned} \tag{4.127}$$

Depending on the sector $\{y,x_1,x_2\} \subset \{\eta_1,\eta_2,\xi_1,\xi_2\}$, where the explicit pole has been taken in the remaining variable $\{\eta_1,\eta_2,\xi_1,\xi_2\} \setminus \{y,x_1,x_2\}$. One of the variables can be identified with $\eta$ or $\xi$ directly. It will be denoted by $y$. In general there is no direct correspondence between one of the remaining variables $\{x_1,x_2\}$ and $x$, where $x = \eta$, if $y = \xi$ and vice versa. Thus, in general $x$ is a functions of the two variables

$$x = x(x_1,x_2) \,. \tag{4.128}$$

It is instructive to understand why the single poles do not cancel. The origin is the sector decomposition of the triple-collinear and the double-collinear sector. The space spanned by the physical variables $\{\hat{\eta}_1,\hat{\eta}_2,\hat{\xi}_1,\hat{\xi}_2\}$ would have a one-to-one correspondence to the space spanned by $\{\eta,\xi\}$ in the real-virtual contribution. But after introducing additional sectors the space is spanned by sector variables $\{\eta_1,\eta_2,\xi_1,\xi_2\}$. Only afterwards subtraction terms are generated, that are minimal in the sector variables. Different sectors take into account different limits and a specific subtraction term will in general only appear in some or only one of the given sectors. If those terms are reexpressed in the physical variables, which correspond to $\{\eta,\xi\}$ directly, the subtraction term is not necessarily the minimal one in those variables. Additionally the integration range is not necessarily the unit square anymore. To obtain a finite result, this has to be compensated by appropriate counterterms. The derivation of these counterterms follows the same pattern. Firstly, subtraction terms in (4.127) that need to be corrected are identified. Secondly, the integral is reexpressed in terms of $y$ and $x$ and finally, the limit $x \to 0$ of the term is inspected to identify the minimal subtraction term and the missing integration region.
The list of pole terms that have to be considered are listed in Tab. 4.7.

| | Case I | | | Case II | Case III | | Case Initial | |
|---|---|---|---|---|---|---|---|---|
| Sector | $\mathcal{S}_4$ | $\mathcal{S}_5$ | $\mathcal{S}_5$ | $\mathcal{S}_2$ | $\mathcal{S}_3$ | $\mathcal{S}_6$ | $\mathcal{S}_3$ | $\mathcal{S}_6$ |
| Pole | $\eta_2$ | $\eta_1$ | $\xi_2$ | $\xi_2$ | $\eta_1$ | $\eta_1$ | $\eta_1$ | $\eta_1$ |

**Table 4.7:** Single pole terms in $\hat{\sigma}^{\mathrm{RR}}_{\mathrm{SU}}$ for which counterterms are derived. Four cases are identified, that have to be treated separately.

### Case I

The pattern of the first case is outlined in the following. The relation between the variables is assumed to be

$$x = x_1\big(1 + c(x_1)x_2\big) \;, \quad c'(0) = 0 \;, \tag{4.129}$$

where c is a function. Subtraction terms in (4.127), in which $x_2 = 0$ do not require any modifications since $x = x_1$. As discussed previously the leading term

$$g(y,x_1,x_2) - g(y,x_1,0) \;, \tag{4.130}$$

is correct by the vanishing of the next-to-leading order cross section. Hence, the relevant term is

$$h(x_2) = -\Big(g(y,0,x_2) - g(0,0,x_2)\Big) \;. \tag{4.131}$$

If only the integrations of $x_1$ and $x_2$ are explicitly written, the integral is rewritten in terms of $x$ as

$$\iint_0^1 \frac{\mathrm{d}x_1}{x_1^{1+b_1\varepsilon}} \frac{\mathrm{d}x_2}{x_2^{1+b_2\varepsilon}}\, h(x_2) = \int_0^1 \frac{\mathrm{d}x}{x^{1+b_1\varepsilon}} \int_0^{x_{2\,\max}(x)} \frac{\mathrm{d}x_2}{x_2^{1+b_2\varepsilon}} \left[\frac{\mathrm{d}x_1}{\mathrm{d}x}(x,x_2) \left(\frac{x}{x_1(x,x_2)}\right)^{1+b_1\varepsilon}\right] h(x_2) \;, \tag{4.132}$$

where

$$x_{2\,\max}(0) = 1 \;. \tag{4.133}$$

The integrand on the right hand side has to be taken in the limit $x \to 0$ to get the contribution that matches the real-virtual subtraction term

$$\lim_{x\to 0} \int_0^{x_{2\,\max}(x)} \frac{\mathrm{d}x_2}{x_2^{1+b_2\varepsilon}} \left[\frac{\mathrm{d}x_1}{\mathrm{d}x}(x,x_2) \left(\frac{x}{x_1(x,x_2)}\right)^{1+b_1\varepsilon}\right] h(x_2) = \int_0^1 \frac{\mathrm{d}x_2}{x_2^{1+b_2\varepsilon}} \big(1 + c(0)x_2\big)^{b_1\varepsilon}\, h(x_2) \;. \tag{4.134}$$

Hence, the correct counterterm is given by the difference of the term and its limit

$$\int_0^1 \frac{\mathrm{d}x}{x^{1+b_1\varepsilon}} \Bigg\{ \int_0^1 \frac{\mathrm{d}x_2}{x_2^{1+b_2\varepsilon}} \big(1 + c(0)x_2\big)^{b_1\varepsilon}\, h(x_2) - \int_0^{x_{2\,\max}(x)} \frac{\mathrm{d}x_2}{x_2^{1+b_2\varepsilon}} \left[\frac{\mathrm{d}x_1}{\mathrm{d}x}(x,x_2) \left(\frac{x}{x_1(x,x_2)}\right)^{1+b_1\varepsilon}\right] h(x_2) \Bigg\} \;. \tag{4.135}$$

Changing the order of integration the integral over $x$ is performed explicitly which leads to the counterterm

$$\int_0^1 \frac{\mathrm{d}x_2}{x_2^{1+b_2\varepsilon}}\, \Delta(x_2)\, h(x_2)\ , \tag{4.136}$$

where restoring the original form it reads

$$-\iint_0^1 \frac{\mathrm{d}y}{y^{1+a\varepsilon}} \frac{\mathrm{d}x_2}{x_2^{1+b_2\varepsilon}}\, \Delta(x_2)\, \big(g(y,0,x_2) - g(0,0,x_2)\big)\ . \tag{4.137}$$

This term is added to the single unresolved contribution and subtracted from the double unresolved contribution. The result depends in general on the scaling of the variables $x_1$ and $x_2$, given by $b_1$ and $b_2$. The scaling is directly obtained from the triple-collinear and double-collinear measures given in Tab. 4.3 and section 4.2.3 respectively. These scalings are correct in CDR and are used for the counterterms of the double unresolved contributions. However, if the scheme is reformulated in the 't Hooft-Veltman regularization, it will be different for the counterterm of the single-unresolved contribution, since one of the resolved partons is treated in four dimensions. The exact procedure how to obtain the correct scaling will be outlined in section 4.6. Nevertheless, the scaling for both schemes will be given for each counterterm.

The triple-collinear sector $\mathcal{S}_4$ follows case I, if the collinear pole in $\eta_2$ is considered. The relation between the variables is

$$y = \eta_1\ , \quad x_1 = \xi_1\ , \quad x_2 = \xi_2\ , \tag{4.138}$$

while $\xi$ corresponds to

$$x = x_1\big(1 + x_2 \min(1, 1/x_1 - 1)\big)\ . \tag{4.139}$$

The counterterm can be calculated and reads

$$\Delta_{\mathcal{S}_4}^{\eta_2} = \frac{1 - (1+\xi_2)^{b_1\varepsilon}}{b_1\varepsilon}\ , \tag{4.140}$$

with

$$b_1^{\mathrm{CDR}} = 4\ , \quad b_1^{\mathrm{HV}} = 2\ . \tag{4.141}$$

The single pole due to $\eta_1$ in sector $\mathcal{S}_5$ is treated in exactly the same way, resulting in the same counterterm

$$\Delta_{\mathcal{S}_5}^{\eta_1} = \Delta_{\mathcal{S}_4}^{\eta_2}\ . \tag{4.142}$$

The last contribution that is covered in case I is sector $\mathcal{S}_5$, if the pole is taken in $\xi_2$. The correspondence between the variables is

$$y = \xi_1\ , \quad x_1 = \eta_2\ , \quad x_2 = \eta_1\ , \tag{4.143}$$

with

$$x = x_1\Big(1 - \frac{x_2}{2}\Big)\ . \tag{4.144}$$

Following the pattern outlined for case I the counterterm can be derived and reads

$$\Delta_{\mathcal{S}_5}^{\xi_2} = \frac{1 - \Big(1 - \frac{\eta_1}{2}\Big)^{b_1\varepsilon}}{b_1\varepsilon}\ , \tag{4.145}$$

with the scaling

$$b_1^{\mathrm{CDR}} = 2\,, \quad b_1^{\mathrm{HV}} = 1\,. \tag{4.146}$$

Case II

The pole in $\xi_2$ in sector $\mathcal{S}_2$ is considered. The unsubtracted contribution only contains the term $g(y,x_1,x_2)$, where the variables are identified to be

$$y = \xi_1\,, \quad x_1 = \eta_1\,, \quad x_2 = \eta_2\,, \quad x = \frac{1}{2}x_1x_2\,. \tag{4.147}$$

It is important to notice that $x(x_1,x_2)$ is symmetric in its arguments. Hence, subtraction terms that contain $x_1$ and $x_2$ have to be considered. The derivation can be done for one variable, say $x_2$. Using the symmetry the whole counterterm can be obtained. The integral can be reparameterized in terms of $x(x_1,x_2)$

$$\iint_0^1 \frac{\mathrm{d}x_1}{x_1^{1+b_1\varepsilon}} \frac{\mathrm{d}x_2}{x_2^{1+b_2\varepsilon}}\, h(x_2) = \int_0^{1/2} \frac{\mathrm{d}x}{x^{1+b_1\varepsilon}} \int_{2x}^1 \frac{\mathrm{d}x_2}{x_2^{1+b_2\varepsilon}} \left(\frac{x_2}{2}\right)^{b_1\varepsilon} h(x_2)\,, \tag{4.148}$$

where $h(x_2)$ summarizes all $x_2$ dependant terms in Eq. (4.127). The parameter $x$ is only integrated in the range [0,1/2] and the second integral still depends on $x$ through the lower boundary of $x_2$. First, the correct behavior as $x \to 0$ is determined by rewriting the above equation as

$$\begin{aligned}\int_0^{1/2} \frac{\mathrm{d}x}{x^{1+b_1\varepsilon}} \Bigg[ &\int_{2x}^1 \frac{\mathrm{d}x_2}{x_2^{1+b_2\varepsilon}} \left(\frac{x_2}{2}\right)^{b_1\varepsilon} h(0) + \int_0^1 \frac{\mathrm{d}x_2}{x_2^{1+b_2\varepsilon}} \left(\frac{x_2}{2}\right)^{b_1\varepsilon} \big(h(x_2) - h(0)\big) \\ &- \int_0^{2x} \frac{\mathrm{d}x_2}{x_2^{1+b_2\varepsilon}} \left(\frac{x_2}{2}\right)^{b_1\varepsilon} \big(h(x_2) - h(0)\big) \Bigg]\,. \end{aligned} \tag{4.149}$$

The first two terms have the correct scaling behavior in the limit $x \to 0$, but need to be integrated in the full range $x \in [0,1/2]$. The last term needs to be removed. Both manipulations are achieved by one counterterm of the form

$$\begin{aligned}\int_{1/2}^1 \frac{\mathrm{d}x}{x^{1+b_1\varepsilon}} \Bigg[ &\int_{2x}^1 \frac{\mathrm{d}x_2}{x_2^{1+b_2\varepsilon}} \left(\frac{x_2}{2}\right)^{b_1\varepsilon} h(0) + \int_0^1 \frac{\mathrm{d}x_2}{x_2^{1+b_2\varepsilon}} \left(\frac{x_2}{2}\right)^{b_1\varepsilon} \big(h(x_2) - h(0)\big) \Bigg] \\ &+ \int_0^{1/2} \frac{\mathrm{d}x}{x^{1+b_1\varepsilon}} \int_0^{2x} \frac{\mathrm{d}x_2}{x_2^{1+b_2\varepsilon}} \left(\frac{x_2}{2}\right)^{b_1\varepsilon} \big(h(x_2) - h(0)\big)\,. \end{aligned} \tag{4.150}$$

The first term can be integrated explicitly, while the rest is further simplified. Taking into account the contribution of $x_1 \leftrightarrow x_2$ the whole counterterm reads in the original variables

$$\begin{aligned} -\frac{1}{b_1 b_2 \varepsilon^2} &\frac{\left(2^{-b_2\varepsilon}-1\right) b_1 - \left(2^{-b_1\varepsilon}-1\right) b_2}{b_1 - b_2} \int_0^1 \frac{\mathrm{d}\xi_1}{\xi_1^{1+a\varepsilon}} \big(g(\xi_1,0,0) - g(0,0,0)\big) \\ &- \iint_0^1 \frac{\mathrm{d}\xi_1}{\xi_1^{1+a\varepsilon}} \frac{\mathrm{d}\eta_1}{\eta_1^{1+b_1\varepsilon}} \frac{1-\left(\frac{\eta_1}{2}\right)^{b_2\varepsilon}}{b_2\varepsilon} \big(g(\xi_1,\eta_1,0) - g(\xi_1,0,0) - g(0,\eta_1,0) + g(0,0,0)\big) \\ &- \iint_0^1 \frac{\mathrm{d}\xi_1}{\xi_1^{1+a\varepsilon}} \frac{\mathrm{d}\eta_2}{\eta_2^{1+b_2\varepsilon}} \frac{1-\left(\frac{\eta_2}{2}\right)^{b_1\varepsilon}}{b_1\varepsilon} \big(g(\xi_1,0,\eta_2) - g(\xi_1,0,0) - g(0,0,\eta_2) + g(0,0,0)\big)\,, \end{aligned} \tag{4.151}$$

where the scaling is given by

$$b_1^{\mathrm{CDR}} = 3 \;, \quad b_2^{\mathrm{CDR}} = 2 \;, \quad b_1^{\mathrm{HV}} = 2 \;, \quad b_2^{\mathrm{HV}} = 1 \;. \tag{4.152}$$

Case III

This case examines the pole due to $\eta_1$ and in sector $\mathcal{S}_3$ and sector $\mathcal{S}_6$. The unresolved parton with momentum $u_1$ is collinear to the reference parton $r$, which is $r$ in the triple-collinear sector and $r_1$ in the double-collinear sector. The variables are

$$y = \eta_2 \;, \quad x_1 = \xi_2 \;, \quad x_2 = \xi_1 \;. \tag{4.153}$$

In order to compare to the real-virtual contribution, the reference parton has to be the collinear parton with momentum

$$r' = r + u_1 \;, \tag{4.154}$$

since the collinear limit has been taken already. It is easier to use rescaled variables

$$r^0 = E_{\max}\, \xi_r\, \xi_{r\,\max} \;, \quad r'^0 = E_{\max}\, \xi_{r'}\, \xi_{r'\,\max} \;, \tag{4.155}$$

where $\xi_{r\,\max}$ denotes the maximum of $r^0/E_{\max}$ and $\xi_{r'\,\max}$ the maximum of $r'^0/E_{\max}$. In this case the reference momentum in $\hat{\sigma}_{\mathrm{SU}}^{\mathrm{RV}}$ and $\hat{\sigma}_{\mathrm{SU}}^{\mathrm{RR}}$ has to be taken into account, hence the energy integration is taken into account explicitly

$$g(y,x_1,x_2) = \int_0^1 \mathrm{d}\xi_r\, h(\xi_r,y,x_1,x_2) \;. \tag{4.156}$$

The derivation is simplified by noticing that two subtraction terms cancel

$$h(\xi_r,y,x_1,0) - h(\xi_r,y,0,0) = 0 \;. \tag{4.157}$$

Additionally, only corrections to the subtraction term $h(\xi_r,y,0,x_2)$ are considered. Corrections to $h(\xi_r,0,0,x_2)$ can be obtained from the first in the limit $y \to 0$. For $x_1 = 0$ there is

$$\xi_{r\,\max}\big|_{x_1=0} = 1 - x_2 \;, \quad \xi_{r'\,\max}\big|_{x_1=0} = 1 \;. \tag{4.158}$$

The relation between the double-real variables and the variables in the real-virtual contribution is given by

$$x = x_1 x_2 x_{2\,\max}(x_2) \;, \quad \xi_{r'} = \xi_r + (1-\xi_r)x_2 \;, \tag{4.159}$$

where

$$x_{2\,\max}(x_2) = \min\left[1,\, \frac{1}{x_2}\frac{1-x_2}{1-\frac{E_{\max}}{\sqrt{\hat{s}}}\left(\hat{u}_1\cdot\hat{u}_2\right)x_2}\right] \;. \tag{4.160}$$

Another variable is introduced

$$\bar{z} = \frac{x_2}{\xi_r + (1-\xi_r)x_2} \;, \tag{4.161}$$

which specifies the soft limit of the unresolved parton of momentum $u_1$, as $\bar{z} \to 0$. The scalar product $\hat{u}_1 \cdot \hat{u}_2$ in (4.160) is equal to $2y$ in the triple-collinear sector, while in the double-collinear

sector it is some function of $y$. It is therefore convenient to define

$$y' = \frac{E_{\max}}{\sqrt{\hat{s}}} \left(\hat{u}_1 \cdot \hat{u}_2\right) \in [0,1] \,, \quad x_{\max} = \frac{1}{1+\sqrt{1-y'}} \,, \tag{4.162}$$

such that

$$x_2 \in [0, x_{\max}] \;\Rightarrow\; x_{2\,\max}(x_2) = 1 \,, \quad x_2 \in [x_{\max}, 1] \;\Rightarrow\; x_{2\,\max}(x_2) = \frac{1}{x_2}\frac{1-x_2}{1-y'x_2} \,. \tag{4.163}$$

At this stage, it is possible to reparameterize the whole integral

$$\begin{aligned}
&\iiiint_0^1 \mathrm{d}\xi_r \frac{\mathrm{d}y}{y^{1+a\varepsilon}} \frac{\mathrm{d}x_1}{x_1^{1+b_1\varepsilon}} \frac{\mathrm{d}x_2}{x_2^{1+b_2\varepsilon}} \, h(\xi_r,y,0,x_2) = \\
&\qquad \iiint_0^1 \frac{\mathrm{d}y}{y^{1+a\varepsilon}} \, \mathrm{d}\xi_{r'} \frac{\mathrm{d}\bar{z}}{\bar{z}^{1+(b_2-b_1)\varepsilon}} \int_0^{\xi_{r'}\bar{z}\,x_{2\,\max}(\xi_{r'}\bar{z})} \frac{\mathrm{d}x}{x^{1+b_1\varepsilon}} \, \xi_{r'}^{(b_1-b_2)\varepsilon} \left(x_{2\,\max}(\xi_{r'}\bar{z})\right)^{b_1\varepsilon} \\
&\qquad\qquad \times \frac{1}{1-\xi_{r'}\bar{z}} \, h\left(\frac{\xi_{r'}(1-\bar{z})}{1-\xi_{r'}\bar{z}}, y, 0, \xi_{r'}\bar{z}\right) = \\
&\qquad\qquad \iiint_0^1 \frac{\mathrm{d}y}{y^{1+a\varepsilon}} \, \mathrm{d}\xi_{r'} \frac{\mathrm{d}\bar{z}}{\bar{z}^{1+(b_2-b_1)\varepsilon}} \int_0^{\xi_{r'}\bar{z}\,x_{2\,\max}(\xi_{r'}\bar{z})} \frac{\mathrm{d}x}{x^{1+b_1\varepsilon}} \, \tilde{h}(\xi_{r'},y,\bar{z}) \,,
\end{aligned} \tag{4.164}$$

where $\tilde{h}$ is just a shorthand notation for the integrand. The order of integration has to be as follows

$$\int \mathrm{d}x \int \mathrm{d}\xi_{r'} \int \mathrm{d}\bar{z} \,, \tag{4.165}$$

to allow for comparison with $\hat{\sigma}^{\mathrm{RV}}_{\mathrm{SU}}$. The integration over $y$ can be safely neglected, since it is not relevant for the discussion. Writing the integral in the demanded order it reads

$$\begin{aligned}
&\iint_0^1 \mathrm{d}\xi_{r'} \frac{\mathrm{d}\bar{z}}{\bar{z}^{1+(b_2-b_1)\varepsilon}} \int_0^{\xi_{r'}\bar{z}\,x_{2\,\max}(\xi_{r'}\bar{z})} \frac{\mathrm{d}x}{x^{1+b_1\varepsilon}} \, \tilde{h}(\xi_{r'},y,\bar{z}) = \\
&\qquad \int_0^{x_{\max}} \frac{\mathrm{d}x}{x^{1+b_1\varepsilon}} \left[ \int_x^1 \mathrm{d}\xi_{r'} \int_{x/\xi_{r'}}^{\min(1,x_{\max}/\xi_{r'})} \frac{\mathrm{d}\bar{z}}{\bar{z}^{1+(b_2-b_1)\varepsilon}} \right. \\
&\qquad\qquad \left. + \int_{x_{\max}}^1 \mathrm{d}\xi_{r'} \int_{x_{\max}/\xi_{r'}}^{\min\left(1,\frac{1}{\xi_{r'}}\frac{1-x}{1-y'x}\right)} \frac{\mathrm{d}\bar{z}}{\bar{z}^{1+(b_2-b_1)\varepsilon}} \right] \tilde{h}(\xi_{r'},y,\bar{z}) \,.
\end{aligned} \tag{4.166}$$

As in the previous cases the limit $x \to 0$ has to be examined and the integration range extended to [0,1]. The result reads

$$\begin{aligned}
&\int_0^1 \frac{\mathrm{d}x}{x^{1+b_1\varepsilon}} \int_0^1 \mathrm{d}\xi_{r'} \left[ \int_{x/\xi_{r'}}^{\min(1,x_{\max}/\xi_{r'})} \frac{\mathrm{d}\bar{z}}{\bar{z}^{1+(b_2-b_1)\varepsilon}} \, \tilde{h}(\xi_{r'},y,0) \right. \\
&\left. + \int_0^{\min(1,x_{\max}/\xi_{r'})} \frac{\mathrm{d}\bar{z}}{\bar{z}^{1+(b_2-b_1)\varepsilon}} \left(\tilde{h}(\xi_{r'},y,\bar{z}) - \tilde{h}(\xi_{r'},y,0)\right) + \int_{\min(1,x_{\max}/\xi_{r'})}^1 \frac{\mathrm{d}\bar{z}}{\bar{z}^{1+(b_2-b_1)\varepsilon}} \, \tilde{h}(\xi_{r'},y,\bar{z}) \right] .
\end{aligned} \tag{4.167}$$

The function is not singular as $\xi_{r'} = 0$, due to a selector function present in $\tilde{h}$. The counterterm is the difference between (4.167) and (4.166). After some simplification and returning to the original variables the full counterterm reads

$$-\iint_0^1 \frac{\mathrm{d}\eta_2}{\eta_2^{1+a\varepsilon}} \frac{\mathrm{d}\xi_1}{\xi_1^{1+b_2\varepsilon}} \frac{1}{b_1\varepsilon} \Big[ \Big(1 - \big(\xi_1 \xi_{2\,\max}(\xi_1,\eta_2)\big)^{b_1\varepsilon}\Big)\, g(\eta_2,0,\xi_1) - \big(1-\xi_1^{b_1\varepsilon}\big)\, g(\eta_2,0,0) \\ - \Big(1 - \big(\xi_1 \xi_{2\,\max}(\xi_1,0)\big)^{b_1\varepsilon}\Big)\, g(0,0,\xi_1) + \big(1-\xi_1^{b_1\varepsilon}\big)\, g(0,0,0) \Big] \,, \quad (4.168)$$

with the scaling

$$b_1^{\mathrm{CDR}} = 3 \,, \quad b_1^{\mathrm{HV}} = 1 \quad (4.169)$$

in sector $\mathcal{S}_3$ and the scaling

$$b_2^{\mathrm{CDR}} = 2 \,, \quad b_2^{\mathrm{HV}} = 0 \,, \quad (4.170)$$

in sector $\mathcal{S}_6$. Even though the general case of the double-collinear parameterization has been treated here (see the first part of section 4.2.3), the special case in the second part of section 4.2.3 can be obtained by the simple replacement

$$\xi_{2\,\max} = 1 \,. \quad (4.171)$$

Case Initial

The last case deals with single poles due to initial state collinear singularities. In this case, the corresponding terms in $\hat{\sigma}_{\mathrm{SU}}^{\mathrm{RR}}$ are compared to $\hat{\sigma}_{\mathrm{SU}}^{\mathrm{C1}}$, since the pole should cancel among these two contributions. The terms in the double real-contributions are the same as in case III: The pole is taken in $\eta_1$ in sector $\mathcal{S}_3$ and sector $\mathcal{S}_6$. In the collinear factorization the convolution with the splitting function has to be taken into account, it reads

$$\iiint_0^1 \mathrm{d}z \frac{\mathrm{d}\eta}{\eta^{1+a\varepsilon}} \frac{\mathrm{d}\xi}{\xi^{1+b\varepsilon}} \Big( f(z,\eta,\xi) - f(z,0,\xi) - f(z,\eta,0) + f(z,0,0) \Big) \,. \quad (4.172)$$

The kinematics are in general given by

$$z p_1 + p_2 \to \text{final state} \,, \quad (4.173)$$

and similarly if the initial state splitting is related to $p_2$. The cross section is usually evaluated in the center-of-mass frame of $zp_1 + p_2$. In order to compare the two contributions, $\hat{\sigma}_{\mathrm{SU}}^{\mathrm{C1}}$ has to be evaluated in a different reference frame. $1-z$ is interpreted as the energy fraction of a collinear parton split from the initial state parton $p_1$. The kinematics are given by

$$p_1 + p_2 \to (1-z) p_1 + \text{final state} \,, \quad (4.174)$$

and the cross section is evaluated in the center-of-mass frame of $p_1 + p_2$, which coincides with the frame in which the double-real contribution is evaluated. The reference momentum $r$ in the triple-collinear parameterization and $r_1$ in the double-collinear parameterization corresponds to $p_1$ (or $p_2$) and the unresolved collinear momentum $u_1$ corresponds to $(1-z)p_1$. The contribution in $\hat{\sigma}_{\mathrm{SU}}^{\mathrm{RR}}$ reads

$$\iiint_0^1 \frac{\mathrm{d}\eta_2}{\eta_2^{1+a\varepsilon}} \frac{\mathrm{d}\xi_1}{\xi_1^{1+b_1\varepsilon}} \frac{\mathrm{d}\xi_2}{\xi_2^{1+b_2\varepsilon}} \Bigg\{ \Bigg[ \Big( g(\eta_2,\xi_1,\xi_2) - g(\eta_2,\xi_1,0) \Big) - \Big( g(0,\xi_1,\xi_2) - g(0,\xi_1,0) \Big) \Bigg]$$

$$- \left[ \Big( g(\eta_2, 0, \xi_2) - g(0, 0, \xi_2) \Big) - \Big( g(\eta_2, 0, 0) - g(0, 0, 0) \Big) \right] \Bigg\} \,, \quad (4.175)$$

where the variables are related to $z$ and $\xi$

$$z = 1 - \frac{2E_{\max}}{\sqrt{\hat{s}}} \xi_1 \,, \quad \xi = \frac{\xi_{2\,\max}}{\xi'_{2\,\max}} \xi_2 \,, \quad \xi_{2\,\max} = \min\left[1,\, \xi'_{2\,\max}\right] \,, \quad \xi'_{2\,\max} = \frac{1}{\xi_1} \frac{1 - \xi_1}{1 - \frac{E_{\max}}{\sqrt{\hat{s}}} \xi_1 \, \hat{r} \cdot \hat{u}_2} \,. \quad (4.176)$$

The terms that need to be considered are

$$g(\eta_2,\xi_1,0) \,, \quad g(0,\xi_1,0) \,, \quad (4.177)$$

since as in case III

$$g(\eta_2,0,\xi_2) - g(\eta_2,0,0) = 0 \,. \quad (4.178)$$

The integral can be reparameterized as

$$\begin{aligned} \iint_0^1 \frac{\mathrm{d}\xi_1}{\xi_1^{1+b_1\varepsilon}} \frac{\mathrm{d}\xi_2}{\xi_2^{1+b_2\varepsilon}} \, g(\eta_2, \xi_1, 0) = \left( \frac{2E_{\max}}{\sqrt{\hat{s}}} \right)^{(b_1-b_2)\varepsilon} \\ \times \int_{1-2E_{\max}/\sqrt{\hat{s}}}^1 \frac{\mathrm{d}z}{(1-z)^{1+(b_1-b_2)\varepsilon}} \int_0^{\xi_{2\,\max}/\xi'_{2\,\max}} \frac{\mathrm{d}\xi}{\xi^{1+b_2\varepsilon}} \left( \frac{\xi_{2\,\max}}{\xi'_{2\,\max}} \right)^{b_2\varepsilon} g(\eta_2, \xi_1(z), 0) \,, \end{aligned} \quad (4.179)$$

where the integration over $\eta_2$ is irrelevant for the discussion. It is only necessary to consider $g(\eta_2,\xi_1,0)$, since $g(0,\xi_1,0)$ can be obtained in the limit $\eta_2 \to 0$. The counterterm can be obtained by adding the missing integration region in $\xi$ and reads

$$\begin{aligned} \left( \frac{2E_{\max}}{\sqrt{\hat{s}}} \right)^{(b_1-b_2)\varepsilon} \int_{1-2E_{\max}/\sqrt{\hat{s}}}^1 \frac{\mathrm{d}z}{(1-z)^{1+(b_1-b_2)\varepsilon}} \\ \times \int_{\xi_{2\,\max}/\xi'_{2\,\max}}^1 \frac{\mathrm{d}\xi}{\xi^{1+b_2\varepsilon}} \left( \frac{\xi_{2\,\max}}{\xi'_{2\,\max}} \right)^{b_2\varepsilon} g(\eta_2, \xi_1(z), 0) = \\ \iint_0^1 \frac{\mathrm{d}\xi_1}{\xi_1^{1+b_1\varepsilon}} \left[ \frac{1}{b_2\varepsilon} \left( 1 - \left( \frac{\xi_{2\,\max}}{\xi'_{2\,\max}} \right)^{b_2\varepsilon} \right) \right] g(\eta_2, \xi_1, 0) \,. \end{aligned} \quad (4.180)$$

The integral has a singularity at $\xi_1 = 0$, respectively $z = 1$. This is an endpoint singularity which is only present in the counterterm, but not in the original contribution to the double-real contribution (4.179), since the integration range of $\xi$ vanishes in the limit $z = 1$. The same singularity appears in the collinear factorization contribution, where it is subtracted. In order that both contributions match, a similar subtraction has to be applied. In practice this is done by the replacement

$$\frac{1}{(1-z)^{1+c\varepsilon}} \;\longrightarrow\; \left[ \frac{1}{(1-z)^{1+c\varepsilon}} \right]_+ \,. \quad (4.181)$$

Finally, the full counterterm for the initial collinear case reads

$$- \iiint_0^1 \frac{\mathrm{d}\eta_2}{\eta_2^{1+a\varepsilon}} \frac{\mathrm{d}\xi_1}{\xi_1^{1+b_1\varepsilon}} \frac{1}{b_2\varepsilon} \left[ \left( 1 - \left( \frac{\xi_{2\,\max}(\eta_2,\xi_1)}{\xi'_{2\,\max}(\eta_2,\xi_1)} \right)^{b_2\varepsilon} \right) g(\eta_2, \xi_1, 0) - \left( 1 - \xi_1^{b_2\varepsilon} \right) g(\eta_2, 0, 0) \right.$$

$$- \left( 1 - \left( \frac{\xi_{2\,\max}(0,\xi_1)}{\xi'_{2\,\max}(0,\xi_1)} \right)^{b_2\varepsilon} \right) g(0,\xi_1,0) + \left(1 - \xi_1^{b_2\varepsilon}\right) g(0,0,0) \Bigg] \,, \quad (4.182)$$

with the scaling

$$b_2^{\mathrm{CDR}} = 3 \,, \quad b_2^{\mathrm{HV}} = 1 \,, \quad (4.183)$$

in sector $\mathcal{S}_3$ and the scaling

$$b_2^{\mathrm{CDR}} = 2 \,, \quad b_2^{\mathrm{HV}} = 0 \,, \quad (4.184)$$

in sector $\mathcal{S}_6$. It is important to notice, that the convolution in $\hat{\sigma}_{\mathrm{SU}}^{\mathrm{C1}}$ has to be evaluated in the boosted frame, using the single-collinear parameterization given in section 4.2.1 with $z \neq 1$. Even though the full contribution $\hat{\sigma}_{\mathrm{SU}}^{\mathrm{C1}}$ is Lorentz invariant, the separation into single- and double-unresolved parts is not Lorentz invariant.

All counterterms given in this section can be added to $\hat{\sigma}_{\mathrm{SU}}$ such that it will be finite in the limit $\varepsilon \to 0$. The same counterterms have to be subtracted from $\hat{\sigma}_{\mathrm{DU}}$ and also give a finite result for this contribution. Up to this point, all manipulations are performed in CDR. In the next section, the step to the 't Hooft-Veltman regularization scheme is explained.

## 4.6 't Hooft-Veltman regularization

The final step in the construction of the subtraction scheme STRIPPER is the restriction of resolved momenta and polarization vectors to four dimensions. As outlined in the introduction to this chapter this amounts to reformulating the scheme in the 't Hooft Veltman regularization scheme as summarized in Tab. 4.1. The procedure for each finite contribution to the cross section in Tab. 4.6 involves two steps: The first one is to replace the full expansion in $\varepsilon$ of tree-level matrix elements and finite remainders by the leading term in the $\varepsilon$ expansion. This corresponds to a restriction of polarization vectors of resolved gluons to four dimensions. Since higher orders in $\varepsilon$ for tree-level matrix contributions and finite remainders are only due to spin sums of external gluons. The second step is to restrict the phase space of resolved particles to four dimensions, which means that their respective momenta are four dimensional vectors.
The following finite contributions need no modifications, since they do not contain any pole term

$$\hat{\sigma}^{B} \,, \quad \hat{\sigma}_{\mathrm{F}}^{\mathrm{R}} \,, \quad \hat{\sigma}_{\mathrm{F}}^{\mathrm{V}} \,, \quad \hat{\sigma}_{\mathrm{F}}^{\mathrm{RR}} \,, \quad \hat{\sigma}_{\mathrm{F}}^{\mathrm{RV}} \,, \quad \hat{\sigma}_{\mathrm{F}}^{\mathrm{VV}} \,. \quad (4.185)$$

In the phase space measure as well the matrix elements $\varepsilon$ can be simply set to zero This simply means that in those contributions all partons are resolved and dimensional regularization is not needed. The remaining contributions contain either $n$ or $n+1$ resolved partons. First, the case of $n$ resolved partons is discussed. The relevant contributions are

$$\hat{\sigma}_{\mathrm{U}} = \hat{\sigma}_{\mathrm{U}}^{\mathrm{R}} + \hat{\sigma}_{\mathrm{U}}^{\mathrm{V}} + \hat{\sigma}^{\mathrm{C}} \,, \quad \hat{\sigma}_{\mathrm{FR}} = \hat{\sigma}_{\mathrm{FR}}^{\mathrm{RV}} + \hat{\sigma}_{\mathrm{FR}}^{\mathrm{VV}} + \hat{\sigma}_{\mathrm{FR}}^{\mathrm{C2}} \,, \quad \hat{\sigma}_{\mathrm{DU}} = \hat{\sigma}_{\mathrm{DU}}^{\mathrm{RR}} + \hat{\sigma}_{\mathrm{DU}}^{\mathrm{RV}} + \hat{\sigma}_{\mathrm{DU}}^{\mathrm{VV}} + \hat{\sigma}_{\mathrm{DU}}^{\mathrm{C1}} + \hat{\sigma}_{\mathrm{DU}}^{\mathrm{C2}} \,. \quad (4.186)$$

In each contribution the cancellation of poles takes place between integrated subtraction terms containing soft and splitting functions in the real contributions, the virtual infrared poles in $\mathbf{Z}^{(1,2)}$ and explicit poles in collinear factorization contributions. This cancellation is independent of the actual matrix element which factorizes in each term. Thus, since the terms are finite, higher orders in $\varepsilon$ for the $n$ parton tree-level matrix elements and finite remainders can be neglected right from the beginning. The above statement is only true if azimuthal averaged splitting functions for the integrated subtraction terms are used (see section 4.4). The phase space is restricted by modifying

the measurement function $F_n$ which defines the infrared safe observable in all of the contributions (4.186). The modification effectively forces the momenta to four dimensions and reads

$$\mathrm{F}_n \longrightarrow \mathrm{F}_n \left( \frac{\mu_R^2 e^{\gamma_\mathrm{E}}}{4\pi} \right)^{-(n-1)\varepsilon} \left[ \prod_{i=1}^{n-1} (2\pi)^{-2\varepsilon} \delta^{(-2\varepsilon)}(q_i) \right] , \tag{4.187}$$

where $q_i$ are the final state resolved partons. It is important to notice that the $\delta$-functions only restrict $n-1$ partons, while the last final state parton is fixed to four dimensions by energy-momentum conservation. Since all contributions are already finite as $\varepsilon \to 0$ the modification of the measurement function has only impact on terms that vanish if $d = 4$. The effect on the phase space parameterizations in section 4.2 can be made explicit. If none of the resolved partons $q_i$ is related to a reference parton, for example if the reference parton is in the initial state then the $\delta$-functions restrict the whole resolved phase space simply to $d = 4$

$$\int \mathrm{d}\boldsymbol{\Phi}_n\Big(p_1 + p_2 \to \sum_{i=1}^{n} q_i\Big) \longrightarrow \int \prod_{i=1}^{n} \frac{\mathrm{d}^3 q_i}{(2\pi)^3 2q_i^0} (2\pi)^4 \delta^{(4)}\Big(\sum_{i=1}^{n} q_i - p_1 - p_2\Big) . \tag{4.188}$$

However, if the reference parton is in the final state, the following factors appear

$$\begin{aligned}
&\delta^{(-2\varepsilon)}(r+u) = (r^0+u^0)^{2\varepsilon}\, \delta^{(-2\varepsilon)}(\hat{r}) && \text{for the single-collinear sector} \\
&\delta^{(-2\varepsilon)}(r+u_1+u_2) = (r^0+u_1^0+u_2^0)^{2\varepsilon}\, \delta^{(-2\varepsilon)}(\hat{r}) && \text{for the triple-collinear sector,} \\
&\delta^{(-2\varepsilon)}(r_1+u_1)\, \delta^{(-2\varepsilon)}(r_2+u_2) = \\
&\quad \big[(r_1^0+u_1^0)(r_2^0+u_2^0)\big]^{2\varepsilon}\, \delta^{(-2\varepsilon)}(\hat{r}_1)\, \delta^{(-2\varepsilon)}(\hat{r}_2) && \text{for the double-collinear sector,}
\end{aligned} \tag{4.189}$$

since a resolved parton momentum in a collinear limit is the sum of the reference momentum and a unresolved momenta. The delta $\delta^{(-2\varepsilon)}(\hat{r})$ restricts the angular integration to four dimensions while the integration for the energy is modified by an energy dependent factor. This factor compensates the higher dimensional contribution to the phase space measure of the resolved momentum. The unresolved momenta are still parameterized in $d = 4 - 2\varepsilon$ dimensions. There are at most two unresolved momenta in the contribution $\hat{\sigma}^{\mathrm{RR}}_{\mathrm{DU}}$. Since all resolved momenta are restricted to four dimensions, by rotational invariance the first unresolved momentum $u_1$ can be explicitly parameterized in five dimensions and the second unresolved momentum can be parameterized in at most six dimensions $u_2$. This is the upper bound on explicit dimensions needed independently of the multiplicity of the considered process. The only function, in which the sixth dimensions arises explicitly is the double soft function. Formulas for the explicit angular integrations beyond four dimensions are given in appendix A.2.1.

The remaining contribution that has to be adapted to the 't Hooft-Veltman scheme is

$$\hat{\sigma}_{\mathrm{SU}} = \hat{\sigma}^{\mathrm{RR}}_{\mathrm{SU}} + \hat{\sigma}^{\mathrm{RV}}_{\mathrm{SU}} + \hat{\sigma}^{\mathrm{C1}}_{\mathrm{SU}} . \tag{4.190}$$

This contribution is however more complicated, since it contains matrix elements with $n+1$ partons and matrix elements with $n$ partons, where $n+1$ partons are resolved and only one particle is unresolved. First, in order to understand the structure of this contribution, the next-to-next-to-leading order measurement function is replaced by a next-to-leading order measurement function, this means $F_n = 0$ and $F_{n+1}$ prevents $n+1$ final state partons to become soft or collinear. Then the previous discussion can be repeated for $n+1$ resolved particles in four dimensions. Returning

to the next-to-next-to-leading order measurement function, i.e. $F_n \neq 0$, one of the resolved particles can become soft and collinear. Appropriate, subtraction terms contain soft and splitting functions. However, since the parton has four dimensional polarization vectors, the correct limit is only obtained if the splitting function at $\varepsilon = 0$ is considered. As an example, the iterated limit, that has already been discussed in section 4.4, is considered. In sector $\mathcal{S}_1$ the collinear pole due to $\eta_2$ is considered, and described by the averaged splitting function. The second collinear limit $\eta_1 \to 0$ of the resolved parton is described by the spin correlated splitting function in four dimensions. The limit in Eq. (4.101) is replaced by

$$\overline{|\mathcal{M}^{(0)}_{a_r,a_1,a_2,\ldots}(r,u_1,u_2,\ldots)|^2} \simeq \frac{\left(8\pi\alpha_s\right)^2}{s_{r2}\, s_{1r2}} \langle \hat{\mathbf{P}}^{(0)}_{a_r a_2}(z_{r2};\varepsilon \neq 0)\rangle \, \langle \mathcal{M}^{(0)}_{a,\ldots}(p,\ldots)|\hat{\mathbf{P}}^{(0)}_{a_1 a_{r2}}(z_{1r2},u_{1\perp};\varepsilon=0)|\mathcal{M}^{(0)}_{a,\ldots}(p,\ldots)\rangle \,, \quad (4.191)$$

if $a_{r2} = g$. The same iterated procedure has to be applied to a soft pole and collinear subtraction and collinear pole and soft subtraction. While the soft pole soft subtraction is not changed since the next-to-leading order soft function does not depend on $\varepsilon$. In this way, matrix elements are only needed in four dimensions. The next step is to restrict the phase space of the $n+1$ resolved partons. This can be achieved in the same way discussed for $n$ resolved partons. The measurement function is modified accordingly

$$\mathrm{F}_{n+1} \longrightarrow \mathrm{F}_{n+1} \left(\frac{\mu_R^2 e^{\gamma_\mathrm{E}}}{4\pi}\right)^{-(n)\varepsilon} \left[\prod_{i=1}^{n} (2\pi)^{-2\varepsilon} \delta^{(-2\varepsilon)}(q_i)\right] . \quad (4.192)$$

The difference to the previous case is that $\delta$-functions will also restrict one of the unresolved momenta in the triple-collinear and double-collinear parameterizations of $\hat{\sigma}^{\mathrm{RR}}_{\mathrm{SU}}$. The list of appearing $\delta$-functions is

$$\begin{aligned}
\delta^{(-2\varepsilon)}(r+u_1)\,\delta^{(-2\varepsilon)}(u_2) &\quad \text{for the collinear pole in } \eta_1 \text{ in sector } \mathcal{S}_3,\\
\delta^{(-2\varepsilon)}(r+u_2)\,\delta^{(-2\varepsilon)}(u_1) &\quad \text{for the collinear pole in } \eta_2 \text{ in sector } \mathcal{S}_1,\\
\delta^{(-2\varepsilon)}(r)\,\delta^{(-2\varepsilon)}(u_1+u_2) &\quad \text{for the collinear pole in } \eta_1 \text{ in sector } \mathcal{S}_5\\
&\quad \text{and in } \eta_2 \text{ in sector } \mathcal{S}_4,\\
\delta^{(-2\varepsilon)}(r)\,\delta^{(-2\varepsilon)}(u_1) &\quad \text{for the soft pole in } \xi_2 \text{ in sectors } \mathcal{S}_1,\ \mathcal{S}_2,\ \mathcal{S}_4 \text{ and } \mathcal{S}_5.\\
\delta^{(-2\varepsilon)}(r_1+u_1)\,\delta^{(-2\varepsilon)}(r_2)\,\delta^{(-2\varepsilon)}(u_2) &\quad \text{for the collinear pole in } \eta_1 \text{ in sector } \mathcal{S}_6\ ,\\
\delta^{(-2\varepsilon)}(r_2+u_2)\,\delta^{(-2\varepsilon)}(r_1)\,\delta^{(-2\varepsilon)}(u_1) &\quad \text{for the collinear pole in } \eta_2 \text{ in sector } \mathcal{S}_6,\\
\delta^{(-2\varepsilon)}(r_1)\,\delta^{(-2\varepsilon)}(r_2)\,\delta^{(-2\varepsilon)}(u_1) &\quad \text{for the soft pole in } \xi_2 \text{ in sector } \mathcal{S}_6.
\end{aligned} \quad (4.193)$$

These restrictions on $u_1$ and $u_2$ influence the scaling of the sector variables as has been anticipated in section 4.5.1. To obtain the correct scaling in the 't Hooft-Veltman regularization the $\delta$-functions in Eq.(4.193) have to be taken into account. As an example, the collinear pole in $\eta_1$ in sector $\mathcal{S}_3$ is discussed. The scaling of $\xi_2^{(-1-b\varepsilon)}$ in CDR can be directly taken from Tab. 4.3 to be $b^{\mathrm{CDR}} = 3$. In the 't Hooft-Veltman scheme the $\delta$-function has to be taken into account additionally

$$\delta^{(-2\varepsilon)}(u_2) = \delta^{(-2\varepsilon)}(\xi_1\xi_2\xi_{2\max}E_{\max}\hat{u}_2) = (\xi_1\xi_2\xi_{2\max}E_{\max})^{2\varepsilon}\delta^{(-2\varepsilon)}(\hat{u}_2)\ . \quad (4.194)$$

Hence, the correct scaling is $b^{\mathrm{HV}} = 1$, as given in Eq. (4.169).

## 4.7 Numerical test of the subtraction scheme in four dimensions

The correctness of the full four-dimensional formulation of the subtraction scheme, is verified for the gluonic channel to the total cross section of $t\bar{t}$-production with up to two additional gluons in the final state. This channel is chosen, since it has the most involved structure, if spin correlation in collinear limits are concerned. Hence, the azimuthal averages, that have been discussed in section 4.4 are tested as well. For this test, the software, that has been used to obtain the results in [34], has been modified. It will be shown that the modifications, that have been discussed in section 4.5.1 and section 4.6, lead to correct results independently of the regularization scheme that is used. The test is performed for the single-unresolved and double-unresolved contributions only. Contributions that include finite remainders of one- and two-loop amplitudes need not to be evaluated, since they have been proven to be explicitly independent of the the regularization scheme, as has been argued in section 4.5. The finite contribution of the subtracted double-real radiation cross section, does not depend on the regularization scheme either, since it can readily evaluated in four dimensions.

The partonic cross section is rescaled, such that it is dimensionless and independent of the strong coupling. It reads

$$\tilde{\sigma}^{(2)} = \frac{m_t^2}{\alpha_s^4}\hat{\sigma}^{(2)} \,, \tag{4.195}$$

where $\hat{\sigma}^{(2)}$ is the total cross section at $\mathcal{O}(\alpha_s^4)$. The renormalization and factorization scales are fixed

$$\mu_R = \mu_F = m_t \,. \tag{4.196}$$

All results were obtained for

$$\beta = \sqrt{1 - \frac{4m_t^2}{\hat{s}}} = 0.5 \,. \tag{4.197}$$

Tables 4.8 and 4.9 contain the separate contributions to the double-unresolved cross section. In Tab. 4.8 the results have been obtained in the CDR scheme, the results in Tab. 4.9 are in the HV scheme. The sum of the different contributions is given in the last row. The given errors are due to the Monte Carlo integration. The integration error of the contributions $\tilde{\sigma}_{\mathrm{DU}}^{\mathrm{VV}}$ and $\tilde{\sigma}_{\mathrm{DU}}^{\mathrm{C2}}$ are negligible, since a deterministic integration routine has been used. By applying the counterterms discussed in section 4.5.1, the double-unresolved contribution should be finite, independently of the the regularization scheme that is used. This is verified in the two tables. All poles cancel within one standard deviation, except the leading pole in CDR, where a consistency with zero is below two standard deviations. The integration has been performed with an optimization of the $\varepsilon^0$ contribution. This is one reason for the lower quality of the leading pole. Additionally, the integrand of the leading pole in CDR is equal to the integrand in HV. Hence, a cancellation in HV implies a cancellation in CDR. Due to large cancellations between the different contributions, it was necessary to use a large sample of integration points. For example, the precision of the double-real contributions has been obtained by using nearly $10^{11}$ points. It has been observed that the convergence in the HV regularization was noticeably better. The precision of the sum of finite parts is of the order of 1%, while the agreement between the result in CDR and HV are at the 0.1% level.

All partial contributions presented in the tables contain only tree-level matrix elements. Their precise definition has been discussed in section 4.5 for general partonic cross sections. In this particular case they are:

| | $1/\varepsilon^4$ | $1/\varepsilon^3$ | $1/\varepsilon^2$ | $1/\varepsilon$ | $\varepsilon^0$ |
|---|---|---|---|---|---|
| $\tilde{\sigma}_{\mathrm{DU}}^{\mathrm{VV}}$ | 0.0321959 | 0.135003 | 0.177418 | 0.04517 | −0.1242 |
| $\tilde{\sigma}_{\mathrm{DU}}^{\mathrm{RV}}$ | −0.0724423(9) | −0.456495(4) | −1.196150(11) | −1.81962(4) | −2.8562(1) |
| $\tilde{\sigma}_{\mathrm{DU}}^{\mathrm{RR}}$ | 0.0402448(2) | 0.321486(1) | 1.045064(6) | 1.61821(4) | 1.3065(3) |
| $\tilde{\sigma}_{\mathrm{DU}}^{\mathrm{C1}}$ | | −0.154649(4) | −0.447655(20) | 0.09385(8) | 1.8313(2) |
| $\tilde{\sigma}_{\mathrm{DU}}^{\mathrm{C2}}$ | | 0.154650 | 0.421336 | 0.06247 | −0.1878 |
| $\tilde{\sigma}_{\mathrm{DU}}^{\mathrm{CDR}}$ | −0.0000016(9) | −0.000005(6) | 0.000013(24) | 0.00007(9) | −0.0304(4) |

**Table 4.8:** Double-unresolved (DU) contributions to the partonic cross section $gg \to t\bar{t} + X$, with $X$ consisting of up to two gluons, evaluated in conventional dimensional regularization (CDR). The error estimates quoted in parentheses are due to Monte Carlo integration. The definition of partial contributions is given in the text.

| | $1/\varepsilon^4$ | $1/\varepsilon^3$ | $1/\varepsilon^2$ | $1/\varepsilon$ | $\varepsilon^0$ |
|---|---|---|---|---|---|
| $\tilde{\sigma}_{\mathrm{DU}}^{\mathrm{VV}}$ | 0.0321959 | 0.086177 | 0.021985 | −0.03200 | 0 |
| $\tilde{\sigma}_{\mathrm{DU}}^{\mathrm{RV}}$ | −0.0724415(9) | −0.346630(3) | −0.702124(8) | −1.04640(3) | −2.3910(1) |
| $\tilde{\sigma}_{\mathrm{DU}}^{\mathrm{RR}}$ | 0.0402447(2) | 0.260452(1) | 0.706469(6) | 1.06119(3) | 1.8461(2) |
| $\tilde{\sigma}_{\mathrm{DU}}^{\mathrm{C1}}$ | | −0.154646(4) | −0.283008(15) | 0.08326(5) | 0.5144(1) |
| $\tilde{\sigma}_{\mathrm{DU}}^{\mathrm{C2}}$ | | 0.154650 | 0.256668 | −0.06603 | 0 |
| $\tilde{\sigma}_{\mathrm{DU}}^{\mathrm{HV}}$ | −0.0000009(9) | 0.000003(6) | −0.000010(17) | 0.00002(6) | −0.0304(2) |

**Table 4.9:** Double-unresolved (DU) contributions to the partonic cross section $gg \to t\bar{t} + X$, with $X$ consisting of up to two gluons, evaluated in 't Hooft-Veltman regularization (HV). The error estimates quoted in parentheses are due to Monte Carlo integration. The definition of partial contributions is given in the text.

$\tilde{\sigma}_{\mathrm{DU}}^{\mathrm{VV}}$ : Double-virtual contributions obtained by integrating the two-loop and one-loop squared amplitudes for $gg \to t\bar{t}$ without their finite remainders.

$\tilde{\sigma}_{\mathrm{DU}}^{\mathrm{RV}}$ : Real-virtual contributions obtained from the integrated subtraction terms of the one-loop amplitude for $gg \to t\bar{t} + g$, without the contribution of the finite remainder of the one-loop amplitude for $gg \to t\bar{t}$.

$\tilde{\sigma}_{\mathrm{DU}}^{\mathrm{RR}}$ : Double-real contributions obtained from the double-unresolved integrated subtraction terms of the Born amplitude for $gg \to t\bar{t} + gg$, including corrections described in section 4.5.1, which make the total double-unresolved contribution finite.

$\tilde{\sigma}_{\mathrm{DU}}^{\mathrm{C1}}$ : Factorization contributions obtained from the convolution of the leading order splitting function with the cross section contribution of the integrated subtraction terms of the Born amplitude for $gg \to t\bar{t} + g$.

$\tilde{\sigma}_{\mathrm{DU}}^{\mathrm{C2}}$ : Factorization contributions obtained from the convolution of the leading order splitting function with the cross section contribution of the one-loop amplitude for $gg \to t\bar{t}$ without its finite remainder, and the convolution of the next-to-leading order splitting function as well as two leading-order splitting functions with the Born cross section for $gg \to t\bar{t}$.

The cross sections in HV have been obtained with azimuthal averaged splitting functions as has been outlined section 4.4. The CDR terms contain the splitting functions with full spin correlations.

| | $1/\varepsilon^2$ | $1/\varepsilon$ | $\varepsilon^0$ |
|---|---|---|---|
| $\tilde{\sigma}_{\mathrm{SU}}^{\mathrm{RR}}$ | 0.064772(4) | 0.42742(3) | 1.0623(3) |
| $\tilde{\sigma}_{\mathrm{SU}}^{\mathrm{RV}}$ | −0.064780(6) | −0.31419(4) | −0.6044(2) |
| $\tilde{\sigma}_{\mathrm{SU}}^{\mathrm{C1}}$ | | −0.11329(3) | −0.1999(1) |
| $\tilde{\sigma}_{\mathrm{SU}}^{\mathrm{A}}$ | | | −0.00737(2) |
| $\tilde{\sigma}_{\mathrm{SU}}^{\mathrm{CDR}}$ | −0.000008(8) | −0.00006(6) | 0.2506(3) |

**Table 4.10:** Single-unresolved (SU) contributions to the partonic cross section $gg \to t\bar{t} + X$, with $X$ consisting of up to two gluons, evaluated in conventional dimensional regularization (CDR). The error estimates quoted in parentheses are due to Monte Carlo integration. The definition of partial contributions is given in the text.

| | $1/\varepsilon^2$ | $1/\varepsilon$ | $\varepsilon^0$ |
|---|---|---|---|
| $\tilde{\sigma}_{\mathrm{SU}}^{\mathrm{RR}}$ | 0.064780(5) | 0.25429(3) | 0.2584(2) |
| $\tilde{\sigma}_{\mathrm{SU}}^{\mathrm{RV}}$ | −0.064770(7) | −0.14096(2) | 0 |
| $\tilde{\sigma}_{\mathrm{SU}}^{\mathrm{C1}}$ | | −0.11329(2) | 0 |
| $\tilde{\sigma}_{\mathrm{SU}}^{\mathrm{A}}$ | | | −0.00734(1) |
| $\tilde{\sigma}_{\mathrm{SU}}^{\mathrm{HV}}$ | 0.000011(8) | 0.00004(4) | 0.2511(2) |

**Table 4.11:** Single-unresolved (SU) contributions to the partonic cross section $gg \to t\bar{t} + X$, with $X$ consisting of up to two gluons, evaluated in 't Hooft-Veltman regularization (HV). The error estimates quoted in parentheses are due to Monte Carlo integration. The definition of partial contributions is given in the text.

In Tabs. 4.10 and 4.11 the partial results for the single-unresolved contribution in the CDR and HV scheme are displayed respectively. Equally to the double-unresolved case the cancellation of poles is observed at the one sigma level. A slight deviation from zero for the leading pole in the HV case beyond one sigma is encountered. The same comments as in the double-unresolved case can be applied here. The agreement between the finite part of the single-unresolved contribution evaluated in the CDR and the HV scheme is within the Monte-Carlo error.

The single contributions, that have been evaluated, read:

$\tilde{\sigma}_{\mathrm{SU}}^{\mathrm{RR}}$ : Double-real contributions obtained from the single-unresolved integrated subtraction terms of the Born amplitude for $gg \to t\bar{t} + gg$, including corrections described in section 4.5.1, which make the total single-unresolved contribution finite. The splitting functions used in the derivation of the integrated subtraction terms are given by the azimuthally averaged expression Eqs. (B.21). The correct result is obtained after adding $\tilde{\sigma}_{\mathrm{SU}}^{\mathrm{A}}$.

$\tilde{\sigma}_{\mathrm{SU}}^{\mathrm{RV}}$ : Real-virtual contributions obtained by integrating the one-loop amplitude for $gg \to t\bar{t} + g$ together with its subtraction terms, after removal of all finite remainders.

$\tilde{\sigma}_{\mathrm{SU}}^{\mathrm{C1}}$ : Factorization contributions obtained from the convolution of the leading order splitting function with the cross section contribution of the Born amplitude for $gg \to t\bar{t} + g$ together with its

subtraction terms.

$\tilde{\sigma}^{\mathrm{A}}_{\mathrm{SU}}$ : Difference between the single-unresolved contributions obtained with spin-correlated and azimuthally-averaged splitting functions in integrated subtraction terms as explained in section 4.4.

The given numerical tests show explicitly that STRIPPER is independent of the regularization scheme. On this basis, the fully general implementation of the scheme in HV regularization is explained in the next chapter.

# CHAPTER 5

## Implementation of STRIPPER

After the subtraction scheme STRIPPER has been fully developed on a theoretical basis in the previous chapter, its explicit implementation is presented in the present chapter. There are several advantages of the four-dimensional formulation that have been taken into account. The most important advantage is that the subtraction scheme is completely independent of the precise process under consideration. Hence, STRIPPER provides a fully general framework to calculate next-to-next-to-leading order corrections in perturbative QCD. The infrared pole structure, that has been discussed in section 4.5, is completely independent of the precise form of the matrix elements. It is only governed by the soft and splitting functions in subtraction terms of real contributions and the infrared operator $\mathbf{Z}$, which incorporates the infrared singular structure of the virtual contributions. Additionally, the phase space decomposition into single-collinear, double-collinear and triple-collinear sectors depends only on the number and flavor of external partons. Hence, the phase space parameterization is uniquely defined for each sector, as outlined in section 4.2.
The subtraction scheme is implemented using the C++11 standard. The explicit implementation follows the theoretical description in the previous chapter. Each contribution that is separately integrable can be evaluated independently. For the evaluation of a specific process, matrix elements are needed. However, the evaluation of matrix elements is separated from the subtraction scheme itself. The connection between matrix elements and the subtraction framework is given through interface classes, which can be adapted to available matrix element generators. Since tree-level matrix elements for Standard Model processes are provided in really sophisticated software libraries, a standard tree-level matrix element generator is already interfaced to the core implementation.
A standard library for one-loop finite remainders, is not yet included, even though several implementations exist, as has been discussed in section 3.3.1. This is because the requirements on the stability of the one-loop amplitude in the singular phase space regions are much higher in a next-to-next-to-leading order computation in comparison to a next-to-leading order computation. It is therefore useful to include one-loop finite remainders on a case by case basis.
The two-loop finite remainder and the one-loop finite remainder squared have to be considered on a case by case basis as well, since only a few two-loop amplitudes have been calculated so far (see section 3.3.2). It is again emphasized that these contributions are finite by themselves. The implemented software is the first fully general event generator to provide fully differential next-to-next-to-leading order predictions.
In the first part of this chapter the adaptation of the (physical) concepts behind STRIPPER to an object-oriented implementation is discussed. Subsequently, specific features of the implementation are presented that go beyond the detailed description of the subtraction scheme in the previous

chapter. In section 5.2, color correlated and spin correlated tree-level matrix elements are discussed. Explicit summations over spin states are replaced by Monte Carlo sums of randomly polarized partons or a helicity sampling, in the case of the reference and the unresolved partons. Therefore, subtraction terms for polarized matrix elements are derived and tested in section 5.3. Some special functions that need to be provided and their implementation is discussed in section 5.4. The effects of missed binning can be minimized. This will be explained in section 5.5. Finally, a first application of the software is demonstrated in section 5.6: Partial results for differential distributions in $t\bar{t}$-production at next-to-next-to-leading order in perturbative QCD are presented.

## 5.1 Overview

In this section, the general structure of the software is presented. The full subtraction scheme is realized in a object-oriented implementation of a Monte Carlo event generator. The main idea is that each (physical) concept that is needed in order evaluate the cross section for specific observables is related to an object of specific properties. In the following, the different classes are presented. In this section, words written in italic letters refer to classes of the C++ implementation or a specific instance of the class. A rough overview of the class dependencies is depicted in Fig. 5.1.

### *Generator*

The software provides a Monte-Carlo event generator for the hadronic cross section given in Eq. (3.9). This is realized by the class *Generator*. The specific instance of *Generator* is defined by an *initial state*, the list of renormalization and factorization *scales* $\mu_{\mathrm{R}}^2$ and $\mu_{\mathrm{F}}^2$ at which the cross section should be evaluated and the *measurement* functions that specify infrared save observables. Different contributions for the partonic subprocesses can be separately included into the generator. All contributions that are separately integrable can be or have to be included separately. The full list of possible contributions and the parameters to identify them are given in Tab. 5.1. The order in $\alpha_s$ is specified for each contribution. Then the number of final state unresolved partons has to be identified $n_u \leq 2$. This number defines how the phase space is divided into sectors using *selector* functions. In order to distinguish single-unresolved and double-unresolved cases, the number of resolved partons $n_r$ out of the unresolved ones has to be provided. The number of loops $n_L$ specifies, if the tree-level matrix elements, the one-loop finite remainder or the two-loop finite and the squared one-loop finite remainder remainder have to be evaluated for the specific contribution. Finally, the presence of convolutions for initial state collinear factorization contributions uniquely defines a single cross section. For a full next-to-next-to-leading order computation, all contributions have to be included into the generator.

*Generator* contains explicitly the implementation of all subtraction and integrated subtraction terms, that are constructed as explained in section 4.3. Explicit formulas for the splitting and soft functions, that appear in the collinear and soft limits of the matrix elements are implemented, see sections 3.4.1 and 4.4 and appendix B.2. Additionally, the splitting functions for the initial state collinear factorization formulas in Eqs.(3.19) and (3.24) are implemented. Separate formulas for the five triple-collinear sectors, the double-collinear sector and the single-unresolved sector are provided. This is necessary in order to factorize the singular part of the collinear and soft limits from a regular piece, which is finite as one or several of the sector variables $\{\xi_1,\xi_2,\eta_1,\eta_2\}$ vanish. Furthermore, the complete set of tree-level polarized subtraction terms is implemented. The infrared singular part of virtual contributions is given by the color space operator $\mathbf{Z}$ as discussed in section 4.5. The explicit formula, given in appendix B.1, is implemented up to second order in $\alpha_s$.

All matrix elements, that appear in the different contributions in Tab. 5.1, are evaluated externally and are called using the interface classes *Born*, *OneLoop* and *TwoLoop*.

| contribution | finite | order in $\alpha_s$ | $n_u$ | $n_r$ | $n_L$ | convolution |
|---|---|---|---|---|---|---|
| $\sigma^{\mathrm{B}}$ | $\surd$ | LO | 0 | 0 | 0 | |
| $\sigma^{\mathrm{V}}_{\mathrm{F}}$ | $\surd$ | NLO | 0 | 0 | 1 | |
| $\sigma^{\mathrm{V}}_{\mathrm{U}}$ | | NLO | 0 | 0 | 0 | |
| $\sigma^{\mathrm{R}}_{\mathrm{F}}$ | $\surd$ | NLO | 1 | 1 | 0 | |
| $\sigma^{\mathrm{R}}_{\mathrm{U}}$ | $\surd$ | NLO | 1 | 0 | 0 | |
| $\sigma^{\mathrm{C}}$ | | NLO | 0 | 0 | 0 | $\surd$ |
| $\sigma^{\mathrm{VV}}_{\mathrm{F}}$ | $\surd$ | NNLO | 0 | 0 | 2 | |
| $\sigma^{\mathrm{VV}}_{\mathrm{FR}}$ | | NNLO | 0 | 0 | 1 | |
| $\sigma^{\mathrm{VV}}_{\mathrm{DU}}$ | | NNLO | 0 | 0 | 0 | |
| $\sigma^{\mathrm{RV}}_{\mathrm{F}}$ | $\surd$ | NNLO | 1 | 1 | 1 | |
| $\sigma^{\mathrm{RV}}_{\mathrm{FR}}$ | $\surd$ | NNLO | 1 | 0 | 1 | |
| $\sigma^{\mathrm{RV}}_{\mathrm{SU}}$ | | NNLO | 1 | 1 | 0 | |
| $\sigma^{\mathrm{RV}}_{\mathrm{DU}}$ | $\surd$ | NNLO | 1 | 0 | 0 | |
| $\sigma^{\mathrm{RR}}_{\mathrm{F}}$ | $\surd$ | NNLO | 2 | 2 | 0 | |
| $\sigma^{\mathrm{RR}}_{\mathrm{SU}}$ | $\surd$ | NNLO | 2 | 1 | 0 | |
| $\sigma^{\mathrm{RR}}_{\mathrm{DU}}$ | $\surd$ | NNLO | 2 | 0 | 0 | |
| $\sigma^{\mathrm{C1}}_{\mathrm{SU}}$ | | NNLO | 1 | 1 | 0 | $\surd$ |
| $\sigma^{\mathrm{C1}}_{\mathrm{DU}}$ | $\surd$ | NNLO | 1 | 0 | 0 | $\surd$ |
| $\sigma^{\mathrm{C2}}_{\mathrm{FR}}$ | | NNLO | 0 | 0 | 1 | $\surd$ |
| $\sigma^{\mathrm{C2}}_{\mathrm{DU}}$ | | NNLO | 0 | 0 | 0 | $\surd$ |

**Table 5.1:** List of contributions of a next-to-next-to-leading order cross section that can be included separately into the Monte Carlo integrator of STRIPPER. The second column tells, whether the contribution contains a finite contribution. The third column notifies to which order in perturbation theory the contribution belongs. The number of unresolved partons $n_u$ is given in column four, while $n_r$ specifies the number of resolved partons out of the unresolved ones. This is necessary in order to distinguish single- and double-unresolved contributions. $n_L$ is the number of loops of the finite remainder in the contribution. To identify the contribution unambiguously, the final column designates, whether a convolution with initial state splitting functions needs to be evaluated.

The Monte Carlo integration is controlled by the instance of *Generator* itself. An one-dimensional version of PARNI [214, 215] provides an implementation of importance sampling in order to generate probability density grids for the generation of random points. It is possible to separate the Monte Carlo integration into an optimization phase, in which grids are generated, and an integration phase, in which the actual integration is performed and the previously generated grids are used. A Monte Carlo sum is performed over all possible sectors that are defined in the class *Selector*. The choice of a specific sector for a single event defines unambiguously the kinematics of all external particles and the phase space measure. The kinematics and the phase space measures are implemented in the class *PhaseSpace*. In particular, the kinematics of the reference and unresolved partons are fixed as explained in section 4.2.

The summation over polarization of all particles, except the reference and the unresolved particles can be performed using random polarization for tree-level matrix elements. The summation over polarization states of the unresolved and the reference parton can be performed by a helicity Monte

Carlo. Both concepts will be explained in detail in section 5.3.

### *Scales*

In order to provide the theoretical error estimate, the calculation has to be performed at different renormalization and factorization scales $\mu_R^2$ and $\mu_F^2$. The class *Scales* provides the possibility to evaluate the cross section for different scale choices, where the scales can be either fixed or depend on the phase space point. A computation for different scales can be performed simultaneously.

### *InitialState*

An initial state is an instance of the class *InitialState* and is defined by the initial state *particles*. Since STRIPPER is equally well defined for decays, the number of initial state particles is either two or one. If the number of initial state particles is two, the center-of-mass energy $\sqrt{s}$ has to be provided. A convolution with PDFs is necessary if one or two of the initial state particles are hadrons, where for now only protons and anti-protons are relevant. The list of PDFs that are considered during an evaluation can be specified. In this form, it is possible to evaluate the cross section for different PDF sets simultaneously. Different PDF sets are interfaced through the newest version of the LHAPDF interpolator, that allows to use all relevant PDF sets, *e.g* [10–13].

### *Particle*

A particle is an instance of the class *Particle*. A particle is identified by a name. The nomenclature is the same as in MadGraph [14]. The class provides default values for the mass, width, number of helicity states and the anti-particle for all Standard Model particles as well as the proton and the anti-proton. All quarks are massless, except the top quark. A function to include new particles is provided. The properties of a particle can in general be changed, although the masses and widths of the gluon, the photon and the proton are fixed. The class provides special functions to identify partons, since they play a special role in STRIPPER.

### *Measurement*

The measurement function given in Eq. (3.11) is implemented into a class *Measurement*. The measurement function controls the output of the calculation, which means each simulated event. It is defined by *cuts* and a *jet-algorithm*. By default, no cuts and jet algorithm is applied. The instance of *Measurement* manages the accumulation of generated weights into histogram bins for different observables of the class *Observable*. Error estimates are provided for each bin. Starting at next-to-leading order a meaningful error estimate for a bin is only obtained, if a weight of an event and the appropriate subtraction term weight are first summed and subsequently squared. Multiple kinematic *observables* can be included into a measurement.

### *Cuts*

A instance of the class *Cuts* decides if a kinematic configuration of the final state is accepted or not in order to preserve infrared safety. The decision is made on the basis of the particle *clusters* constructed by the *jet-algorithm*.

### *JetAlgorithm*

The class *JetAlgorithm* provides, currently, two different implementations of jet algorithms presented in [216]. The instance of a jet algorithm defines clusters of final state particles on basis of their momenta and the parameters that define the jet.

### *Cluster*

A cluster, as an instance of *Cluster*, has two attributes. The list of particles in the cluster an its total momentum. A cluster is either a single particle or a jet.

### *Observable*

The class *Observable* provides an interface for kinematic observables in order to compute differential cross sections. The list of observables should be included into the measurement function, as described before. The following observables are already defined. The *InvariantMass* can be specified by the list of clusters for which the invariant mass should be defined. The *Rapidity* for the set of clusters and the *TransverseMomentum* for a set of particle clusters.

### *Histogram*

An object of the class *Histogram* is defined by the number of bins and a vector that defines the left and right bound of each bin. The number and size of histogram bins can be specified individually, where one as well as two dimensional histograms are possible. A smearing parameter can be specified in order to reduce the effects of missed binning. This will be explained in detail in section 5.5. The set up allows to evaluate different differential cross sections in one run. The *measurement* class manages the accumulation of the weights and errors to each bin.

### *Process*

The *Process* class implements a general process which is defined by the initial and final state *particles*.

### *Selector*

The number of unresolved partons and the partonic *process* defines a instance of the *Selector* class. This is the explicit realization of selector functions that were discussed in section 4.1. Based on the specific process it determines the number of independent single-collinear, double-collinear and triple-collinear sectors, where each triple-collinear sector is divided in five subsectors $\mathcal{S}_1$ to $\mathcal{S}_5$ as explained in section 4.2. A Monte-Carlo sum over all sectors is realized in the class *Generator*.

### *PhaseSpace*

The parameterizations of the phase space are implemented in a class *PhaseSpace*. It is sufficient to provide the partonic center-of-mass energy and a current sector of the *Selector* instance. This defines the unresolved and the reference particle, which are parameterized according to section 4.2. The momenta of the remaining partons in $\mathrm{d}\boldsymbol{\Phi}_{n-n_{fr}}(Q)$, see Eq. (4.12), are evaluated independently in the center-of-mass frame of $Q$ and then boosted back to the partonic center-of-mass frame. The class provides methods to adapt the kinematics as one or more sector variables go to zero, which are $\{\xi_1,\xi_2,\eta_1,\eta_2\}$ in the double- and triple-collinear sectors or $\{\xi,\eta\}$ in the single-collinear sector. This is necessary in order to obtain the correct kinematics in subtraction terms. Resolved particles are always four-dimensional by applying $\delta$-functions as explained in section 4.6. The class provides also the weight of the measure of the phase space, including the explicit weight due to the selector function.

### *Born*

This interface class provides all tree-level matrix elements that are needed in STRIPPER. The full list reads

$$\langle\mathcal{M}_n^{(0)}|\mathcal{M}_n^{(0)}\rangle\,, \qquad \langle\mathcal{M}_n^{(0)}|\mathbf{T}_i\cdot\mathbf{T}_j|\mathcal{M}_n^{(0)}\rangle\,, \qquad \langle\mathcal{M}_n^{(0)}|\lambda_i\rangle\langle\lambda_i'|\mathcal{M}_n^{(0)}\rangle\,,$$
$$\langle\mathcal{M}_n^{(0)}|\big\{\mathbf{T}_i\cdot\mathbf{T}_j,\mathbf{T}_k\cdot\mathbf{T}_l\big\}|\mathcal{M}_n^{(0)}\rangle\,, \qquad \langle\mathcal{M}_n^{(0)}|f^{abc}T_i^aT_j^bT_k^c|\mathcal{M}_n^{(0)}\rangle\,, \qquad \langle\mathcal{M}_n^{(0)}|\mathbf{T}_i\cdot\mathbf{T}_j|\lambda_k\rangle\langle\lambda_k'|\mathcal{M}_n^{(0)}\rangle\,,$$

$$\langle \mathcal{M}_n^{(0)}|\lambda_i\lambda_j\rangle\langle\lambda_i'\lambda_j'|\mathcal{M}_n^{(0)}\rangle\,, \qquad \langle \mathcal{M}_{n+1}^{(0)}|\mathcal{M}_{n+1}^{(0)}\rangle\,, \qquad \langle \mathcal{M}_{n+1}^{(0)}|\mathbf{T}_i\cdot\mathbf{T}_j|\mathcal{M}_{n+1}^{(0)}\rangle\,,$$
$$\langle \mathcal{M}_{n+1}^{(0)}|\lambda_i\rangle\langle\lambda_i'|\mathcal{M}_{n+1}^{(0)}\rangle\,, \qquad \langle \mathcal{M}_{n+2}^{(0)}|\mathcal{M}_{n+2}^{(0)}\rangle\,,$$

where in principle different matrix element libraries can be interfaced. By default the matrix elements are provided by [214, 215] and most of the Standard Model matrix elements can be evaluated. The implementation of color correlators is outlined in section 5.2.1. The class provides matrix elements for specific helicities or spin summed amplitudes. Additionally, randomly polarized external states are supported. In order to implement spin correlations and polarized subtraction terms access to the polarization vectors of gluons is provided. Spin correlations, denoted by $|\lambda_i\rangle\langle\lambda_i'|$, are explained in section 5.2.2.

*OneLoop*

This interface class provides the necessary one-loop amplitudes at a specific renormalization scale $\mu_{\mathrm{R}}^2$, which read

$$2\mathrm{Re}\langle \mathcal{M}_n^{(0)}|\mathcal{F}_n^{(1)}\rangle\,, \quad 2\mathrm{Re}\langle \mathcal{M}_n^{(0)}|\mathbf{T}_i\cdot\mathbf{T}_j|\mathcal{F}_n^{(1)}\rangle\,, \quad 2\mathrm{Re}\langle \mathcal{M}_n^{(0)}|\lambda_i\rangle\langle\lambda_i'|\mathcal{F}_n^{(1)}\rangle\,, \quad 2\mathrm{Re}\langle \mathcal{M}_{n+1}^{(0)}|\mathcal{F}_{n+1}^{(1)}\rangle\,.$$

The one-loop four point functions including spin and color correlations for $t\bar{t}$ are already provided. The one-loop five-point functions for $t\bar{t}$-production at next-to-next-to-leading order are already provided using the software of [217, 218] that has been used for $t\bar{t}$ production plus an additional jet at next-to-leading order.

*TwoLoop*

This interface class provides the two-loop contribution for a specific renormalization scale $\mu_{\mathrm{R}}^2$, which read

$$2\mathrm{Re}\langle \mathcal{M}_n^{(0)}|\mathcal{F}_n^{(2)}\rangle + \langle \mathcal{F}_n^{(1)}|\mathcal{F}_n^{(1)}\rangle\,.$$

The first two-loop contributions that will be provided are the ones for $t\bar{t}$-production, that have been used to calculate the total cross section at next-to-next-to-leading order [34].

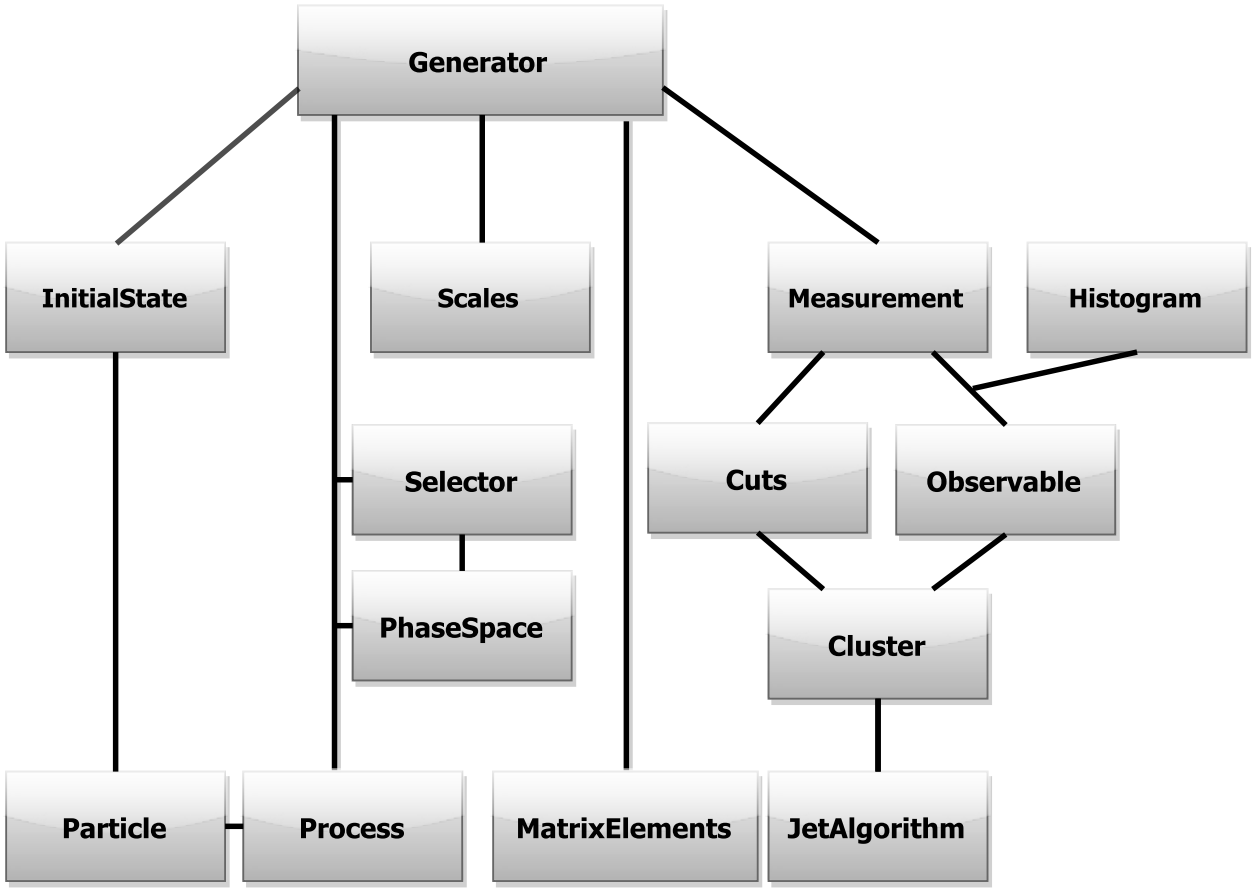


**Figure 5.1:** Diagrammatic representation of the class dependencies. Each concept in STRIPPER is implemented in a C++-class. A short description of the classes is given in the main text.

## 5.2 Tree-level matrix elements

Tree-level matrix elements are evaluated using the FORTRAN software library [214, 215]. The library provides amplitude in the color-flow basis (see Appendix A.1) for a specific helicity configuration of external particles

$$\langle \lambda_1 \dots \lambda_n | \mathcal{M}_n^{(0)} \rangle = \sum_{I=P(2,\dots n)} \delta^{i_1}_{j_{\sigma_I(1)}} \delta^{i_2}_{j_{\sigma_I(2)}} \dots \delta^{i_n}_{j_{\sigma_I(n)}} \mathcal{M}_I^{(0)} \left(\lambda_1 \dots \lambda_n\right) \ . \tag{5.1}$$

### 5.2.1 Color correlations

Since $|\mathcal{M}_n^{(0)}\rangle$ is a vector in color and spin space, the left hand side of Eq. (5.1) is still a vector in color space, where $n$ is the number of external partons. The squared matrix element summed over

helicities and colors of external particles reads

$$\begin{aligned}|\mathcal{M}|^2 &= \sum_{\lambda_1\ldots\lambda_n} \langle \mathcal{M}_n^{(0)}|\lambda_1\ldots\lambda_n\rangle\langle\lambda_1\ldots\lambda_n|\mathcal{M}_n^{(0)}\rangle \\ &= \sum_{\lambda_1\ldots\lambda_n}\sum_{I,J} \mathcal{M}_I^{(0),\dagger}(\lambda_1\ldots\lambda_n)\,\mathcal{M}_J^{(0)}(\lambda_1\ldots\lambda_n)\times \\ &\times \delta_{k_1}^{\bar{k}_{\sigma_I(1)}}\ldots\delta_{k_n}^{\bar{k}_{\sigma_I(n)}}\left[\mathbf{O}^{k_1\ldots k_n;\bar{j}_{\sigma_J(1)}\ldots\bar{j}_{\sigma_J(n)}}_{\bar{k}_{\sigma_I(1)}\ldots\bar{k}_{\sigma_I(n)};j_1\ldots j_n}\right]\delta^{j_1}_{\bar{j}_{\sigma_J(1)}}\ldots\delta^{j_n}_{\bar{j}_{\sigma_J(n)}}\,,\end{aligned} \tag{5.2}$$

where a summation over equal indices is understood. Each operator in color space $\mathbf{O}$ in the color flow representation can be written in terms of Kronecker deltas connecting open color indices of the amplitude with open color indices of the complex conjugate amplitude. If there are no color correlations the operator connects each quark color index with the corresponding antiquark color index of the complex conjugate amplitude [1], which effectively just sums then number of colors of external particles. Explicitly the operator reads

$$\mathbf{O}\equiv\mathbf{1} = \delta_{j_1}^{k_1}\delta^{\bar{j}_{\sigma_J(1)}}_{\bar{k}_{\sigma_I(1)}}\ldots\delta_{j_n}^{k_n}\delta^{\bar{j}_{\sigma_J(n)}}_{\bar{k}_{\sigma_I(n)}} = \delta_1^1\delta_{\sigma_1}^{\sigma_1}\ldots\delta_n^n\delta_{\sigma_n}^{\sigma_n}\,, \tag{5.3}$$

where on the right hand side, a short hand notation for the indices has been introduced

$$k_i\to i\,,\quad j_i\to i\,,\quad \bar{k}_{\sigma_I(i)}\to\sigma_i\,,\quad \bar{j}_{\sigma_J(i)}\to\sigma_i\,.$$

In this form a distinction between upper and lower indices as they appear in Eq. (5.2) is necessary in order to identify contractions with the amplitude or its complex conjugate.
Color correlations can be implemented on the same footing by writing the color charge operator of parton $i$, $\mathbf{T}_i$, in the color flow representation

$$\begin{aligned}\mathbf{T}_{i;\mathrm{q}} &= (t^a)^i_i\,\delta^{\sigma_i}_{\sigma_i}\,,\\ \mathbf{T}_{i;\bar{\mathrm{q}}} &= (-t^a)^{\sigma_i}_{\sigma_i}\,\delta^i_i\,,\\ \mathbf{T}_{i;\mathrm{g}} &= (t^a)^i_i\,\delta^{\sigma_i}_{\sigma_i} - (t^a)^{\sigma_i}_{\sigma_i}\,\delta^i_i\,.\end{aligned} \tag{5.4}$$

It should be emphasized, that in the context of color flows, the indices i,j,... always belong to a quark-anti-quark pair. In contrast to the previous chapter, where each parton is labeled by its own index. The objects that actual appear in the color correlated matrix elements $\mathbf{T}_i\cdot\mathbf{T}_j$ can be determined by using the identity

$$(t^a)^i_j(t^a)^k_l = \frac{1}{2}\left(\delta^i_l\,\delta^k_j - \frac{1}{N_c}\delta^i_j\,\delta^k_l\right)\,. \tag{5.5}$$

The correlation operators for $i=j$ read

$$\begin{aligned}\mathbf{T}_{i;\mathrm{q}}\cdot\mathbf{T}_{i;\mathrm{q}} = \mathbf{T}_{i;\bar{\mathrm{q}}}\cdot\mathbf{T}_{i;\bar{\mathrm{q}}} &= C_F\,\mathbf{1}\,,\\ \mathbf{T}_{i;\mathrm{g}}\cdot\mathbf{T}_{i;\mathrm{g}} &= C_A\,\mathbf{1}\,,\\ \mathbf{T}_{i;\mathrm{q}}\cdot\mathbf{T}_{i;\bar{\mathrm{q}}} &= -\frac{1}{2}\left(\delta^i_{\sigma_i}\,\delta^{\sigma_i}_i - \frac{1}{N_c}\delta^i_i\,\delta^{\sigma_i}_{\sigma_i}\right)\,,\end{aligned} \tag{5.6}$$

1 The gluon has a quark and antiquark index. See: A.1

whereas for different indices $i \neq j$ they read

$$\begin{aligned}
\mathbf{T}_{i;\mathrm{g}} \cdot \mathbf{T}_{j;\mathrm{g}} &= \frac{1}{2}\left(-\delta^i_{\sigma_j}\,\delta^j_{\sigma_i}\,\delta^{\sigma_i}_{\sigma_j}\,\delta^{\sigma_j}_{i} - \delta^i_{i}\,\delta^j_{\sigma_i}\,\delta^{\sigma_i}_{j}\,\delta^{\sigma_j}_{\sigma_j} + \delta^i_{i}\,\delta^j_{j}\,\delta^{\sigma_i}_{\sigma_j}\,\delta^{\sigma_j}_{\sigma_i} + \delta^i_{j}\,\delta^j_{i}\,\delta^{\sigma_i}_{\sigma_i}\,\delta^{\sigma_j}_{\sigma_j}\right) , \\
\mathbf{T}_{i;\mathrm{g}} \cdot \mathbf{T}_{j;\mathrm{q}} &= \frac{1}{2}\left(-\delta^i_{i}\,\delta^j_{\sigma_i}\,\delta^{\sigma_i}_{j}\,\delta^{\sigma_j}_{\sigma_j} + \delta^i_{j}\,\delta^j_{i}\,\delta^{\sigma_i}_{\sigma_i}\,\delta^{\sigma_j}_{\sigma_j}\right) , \\
\mathbf{T}_{i;\mathrm{g}} \cdot \mathbf{T}_{j;\bar{\mathrm{q}}} &= \frac{1}{2}\left(-\delta^i_{\sigma_j}\,\delta^j_{j}\,\delta^{\sigma_i}_{\sigma_i}\,\delta^{\sigma_j}_{i} + \delta^i_{i}\,\delta^j_{j}\,\delta^{\sigma_i}_{\sigma_j}\,\delta^{\sigma_j}_{\sigma_i}\right) , \\
\mathbf{T}_{i;\mathrm{q}} \cdot \mathbf{T}_{j;\mathrm{q}} &= \frac{1}{2}\left(\delta^i_{j}\,\delta^j_{i} - \frac{1}{N_c}\delta^i_{i}\,\delta^j_{j}\right)\,\delta^{\sigma_i}_{\sigma_i}\,\delta^{\sigma_j}_{\sigma_j} , \\
\mathbf{T}_{i;\bar{\mathrm{q}}} \cdot \mathbf{T}_{j;\bar{\mathrm{q}}} &= \frac{1}{2}\delta^i_{i}\,\delta^j_{j}\left(\delta^{\sigma_i}_{\sigma_j}\,\delta^{\sigma_j}_{j} - \frac{1}{N_c}\delta^{\sigma_i}_{\sigma_i}\,\delta^{\sigma_j}_{\sigma_j}\right) , \\
\mathbf{T}_{i;\mathrm{q}} \cdot \mathbf{T}_{j;\bar{\mathrm{q}}} &= \frac{1}{2}\left(-\delta^i_{\sigma_j}\,\delta^j_{j}\delta^{\sigma_i}_{\sigma_i}\,\delta^{\sigma_j}_{i} + \frac{1}{N_c}\delta^i_{i}\,\delta^j_{j}\delta^{\sigma_i}_{\sigma_i}\,\delta^{\sigma_j}_{\sigma_j}\right) ,
\end{aligned}$$

where an operator **1** for the remaining uncorrelated color flows is always understood.
In Stripper two functions are implemented that calculate the double and quadruple correlation operators. They are subsequently contracted with the matrix elements in the color flow basis.
The remaining triple color correlator

$$\langle \mathcal{M}^{(0)}_n | f^{abc} T^a_i T^b_j T^c_k | \mathcal{M}^{(0)}_n \rangle \, , \tag{5.7}$$

can be obtained using the quadruple correlator and the identity

$$i f^{abc} T^a_i T^b_j T^c_k = [\mathbf{T}_i \cdot \mathbf{T}_j, \mathbf{T}_i \cdot \mathbf{T}_k,] \ . \tag{5.8}$$

It is important to notice that the triple color correlator always vanishes, if matrix elements are summed over color and spin and do not contain any complex parameters. This has been shown in [219] using the following argument. The matrix element can be expanded in an arbitrary color basis

$$|\mathcal{M}^{(0)}\rangle = \sum_\alpha |\mathcal{M}^{(0)}_\alpha\rangle \times |c_\alpha\rangle \, , \tag{5.9}$$

where the basis vectors $|c_\alpha\rangle$ are made of the generators in the fundamental representation of SU(3) $t^c_{ab}$ or the adjoint representation $if^{abc}$. The argument holds equally for any kind of basis representation. The triple color correlator is evaluated as follows

$$\langle \mathcal{M}^{(0)}_n | i f^{abc} T^a_i T^b_j T^c_k | \mathcal{M}^{(0)}_n \rangle = \sum_{\alpha\beta} \langle \mathcal{M}^{(0)}_\alpha | \mathcal{M}^{(0)}_\beta \rangle \langle c_\alpha | i f^{abc} T^a_i T^b_j T^c_k | c_\beta \rangle \, . \tag{5.10}$$

The color charge operators are hermitian and commute with each other, as all parton indices $i$,$j$,$k$ are different. Therefore, the color contribution is

$$\langle c_\alpha | i f^{abc} T^a_i T^b_j T^c_k | c_\beta \rangle = -\langle c_\beta | i f^{abc} T^a_i T^b_j T^c_k | c_\alpha \rangle \, , \tag{5.11}$$

as the contribution is always real. Hence, the color contribution is antisymmetric under the exchange of $\alpha$ and $\beta$. The whole correlator 5.10 is thus

$$\langle \mathcal{M}_n^{(0)}|if^{abc}T_i^aT_j^bT_k^c|\mathcal{M}_n^{(0)}\rangle = \frac{1}{2}\sum_{\alpha\beta}\left(\langle \mathcal{M}_\alpha^{(0)}|\mathcal{M}_\beta^{(0)}\rangle - \langle \mathcal{M}_\beta^{(0)}|\mathcal{M}_\alpha^{(0)}\rangle\right)\langle c_\alpha|if^{abc}T_i^aT_j^bT_k^c|c_\beta\rangle \ . \tag{5.12}$$

If $\langle \mathcal{M}_\alpha^{(0)}|\mathcal{M}_\beta^{(0)}\rangle$ is real, the correlator vanishes. This is the case, if the amplitude is summed over polarizations of the external particles and if there are no other complex parameters, e.g. masses or coupling constants, in the matrix element.
For a squared amplitude of a given polarization the correlator does not vanish in general, because

$$\langle \mathcal{M}_\alpha^{(0)}|\lambda_1\dots\lambda_n\rangle\langle\lambda_1\dots\lambda_n|\mathcal{M}_\beta^{(0)}\rangle^* \neq \langle \mathcal{M}_\beta^{(0)}|\lambda_1\dots\lambda_n\rangle\langle\lambda_1\dots\lambda_n|\mathcal{M}_\alpha^{(0)}\rangle \ . \tag{5.13}$$

### 5.2.2 Spin correlations

Collinear limits of matrix elements are described by splitting functions $\hat{P}_{qg}^{(0)\,ss'}$, if the splitting particle is a quark and $\hat{P}^{(0),\mu\nu}$, if the splitting particle is a gluon. In the latter case, the collinear subtraction term contains single spin correlated matrix elements indicated by

$$|\lambda_i\rangle\langle\lambda_i'| \ , \tag{5.14}$$

or double spin correlations indicated by

$$|\lambda_i\lambda_j\rangle\langle\lambda_i'\lambda_j'| \ , \tag{5.15}$$

where in the first case the polarization of gluon $i$ is fixed to be $\lambda_i'$ in the matrix element and $\lambda_i$ in the complex conjugated matrix element. Correspondingly, in the second case two polarizations of two gluons are fixed in the matrix element and its complex conjugated counterpart. A spin correlated matrix element can then be calculated using the identity

$$\langle \mathcal{M}_n|k_\perp^{\mu_i}k_\perp^{\nu_i}|\mathcal{M}_n\rangle = \sum_{\lambda_i\lambda_i'}\varepsilon^*(p_i,\lambda_i')\cdot k_\perp\varepsilon(p_i,\lambda_i)\cdot k_\perp\langle \mathcal{M}_n^{(0)}|\lambda_i\rangle\langle\lambda_i'|\mathcal{M}_n^{(0)}\rangle \ , \tag{5.16}$$

where $\varepsilon(p_i,\lambda_i')$ is the polarization vector of gluon with momentum $p_i$. Another possibility is to replace the polarization vector of the gluon in the matrix element, directly by the transverse vector $k_\perp$, if this is possible.

## 5.3 Random polarization and polarized subtraction terms

The complexity of higher order calculation has two origins. On the one hand there is the conceptual complexity to find appropriate methods and techniques to calculate next-to-next-to-leading order corrections to a given process. This has been discussed at length in the preceding chapters of this work.
On the other hand, calculations become challenging from a computational point of view. In practical scattering problems, unpolarized results are needed and therefore a summation/average over external polarization states has to be performed during the calculation. The number of summations that have to be performed is in principle $2^{n_2}3^{n_3}$, where $n_2$ is the number of external particles with two polarization states and $n_3$ the number of external particles with three polarization states. From this perspective the computationally complexity increases rapidly as the number of external particles

rises. For a next-to-leading order calculation the real radiation contribution $\hat{\sigma}_F^R$ with one additional parton in the final state is therefore the bottleneck. At next-to-next-to-leading order the double-real radiation contribution $\hat{\sigma}_F^{RR}$ is the most complex one in this sense, since it contains two additional partons in the final state.
A replacement of the deterministic summation over helicity states by Monte Carlo methods will speed up the calculation basically up to a factor of $2^{n_2}3^{n_3}$. There are two general methods, how replace the summation by a Monte Carlo sampling. Here, only particles with two polarization states are discussed, namely massless gauge bosons and fermions. The first method is to sample over discrete helicity configurations of the external partons. This has however the disadvantage that different polarization contributions can differ by orders of magnitude. If a uniform distribution for the sampling is used, a large number of points have to be evaluated to get a reliable error estimate of the final result.
The second method is to replace the helicity summation by an integral that can be evaluated using Monte Carlo integration. A naive way is to write

$$\int \mathrm{d}\boldsymbol{\Phi}_n \langle \mathcal{M}_n^{(0)} | \mathcal{M}_n^{(0)} \rangle = \int_{[0,1]} \mathrm{d}^{n+2} l \int \mathrm{d}\boldsymbol{\Phi}_n \langle \mathcal{M}_n^{(0)} | \lambda_1(l_1) \ldots \rangle \langle \lambda_1(l_1) \ldots | \mathcal{M}_n^{(0)} \rangle \ , \tag{5.17}$$

where

$$\lambda_i(l_i) = \begin{cases} +1 & \text{for} \quad 0 \leq l < \frac{1}{2} \\ -1 & \text{for} \quad \frac{1}{2} \leq l < 1 \end{cases} \ . \tag{5.18}$$

However, this is essentially the helicity sampling method explained above, since the strength of the discontinuity at $l_i = \frac{1}{2}$ reflects the difference between the different helicity configurations. It is possible to bypass this problem using *random polarizations* [220]. The summation over gluon (or photon) polarization states is replaced by

$$\sum_{\lambda=\pm} \varepsilon_\mu^{\lambda *} \varepsilon_\nu^\lambda = \frac{1}{2\pi} \int_0^{2\pi} \mathrm{d}\phi \, \varepsilon_\mu^*(\phi) \varepsilon_\nu(\phi) \ , \tag{5.19}$$

where the randomly polarized vectors are

$$\varepsilon_\mu(\phi) = e^{i\phi} \varepsilon_\mu^+ + e^{-i\phi} \varepsilon_\mu^- \ . \tag{5.20}$$

The method can be straightforwardly extended to fermions using the replacements

$$\begin{aligned} u(\phi) &= e^{-i\phi} u^+ + e^{i\phi} u^- \ , \quad \bar{u}(\phi) = e^{i\phi} \bar{u}^+ + e^{-i\phi} \bar{u}^- \ , \\ v(\phi) &= e^{-i\phi} v^+ + e^{i\phi} v^- \ , \quad \bar{v}(\phi) = e^{i\phi} \bar{v}^+ + e^{-i\phi} \bar{v}^- \ . \end{aligned} \tag{5.21}$$

The spin summation becomes

$$\sum_{\lambda=\pm} u^\lambda \bar{u}^\lambda = \frac{1}{2\pi} \int_0^{2\pi} \mathrm{d}\phi \, u(\phi) \bar{u}(\phi) \ , \quad \sum_{\lambda=\pm} v^\lambda \bar{v}^\lambda = \frac{1}{2\pi} \int_0^{2\pi} \mathrm{d}\phi \, v(\phi) \bar{v}(\phi) \ . \tag{5.22}$$

The phase space integral and the polarization integral is now performed over a continuous integrand, contributions for different polarization angles $\{\phi_i\}$ will be of similar size and no spoiling of the Monte Carlo convergence is expected.

The random polarization method can be readily used for evaluation of contributions that are finite without subtraction terms. Contributions that do need subtraction are not finite anymore, since the subtraction terms are summed over polarizations configurations, as discussed in section 3.4.1. The locality of the subtraction terms will be lost. At next-to-leading order this problem has been solved by introducing randomly polarized subtraction terms for the real radiation contribution in the Catani-Seymour dipole subtraction formalism [221].
Another approach is to use a hybrid scheme of helicity sampling and random polarization [222]. In this context, subtraction terms for matrix elements of fixed polarization have been derived for the real radiation contribution at next-to-leading order in the dipole formalism. The splitting and soft partons have therefore fixed helicity states, while all other particles in the process are randomly polarized.
For the implementation of STRIPPER one of the above methods had to be chosen and extended to next-to-next-to-leading order subtractions. As it is not clear how to extend the former method to obtain randomly polarized subtraction terms as two particles become unresolved, the latter method has been chosen.
In the parameterization of STRIPPER it means that the reference partons $r$ or $r_1$ and $r_2$ and the unresolved partons $u$ or $u_1$ and $u_2$ have definite helicities and a sample over different helicity configurations is performed. The remaining particles in the process are randomly polarized. In the next sections, we explain how polarized subtraction terms are obtained as one or two particles become unresolved.

### 5.3.1 Soft polarized limits

A matrix element for a given polarization $\lambda$ of one soft gluon with momentum $q \to 0$ factorizes into a reduced matrix element and the eikonal current [138]

$$\langle c;\lambda|\mathcal{M}_{g,a1,\ldots,a_n}\rangle = g_s\,\varepsilon_\mu(q,\lambda)J^{c,\mu}(q)|\mathcal{M}_{a_1,\ldots,a_2}\rangle, \tag{5.23}$$

where the eikonal current is given by

$$\mathbf{J}^\mu = \sum_{i=1}^{n} \mathbf{T}_i \frac{p_i^\mu}{p_i\cdot q}\ . \tag{5.24}$$

It is important to notice that this factorization formula is independent of the polarizations of the remaining hard partons. It can be easily shown that no modifications of the spin summed subtraction term is necessary [222]. The squared matrix element contains the factor

$$\mathbf{J}^{c,\mu\,\dagger}\mathbf{J}^{c,\nu}\varepsilon_\mu(q,\lambda)\varepsilon^*_\nu(q,\lambda) = \mathbf{J}^{c,\mu\,\dagger}\mathbf{J}^{c,\nu}\varepsilon_\mu(q,-\lambda)\varepsilon^*_\nu(q,-\lambda) = \frac{1}{2}\mathbf{J}^{c,\mu\,\dagger}\mathbf{J}^{c}_\mu\ . \tag{5.25}$$

The equality is obtained by using the relation between positive and negative helicity polarization vectors

$$\varepsilon^*_\mu(p,\lambda) = e^{i\psi}\varepsilon_\mu(p,-\lambda)\ , \tag{5.26}$$

where $\psi$ is an arbitrary phase, and the hermiticity of the eikonal current has been used. Equation (5.25) proves that the polarized single soft subtraction term is just half the subtraction term of the related spin summed limit.
At next-to-next-to-leading order we consider the limit of two soft particles with momentum $q_1 \to 0$ and momentum $q_2 \to 0$. We consider the limit of a soft quark anti-quark pair with given helicity $\lambda_1$ and $\lambda_2$. The soft singularity is only present, if the quark pair is produced by a single gluon. In this

way a soft current can be derived by using the soft gluon insertion rules as in the single soft case [138]. The soft limit can be written as

$$\langle\lambda_1\lambda_2|\mathcal{M}_{q,\bar{q},a_1,\ldots,a_n}\rangle \simeq (4\pi\alpha_s)\,\frac{t^c_{c_1c_2}}{\sqrt{2}\langle q_1q_2\rangle}\,\tilde{\varepsilon}_\mu(q_1,q_2;\lambda_1,\lambda_2)\,\mathbf{J}^{c,\mu}(q_1+q_2)|\mathcal{M}_{a_1,\ldots,a_n}\rangle\,, \tag{5.27}$$

where the polarization vector $\tilde{\varepsilon}_\mu(q_1+q_2;\lambda_1,\lambda_2)$ in terms of the polarizations of the quark and anti-quark can be explicitly calculated using Feynman rules in the Spinor-Helicity formalism (see appendix A.3)

$$\begin{aligned}\tilde{\varepsilon}_\mu(q_1,q_2;+1,-1) &= \frac{[q_1|\gamma_\mu|q_2\rangle}{\sqrt{2}[q_2q_1]}\,,\\ \tilde{\varepsilon}_\mu(q_1,q_2;-1,+1) &= \frac{\langle q_1|\gamma_\mu|q_2]}{\sqrt{2}[q_2q_1]}\,.\end{aligned} \tag{5.28}$$

By helicity conservation, the two quarks have opposite helicity. As in the case of a single soft gluon there exist a simple relation between the polarization vector and its complex conjugate

$$\tilde{\varepsilon}^*_\mu(q_1,q_2;+1,-1) = e^{i\psi}\tilde{\varepsilon}_\mu(q_1,q_2;-1,+1)\,. \tag{5.29}$$

We square the limit of the amplitude and sum colors of the outgoing quark and anti-quark pair $c_1$ and $c_2$. Using the hermiticity of the soft current we obtain the factorization formula

$$\begin{aligned}\langle\mathcal{M}_{q,\bar{q},a_1,\ldots,a_n}(q_1,q_2,\ldots)|\lambda_1\lambda_2\rangle\langle\lambda_1\lambda_2|\mathcal{M}_{q,\bar{q},a_1,\ldots,a_n}(q_1,q_2,\ldots)\rangle \simeq\\ \frac{1}{2}\,(4\pi\alpha_s)^2\,T_F\sum_{ij}\mathcal{I}_{ij}(q_1,q_2)\,\langle\mathcal{M}^{(0)}_{a_1,\ldots}(p_1,\ldots)|\mathbf{T}_i\cdot\mathbf{T}_j|\mathcal{M}^{(0)}_{a_1,\ldots}(p_1,\ldots)\rangle\,,\end{aligned} \tag{5.30}$$

if $\lambda_1=+1$ and $\lambda_2=-1$ or $\lambda_1=-1$ and $\lambda_2=+1$. The right hand side is just half the soft limit of the matrix elements summed over helicities of the quark anti-quark pair. Again we remark that the soft limit is independent of the polarization of the remaining hard partons.
The soft limit of two gluons is described by the two-gluon eikonal current

$$\langle\lambda_1\lambda_2|\mathcal{M}_{g,g,a_1,\ldots,a_n}(q_1,q_2,p_1,\ldots)\rangle \simeq (4\pi\alpha_s)\,\varepsilon^{\mu*}(q_1,\lambda_1)\varepsilon^{\nu*}(q_2,\lambda_2)\,\mathbf{J}^{c_1,c_2}_{\mu\nu}(q_1,q_2)|\mathcal{M}(p_1,\ldots)\rangle\,, \tag{5.31}$$

where $q_i\to 0$ are the momenta of the soft gluons and $\varepsilon^\mu(q_i,\lambda_i)$ their polarization vectors, with $i=1,2$. The explicit form of the two-gluon current can be derived by taking into account all singular insertions of two soft gluons [20, 138]

$$\begin{aligned}\mathbf{J}^{c_1c_2}(q_1,q_2,\lambda_1,\lambda_2) \equiv \varepsilon_1^{\mu*}\varepsilon_2^{\nu*}\,\mathbf{J}^{c_1c_2}_{\mu\nu}(q_1,q_2) =\\ \frac{1}{2}\sum_{i,j}\{\mathbf{T}^{c_1}_i,\mathbf{T}^{c_2}_j\}J_{1,ij}(q_1,q_2;\lambda_1,\lambda_2) + if^{c_1c_2c_3}\sum_i\mathbf{T}^{c_3}_i\,J_{2,i}(q_1,q_2,\lambda_1,\lambda_2)\,,\end{aligned} \tag{5.32}$$

where the abbreviations $\varepsilon^\mu_i\equiv\varepsilon^\mu(q_i,\lambda_i)$, were introduced. The two auxiliary soft functions are given by

$$J_{1,ij}(q_1,q_2;\lambda_1,\lambda_2) = \frac{p_i\cdot\varepsilon^*_1\,p_j\cdot\varepsilon^*_2}{p_i\cdot q_1\,p_j\cdot q_2}\,, \tag{5.33}$$

and

$$J_{2,i}(q_1,q_2;\lambda_1,\lambda_2) = \frac{p_i\cdot\varepsilon_1^*\, q_1\cdot\varepsilon_2^* - p_i\cdot\varepsilon_2^*\, q_2\cdot\varepsilon_1^*}{(q_1\cdot q_2)\,[p_i\cdot(q_1+q_2)]} - \frac{p_i\cdot(q_1-q_2)}{2\,[p_i\cdot(q_1+q_2)]}\left[\frac{p_i\cdot\varepsilon_1^*\, p_i\cdot\varepsilon_2^*}{(p_i\cdot q_1)(p_i\cdot q_2)} + \frac{\varepsilon_1^*\cdot\varepsilon_2^*}{q_1\cdot q_2}\right] . \tag{5.34}$$

In the following the arguments of the functions $J_{1,ij}$ and $J_{2,i}$ are dropped for simplicity. The factorization formula squared provides the limit of the matrix element for a fixed helicity configuration of the soft gluons

$$\begin{aligned}\mathbf{J}^{c_1c_2\,\dagger}(q_1,q_2,\lambda_1,\lambda_2)\mathbf{J}^{c_1c_2}(q_1,q_2,\lambda_1,\lambda_2) = \\ &\frac{1}{4}\sum_{i,j,k,l} J_{1,ij}J_{1,kl}^*\{\mathbf{T}_k^{c_1},\mathbf{T}_l^{c_2}\}\{\mathbf{T}_i^{c_1},\mathbf{T}_j^{c_2}\} \\ &+\frac{1}{2}\sum_{i,j,k} if^{c_1c_2c_3}(J_{1,ij}^*J_{2,k}\{\mathbf{T}_i^{c_1},\mathbf{T}_j^{c_2}\}\mathbf{T}_k^{c_3} - J_{1,ij}J_{2,k}^*\mathbf{T}_k^{c_3}\{\mathbf{T}_i^{c_1},\mathbf{T}_j^{c_2}\}) \\ &+C_A\sum_{i,j} J_{2,i}^*J_{2,j}\mathbf{T}_i\cdot\mathbf{T}_j\ ,\end{aligned} \tag{5.35}$$

where a summation over the color indices is understood. The color algebra is simplified using the identities

$$if^{c_1c_2c_3}\mathbf{T}_k^{c_3}\{\mathbf{T}_i^{c_1},\mathbf{T}_j^{c_2}\} = 2if^{c_1c_2c_3}\mathbf{T}_k^{c_3}\mathbf{T}_i^{c_1}\mathbf{T}_j^{c_2}(1-\delta_{ik})(1-\delta_{ij})(1-\delta_{jk}) - C_A\mathbf{T}_i\cdot\mathbf{T}_j(\delta_{ik}-\delta_{jk})\ , \tag{5.36}$$

and

$$\begin{aligned}\{\mathbf{T}_i^{c_1},\mathbf{T}_j^{c_2}\}\{\mathbf{T}_k^{c_1},\mathbf{T}_l^{c_2}\} = &\,2\{\mathbf{T}_i\cdot\mathbf{T}_k,\mathbf{T}_j\cdot\mathbf{T}_l\} + C_A[\delta_{ij}\delta_{kl}\mathbf{T}_i\cdot\mathbf{T}_k + 2\delta_{il}\delta_{jk}\mathbf{T}_i\cdot\mathbf{T}_j \\ &-\delta_{ij}\delta_{ik}\mathbf{T}_i\cdot\mathbf{T}_l - \delta_{ij}\delta_{il}\mathbf{T}_i\cdot\mathbf{T}_k - \delta_{il}\delta_{ik}\mathbf{T}_i\cdot\mathbf{T}_j - \delta_{jl}\delta_{jk}\mathbf{T}_i\cdot\mathbf{T}_j] \\ &+2if^{c_1c_2c_3}\mathbf{T}_i^{c_1}\mathbf{T}_l^{c_2}\mathbf{T}_k^{c_3}\,\delta_{jk}(1-\delta_{il})(1-\delta_{ik})(1-\delta_{kl}) \\ &+2if^{c_1c_2c_3}\mathbf{T}_k^{c_1}\mathbf{T}_j^{c_2}\mathbf{T}_i^{c_3}\,\delta_{il}(1-\delta_{ik})(1-\delta_{jk})(1-\delta_{ij})\ .\end{aligned} \tag{5.37}$$

We recast the result into terms proportional to different color correlated matrix elements. The final form of the factorization formula in the double soft limit of two gluons reads

$$\begin{aligned}\langle\mathcal{M}_{g,g,a_1,\ldots,a_n}(q_1,q_2,\ldots)|\lambda_1\lambda_2\rangle\langle\lambda_1\lambda_2|\mathcal{M}_{g,g,a_1,\ldots,a_n}(q_1,q_2,\ldots)\rangle \simeq \\ (4\pi\alpha_s)^2\Big[&\frac{1}{2}\sum_{i,j,k,l} J_{1,ij}^*J_{1,kl}\langle\mathcal{M}^{(0)}_{a_1,\ldots,a_n}|\{\mathbf{T}_i\cdot\mathbf{T}_j,\mathbf{T}_k\cdot\mathbf{T}_l\}|\mathcal{M}^{(0)}_{a_1,\ldots,a_n}\rangle \\ &-\sum_{(i,j,k)}\Big(2\mathrm{Im}(J_{1,ij}^*J_{2,k}) + \mathrm{Im}(J_{1,kj}^*J_{1,ik}))\Big)\langle\mathcal{M}^{(0)}_{a_1,\ldots,a_n}|f^{abc}T_i^aT_j^bT_k^c|\mathcal{M}^{(0)}_{a_1,\ldots,a_n}\rangle \\ &-C_A\sum_{i,j}\tilde{\mathcal{S}}_{i,j}(q_1,q_2,\lambda_1,\lambda_2)\langle\mathcal{M}^{(0)}_{a_1,\ldots,a_n}|\mathbf{T}_i\cdot\mathbf{T}_j|\mathcal{M}^{(0)}_{a_1,\ldots,a_n}\rangle\Big]\ ,\end{aligned} \tag{5.38}$$

where the polarized two-gluon soft function is

$$\begin{aligned}\tilde{\mathcal{S}}_{i,j}(q_1,q_2,\lambda_1,\lambda_2) = \frac{1}{4}(&J_{1,ii}(J_{1,ij}^* + J_{1,ji}^* - J_{1,jj}^*) + J_{1,ji}J_{1,jj}^* - 2J_{1,ij}^*J_{2,i} + 2J_{1,ij}^*J_{2,j} \\ &- 4J_{2,i}J_{2,j}^* - J_{1,ij}(2J_{1,ji}^* - J_{1,jj}^* + 2J_{2,i}^* - 2J_{2,j}^*))\ .\end{aligned} \tag{5.39}$$

The triple color correlator only vanishes after summing over the polarizations of the soft gluons.

### 5.3.2 Polarized splitting functions

In section 3.4.1 the factorization of the unpolarized squared matrix element in the collinear limit of two or three partons has been discussed. Factorization remains valid, if the collinear partons are polarized. While for the $1 \to 2$ splitting the polarized splitting functions for the squared amplitude are still manageable [222], the splitting functions for the polarized $1 \to 3$ splittings are cumbersome. It turns out to be simpler to consider the collinear limit of the matrix element itself before squaring it.

The collinear limit of two final state partons with momentum $p_1$ and $p_2$ can be defined using the Sudakov parametrization (3.48) in the limit $k_\perp^2 \to 0$. The factorization formula for the matrix element reads [139, 223, 224]

$$\langle \lambda_1 \lambda_2 | \mathcal{M}_{a_1,a_2,\dots}(p_1,p_2,\dots)\rangle \simeq \sum_\lambda \mathrm{Split}_\lambda^{a\to a_1 a_2}(p_1^{\lambda_1},p_2^{\lambda_2}) \langle \lambda | \mathcal{M}_{a,\dots}(p,\dots)\rangle \,, \tag{5.40}$$

where the collinear factors depend on the helicity $\lambda$ of the splitting particle, which is chosen to be in the final state and the polarization of the collinear partons $\lambda_1$ and $\lambda_2$. Explicit formulas are given in the mentioned references. It is common to define a splitting matrix for the squared amplitude

$$\mathbf{P}^{a\to a_1 a_2}(p_1^{\lambda_1},p_2^{\lambda_2}) = \begin{pmatrix} P_{++}^{a\to a_1 a_2}(p_1^{\lambda_1},p_2^{\lambda_2}) & P_{+-}^{a\to a_1 a_2}(p_1^{\lambda_1},p_2^{\lambda_2}) \\ P_{-+}^{a\to a_1 a_2}(p_1^{\lambda_1},p_2^{\lambda_2}) & P_{--}^{a\to a_1 a_2}(p_1^{\lambda_1},p_2^{\lambda_2}) \end{pmatrix} \,, \tag{5.41}$$

where the entries are defined by

$$P_{\lambda'\lambda}^{a\to a_1 a_2}(p_1^{\lambda_1},p_2^{\lambda_2}) = [\mathrm{Split}_{\lambda'}^{a\to a_1 a_2}(p_1^{\lambda_1},p_2^{\lambda_2})]^\dagger \mathrm{Split}_\lambda^{a\to a_1 a_2}(p_1^{\lambda_1},p_2^{\lambda_2}) \,. \tag{5.42}$$

The summation of open color indices is always understood. The polarized subtraction term for the squared matrix element is finally written as a matrix-vector multiplication in helicity space

$$\begin{aligned} &\langle \mathcal{M}^{(0)}_{a_1,a_2,\dots}(p_1,p_2,\dots)|\lambda_1\lambda_2\rangle\langle\lambda_1\lambda_2|\mathcal{M}^{(0)}_{a_1,a_2,\dots}(p_1,p_2,\dots)\rangle \simeq \\ &\qquad (\langle \mathcal{M}_{a,\dots}(p,\dots)|+\rangle \ \langle \mathcal{M}_{a,\dots}(p,\dots)|-\rangle)\, \mathbf{P}^{a\to a_1 a_2}(p_1^{\lambda_1},p_2^{\lambda_2}) \begin{pmatrix} \langle +|\mathcal{M}_{a,\dots}(p,\dots)\rangle \\ \langle -|\mathcal{M}_{a,\dots}(p,\dots)\rangle \end{pmatrix} \,. \end{aligned} \tag{5.43}$$

The unpolarized splitting functions are recovered by summing over the polarizations of the collinear partons.

The same reasoning can be generalized to the more involved case of the triple-collinear limit. It is parameterized using the Sudakov parametrization for three final state partons of momentum $p_i$, Eq. (3.52), where again $p^2 = n^2 = p \cdot k_{\perp i} = n \cdot k_{\perp i} = 0$. The matrix element factorizes in the limit $k_{\perp i} \to 0$ [138, 225]

$$\langle \lambda_1 \lambda_2 \lambda_3 | \mathcal{M}_{a_1,a_2,a_3,\dots}(p_1,p_2,p_3\dots)\rangle \simeq \sum_\lambda \mathrm{Split}_\lambda^{a\to a_1 a_2 a_3}(p_1^{\lambda_1},p_2^{\lambda_2},p_3^{\lambda_3}) \langle \lambda | \mathcal{M}_{a,\dots}(p,\dots)\rangle \,, \tag{5.44}$$

where the triple splitting functions have been rederived for the implementation in Stripper. They are given in appendix B.4 and have been firstly calculated in [224]. A general recipe is discussed in the following how they can be obtained using the spinor helicity formalism (see A.3).

First, the diagrams contributing to given $a \to a_1 a_2 a_3$ process are generated. This has been done using the Mathematica packages FeynArts and FormCalc [226, 227]. Some modifications have to

be applied, since the Feynman amplitude has to be given in an axial gauge, which is not available a priori in FeynArts. There are five different processes that have to be taken into account

$$\begin{aligned} q &\to q\bar{q}'q' \,, \\ q &\to q\bar{q}q \,, \\ q &\to qgg \,, \\ g &\to g\bar{q}q \,, \\ g &\to ggg \,. \end{aligned} \tag{5.45}$$

Each contribution is expressed in terms of helicity spinors for a given polarization of the four involved partons, where spinors and polarization vectors are replaced as discussed in A.3. The spinor of the parton $a$ which is either $|p\rangle$ or $|p]$ is then replaced by

$$\not{p} = \not{p}_1 + \not{p}_2 + \not{p}_3 \,, \tag{5.46}$$

using energy-momentum conservation. The slashed contributions are reexpressed in terms of helicity spinors

$$\not{p}_i = |p_i\rangle[p_i| + |p_i]\langle p_i| \,. \tag{5.47}$$

They connect the splitting function and the actual matrix element. By simple power counting arguments, the spinor connected to the matrix element can be expanded to leading order in $k_\perp$

$$|p_i\rangle \simeq \sqrt{z_i}|p\rangle \,. \tag{5.48}$$

The factor $\sqrt{z_i}$ is kept in in the splitting function, while the spinor provides the full factorization of the matrix element. Apart from color factors and constants the splitting function only depends on Spinor invariants, if invariants $s_{ij}$ are appropriately replaced by $[p_ip_j]\langle p_jp_i\rangle$. The list of possible invariants is

$$\{[p_ip_j],[k_ip_j],[k_ik_j],\langle p_ip_j\rangle,\langle k_ip_j\rangle,\langle k_ik_j\rangle\}, \tag{5.49}$$

where $k_i$, $i = 0,1,2,3$, are reference momenta of the external gluons $a_i$ and the axial gauge vector $k_0$, which is also the reference vector of a splitting gluon, $a = g$ in the axial gauge.
In order to obtain the collinear limit of the splitting function just the leading terms in the collinear limit $k_\perp \to 0$ are retained. In practice this amounts to keep $[p_ip_j]$ and $\langle p_ip_j\rangle$, which scale as

$$[p_ip_j] = \sqrt{2p_i\cdot p_j}e^{i\psi} \sim \sqrt{-k_\perp^2} \,, \quad \langle p_ip_j\rangle = \sqrt{2p_i\cdot p_j}e^{-i\psi} \sim \sqrt{-k_\perp^2} \,, \tag{5.50}$$

while all remaining spinor products are expanded to leading order using (5.48). $\psi$ is a yet unspecified phase which is irrelevant for the discussion. The leading collinear behavior does not depend on the reference momenta $k_i$ anymore. The obtained functions are the splitting functions $\mathrm{Split}^{a\to a_1a_2a_3}$.
Similar to the collinear limit of two partons, a splitting matrix can be defined for the triple-collinear limit

$$\mathbf{P}^{a\to a_1a_2a_3}(p_1^{\lambda_1},p_2^{\lambda_2},p_3^{\lambda_3}) = \begin{pmatrix} P_{++}^{a\to a_1a_2a_3}(p_1^{\lambda_1},p_2^{\lambda_2},p_3^{\lambda_3}) & P_{+-}^{a\to a_1a_2a_3}(p_1^{\lambda_1},p_2^{\lambda_2},p_3^{\lambda_3}) \\ P_{-+}^{a\to a_1a_2a_3}(p_1^{\lambda_1},p_2^{\lambda_2},p_3^{\lambda_3}) & P_{--}^{a\to a_1a_2a_3}(p_1^{\lambda_1},p_2^{\lambda_2},p_3^{\lambda_3}) \end{pmatrix} \,, \tag{5.51}$$

where the definition of the entries can be easily adapted from (5.42).
The entries of the splitting matrices $\mathbf{P}$ for all possible flavor and helicity configurations are imple-

mented in STRIPPER and serve as collinear and soft-collinear subtraction terms. Initial state collinear limits are obtained by the crossing relations outlined in appendix B.5. For the implementation, the parameterization in the spinor helicity framework has to be related to the parameterization of resolved and unresolved particles given in section 4.2. Therefore, the flavor of the reference momentum $r$ has to be fixed to obtain all possible subtraction terms. For the $1 \to 2$ splitting the list of possible splitting matrices is

$$\{g \to \bar{q}q,\, q \to qg,\, q \to gq,\, g \to gg\}\,, \tag{5.52}$$

providing subtraction terms for single collinear limits in $\hat{\sigma}^F_{\mathrm{R}}$ and $\hat{\sigma}^F_{\mathrm{RR}}$. The list of splitting matrices for the $1 \to 3$ splittings is

$$\begin{aligned}\{&q \to \bar{q}'q'q,\ q \to \bar{q}'qq',\ q \to q\bar{q}'q',\ q \to \bar{q}qq,\ q \to qq\bar{q},\ q \to q\bar{q}q,\ q \to ggq,\\ &q \to qgg,\ q \to gqg,\ g \to qqg,\ g \to gqq,\ g \to qgq,\ g \to ggg\}\,,\end{aligned} \tag{5.53}$$

providing subtraction terms for the five triple-collinear sectors in $\hat{\sigma}^F_{\mathrm{RR}}$. The momentum assignments in the given lists are ordered like $a \to a_1(u)a_2(r)$ and $a \to a_1(u_1)a_2(u_2)a_3(r)$ respectively. Each of the five triple collinear sectors contains $13 \cdot 8 = 104$ polarized splitting matrices. The related spinor invariants are converted to the momentum parameterizations available in Stripper. Here, only the parameterization of triple-collinear splitting functions is discussed, the single-collinear functions are obtained as a special case.
The set of spinor invariants that appear in the splitting functions are

$$\{[u_1u_2], [ru_1], [ru_2], \langle u_1u_2\rangle, \langle ru_1\rangle, \langle ru_2\rangle\}. \tag{5.54}$$

Beforehand, it is useful to recognize that only two of the three are linearly independent

$$\langle u_1u_2\rangle = \frac{\sqrt{z_1}\langle ru_2\rangle - \sqrt{z_2}\langle ru_1\rangle}{\sqrt{z_r}} + \mathcal{O}((k_\perp)^2)\,. \tag{5.55}$$

Given the sector parameterizations, it is useful to choose $\langle ru_2\rangle$ and $\langle ru_1\rangle$ as the minimal set in sectors $\mathcal{S}_1 - \mathcal{S}_3$. Due to the fact that $r$ points already towards the triple-collinear direction, the invariants are directly related to the momenta and vectors in STRIPPER

$$\langle ru_1\rangle = \sqrt{2\,r\cdot u_1}(\sqrt{2}\,u_{1\perp}\cdot\varepsilon^*(r,+1))\,, \quad \langle ru_2\rangle = \sqrt{2\,r\cdot u_2}(\sqrt{2}\,u_{2\perp}\cdot\varepsilon^*(r,+1))\,, \tag{5.56}$$

where $\varepsilon(r,\lambda)$ is the polarization vector of a gluon in the collinear direction $r$. It is worth to recognize that the term in the brackets are pure phases.
In sectors $\mathcal{S}_4$ and $\mathcal{S}_5$ it is however more appropriate to choose $\langle ru_1\rangle$ and $\langle u_1u_2\rangle$ as the minimal set of invariants, where

$$\langle u_1u_2\rangle = \sqrt{2\,r\cdot u_1}(\sqrt{2}\,u_{3\perp}\cdot\varepsilon^*(r,+1))\,. \tag{5.57}$$

The choice of independent spinor invariants, depends on the allowed single-collinear limit within a triple-collinear sector. In sector $\mathcal{S}_1$ this is the limit $r||u_2$, in sector $\mathcal{S}_2$ and $\mathcal{S}_3$ it is the limit $r||u_1$, whereas in sector $\mathcal{S}_4$ and $\mathcal{S}_5$ it is $u_1||u_2$, as can be read off in Tab. 4.2.

### 5.3.3 Numerical tests

The implementation of the soft and collinear limits has been tested. Here, the tests for the triple-collinear limit and the double soft limits are explained. The correctness of the remaining cases, that

are not outlined here, has been verified in a similar way.
The triple-collinear limits of the matrix elements are implemented independently for each of the five triple-collinear sectors. The number of possible flavor assignments of the collinear partons has been counted in (5.53) to be 13. The total number of splitting functions, that provide collinear subtraction terms for amplitudes of a fixed helicity, is about $8 \times 13 = 104$ for each sector, where 8 is the number of possible helicity configurations of the reference and the two unresolved partons. Some of the limits are not possible by helicity conservation. The convergence of the matrix elements and their subtraction terms can be tested numerically. This test provides an important verification, whether the helicity subtraction terms are correct. It is useful to introduce the relative deviation of the integrand in the double-real radiation cross section for a specific sector $\mathcal{S}$

$$\delta_{\mathcal{S}}(x) = \left| \frac{\mathrm{d}\hat{\sigma}^{\mathrm{RR}}(x) - \mathrm{d}\hat{\sigma}^{\mathrm{RR,Limit}}(x)}{\mathrm{d}\hat{\sigma}^{\mathrm{RR}}(x)} \right| . \tag{5.58}$$

The partonic cross section $\mathrm{d}\hat{\sigma}^{\mathrm{RR}}(x)$ contains the full $n+2$ parton matrix element, where the helicities of the reference parton and the unresolved partons ($\lambda_{u_1}$,$\lambda_{u_2}$,$\lambda_r$) are fixed. The remaining partons are randomly polarized. The cross section $\mathrm{d}\hat{\sigma}^{\mathrm{RR,Limit}}(x)$ represents the limit of $\mathrm{d}\hat{\sigma}^{\mathrm{RR}}(x)$. The $n+2$ parton matrix element is replaced by the appropriate splitting matrix and reduced matrix elements. The variable $x$ is equal to $\eta_1$ in sector $\mathcal{S}_1$ and $\mathcal{S}_4$ and $\eta_2$ in sector $\mathcal{S}_2$, $\mathcal{S}_3$ and $\mathcal{S}_5$. In the triple-collinear limit, *i.e.* $x \to 0$, the quantity $\delta_{\mathcal{S}}(x) \to 0$. This behavior has been tested numerically for each possible configuration of flavor and helicity. It is important to test the collinear limits in the initial and final state to exclude possible errors related to the crossing of splitting functions.
The Figs. 5.2, 5.3, 5.4 and 5.5 display a selection of tests. All integration parameters have been fixed randomly. The function $\delta_{\mathcal{S}}(x)$ has been evaluated at 1000 points $x$ between $10^{-6}$ and $10^{-10}$ in double precision. It has been observed that this region provide numerical stable results for all functions. Each plot contains all possible helicity configurations of the collinear partons, which are represented using different colors: orange: $(+,+,+)$, pink: $(+,+,-)$, black: $(+,-,+)$, brown: $(-,+,+)$, purple: $(+,-,-)$, green: $(-,+,-)$, blue: $(-,-,+)$ and red: $(-,-,-)$. Especially, if only massless partons are considered in the partonic matrix element, different helicity configurations return the same matrix element. Hence, only a subset of the 8 curves is present in general. The displayed plots, verify the correct behavior in different sectors for different splitting functions.
The soft limit of two polarized gluons can be tested similarly using the function $\delta(x)$ in Eq. (5.58). The cross section $\mathrm{d}\hat{\sigma}^{\mathrm{RR,Limit}}(x)$ contains the polarized double soft limit of the $n+2$ matrix element, which has been calculated in (5.38). In this case, $x$ is equal to $\xi_2$ in all sectors and indicates the double soft limit. It is important to notice that these numerical tests not only demonstrate the correctness of the soft and splitting functions, but also confirm the correctness of all color correlated tree-level matrix elements. The numerical test for two different partonic processes is shown in Fig. 5.6. The left plot shows the behavior in the soft limit including massive partons. In this case, all possible helicity configurations of the two gluons are different. In the purely massless case the matrix element in the double soft limit for the helicity configuration (+,+) coincides with the matrix element of the helicity configuration (−,−) and the configuration (+,−) coincides with the configuration (−,+). In the very low $x$ region the linear behavior is spoiled due to numerical instabilities in evaluating the $n+2$ parton matrix element in double precision.
The tests nicely reflect the behavior of the regularized matrix elements in the soft and collinear limits. In the triple-collinear limit $\delta(x)$ behaves as $\sqrt{x}$, while in the double-soft limit it behaves as $x$.

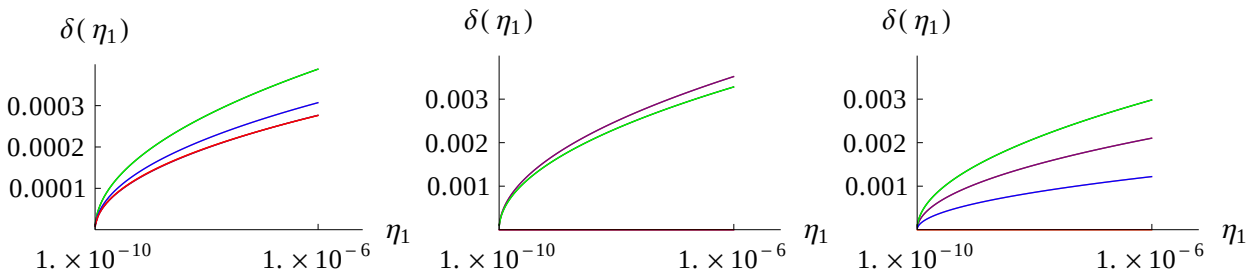


**Figure 5.2:** Numerical test of the triple-collinear limit in sector $\mathcal{S}_1$, where the three collinear partons with momentum $u_1$ ,$u_2$ and $r$ are in the final state. All 8 different helicities for the collinear partons are tested. Depending on the flavor assignment, some of them vanish or are identical. In the latter case the lines in the plot overlap. The assignment of different colors is explained in the main text.
**Left:** The partonic process is $ug \to ugggg$, where $a_r = g$, $a_{u_1} = g$ and $a_{u_2} = g$.
**Middle:** The partonic process is $ug \to ugd\bar{d}$, where $a_r = g$, $a_{u_1} = d$ and $a_{u_2} = \bar{d}$
**Right:** The partonic process is $u\bar{u} \to u\bar{u}u\bar{u}$, where $a_r = \bar{u}$, $a_{u_1} = u$ and $a_{u_2} = \bar{u}$ .

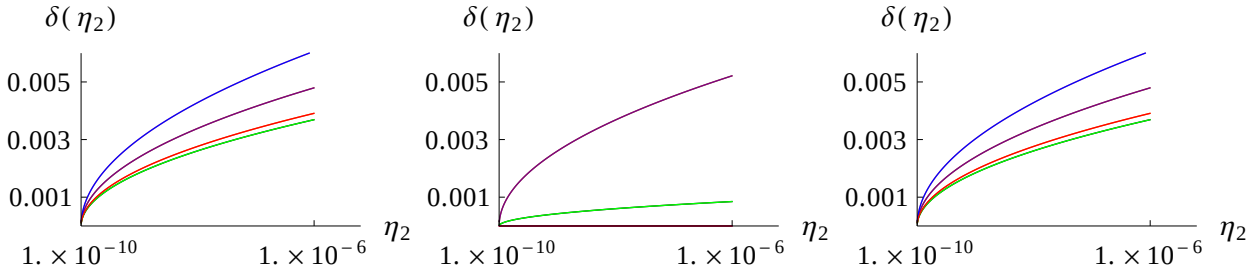


**Figure 5.3:** Numerical test of the triple-collinear limit in sector $\mathcal{S}_5$, where the three collinear partons with momentum $u_1$ ,$u_2$ and $r$ are in the final state. All 8 different helicities for the collinear partons are tested. Depending on the flavor assignment, some of them vanish or are identical. In the latter case the lines in the plot overlap. The assignment of different colors is explained in the main text.
**Left:** The partonic process is $ug \to ugggg$, where $a_r = u$, $a_{u_1} = g$ and $a_{u_2} = g$.
**Middle:** The partonic process is $ug \to ugd\bar{d}$, where $a_r = u$, $a_{u_1} = d$ and $a_{u_2} = \bar{d}$
**Right:** The partonic process is $\bar{u}g \to \bar{u}ggg$, where $a_r = \bar{u}$, $a_{u_1} = g$ and $a_{u_2} = g$ .

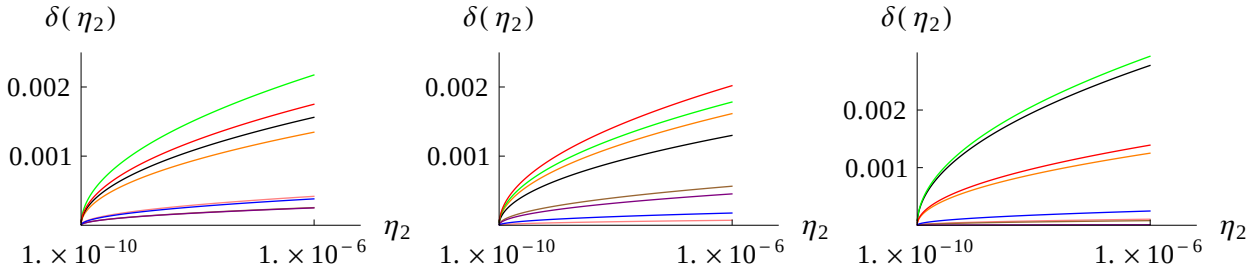


**Figure 5.4:** Numerical test of the triple-collinear limit in sector $\mathcal{S}_2$, where the reference parton $r$ is in the initial state. All 8 different helicities for the collinear partons are tested. Depending on the flavor assignment, some of them vanish or are identical. In the latter case the lines in the plot overlap. The assignment of different colors is explained in the main text.
**Left:** The partonic process is $u\bar{u} \to ggt\bar{t}$, where $a_r = \bar{u}$, $a_{u_1} = g$ and $a_{u_2} = g$
**Middle:** The partonic process is $ug \to ugt\bar{t}$, where $a_r = g$, $a_{u_1} = u$ and $a_{u_2} = g$
**Right:** The partonic process is $gg \to ggt\bar{t}$, where $a_r = g$, $a_{u_1} = g$ and $a_{u_2} = g$.

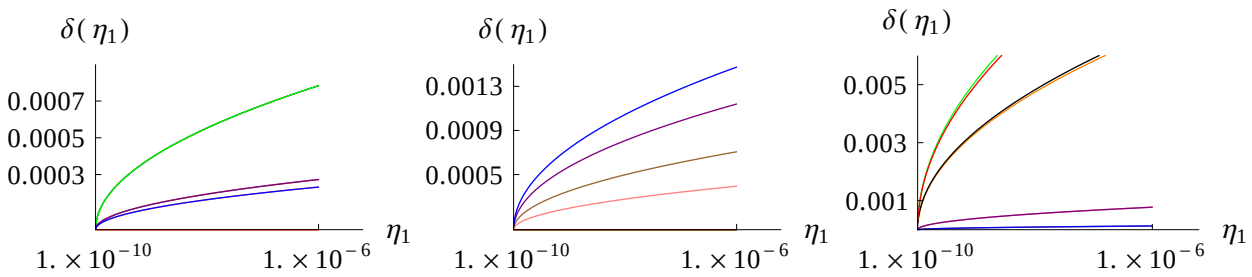


**Figure 5.5:** Numerical test of the triple-collinear limit in sector $\mathcal{S}_4$, where the reference parton $r$ is in the initial state. All 8 different helicities for the collinear partons are tested. Depending on the flavor assignment, some of them vanish or are identical. In the latter case the lines in the plot overlap. The assignment of different colors is explained in the main text.
**Left:** The partonic process is $u\bar{u} \to u\bar{u}d\bar{d}$, where $a_r = \bar{u}$, $a_{u_1} = u$ and $a_{u_2} = \bar{u}$.
**Middle:** The partonic process is $u\bar{d} \to u\bar{d}t\bar{t}$, where $a_r = \bar{d}$, $a_{u_1} = d$ and $a_{u_2} = \bar{u}$
**Right:** The partonic process is $\bar{u}g \to \bar{u}gt\bar{t}$, where $a_r = g$, $a_{u_1} = \bar{u}$ and $a_{u_2} = g$

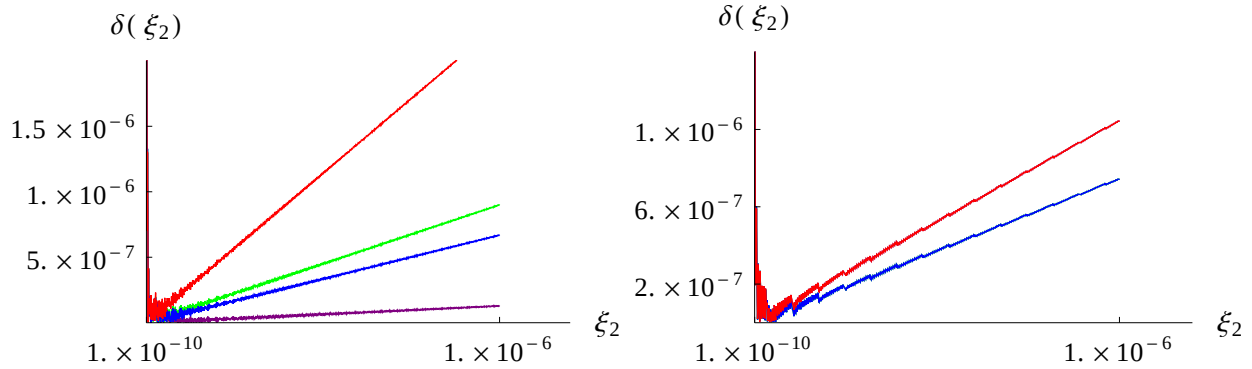


**Figure 5.6:** Numerical test of the soft limit of two polarized gluons in sector $\mathcal{S}_1$. The four possible helicity assignments for the unresolved gluons are displayed: purple: (+,+), green: (+,−), blue: (−,+) and red: (−,−). In the purely massless case respectively two helicity states coincide.
**Left:** The partonic process is $gg \to t\bar{t}gg$
**Right:** The partonic process is $gg \to d\bar{d}gg$

## 5.4 Special functions

The limits of one-loop matrix elements elements contain special functions that have to be evaluated for every point of the Monte Carlo integration. These functions are implemented efficiently in STRIPPER as will be outlined in this section.

### 5.4.1 Polylogarithms

Setting up the subtraction scheme at next-to-next-to-leading order, the evaluation of harmonic polylogarithms up to weight four is needed. Polylogarithms in the context of multi-loop calculations have been extensively studied and libraries exist to evaluate the real and imaginary part of these functions for arbitrary, complex arguments [228]. For the present application to physical cross sections only real parts of harmonic polylogarithms of real arguments are needed. Consequently, a independent implementation is useful. The polylogarithms are defined recursively as

$$\mathrm{Li}_n(x) = -\int_0^x \frac{\mathrm{d}t}{t}\,\mathrm{Li}_{n-1}(t)\;,\;\text{with}\,x\in(-\infty,1)\;, \tag{5.59}$$

where

$$\mathrm{Li}_1(x) = \log(1-x)\;. \tag{5.60}$$

For the numerical evaluation of the functions for $n\in\{2,3,4\}$, Eq. (5.59) is expanded in a Taylor-series in the Bernoulli variable $u$, which is defined as [228]

$$x = 1-e^{-u}\;,\quad u = -\log(1-x)\,. \tag{5.61}$$

This change of variables improves the convergence of the series significantly. This expansion is used in the range $\left[-1,\frac{1}{2}\right]$. A sufficient precision is obtained, if 7 terms for $\mathrm{Li}_2$, 13 terms for $\mathrm{Li}_3$ and 13 terms for $\mathrm{Li}_4$ are kept, if a Chebychev economization of the series is performed. The range $\left(\frac{1}{2},1\right)$ is obtained by using the transformation properties of the polylogarithms under the transformation $x\to 1-x$

$$\begin{aligned}
\mathrm{Li}_2(1-x) &= -\mathrm{Li}_2(x) - \log(x)\log(1-x) + \zeta_2\,,\\
\mathrm{Li}_3(1-x) &= -S_{1,2}(x) + \log(1-x)\left(\mathrm{Li}_2(1-x) + \frac{1}{2}\log(x)\log(1-x)\right) + \zeta_3\,,\\
\mathrm{Li}_4(1-x) &= -S_{1,3}(x) + \zeta_4\\
&\quad - \log(1-x)\left(S_{1,2}(x) - \frac{1}{2}\log(1-x)\left(\zeta_2 - \mathrm{Li}_2(x) - \frac{1}{3}\log(x)\log(1-x)\right) - \zeta_3\right)\;,
\end{aligned}$$

where $\zeta_n$ is the Riemann $\zeta$-function. The Nielsen polylogarithms $S_{1,p}(x)$ are defined by

$$S_{1,p}(x) = \frac{(-1)^p}{p!}\int_0^1 \frac{\mathrm{d}t}{t}\log^p(1-xt)\;. \tag{5.62}$$

They are only needed in the range $\left[0,\frac{1}{2}\right]$ and are evaluated using an optimized series expansion as well. For $S_{1,2}(x)$ 6 coefficients are needed, while for $S_{1,3}(x)$ 7 coefficients are kept.
The evaluation of $\mathrm{Li}_n$ in the range $(-\infty,-1)$ is done using identities of the functions for the

transformation $x \to 1/x$. They read

$$\begin{aligned}
\mathrm{Li}_2(\frac{1}{x}) &= -\mathrm{Li}_2(x) - \frac{1}{2}\log^2(-x) - \zeta_2, \\
\mathrm{Li}_3(\frac{1}{x}) &= \mathrm{Li}_3(x) + \log(-x)\left(\zeta_2 + \frac{1}{6}\log^2(-x)\right), \\
\mathrm{Li}_4(\frac{1}{x}) &= -\mathrm{Li}_4(x) - \frac{1}{2}\log^2(-x)\left(\zeta_2 + \frac{1}{12}\log^2(-x)\right) - \frac{7}{4}\zeta_4.
\end{aligned}$$

The relative precision of the numerical implementation has been tested and is depicted in Fig. 5.7. It is described by the function

$$\delta_i = \frac{(\mathrm{Li}_i^{\mathrm{exact}}(x) - \mathrm{Li}_i^{\mathrm{num}}(x))}{\mathrm{Li}_i^{\mathrm{exact}}(x)}\,, \tag{5.63}$$

where the superscript *num* refers to the numerically evaluated function in double precision and the superscript *exact* refers to an arbitrary precision evaluation in MATHEMATICA. A overall precision of better than $10^{-15}$ is achieved.

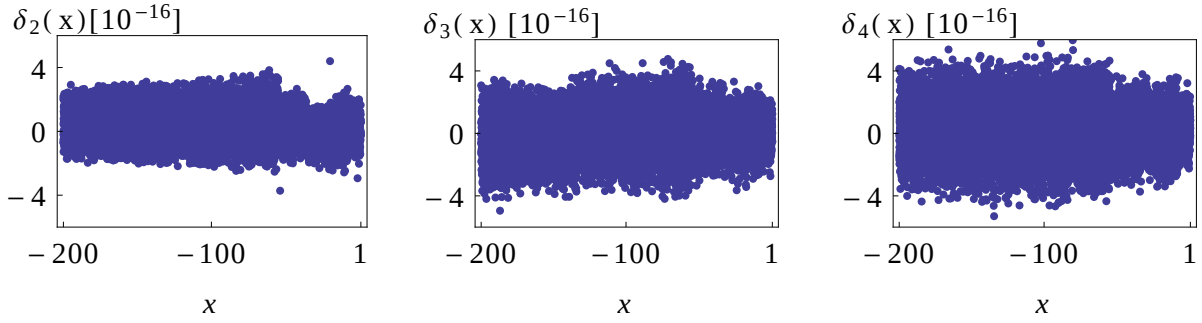


**Figure 5.7:** Relative precision of the numerical evaluation of $\mathrm{Li}_2(x)$, $\mathrm{Li}_3(x)$ and $\mathrm{Li}_4(x)$ in the range $[-200,1]$. The overall relative precision is better than $10^{-15}$

### 5.4.2 One-loop soft function

The soft limit of a one-loop matrix element, which has been discussed in Eq. (3.59), contains the function $R_{ij}$ which can be found in [146]. The explicit form of this function depends on whether the hard partons $i$ and $j$ are massless or massive. In the case that both partons are massive, $i = I$ and $j = J$, $R_{IJ}$ contains the following function

$$F_c(x_1,x_2) = \int_0^1 \mathrm{d}t \frac{\ln(1-t)\ln(1-t\frac{x_2}{x_1})}{\frac{1}{x_2} - t}\,, \tag{5.64}$$

where the arguments are defined by the momenta of the massive partons $p_I$ and $p_J$ and the momentum of the soft parton $q$. They read

$$x_1 = \frac{\alpha_J}{\alpha_J - v + 1}\,, \quad x_2 = \frac{\alpha_J}{\alpha_J + v + 1}\,, \tag{5.65}$$

where

$$v = \sqrt{1 - \frac{m_I^2 m_J^2}{(p_I \cdot p_J)^2}}\,, \quad \alpha_J = \frac{m_J^2 (p_J \cdot q)}{(p_J \cdot q)(p_I \cdot p_J)}\,. \tag{5.66}$$

The physical domain of the function is easily obtained by replacing the first variable

$$\tilde{x}_1(x_1,x_2) = \frac{x_2}{x_1}\,. \tag{5.67}$$

The function reads

$$F_c(x_1,x_2) = x_2 \int_0^1 \mathrm{d}t \frac{\ln(1-t)\ln(1-t\,\tilde{x}_1(x_1,x_2))}{1-x_2 t}\,. \tag{5.68}$$

The kinematic parameters $v$ and $\alpha_J$ are Lorentz invariant and can be written in the rest frame of $p_J$

$$\begin{aligned} v &= \frac{|\vec{p}_I|}{E_I} && \to && v \in [0,1)\,, \\ \alpha_J &= 1 - \frac{|\vec{p}_I|}{E_I}\cos\theta && \to && \alpha_J \in (0,2)\,, \end{aligned} \tag{5.69}$$

where $\theta$ is the angle between the soft particle and $p_I$ in the chosen frame. After rewriting the two variables $\tilde{x}_1$ and $x_2$, the domain of the function is obtained

$$\begin{aligned} \tilde{x}_1 &= \frac{2 - v(1+\cos\theta)}{2 + v(1-\cos\theta)} \in (0,1]\,, \\ x_2 &= \frac{1 - v\cos\theta}{2 + v(1-\cos\theta)} \in \left(0,\frac{1}{2}\right]\,. \end{aligned} \tag{5.70}$$

For the numerical evaluation, the function is expanded in a two-dimensional Taylor series around zero. The convergence can be improved substantially by using the Bernoulli change of variables, Eq. (5.61), in both variables. This expansion is only valid as $x_2$ and $\tilde{x}_1$ are small. For $\tilde{x}_1 \sim 1$ it breaks down, since the Bernoulli change of variable is not defined anymore. The integration domain is split into two regions. The first region is

$$\tilde{x}_1 \in \left(0,\frac{1}{2}\right] \quad x_2 \in \left(0,\frac{1}{2}\right]\,. \tag{5.71}$$

In this region the expansion can be used and the aimed precision is achieved, if $17 \times 16 = 272$ coefficients are kept. The second region is defined by

$$\tilde{x}_1 \in \left(\frac{1}{2},1\right] \quad x_2 \in \left(0,\frac{1}{2}\right]\,. \tag{5.72}$$

A expansion in $u_2 = -\log(1-x_2)$ is still convergent and reads

$$F_c(\tilde{x}_1,x_2) \simeq \sum_{i=0}^{n} f_i(\tilde{x}_1) u_2^i\,, \tag{5.73}$$

where $n = 20$ terms are kept. The coefficients $f_i(x_1)$ are integrated analytically and can be written in the following form

$$f_i(\tilde{x}_1) = \sum_{j=0}^{i} \left[ a_{ij} + \frac{1-\tilde{x}_1}{\tilde{x}_1} \log(1-\tilde{x}_1) b_{ij} + \frac{1-\tilde{x}_1}{\tilde{x}_1} \mathrm{Li}_2\left(\frac{\tilde{x}_1}{\tilde{x}_1 - 1}\right) c_{ij} \right] \cdot \tilde{x}_1^{-j} \,, \tag{5.74}$$

where it should be recognized that the coefficient matrices $a_{ij}$, $b_{ij}$ and $c_{ij}$ are triangular. The relative precision of the numerical evaluation of the function has been verified and is depicted in Fig. 5.8, where

$$\delta(\tilde{x}_1,x_2) = \left| \frac{F_c^{\text{exact}}(\tilde{x}_1,x_2) - F_c^{\text{num}}(\tilde{x}_1,x_2)}{F_c^{\text{exact}}(\tilde{x}_1,x_2)} \right| \,. \tag{5.75}$$

The exact evaluation of the function has been performed using MATHEMATICA.

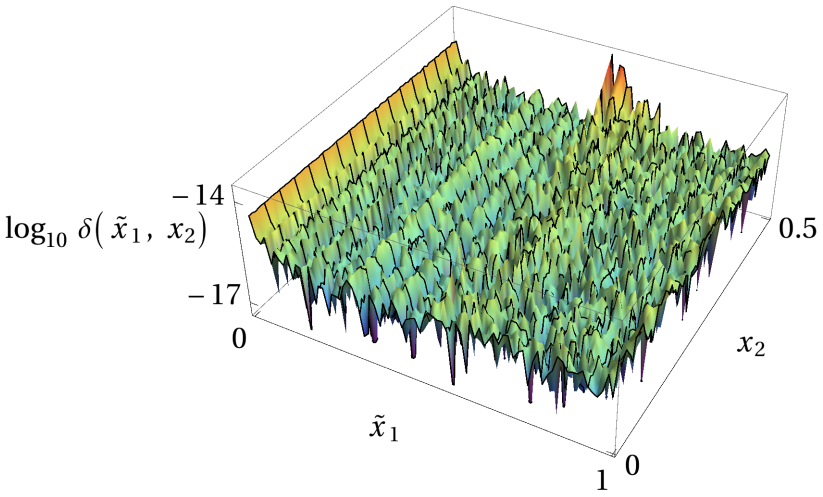


**Figure 5.8:** . Comparison of the numerical implementation of the function $F_c(\tilde{x}_1,x_2)$ with an arbitrary precision evaluation in MATHEMATICA. A grid of $80 \times 80$ points is used. The relative precision in all points is better than $10^{-13}$.

## 5.5 Missed binning

Differential cross section calculations suffer from *missed binning* effects starting at next-to-leading order. These effects occur if additional partons in the phase space become unresolved. At next-to-leading order this would be the finite real contribution $\hat{\sigma}^{\mathrm{R}}_{\mathrm{F}}$. The kinematics of the $n+1$ parton phase space contribution could correspond to a different histogram bin than the corresponding kinematics of the $n$ parton subtraction term. If this configuration occurs close to a singular point of the $n+1$ parton phase space, the subtraction term does not provide a regularization of the integrand. The same phenomenon occurs not only at the edge of histogram bins, but also if cuts are applied. The $n+1$ contribution can be accepted by the cut, while the subtraction term could be dismissed. In both cases, the Monte Carlo integration error is enhanced and more evaluations of the integrand are needed in order to keep the error acceptable. At next-to-next-to-leading order the effect of missed binning is expected to be larger, since more possibilities of singular limits are possible, for example in the double-real contribution $\hat{\sigma}^{\mathrm{RR}}_{\mathrm{FF}}$.

An approach to diminish the effects of missed binning is bin *smearing*. The fixed boundaries of a bin (or the position of the cut) are replaced by a Gaussian distribution around some mean position

$\mu$ and the standard deviation $\sigma$

$$P(x) = \frac{1}{\sigma\sqrt{2\pi}} e^{-\frac{(x-\mu)^2}{2\sigma^2}} \ . \tag{5.76}$$

The probability that the event at $x$ is distributed into the left bin is given by

$$s(x) \equiv \int_x^\infty \mathrm{d}x' P(x') = \frac{1}{2}\mathrm{erfc}\left(\frac{(x-\mu)}{\sqrt{2}\sigma}\right) \ , \tag{5.77}$$

which is the probability that the bin edge is to the right of $x$. The weight of the event $w(x)$ is distributed into the left and the right bin, where the modified weights are given by $s(x)w(x)$ and $(1-s(x))w(x)$ respectively. The distribution of a given event between two neighboring bins is called smearing. Smearing reduces the statistical error, but it also changes the edges of the bins. It should therefore only be applied to cases which contribute little to the cross section, such that the effect on the bins is small.
The effects of missed binning at next-to-leading order using STRIPPER are depicted in Figs. 5.9 and 5.10. The hadronic differential cross-sections $\mathrm{d}\hat{\sigma}_{\mathrm{F}}^{\mathrm{R}}$ for $pp \to t\bar{t} + X$ in the rapidity $y_t$ of the top quark are shown. Each plot shows the same contribution for a different smearing parameter $s$, which defines the width of the Gaussian distribution

$$\sigma = s\Delta_{\mathrm{bin}} \ , \tag{5.78}$$

where $\Delta_{\mathrm{bin}}$ is the width of a single bin. The error band is due to the statistical error of the Monte-Carlo integration. In each plot of Fig. 5.9 1 million events are evaluated. If no smearing

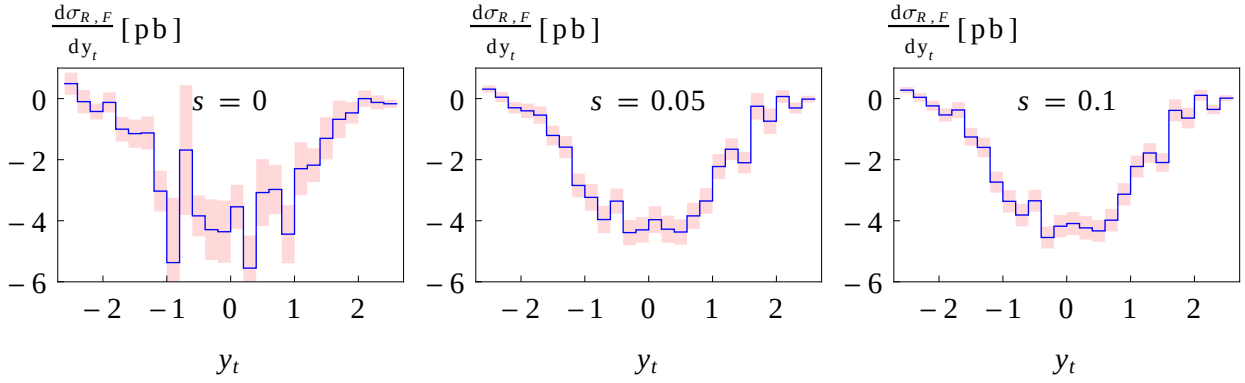


**Figure 5.9:** The effects of bin smearing on the statistical error of differential hadronic cross section $\mathrm{d}\hat{\sigma}_{\mathrm{F}}^{\mathrm{R}}$, for 1 million integration points. The center-of-mass energy is 8 TeV. The differential distributions are taken in the rapidity of the top quark $y_t$ for different values of the smearing parameter $s$, which is defined in the text.

is applied, $s = 0$, the contribution has a huge statistical uncertainty in each bin, which is due to missed binning. The error decreases significantly, if a smearing is applied $s = 0.05$. The difference between $s = 0.05$ and $s = 0.1$ is not significant. Hence, already for $s = 0.05$ the main part of missed binning effects that spoil the convergence of the integration are regularized by the smearing. In Fig. 5.10 the same integration has been performed, only the statistics have been increased by a factor 10. This increase already reduces the impact of missed binning effects considerably. Including bin smearing $s = 0.05$ and $s = 0.1$ reduces the effects further. The contribution of $\mathrm{d}\hat{\sigma}_{\mathrm{F}}^{\mathrm{R}}$ to the full next-to-leading order cross section is rather small. In the given example case it amounts of less than 10%, such that smearing uncertainties are negligible.

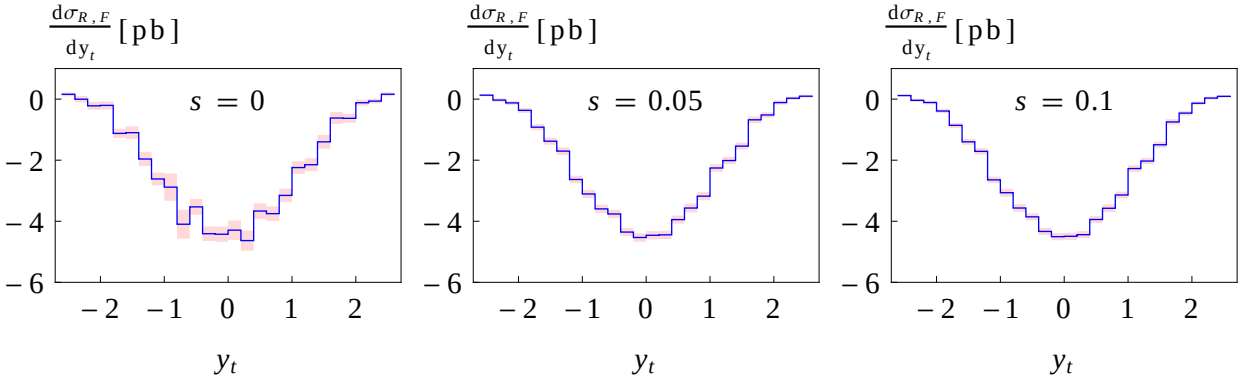


**Figure 5.10:** The effects of bin smearing on the statistical error of differential hadronic cross section $d\hat{\sigma}_F^R$, for 10 million integration points. The center-of-mass energy is 8 TeV. The differential distributions are taken in the rapidity of the top quark $y_t$ for different values of the smearing parameter $s$, which is defined in the text.

### 5.5.1 Missed binning in integrated subtraction terms

Integrated subtraction terms suffer from missed binning in the same way as the finite subtracted contributions discussed previously. In principle, the same treatment can be applied to minimize its effect on the distribution. The difference to the finite subtracted contributions $\hat{\sigma}_F^R$ and $\hat{\sigma}_F^{RR}$ is that in the unresolved contributions the pole term and the subtraction term contain the same resolved and unresolved partons. However, the kinematics in the collinear and the soft-collinear limit are different due to the specific parameterization. This leads to missed binning. A mapping of the kinematics in the collinear limit to the kinematics in the soft-collinear limit is however possible and this treatment avoids effects of missed binning completely. There are several cases to distinguish. One parton can become soft and collinear to an initial or final state parton, which occurs in the single-collinear sector. Two partons can become collinear to an initial or final state parton, where either both or only one can become soft. This occurs in the triple-collinear sector. Finally, two partons can become collinear to two different partons, which can be both in the final state, both in the initial state or one in the final state and one in the initial state. Either both unresolved partons can become soft or only one of them. This configuration occurs in the double-collinear sector.

#### Single-collinear sector

In this section the reparameterization of the collinear pole term in $\hat{\sigma}_U^R$ and $\hat{\sigma}_{DU}^{RV}$. The case of an initial-state collinear limit is discussed first. Including the convolution with the parton distribution function the collinear configuration is

$$\int_0^1 d\xi \int_{x_{\min}}^1 dx\, f(x)\sigma(x,\xi) \,, \tag{5.79}$$

where $f(x)$ is the parton distribution function, given in Eq. (3.9). The variable $x$ is the convolution parameter $x_1$, if the reference momentum is $p_1$, or $x_2$, if the reference momentum is $p_2$. The soft variable of the collinear parton is $\xi$. The minimal value $x_{\min} = (Q_{\min}/\sqrt{s})^2$ is related to the sum of external masses and is given in Eq. (4.14). The resolved particle entering the matrix element in the

collinear limit has energy

$$\frac{1}{2}E_{\mathrm{cms}}(x) - E_{\mathrm{max}}(x)\xi \;, \tag{5.80}$$

where the partonic center-of-mass energy $E_{\mathrm{cms}}(x)$ is obtained from the hadronic center-of-mass energy $\sqrt{s}$ by

$$\frac{1}{2}E_{\mathrm{cms}}(x) = \sqrt{xs} \;. \tag{5.81}$$

The unresolved parton energy is rescaled as in Eq. (4.25), where the maximal energy depends on the momentum fraction $x$

$$E_{\mathrm{max}}(x) = \frac{E_{\mathrm{cms}}(x)}{2}\left(1 - \left(\frac{Q_{\mathrm{min}}}{E_{\mathrm{cms}}(x)}\right)^2\right) \;. \tag{5.82}$$

By a change of the convolution variable $x \to x'$ it is possible to change the energy of the collinear parton, such that the center-of-mass energy is the same as in the soft-collinear limit, where $\xi \to 0$. This requirement reads

$$2\left(\frac{1}{2}E_{\mathrm{cms}}(x) - E_{\mathrm{max}}(x)\xi\right)E_{\mathrm{cms}}(x) = E^2_{\mathrm{cms}}(x') \;, \tag{5.83}$$

which leads to the transformation rule

$$z(x') \equiv \frac{x'}{x} = \frac{1-\xi}{1 - \left(\frac{Q_{\mathrm{min}}}{E_{\mathrm{cms}}(x')}\right)^2\xi} \;. \tag{5.84}$$

The integral is rewritten in terms of the new convolution variable

$$\int_0^1 \mathrm{d}\xi \int_{x_{\mathrm{min}}}^1 \mathrm{d}x\, f(x)\sigma(x,\xi) = \int_0^1 \mathrm{d}\xi \frac{\mathrm{d}x'}{1-\xi}\,\theta(z(x') - x')f\left(\frac{x'}{z(x')}\right)\sigma(\frac{x'}{z(x')},\xi) \;. \tag{5.85}$$

The kinematics entering the matrix element in $\sigma$ are as if $\xi = 0$. The transformation $x \to x'$ is nothing but a boost along the beam axis.
If the reference particle is in the final state, the same reasoning can be applied. The reference energy is rescaled by its maximal energy $r^0_{\mathrm{max}}$, given in Eq. (4.22) with $z = 1$, in the collinear limit it reads

$$r^0 = E_{\mathrm{max}}(1-\xi)\xi_r \;. \tag{5.86}$$

The energy of the parton that enters the matrix element in the collinear limit is the sum of the energy of the reference parton and the unresolved parton. A transformation of the energy variable $\xi_r \to \xi_{r'}$ can be determined, such that the kinematics in the collinear limit are the same as the kinematics in the soft-collinear limit. The requirement reads

$$E_{\mathrm{max}}(1-\xi)\xi_r + E_{\mathrm{max}}\xi = E_{\mathrm{max}}\xi_{r'} \;, \tag{5.87}$$

which is rewritten as

$$\xi_r = \frac{\xi_{r'} - \xi}{1-\xi} \;. \tag{5.88}$$

The transformation of the relevant integral is finally given by

$$\int_0^1 \mathrm{d}\xi \int_0^1 \mathrm{d}\xi_r \sigma(\xi_r,\xi) = \int_0^1 \mathrm{d}\xi \int_0^1 \frac{\mathrm{d}\xi_{r'}}{1-\xi} \theta(\xi_{r'}-\xi) \sigma\left(\frac{\xi_{r'}-\xi}{1-\xi},\xi\right) . \tag{5.89}$$

Single-collinear sector in a boosted reference frame

There is yet another situation that has to be taken into account for a single-collinear sector. The collinear renormalization contribution $\hat{\sigma}^{\mathrm{C1}}$, as given in Eq. (3.24) contains a convolution of $\hat{\sigma}^{\mathrm{R}}$ with a splitting function. The reference and the unresolved parton are defined in the center-of-mass frame of $p_1 + p_2$, while the contribution is evaluated for a boosted initial state momentum $zp_1 + p_2$. The case $p_1 + zp_2$ is obtained by symmetry. Missed binning is related to the different kinematics of the case $z = 1$ and $z \neq 1$. It can be avoided by changing the convolution variable $x_1 \to x_1/z$, if $z \neq 1$. The center-of-mass energy is as if $z = 1$, since effectively the partonic momentum $p_1$ is replaced by $p_1/z$. This is effectively a boost along the beam axis, where the corresponding rapidity is

$$y = \frac{1}{2} \log z . \tag{5.90}$$

Unfortunately, the reference momentum and the unresolved momentum in $\hat{\sigma}^{\mathrm{R}}$ are now defined in the center-of-mass frame of $p_1/z + p_2$. In order to match the kinematics at $z = 1$ they have to be boosted to the center-of-mass frame of $p_1 + p_2$, by a boost in $z$-direction of rapidity $y$. The corresponding Lorentz-matrix for the transformation of the energy and the $z$-component reads

$$\Lambda(z) = \frac{1}{2\sqrt{z}} \begin{pmatrix} 1+z & z-1 \\ z-1 & 1+z \end{pmatrix} . \tag{5.91}$$

Since, the unresolved parton is parameterized with respect to the resolved parton, as explained in section 4.2.1, only the angle of the reference momentum with respect to the $z$-axis, $\alpha_1$, is effected by the boost. In this particular case the rescaled energy parameters $\xi_r$ and $\xi$ do not change, as they describe the same energy fraction in both frames. The transformation of the cosine of the angle reads

$$\cos\alpha_1 \longrightarrow \frac{(1+z)\cos\alpha_1 - (1-z)}{(1+z) - (1-z)\cos\alpha_1} . \tag{5.92}$$

Triple-collinear sector

The triple-collinear contribution to $\hat{\sigma}^{\mathrm{RR}}_{\mathrm{DU}}$ is considered. The energy of the collinear parton entering the matrix element is given by the sum of the reference parton and the unresolved partons

$$r^0 + u_1^0 + u_2^0 , \tag{5.93}$$

where the parameterization in terms of sector variables is given in Eq. (4.35) and Tab. 4.2. A transformation of the integration variable in the collinear limit should either reproduce the triple-collinear double soft kinematics, if both unresolved partons can become soft or the triple-collinear single soft kinematics, if only one of the partons can become soft. The former case corresponds to a mapping of $r^0 + u_1^0 + u_2^0 \to r^0$, while the latter corresponds to a mapping $r^0 + u_1^0 + u_2^0 \to r^0 + u_1^0$. The mappings given in Tab. 4.2 allow that either both partons are soft or $u_2$ is soft. Another possible case is, when $u_2$ is already soft. Then the mapping should be $r^0 + u_1^0 \to r^0$. As in the single-collinear case the reference parton can be in the initial state or in the final state. If the reference parton is in

the initial state the condition Eq. (5.83) can be generalized and reads

$$2\left(\frac{1}{2}E_{\mathrm{cms}}(x)-E_{\max}(x)\xi\right)E_{\mathrm{cms}}(x)=2\left(\frac{1}{2}E_{\mathrm{cms}}(x')-E_{\max}(x')\xi'\right)E_{\mathrm{cms}}(x')\,, \tag{5.94}$$

where depending on the mapping the variables $\xi$ and $\xi'$ are given in Tab. 5.2. The solution is easily obtained

$$z(x')\equiv\frac{x'}{x}=\frac{1-\xi}{1-\xi'-\left(\frac{Q_{\min}}{E_{\mathrm{cms}}(x')}\right)^2(\xi-\xi')}\,. \tag{5.95}$$

The integral reads

$$\int_{x_{\min}}^{1}\mathrm{d}x\,f(x)\sigma(x,\xi)=\mathrm{d}x'\frac{1-\xi'}{1-\xi}\,\theta(z(x')-x')f\left(\frac{x'}{z(x')}\right)\sigma\left(\frac{x'}{z(x')},\xi\right)\,. \tag{5.96}$$

If the reference momentum is in the final state, the reasoning of the single-collinear case can be easily generalized, see Eq. (5.97). The condition that the kinematics of the triple-collinear limit are the same as in the soft triple-collinear limit is given by

$$E_{\max}(1-\xi)\xi_r+E_{\max}\xi=E_{\max}(1-\xi')\xi_{r'}+E_{\max}\xi'\,. \tag{5.97}$$

The transformation rule is

$$\xi_r=\frac{\xi_{r'}(1-\xi')-(\xi-\xi')}{1-\xi}\,, \tag{5.98}$$

and the transformed integral reads

$$\int_0^1\mathrm{d}\xi_r\sigma(\xi_r)=\int_0^1\mathrm{d}\xi\int_0^1\mathrm{d}\xi_{r'}\frac{1-\xi'}{1-\xi}\theta(\xi_{r'}(1-\xi')-(\xi-\xi'))\sigma\left(\frac{\xi_{r'}(1-\xi')-(\xi-\xi')}{1-\xi}\right)\,. \tag{5.99}$$

The relation of the variables $\xi$ and $\xi'$ to the sector variables for the different mapping. is given in Tab. 5.2.

| mapping | $\xi$ | $\xi'$ |
|---|---|---|
| $r^0+u_1^0+\to r^0$ | $\xi_1$ | 0 |
| $r^0+u_1^0+u_2^0\to r^0$ | $\xi_1+\xi_2'\min[\xi_1,1-\xi_1]$ | 0 |
| $r^0+u_1^0\to r^0+u_1^0$ | $\xi_1+\xi_2'\min[\xi_1,1-\xi_1]$ | $\xi_1$ |

**Table 5.2:** Identification of the auxiliary variable $\xi$ and $\xi'$ with the sector variables of the two unresolved partons in the triple-collinear sector. The variable $\xi_2'=\xi_2$ in all sectors but sector $\mathcal{S}_2$, where it is $\xi_2'=\eta_1\xi_2$. The remappings are performed in the triple-collinear limit of the three partons, where the function $\xi_{2\max}=\min\left[1,\frac{1-\xi_1}{\xi_1}\right]$.

### Double-collinear sector

The transformations for the double-collinear sector are obtained in a similar way and are mixed cases of the ones, that have been discussed already. In the double-collinear limit the hard momenta that enter the matrix elements are $r_1+u_1$ and $r_2+u_2$. The possible mappings have to reproduce the kinematics as additionally, $u_2^0=0$ or $u_1^0=0$ and $u_2^0=0$. The list of possible mappings is

$$\{r_1^0+u_1^0,r_2^0+u_2^0\}\to\{r_1^0+u_1^0,r_2^0\}\,,$$

$$\{r_1^0 + u_1^0, r_2^0 + u_2^0\} \to \{r_1^0, r_2^0\} \,.$$

These mappings can be related to the mappings in the single-collinear case. Similar remappings are applied iteratively to the collinear pairs. Additionally, if at least one of the reference momentum is in the initial state and a mapping as in Eq. (5.84) is applied, the second collinear parton pair is effectively boosted by $z(x')$. A boost as in Eq. (5.91) has to be applied to the second pair in order to match the kinematics.

The presented mappings improve the convergence of the Monte Carlo integration and completely avoid missed binning.

## 5.6 Functionality of the software

In this section, the functionality of the software is presented and first histograms are obtained. A full phenomenological study of processes is beyond the scope of this work and will be presented elsewhere.

In order to verify the concept of the implementation first differential distributions for different observables are presented. Since the one-loop matrix elements for $pp \to t\bar{t}$ are already interfaced, first tests can be performed for this process. Differential distributions at leading order and next-to-leading order are shown in Figs. 5.11 and 5.12 respectively. The center-of-mass energy is fixed to $\sqrt{s} = 8\text{TeV}$. The left plot shows the rapidity distribution of the top quark, while the right plot shows the distribution in the transverse momentum $p_t$ of the top quark. The theoretical uncertainty is obtained by varying the factorization and renormalization scale independently in the range $m_t/2 \leq \mu_{\text{F,R}} \leq 2m_t$, where $1/4 < \mu_\text{F}/\mu_\text{R} < 4$. The modular structure of the software allows to evaluate the cross section for different scales in one integration run. Different scale choices are organized by the class *Scales*. For the presented example, the evaluation has been performed at seven different combinations of scales, where the depicted error band is given for the largest difference between two choices. The central value is evaluated at the scales $\mu_\text{R} = \mu_\text{F} = m_t$. The rapidity distribution is shown for the CT10 PDF sets and the $p_t$-distribution for the MSTW2008(nn)lo68cl PDF sets are depicted. The evaluation of the different contributions has been performed for four different PDF sets at the same time. As explained in section 5.1 the management of the different sets is controlled by the class *InitialState*. Another important feature of the implementation is that the output is completely managed by the *Measurement* class, where different observables can be defined simultaneously. Therefore, both plots in the shown figures have been obtained in the course of one evaluation.

First partial contributions to the differential distributions at next-to-next-to-leading order are presented in Fig. 5.13. The previously given comments apply to this differential distributions as well. The cross section is denoted by $\sigma^{\text{nnLO}}$ in order to highlight that it contains only partially contributions to the next-to-next-to-leading order cross section. It is therefore phenomenologically not relevant yet. On top of the full next-to-leading order contribution it contains the following parts. The finite part of the real-virtual contribution $\sigma_\text{F}^\text{RV}$ is included. This contribution includes the $n+1$-parton one-loop finite remainder and is finite due to the appropriate subtraction terms, that include the infrared limits of the one-loop finite remainder. In general high statistics are required to obtain a reliable result. In the present case $2 \times 10^8$ points have been evaluated for this contribution, which took about 8 hours on cluster of 800 cores. In addition, the finite part of the double-real contribution $\sigma_\text{F}^\text{RR}$ is included, where in the presented plots only the partonic contributions $gg \to t\bar{t}gg$ and $gg \to t\bar{t}u\bar{u}$ are considered. The summation over spin states has been performed by a deterministic summation for all external particles except the reference and unresolved partons. The

sum over polarization states of the reference and the unresolved partons has been performed by a helicity Monte Carlo, as explained in section 5.3. Hence, the convergence of the calculation provides another important test of the polarized subtraction terms in a more realistic context. Additionally, a smearing has been applied in order to reduce the effects of missed binning. The evaluation of $2 \times 10^9$ integration points in the presented set up, requires 2 hours on a 800 core cluster. These two contributions are the most costly parts in terms of computation time, since they are the only contributions that contain the one-loop $n+1$ parton finite remainder and the $n+2$ parton tree-level matrix element respectively. Finally, the full contribution that contains the $n$ particle one-loop finite remainder $\sigma_{\mathrm{FR}}$ is included in both plots in Fig. 5.13

The given examples show already the main functionality of the software. Differential distributions for cross sections that are relevant at the LHC will be available on a short computational time scale, while the observable can be tailored individually to a multitude of experimental setups.

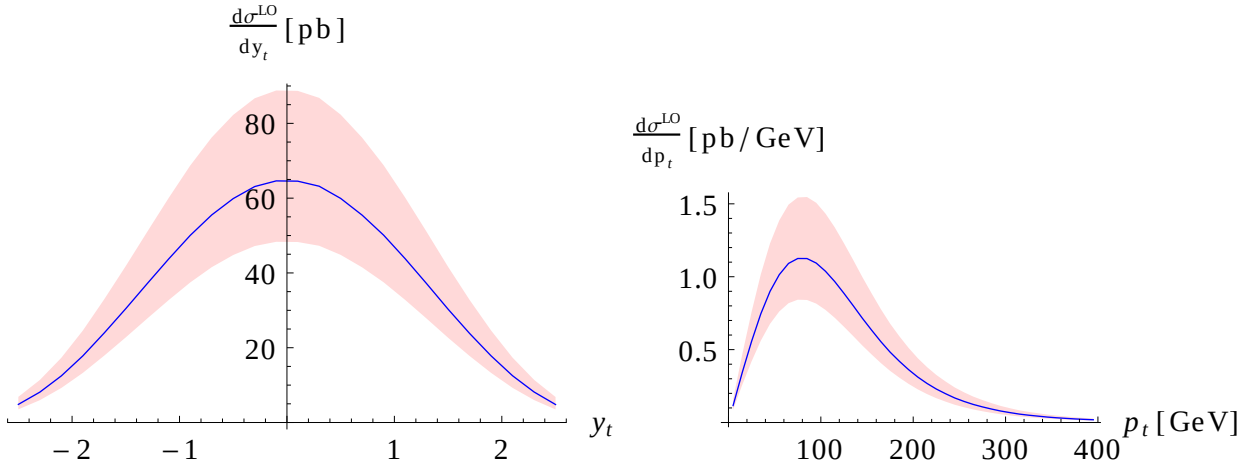


**Figure 5.11:** Differential distributions for top-pair production at hadron collisions at leading order obtained with STRIPPER. The error band is due to the variation of the renormalization and factorization scales in the range $m_t/2 \leq \mu_{\mathrm{F,R}} \leq 2m_t$. The central value is given at $\mu_{\mathrm{F,R}} = m_t$. The total cross section is $172.2 \pm 66.7(\mathrm{scale}) \pm 44.4(\mathrm{PDF})$ pb.
**Left:** Differential distribution in the rapidity $y_t$ of the $t$-quark. The PDF set is CT10.
**Right:** Differential distribution in the transverse momentum $p_t$ of the $t$-quark. The PDF set is MSTW2008lo68cl.

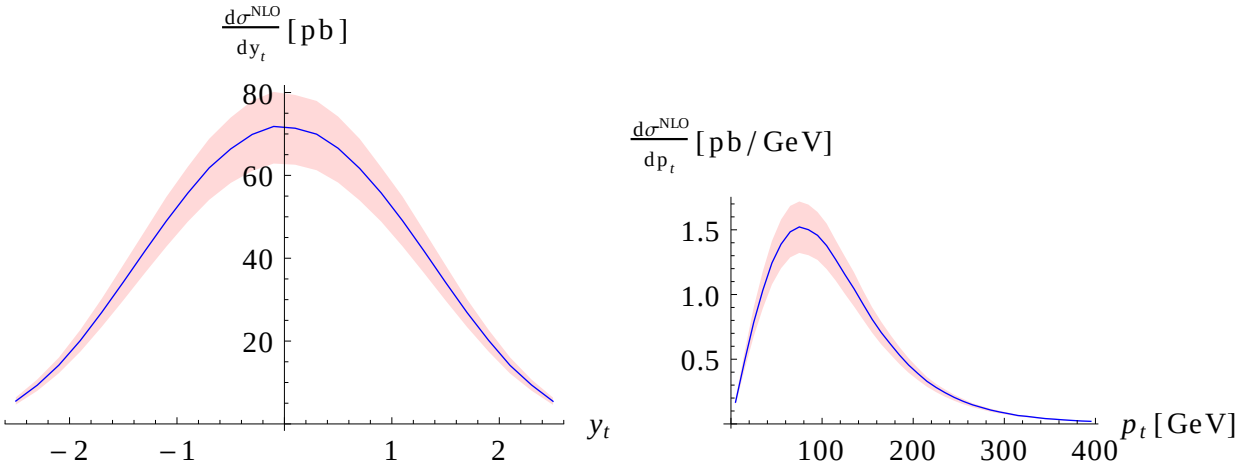


**Figure 5.12:** Differential distributions for top-pair production at hadron collisions at next-to-leading order obtained with STRIPPER. The error band is due to the variation of the renormalization and factorization scales in the range $m_t/2 \leq \mu_{\mathrm{F,R}} \leq 2m_t$. The central value is given at $\mu_{\mathrm{F,R}} = m_t$. The total cross section is $226.2 \pm 27.8(\text{scale}) \pm 29.6(\text{PDF})$ pb.
**Left:** Differential distribution in the rapidity $y_t$ of the $t$-quark. The PDF set is CT10NLO.
**Right:** Differential distribution in the transverse momentum $p_t$ of the $t$-quark. The PDF set is MSTW2008nlo68cl.

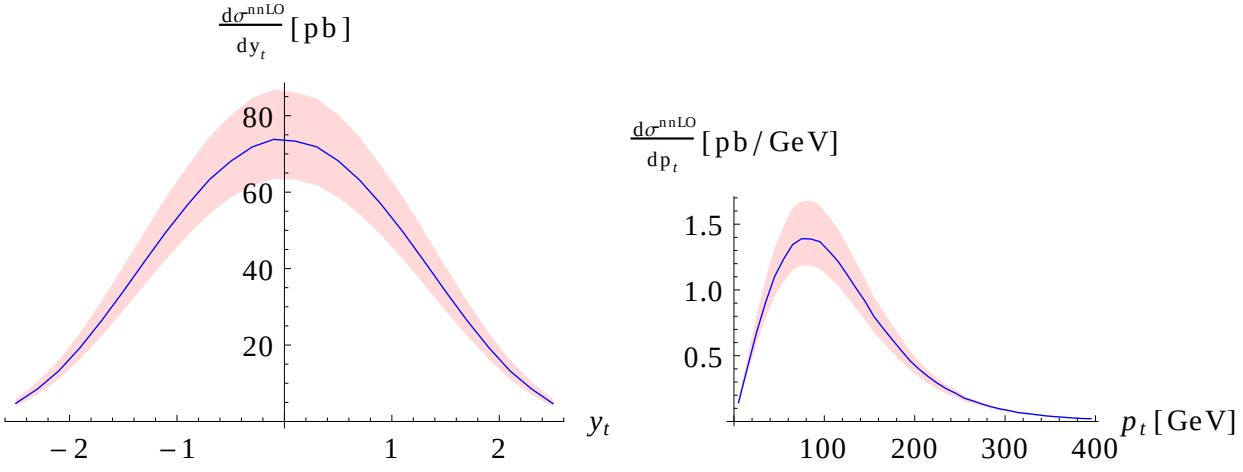


**Figure 5.13:** Differential distributions for top-pair production at hadron collisions at next-to-leading order and parts of the next-to-next-to-leading order contributions obtained with STRIPPER. In addition to the next-to-leading order cross section the contributions $\sigma_{\mathrm{F}}^{\mathrm{RV}}$, $\sigma_{\mathrm{FR}}$ and $\sigma_{\mathrm{F}}^{\mathrm{RR}}$ are included, where in the last case only the partonic channels $gg \to t\bar{t}gg$ and $gg \to t\bar{t}u\bar{u}$ are included. The error band is due to the variation of the renormalization and factorization scales in the range $m_t/2 \leq \mu_{\mathrm{F,R}} \leq 2m_t$. The central value is given at $\mu_{\mathrm{F,R}} = m_t$.
**Left:** Differential distribution in the rapidity $y_t$ of the $t$-quark. The PDF set is CT10NNLO.
**Right:** Differential distribution in the transverse momentum $p_t$ of the $t$-quark. The PDF set is MSTW2008nnlo68cl.

# CHAPTER 6

## Summary and Outlook

The main result of this work is a complete general construction of the sector improved residue subtraction scheme STRIPPER, which has been outlined in chapter 4. STRIPPER provides a subtraction framework that allows to compute fully differential next-to-next-to-leading order corrections in perturbative QCD to arbitrary processes and in particular to processes that are relevant for the interpretation of data at the LHC.
The main features of the scheme are summarized in the following:

- The cross section is separated into several finite and integrable pieces by providing all necessary subtraction terms.
- A numerical cancellation of pole contributions between virtual and real corrections is ensured by the explicit construction of the scheme.
- Subtraction terms are local, which allows a numerically stable efficient Monte-Carlo integration.
- The subtraction scheme is formulated in such a way that only four-dimensional matrix elements are needed. Hence, it can be interfaced to available matrix element generators.
- The subtraction scheme is process independent due to universal factorization properties of matrix elements in soft and collinear limits.
- The full color information is treated directly and no additional approximations are made.

The explicit implementation of the scheme has been discussed in chapter 5. The structure of the software reflects the fact that the subtraction scheme is process independent. This means that the implementation of the subtractions scheme is completely decoupled from the evaluation of single matrix elements. General features of the implementation that improve efficiency and stability of a numerical evaluation have been outlined. In particular, deterministic sums over polarization states of external particles in the most time consuming contributions are replaced by Monte Carlo sums over randomly polarized particles for all particles but the reference and unresolved partons. For the reference and the unresolved partons the deterministic sum is replaced by a Monte Carlo sampling over helicity states. Therefore complete polarized subtraction terms have been derived and implemented.
In addition to the full subtraction scheme, the software includes already all necessary tree-level amplitudes for first Standard Model applications. One-loop and two-loop amplitudes have to be provided additionally. A standardized interface exists that can be adapted to existing one-loop matrix element generators. Currently, all one-loop matrix elements for $t\bar{t}$ production at next-to-next-to-leading order are included. Available two-loop matrix elements can be readily interfaced

to the subtraction scheme. The functionality of the software has been shown for a specific, non-trivial example. Fully differential distributions for $t\bar{t}$ production at next-to-leading order have been presented. Partial results for the same distributions at next-to-next-to-leading order have been presented as well.
STRIPPER represents the first next-to-next-to-leading order event generator that can be modularly extended to new processes, if the corresponding two-loop matrix elements are available.

### Outlook

Following the first partial application to $t\bar{t}$-production, the next step is to include all missing contributions at next-to-next-to-leading order. In particularly the two-loop finite-remainder will be included, which has been calculated in [103, 104]. This allows to present fully differential next-to-next-to-leading order predictions for $t\bar{t}$-production in hadron collisions.
An important additional verification of the subtraction scheme and its implementation would be an application to further processes of phenomenological relevance. The modular implementation of STRIPPER allows, in principle, a straightforward inclusion of further processes, if the two-loop matrix elements are available. An application of physical interest would be therefore dijet production in hadron collisions at next-to-next-to-leading order. Currently, a computation of the purely gluonic contribution exists [49, 50]. A full computation would allow to include dijet data from proton-proton collisions in the determination of PDF sets at next-to-next-to-leading order.
In the future, it would be interesting to apply the software to processes with 3 final state particles. Observing the rapid progress in the computation of two-loop matrix elements in the past few years, first results for two-loop matrix elements with five external states are expected within a few years. There are several extensions to the current implementation that can be thought of in the near future. For example, the inclusion of decays of final state unstable particles is important in order to match the measured quantities precisely.
Finally, the event generator will be made publicly available, after first benchmark processes are successfully calculated.

STRIPPER is an important step towards fully automated next-to-next-to-leading order computations, which are necessary to understand measurements at the LHC in context of the Standard Model, especially in the light of Run II.

# Acknowledgments

I thank Professor Michal Czakon for giving me the opportunity to write this phd thesis at the institute for theoretical particle physics and cosmology at RWTH Aachen university, and for his professional advice.

In addition, I would also like to thank all people who supported me in writing this thesis.

# APPENDIX A

## Notation and conventions

The spacetime dimension is continued to the complex plane and denoted by

$$d = 4 - 2\varepsilon \ , \tag{A.1}$$

where $\varepsilon \to 0$ lead to a finite result for physical quantities.
The relation between the bare and the renormalized strong coupling constant is given by

$$\alpha_s^0 = \left(\frac{\mu_{\mathrm{R}}^2 e^{\gamma_{\mathrm{E}}}}{4\pi}\right)^{\varepsilon} Z_{\alpha_s} \zeta_{\alpha_s} \alpha_s \ , \tag{A.2}$$

with

$$\begin{aligned} \mu_R &- \text{ renormalization scale ,} \\ Z_{\alpha_s} &- \overline{\mathrm{MS}} \text{ renormalization constant ,} \\ \zeta_{\alpha_s} &- \text{ heavy-quark decoupling constant [66] .} \end{aligned} \tag{A.3}$$

Matrix elements are given as vectors in color- and spin space

$$\mathcal{M}^{c_1,\ldots,c_n;s_1,\ldots,s_n}_{a_1,\ldots,a_n}(p_1,\ldots,p_n) = \Big(\langle c_1,\ldots,c_n| \otimes \langle s_1,\ldots,s_n|\Big) \, |\mathcal{M}_{a_1,\ldots,a_n}(p_1,\ldots,p_n)\rangle \ , \tag{A.4}$$

$$|\mathcal{M}_n\rangle = |\mathcal{M}_{a_1,\ldots,a_n}(p_1,\ldots,p_n)\rangle \ , \quad \sum_{\substack{\text{color}\\ \text{spin}}} |\mathcal{M}_n|^2 = \langle \mathcal{M}_n|\mathcal{M}_n\rangle \ , \tag{A.5}$$

$$|\mathcal{M}_n\rangle = \left(\frac{\mu_R^2 e^{\gamma_{\mathrm{E}}}}{4\pi}\right)^{-l\varepsilon} \Big(|\mathcal{M}_n^{(0)}\rangle + |\mathcal{M}_n^{(1)}\rangle + |\mathcal{M}_n^{(2)}\rangle + \ldots\Big) \ . \tag{A.6}$$

$c_i$ – color of parton $i$,
$a_i$ – flavor of parton $i$,
$s_i$ – spin of parton $i$,
$p_i$ – momentum of parton $i$,
$|c_1,\ldots,c_n\rangle$ – color basis vectors,
$|s_1,\ldots,s_n\rangle$ – spin basis vectors,
$l$ – $\alpha_s$ power of Born approximation.

Phase space integrals over $n$ final state particles are

$$\int \mathrm{d}\boldsymbol{\Phi}_n\Big(p_1+p_2\to\sum_{i=1}^n q_i\Big)=\left(\frac{\mu_R^2 e^{\gamma_\mathrm{E}}}{4\pi}\right)^{(n-1)\varepsilon}\int\prod_{i=1}^n\frac{\mathrm{d}^{d-1}q_i}{(2\pi)^{d-1}2q_i^0}\,(2\pi)^d\delta^{(d)}\Big(\sum_{i=1}^n q_i-p_1-p_2\Big)\,. \tag{A.7}$$

Sums over massive, massless and arbitrary partons are distinguished

$$\sum_{ij\ldots}\ -\text{ sum over all indices } i,j,\ldots\,,\qquad \sum_{(i,j,\ldots)}\ -\text{ sum over distinct indices } i,j,\ldots\,.$$

$$\begin{aligned} i,j,k,\ldots &-\text{ indices for arbitrary partons, both massless and massive,}\\ i_0,j_0,k_0,\ldots &-\text{ indices for massless partons,}\\ I,J,K,\ldots &-\text{ indices for massive partons.}\end{aligned} \tag{A.8}$$

The following kinematic invariants are used in several places of the text

$$p_I^2=m_I^2\,, \tag{A.9}$$

$$v_I=p_I/m_I\,, \tag{A.10}$$

$$v_{IJ}=\sqrt{1-\frac{m_I^2m_J^2}{(p_Ip_J)^2}}\,, \tag{A.11}$$

$$s_{ij}=2\sigma_{ij}p_i\cdot p_j+i0^+\,, \tag{A.12}$$

where $\sigma_{ij}=+1$ if the momenta $p_i$ and $p_j$ are both incoming or outgoing and $\sigma_{ij}=-1$ otherwise.

$$\sigma_{ij}=+1\ -\text{ if the momenta } p_i \text{ and } p_j \text{ are both incoming or outgoing}\,,\quad \sigma_{ij}=-1\ -\text{ otherwise.}$$

## A.1 Color decomposition and color algebra

Matrix elements are given as vectors in color space. Operators in this space are the color charge operators that are defined by [16]

$$\begin{aligned}\langle c_1,\ldots,c_i,\ldots,c_n,c|\mathbf{T}_i|b_1,\ldots,b_i,\ldots,b_n\rangle&=\langle c_1,\ldots,c_i,\ldots,c_n|T_i^c|b_1,\ldots,b_i,\ldots,b_n\rangle\\&=\delta_{c_1b_1}\ldots T^c_{c_ib_i}\ldots\delta_{c_nb_n}\,.\end{aligned} \tag{A.13}$$

$$\sum_i\mathbf{T}_i|\mathcal{M}_n\rangle=0\,,\quad T_i^cT_j^c=\mathbf{T}_i\cdot\mathbf{T}_j=\mathbf{T}_j\cdot\mathbf{T}_i,\quad \mathbf{T}_i\cdot\mathbf{T}_i=\mathbf{T}_i^2=C_i=C_{a_i}\,, \tag{A.14}$$

$$C_g=C_A\,,\quad C_q=C_{\bar q}=C_F\,. \tag{A.15}$$

$$\begin{aligned} T^c_{c_1c_2}&=if^{c_1cc_2}\ -\text{ emitter is a gluon}\,, &(A.16)\\ T^c_{c_1c_2}&=t^c_{c_1c_2}(=-t^c_{c_2c_1})\ -\text{ emitter is an outgoing quark (anti-quark)}\,, &(A.17)\\ T^c_{c_1c_2}&=-t^c_{c_2c_1}(=t^c_{c_1c_2})\ -\text{ emitter is an ingoing quark (anti-quark)}\,. &(A.18)\end{aligned}$$

$$\mathrm{Tr}\left[t^at^b\right]=T_F\delta^{ab}=\frac{1}{2}\delta^{ab}\,. \tag{A.20}$$

The above treatment assumes that the gluon is treated as a eight dimensional vector in the adjoint representation of $SU(3)$, while the quarks are in the three-dimensional fundamental representation of $SU(3)$, where the number of colors is $N_c = 3$.
Another basis, which is also used in this work, is the color flow representation of matrix elements [229, 230]. The single gluon index $c$ ($c = 1,\ldots,N_c^2 - 1$) is traded for two indices in the fundamental representation and the complex conjugate fundamental representation. On a Langrangian level this can be achieved by replacing the gluon field by

$$A_\mu^c \to \frac{1}{\sqrt{2}} A_\mu^c (t^c)_j^i, \tag{A.21}$$

where upper indices are in the fundamental representation and lower indices in the conjugate fundamental representation. The indices of the color flow basis should not be confused with the indices labeling the partons introduced in Eq. (A.8). Each matrix element, that contains $n$ external partons can be decomposed according to its color structure as

$$|\mathcal{M}_n^{(0)}\rangle = \sum_{I=P(2,\ldots n)} \delta^{i_1}_{j_{\sigma_I(1)}} \delta^{i_2}_{j_{\sigma_I(2)}} \ldots \delta^{i_n}_{j_{\sigma_I(n)}} \mathcal{M}_I^{(0)}(p_1 \ldots p_n) \equiv D_I \mathcal{M}_I^{(0)}(p_1 \ldots p_n) \ , \tag{A.22}$$

where $\mathcal{M}_I^{(0)}$ is the color ordered amplitude. The summation runs over all $(n-1)!$ permutations $\sigma_I$ of $(2,\ldots,n)$. The $k$-th external gluon is labeled by the double index $(i_k,j_{\sigma_I(k)})$, while the $k$-th quark is labeled by $(i_k,0)$ and the $k$-th antiquark by $(0,j_{\sigma_I(k)})$. Squaring the amplitude and summing over all colors the color matrix is given by

$$C_{IJ} = \sum_{\text{color}} D_I D_J^\dagger = N_c^{m(\sigma_I,\sigma_J)} \ . \tag{A.23}$$

The function $1 \leq m(\sigma_I,\sigma_J) \leq N$ counts the number of closed delta contractions, where $N$ is the number of gluons and $q\bar{q}$-pairs. In the leading color approximation (LC), only diagonal terms $I = J$ are kept, with $m(\sigma_I,\sigma_J) = N$. The squared matrix element reads

$$\langle \mathcal{M}_n^{(0)} | \mathcal{M}_n^{(0)} \rangle = N_c^N \sum_I |\mathcal{M}_I^{(0)}(p_1 \ldots p_n)|^2 + \mathcal{O}(N_c^{N-2}) \ . \tag{A.24}$$

Even though here the color flow representation is only given for tree-level amplitudes it can be generalized to amplitudes containing loops.

## A.2 Spherical coordinates in $d$-dimensions

The parameterization of momenta for the subtraction scheme STRIPPER relies on spherical coordinates in $d$-dimensions. It is therefore useful to have a consistent notation for vectors and integration measures in those coordinates.
The notation has been established in [1].

Let $\mathrm{d}^d\boldsymbol{r}$ be the Euclidean integration measure in $\mathbb{R}^d$. It is decomposed into a radial and an angular part with the help of a $\delta$-function insertion, if the $\boldsymbol{r}$ vector is rescaled as $\boldsymbol{r} = r\,\hat{\boldsymbol{n}}$

$$\int_{\mathbb{R}^d} \mathrm{d}^d\boldsymbol{r} = \int_0^\infty \mathrm{d}r\, r^{d-1} \int_{\mathbb{R}^d} \mathrm{d}^d\hat{\boldsymbol{n}}\, \delta(1 - \|\hat{\boldsymbol{n}}\|) = \int_0^\infty \mathrm{d}r\, r^{d-1} \int_{\mathcal{S}_1^{d-1}} \mathrm{d}\boldsymbol{\Omega} \ . \tag{A.25}$$

This defines a rotationally invariant measure, $\mathrm{d}\boldsymbol{\Omega}$, on the unit $(d-1)$-sphere, $\mathbb{S}_1^{d-1}$. The versors $\hat{\boldsymbol{n}}$ are always further specified by their dimensionality and are recursively defined in terms of angles

$$\hat{\boldsymbol{n}}^{(d)}(\theta_1, \theta_2, \ldots, \theta_{d-1}) = \begin{pmatrix} \cos\theta_1 \\ \\ \sin\theta_1 \; \hat{\boldsymbol{n}}^{(d-1)}(\theta_2, \ldots, \theta_{d-1}) \end{pmatrix} , \quad \hat{\boldsymbol{n}}^{(1)} = 1 , \tag{A.26}$$

where

$$\theta_1, \ldots, \theta_{d-2} \in [0, \pi] , \quad \theta_{d-1} \in [0, 2\pi] . \tag{A.27}$$

An important property of this parameterization is

$$\begin{aligned} \hat{\boldsymbol{n}}^{(d)}(\theta_1, \ldots, \theta_{n-1}, 0, \theta_{n+1}, \ldots, \theta_{d-1}) &= \hat{\boldsymbol{n}}^{(d)}(\theta_1, \ldots, \theta_{n-1}, 0, 0, \ldots) , \\ \hat{\boldsymbol{n}}^{(d)}(\theta_1, \ldots, \theta_{n-1}, \pi, \theta_{n+1}, \ldots, \theta_{d-1}) &= \hat{\boldsymbol{n}}^{(d)}(\theta_1, \ldots, \theta_{n-1}, \pi, 0, 0, \ldots) . \end{aligned}$$

The recursive definition of the versor can be implemented in the integration measure

$$\int_{\mathbb{S}_1^{d-1}} \mathrm{d}\boldsymbol{\Omega}(\theta_1, \theta_2, \ldots, \theta_{d-1}) = \int_0^\pi \mathrm{d}\theta_1 \, \sin^{d-2}\theta_1 \int_{\mathbb{S}_1^{d-2}} \mathrm{d}\boldsymbol{\Omega}(\theta_2, \ldots, \theta_{d-1}) . \tag{A.28}$$

The volume of the unit $(d-1)$-sphere is

$$\int_{\mathbb{S}_1^{d-1}} \mathrm{d}\boldsymbol{\Omega} \, 1 = \frac{2\pi^{\frac{d}{2}}}{\Gamma\left(\frac{d}{2}\right)} . \tag{A.29}$$

The following formular is essential for the four dimensional formulation of STRIPPER and is used in section 4.6

$$\int_{\mathbb{S}_1^{d-1}} \mathrm{d}\boldsymbol{\Omega} \, \delta^{(d)}\left(\alpha\hat{\boldsymbol{n}}^{(d)}\right) = \alpha^{1-d} \int_{\mathbb{R}^d} \mathrm{d}^d\left(\alpha\hat{\boldsymbol{n}}^{(d)}\right) \, \delta\left(\alpha - \left\|\alpha\hat{\boldsymbol{n}}^{(d)}\right\|\right) \, \delta^{(d)}\left(\alpha\hat{\boldsymbol{n}}^{(d)}\right) = \frac{1}{\alpha^{d-1}} \, \delta(\alpha) , \tag{A.30}$$

as it takes care of the correct reduction of the dimensionality of space

$$\int_{\mathbb{S}_1^{d-1}} \mathrm{d}\boldsymbol{\Omega} \, \delta^{(d-n)}\left(\hat{\boldsymbol{n}}^{(d)}\right) = \int_{\mathbb{S}_1^{n-1}} \mathrm{d}\boldsymbol{\Omega} , \tag{A.31}$$

In the context of STRIPPER, unit vectors are defined through rotations of a single basis vector pointing along the $z$-direction

$$\hat{\boldsymbol{n}}_{\boldsymbol{0}}^{(d)} = \begin{pmatrix} 1 \\ 0 \\ 0 \\ \vdots \end{pmatrix} , \tag{A.32}$$

where $d \times d$ rotation matrices transforming the coordinates $i$ and $j$ are defined by

$$\boldsymbol{R}_{ij}^{(d)}(\theta) = \begin{pmatrix} & & & i & & & j & & & \\ 1 & & & & & & & & & \\ & \ddots & & & & & & & & \\ & & 1 & & & & & & & \\ & & & \cos\theta & & & \sin\theta & & & i \\ & & & & 1 & & & & & \\ & & & & & \ddots & & & & \\ & & & & & & 1 & & & \\ & & & -\sin\theta & & & \cos\theta & & & j \\ & & & & & & & 1 & & \\ & & & & & & & & \ddots & \\ & & & & & & & & & 1 \end{pmatrix} , \tag{A.33}$$

The unspecified entries vanish. If rotations act in different planes, then the respective rotation matrices commute

$$\{i,j\} \cap \{k,l\} = \emptyset \implies \left[\boldsymbol{R}_{ij}^{(d)}(\theta_1),\, \boldsymbol{R}_{kl}^{(d)}(\theta_2)\right] = 0 \,. \tag{A.34}$$

The versor parameterization can be expressed through rotations as

$$\hat{\boldsymbol{n}}^{(d)}(\theta_1,\ldots,\theta_{d-1}) = \boldsymbol{R}_1^{(d)}(\theta_1,\ldots,\theta_{d-1})\hat{\boldsymbol{n}}_{\boldsymbol{0}}^{(d)} \,, \tag{A.35}$$

where useful shorthand notation is given by

$$\boldsymbol{R}_n^{(d)}(\theta_1,\ldots,\theta_{d-n}) = \boldsymbol{R}_{d,d-1}^{(d)}(\theta_{d-n})\ldots\boldsymbol{R}_{n+1,n}^{(d)}(\theta_1) \,. \tag{A.36}$$

Due to the commutation properties of the rotation matrices, there is

$$\left[\boldsymbol{R}_1^{(d)}(\theta_1,\ldots,\theta_{n-1},0,0,\ldots),\, \boldsymbol{R}_{n+1}^{(d)}(\theta_{n+1},\ldots,\theta_{d-1})\right] = 0 \,. \tag{A.37}$$

### A.2.1 Angular integration beyond four dimensions

The subtraction scheme STRIPPER presented in chapter 4 relies on a parametrization of momenta in angles and energies in $d = 4-2\varepsilon$. The formulation of the scheme in 't Hooft-Veltman regularization however restricts resolved momenta to $d = 4$ dimensions. The unresolved momenta are explicitly integrated beyond four dimensions, where the relevant dimensions are restricted to five for the first unresolved momentum and to six for the second unresolved momentum in the worst case of the double soft limit. Here the angular integration measure is explicitly given, if four, five or six dimensions need to be integrated explicitly.
If the integrand only depends on four dimensional parameters the remaining angular space can be analytically integrated using

$$\int_{\mathcal{S}_1^{-2\varepsilon}} \mathrm{d}\boldsymbol{\Omega}\, 1 = 2\frac{(4\pi)^{-\varepsilon}\Gamma(1-\varepsilon)}{\Gamma(1-2\varepsilon)} \,. \tag{A.38}$$

If there is only one unresolved momentum five dimensions need to be integrated explicitly. The corresponding angular integration is [20]

$$\int_{\mathbb{S}_1^{-2\varepsilon}} \mathrm{d}\boldsymbol{\Omega}(\rho_1,\ldots) = \frac{(4\pi)^{-\varepsilon}\Gamma(1-\varepsilon)}{\Gamma(1-2\varepsilon)} \times \int_{-1}^{+1} \mathrm{d}\cos\rho_1 \left(\delta(1-\cos\rho_1)+\delta(1+\cos\rho_1) - 2\varepsilon\,\frac{4^\varepsilon\Gamma(1-2\varepsilon)}{\Gamma^2(1-\varepsilon)}\left[\frac{1}{(1-\cos^2\rho_1)^{1+\varepsilon}}\right]_+\right) . \quad \text{(A.39)}$$

In the worst case scenario two unresolved momenta are present in the integrand and six dimensions have to be integrated explicitly for the second unresolved parton. The corresponding formula reads

$$\begin{aligned}\int_{\mathbb{S}_1^{-2\varepsilon}} \mathrm{d}\boldsymbol{\Omega}(\sigma_1,\sigma_2,\ldots) &= \frac{(4\pi)^{-\varepsilon}\Gamma(1-\varepsilon)}{2\Gamma(1-2\varepsilon)} \\ &\times \int_{-1}^{+1} \mathrm{d}\cos\sigma_1 \int_{-1}^{+1} \mathrm{d}\cos\sigma_2 \left( \big(\delta(1-\cos\sigma_1)+\delta(1+\cos\sigma_1)\big)\big(\delta(1-\cos\sigma_2)+\delta(1+\cos\sigma_2)\big) \right. \\ &- 2\varepsilon\,\frac{4^\varepsilon\Gamma(1-2\varepsilon)}{\Gamma^2(1-\varepsilon)}\left[\frac{1}{(1-\cos^2\sigma_1)^{1+\varepsilon}}\right]_+ \big(\delta(1-\cos\sigma_2)+\delta(1+\cos\sigma_2)\big) \\ &\left. - \frac{2+4\varepsilon}{\pi}\left[\frac{1}{(1-\cos^2\sigma_1)^{1+\varepsilon}}\right]_+ \left[\frac{1}{(1-\cos^2\sigma_2)^{\frac{3}{2}+\varepsilon}}\right]_+ \right) .\end{aligned} \quad \text{(A.40)}$$

The distributions present in the given formulas are defined by

$$\begin{aligned}\int_{-1}^{+1} \mathrm{d}\cos\rho \left[\frac{1}{(1-\cos^2\rho)^\alpha}\right]_+ f(\cos\rho) &= \int_{-1}^{0} \mathrm{d}\cos\rho\,\frac{f(\cos\rho)-f(-1)}{(1-\cos^2\rho)^\alpha} \\ &+ \int_{0}^{+1} \mathrm{d}\cos\rho\,\frac{f(\cos\rho)-f(+1)}{(1-\cos^2\rho)^\alpha} .\end{aligned} \quad \text{(A.41)}$$

## A.3 Spinor helicity formalism

Matrix elements for a fixed polarization can be described in a compact way using the *Spinor-Helicty formalism*. Massless Dirac spinors are separated into right- and left-handed Weyl spinors

$$u(p_i) = \begin{pmatrix} u_L(p_i) \\ u_R(p_i) \end{pmatrix} , \quad v(p_i) = \begin{pmatrix} v_L(p_i) \\ u_R(p_i) \end{pmatrix} . \quad \text{(A.42)}$$

The left and right-handed spinors are represented using a bra-ket notation:

$$u_+ = u_R(p) = P_+u(p) = P_+v(p) = |p\rangle , \qquad u_- = u_L(p) = P_-u(p) = P_-v(p) = |p] , \quad \text{(A.43)}$$

$$\bar{u}(p)P_- = \bar{v}(p)P_- = [p| , \qquad \bar{u}(p)P_+ = \bar{v}(p)P_+ = \langle p| . \quad \text{(A.44)}$$

In Tab. A.1 the corresponding spinors for a fixed helicity of outgoing and incoming massless fermions are given. The following identities are fulfilled by the spinor representation

$$\langle p_i p_j\rangle = -\langle p_j p_i\rangle , \quad \text{(A.45)}$$

| particle type | helicity | spinor |
|---|---|---|
| outgoing particle | $-1$ | $\langle p\vert$ |
| | $+1$ | $[p\vert$ |
| incoming particle | $-1$ | $\vert p]$ |
| | $+1$ | $\vert p\rangle$ |
| outgoing antiparticle | $-1$ | $\vert p\rangle$ |
| | $+1$ | $\vert p]$ |
| incoming antiparticle | $-1$ | $[p\vert$ |
| | $+1$ | $\langle p\vert$ |

**Table A.1:** Identification of left and right handed massless spinors with fermions of definite helicity.

$$[p_i p_j] = -[p_j p_i] \,, \tag{A.46}$$

$$\langle p_i p_j \rangle^* = \mathrm{sign}(p_i^0 p_j^0)[p_j p_i] \,, \tag{A.47}$$

$$\langle p_i p_j \rangle [p_j p_i] = 2 p_i \cdot p_j, \tag{A.48}$$

where incoming momenta are treated as outgoing with negative energy component $p^0$. Polarization vectors up to a term proportional to the direction of the gluon as eigenstates of the helicity operator with eigenvalues $\pm 1$

$$\varepsilon^\mu(p_z,+1) = \frac{1}{\sqrt{2}} \begin{pmatrix} 0 \\ -i \\ 1 \\ 0 \end{pmatrix} \,, \quad \varepsilon^\mu(p_z,-1) = \frac{1}{\sqrt{2}} \begin{pmatrix} 0 \\ i \\ 1 \\ 0 \end{pmatrix} \,, \text{ with } p_z = \begin{pmatrix} E \\ 0 \\ 0 \\ E \end{pmatrix} \,. \tag{A.49}$$

The polarization vectors can be expressed using helicity spinors, an additional reference momentum $k$ has to be introduced

$$\varepsilon_-^\mu(p,k) \equiv \varepsilon^\mu(p,-1,k) = \frac{\langle k|\gamma^\mu|p]}{\sqrt{2}\langle pk\rangle} \,, \quad \varepsilon_+^\mu \equiv \varepsilon^\mu(p,+1,k) = \frac{\langle p|\gamma^\mu|k]}{\sqrt{2}[kp]} \,. \tag{A.50}$$

This representation is equivalent to the axial gauge, which is reflected by the following properties

$$\varepsilon_\pm^{\mu *}(p,k) = \varepsilon_\mp^\mu(p,k) \,, \tag{A.51}$$

$$p \cdot \varepsilon_\pm(p,k) = k \cdot \varepsilon_\pm(p,k) = 0 \,, \tag{A.52}$$

$$\sum_{\lambda=\pm} \varepsilon_\lambda^\mu(p,k) \varepsilon_\lambda^{\nu *}(p,k) = -g^{\mu\nu} + \frac{p^\mu k^\nu + p^\nu k^\mu}{2p \cdot k} \,. \tag{A.53}$$

# APPENDIX B

## Infrared limits

### B.1 Infrared divergences of virtual amplitudes

The IR renormalization constant $\mathbf{Z}(\varepsilon,\{p_i\},\{m_i\},\mu_R)$ introduced in section 4.5 satisfies the renormalization group equation

$$\frac{\mathrm{d}}{\mathrm{d}\ln\mu_R}\,\mathbf{Z}(\varepsilon,\{p_i\},\{m_i\},\mu_R) = -\boldsymbol{\Gamma}(\{p_i\},\{m_i\},\mu_R)\,\mathbf{Z}(\varepsilon,\{p_i\},\{m_i\},\mu_R)\,, \tag{B.1}$$

where the anomalous dimension operator $\boldsymbol{\Gamma}$ is given by [231–236]

$$\begin{aligned}\boldsymbol{\Gamma}(\{p_i\},\{m_i\},\mu_R) \,=\, & \sum_{(i_0,j_0)} \frac{\mathbf{T}_{i_0}\cdot\mathbf{T}_{j_0}}{2}\,\gamma_{\mathrm{cusp}}(\alpha_s)\,\ln\left(\frac{\mu_R^2}{-s_{i_0j_0}}\right) + \sum_{i_0}\gamma^{i_0}(\alpha_s) \\ & - \sum_{(I,J)} \frac{\mathbf{T}_I\cdot\mathbf{T}_J}{2}\,\gamma_{\mathrm{cusp}}(v_{IJ},\alpha_s) + \sum_I \gamma^I(\alpha_s) + \sum_{I,j_0}\mathbf{T}_I\cdot\mathbf{T}_{j_0}\,\gamma_{\mathrm{cusp}}(\alpha_s)\,\ln\left(\frac{m_I\,\mu_R}{-s_{Ij_0}}\right) \\ & + \sum_{(I,J,K)} i\,f^{abc}\,T_I^a\,T_J^b\,T_K^c\,F_1(v_{IJ},v_{JK},v_{KI}) \\ & + \sum_{(I,J)}\sum_{k_0} i\,f^{abc}\,T_I^a\,T_J^b\,T_{k_0}^c\,f_2\left(v_{IJ},\ln\left(\frac{-\sigma_{Jk_0}\,v_J\cdot p_{k_0}}{-\sigma_{Ik_0}\,v_I\cdot p_{k_0}}\right)\right) + \mathcal{O}(\alpha_s^3)\,.\end{aligned} \tag{B.2}$$

The explicit solution of the RGE (B.1) can be found in [237], and reads up to order $\alpha_s^2$

$$\begin{aligned}\mathbf{Z} = 1 &+ \frac{\alpha_s}{4\pi}\left(\frac{\Gamma_0'}{4\varepsilon^2} + \frac{\boldsymbol{\Gamma}_0}{2\varepsilon}\right) \\ &+ \left(\frac{\alpha_s}{4\pi}\right)^2\left[\frac{(\Gamma_0')^2}{32\varepsilon^4} + \frac{\Gamma_0'}{8\varepsilon^3}\left(\boldsymbol{\Gamma}_0 - \frac{3}{2}\,\beta_0\right) + \frac{\boldsymbol{\Gamma}_0}{8\varepsilon^2}\,(\boldsymbol{\Gamma}_0 - 2\beta_0) + \frac{\Gamma_1'}{16\varepsilon^2} + \frac{\boldsymbol{\Gamma}_1}{4\varepsilon}\right] + \mathcal{O}(\alpha_s^3)\,,\end{aligned} \tag{B.3}$$

where the lading contribution to the beta-function is

$$\beta_0 = \frac{11}{3}C_A - \frac{4}{3}T_F n_l\,, \tag{B.4}$$

with $n_l$ the number of massless quark flavors. The expression contains the anomalous dimension $\boldsymbol{\Gamma}$ and its derivative

$$\Gamma'(\alpha_s) = \frac{\partial}{\partial \ln \mu_R} \boldsymbol{\Gamma}(\{p_i\},\mu_R,\alpha_s) \,, \tag{B.5}$$

expanded according to

$$\boldsymbol{\Gamma} = \sum_{n=0}^{\infty} \boldsymbol{\Gamma}_n \left(\frac{\alpha_s}{4\pi}\right)^{n+1}, \quad \Gamma' = \sum_{n=0}^{\infty} \Gamma'_n \left(\frac{\alpha_s}{4\pi}\right)^{n+1} \,. \tag{B.6}$$

$\boldsymbol{\Gamma}$ is given in terms of the anomalous dimensions $\gamma_{\text{cusp}}$, $\gamma^q$, $\gamma^Q$, $\gamma^g$, and two functions $F_1$ and $f_2$. The explicit formulae for the coefficients of the expansion in $\alpha_s$ read

$$\gamma(\alpha_s) = \sum_{n=0}^{\infty} \gamma_n \left(\frac{\alpha_s}{4\pi}\right)^{n+1} \,, \tag{B.7}$$

which are taken literally from [232, 237]. The massless cusp anomalous dimension is

$$\begin{aligned} \gamma_0^{\text{cusp}} &= 4 \,, \\ \gamma_1^{\text{cusp}} &= \left(\frac{268}{9} - \frac{4\pi^2}{3}\right) C_A - \frac{80}{9} T_F n_l \,. \end{aligned} \tag{B.8}$$

In the massive case the cusp anomalous dimension can be written as

$$\begin{aligned} \gamma_{\text{cusp}}(v,\alpha_s) = {} & \gamma_{\text{cusp}}(\alpha_s) \frac{1}{v} \left[\frac{1}{2} \ln\left(\frac{1+v}{1-v}\right) - i\pi\right] \\ & + 8C_A \left(\frac{\alpha_s}{4\pi}\right)^2 \left\{ \zeta_3 - \frac{5\pi^2}{6} + \frac{1}{4} \ln^2\left(\frac{1+v}{1-v}\right) \right. \\ & \quad + \frac{1}{v^2} \left[\frac{1}{24} \ln^3\left(\frac{1+v}{1-v}\right) + \ln\left(\frac{1+v}{1-v}\right) \left(\frac{1}{2} \text{Li}_2\left(\frac{1-v}{1+v}\right) - \frac{5\pi^2}{12}\right) \right. \\ & \quad \left. + \text{Li}_3\left(\frac{1-v}{1+v}\right) - \zeta_3 \right] \\ & \quad + \frac{1}{v} \left[\frac{5\pi^2}{6} + \frac{5\pi^2}{12} \ln\left(\frac{1+v}{1-v}\right) - \ln\left(\frac{2v}{1+v}\right) \ln\left(\frac{1+v}{1-v}\right) \right. \\ & \qquad \left. - \frac{1}{4} \ln^2\left(\frac{1+v}{1-v}\right) - \frac{1}{24} \ln^3\left(\frac{1+v}{1-v}\right) + \text{Li}_2\left(\frac{1-v}{1+v}\right) \right] \\ & \quad + i\pi \left\{ \frac{1}{v^2} \left[\frac{\pi^2}{6} - \frac{1}{4} \ln^2\left(\frac{1+v}{1-v}\right) - \text{Li}_2\left(\frac{1-v}{1+v}\right) \right] \right. \\ & \qquad + \frac{1}{v} \left[-\frac{\pi^2}{6} + 2 \ln\left(\frac{2v}{1+v}\right) + \ln\left(\frac{1+v}{1-v}\right) + \frac{1}{4} \ln^2\left(\frac{1+v}{1-v}\right) \right] \\ & \qquad \left. \left. - \ln\left(\frac{1+v}{1-v}\right) \right\} \right\} \,, \end{aligned} \tag{B.9}$$

where $v = v_I$ for the massive parton $I$. For massless quarks (anti-quarks)

$$\gamma_0^q = -3C_F \,,$$

$$\gamma_1^q = C_F^2\left(-\frac{3}{2}+2\pi^2-24\zeta_3\right)+C_FC_A\left(-\frac{961}{54}-\frac{11\pi^2}{6}+26\zeta_3\right)+C_FT_Fn_l\left(\frac{130}{27}+\frac{2\pi^2}{3}\right)\,, \tag{B.10}$$

whereas the massive quark (anti quark) anomalous dimension is

$$\begin{aligned}\gamma_0^Q &= -2C_F\,,\\ \gamma_1^Q &= C_FC_A\left(\frac{2\pi^2}{3}-\frac{98}{9}-4\zeta_3\right)+\frac{40}{9}\,C_FT_Fn_l\,.\end{aligned} \tag{B.11}$$

The anomalous dimension for gluons reads

$$\begin{aligned}\gamma_0^g &= -\beta_0 = -\frac{11}{3}\,C_A+\frac{4}{3}\,T_Fn_l\,,\\ \gamma_1^g &= C_A^2\left(-\frac{692}{27}+\frac{11\pi^2}{18}+2\zeta_3\right)+C_AT_Fn_l\left(\frac{256}{27}-\frac{2\pi^2}{9}\right)+4C_FT_Fn_l\,.\end{aligned} \tag{B.12}$$

Finally, the functions $F_1$ and $f_2$ are [235]

$$\begin{aligned}F_1(v_{12},v_{23},v_{31}) &= \frac{1}{3}\sum_{I,J,K=1}^{3}\varepsilon_{IJK}\,\frac{\alpha_s}{4\pi}\,g(v_{IJ})\,\gamma_{\text{cusp}}(v_{KI},\alpha_s)\,,\\ f_2\Big(v_{12},\ln\frac{-\sigma_{23}\,v_2\cdot p_3}{-\sigma_{13}\,v_1\cdot p_3}\Big) &= -\frac{\alpha_s}{4\pi}\,g(v_{12})\,\gamma_{\text{cusp}}(\alpha_s)\,\ln\left(\frac{-\sigma_{23}\,v_2\cdot p_3}{-\sigma_{13}\,v_1\cdot p_3}\right)\,,\end{aligned} \tag{B.13}$$

where

$$\begin{aligned}g(v) = {}& \frac{5\pi^2}{6}-\frac{1}{4}\ln^2\left(\frac{1+v}{1-v}\right)\\ &+\frac{1}{v}\left[-\frac{5\pi^2}{6}+\ln\left(\frac{2v}{1+v}\right)\ln\left(\frac{1+v}{1-v}\right)+\frac{1}{4}\ln^2\left(\frac{1+v}{1-v}\right)-\text{Li}_2\left(\frac{1-v}{1+v}\right)\right]\\ &+i\pi\left\{\ln\left(\frac{1+v}{1-v}\right)-\frac{1}{v}\left[2\ln\left(\frac{2v}{1+v}\right)+\ln\left(\frac{1+v}{1-v}\right)\right]\right\}\,.\end{aligned} \tag{B.14}$$

## B.2 Soft and collinear limits of tree-level matrix elements

Soft- and collinear limits of tree-level matrix elements as discussed in section 3.4.1. Here, some explicit expressions for soft and splitting functions are summarized.

### B.2.1 Splitting functions

The collinear limit of two partons is described in Eq. (3.48), while the factorization formula is given in Eq. (3.49). The possible splitting functions are defined as operators in spin space that act on the spin of parton $a$

$$\langle s|\hat{\mathbf{P}}^{(0)}_{a_1a_2}|s'\rangle = \hat{P}^{(0),\,ss'}_{a_1a_2}\,. \tag{B.15}$$

The splitting functions are

$$\hat{P}^{(0),\,\mu\nu}_{gg}(z,k_\perp;\varepsilon) = 2C_A\,\left[-g^{\mu\nu}\left(\frac{z}{1-z}+\frac{1-z}{z}\right)-2(1-\varepsilon)z(1-z)\frac{k_\perp^\mu k_\perp^\nu}{k_\perp^2}\right]\,, \tag{B.16}$$

$$\hat{P}^{(0),\,\mu\nu}_{q\bar{q}}(z,k_\perp;\varepsilon) = \hat{P}^{(0),\,\mu\nu}_{\bar{q}q}(z,k_\perp;\varepsilon) = T_F\left[-g^{\mu\nu} + 4z(1-z)\frac{k_\perp^\mu k_\perp^\nu}{k_\perp^2}\right] , \tag{B.17}$$

$$\hat{P}^{(0),\,ss'}_{qg}(z,k_\perp;\varepsilon) = \hat{P}^{(0),\,ss'}_{\bar{q}g}(z,k_\perp;\varepsilon) = \delta^{ss'}\,C_F\,\left[\frac{1+z^2}{1-z} - \varepsilon(1-z)\right] , \tag{B.18}$$

$$\hat{P}^{(0),\,ss'}_{gq}(z,k_\perp;\varepsilon) = \hat{P}^{(0),\,ss'}_{g\bar{q}}(z,k_\perp;\varepsilon) = \hat{P}^{(0),\,ss'}_{qg}(1-z,k_\perp;\varepsilon) , \tag{B.19}$$

while averaging over the transverse direction leads to the factorization formula

$$\overline{|\mathcal{M}^{(0)}_{a_1,a_2,\ldots}(p_1,p_2,\ldots)|^2} \simeq 4\pi\alpha_s\,\frac{2}{s_{12}}\,\langle\hat{\mathbf{P}}^{(0)}_{a_1a_2}(z;\varepsilon)\rangle\,|\mathcal{M}^{(0)}_{a,\ldots}(p,\ldots)|^2 , \tag{B.20}$$

where the averaged splitting functions read

$$\langle\hat{\mathbf{P}}^{(0)}_{gg}(z;\varepsilon)\rangle = 2C_A\left[\frac{z}{1-z} + \frac{1-z}{z} + z(1-z)\right] , \tag{B.21}$$

$$\langle\hat{\mathbf{P}}^{(0)}_{q\bar{q}}(z;\varepsilon)\rangle = \langle\hat{\mathbf{P}}^{(0)}_{\bar{q}q}(z;\varepsilon)\rangle = T_F\left[1 - \frac{2z(1-z)}{1-\varepsilon}\right] , \tag{B.22}$$

$$\langle\hat{\mathbf{P}}^{(0)}_{qg}(z;\varepsilon)\rangle = \langle\hat{\mathbf{P}}^{(0)}_{\bar{q}g}(z;\varepsilon)\rangle = C_F\,\left[\frac{1+z^2}{1-z} - \varepsilon(1-z)\right] , \tag{B.23}$$

$$\langle\hat{\mathbf{P}}^{(0)}_{gq}(z;\varepsilon)\rangle = \langle\hat{\mathbf{P}}^{(0)}_{g\bar{q}}(z;\varepsilon)\rangle = \langle\hat{\mathbf{P}}^{(0)}_{qg}(1-z;\varepsilon)\rangle . \tag{B.24}$$

The triple collinear limit is defined in Eq. (3.52) and the factorization formula is given in (3.53). Possible splitting functions are

$$\begin{gathered}\langle\hat{\mathbf{P}}_{\bar{q}_1'q_2'q_3}\rangle , \quad \langle\hat{\mathbf{P}}_{\bar{q}_1q_2q_3}\rangle , \quad \langle\hat{\mathbf{P}}_{g_1g_2q_3}\rangle , \\ \hat{P}^{\mu\nu}_{g_1q_2\bar{q}_3} , \quad \hat{P}^{\mu\nu}_{g_1g_2g_3} ,\end{gathered} \tag{B.25}$$

where in the case of a quark splitting spin correlations are absent and only averaged functions are needed. Explicit formulas can be found in [1, 138].

### B.2.2 Soft functions

The soft limit of a $q\bar{q}$-pair (3.55) is described by the soft function

$$\mathcal{J}_{ij}(q_1,q_2) = \frac{(p_i\cdot q_1)\,(p_j\cdot q_2) + (p_j\cdot q_1)\,(p_i\cdot q_2) - (p_i\cdot p_j)\,(q_1\cdot q_2)}{(q_1\cdot q_2)^2\,[p_i\cdot(q_1+q_2)]\,[p_j\cdot(q_1+q_2)]} . \tag{B.26}$$

The soft limit of two gluons is described by the soft function

$$\mathcal{S}_{ij}(q_1,q_2) = \mathcal{S}^{m=0}_{ij}(q_1,q_2) + \left(m_i^2\,\mathcal{S}^{m\neq0}_{ij}(q_1,q_2) + m_j^2\,\mathcal{S}^{m\neq0}_{ji}(q_1,q_2)\right) , \tag{B.27}$$

where [138]

$$\begin{aligned}\mathcal{S}_{ij}^{m=0}(q_1,q_2) = &\frac{(1-\varepsilon)}{(q_1\cdot q_2)^2}\frac{p_i\cdot q_1\; p_j\cdot q_2 + p_i\cdot q_2\; p_j\cdot q_1}{p_i\cdot(q_1+q_2)\; p_j\cdot(q_1+q_2)}\\ &-\frac{(p_i\cdot p_j)^2}{2\; p_i\cdot q_1\; p_j\cdot q_2\; p_i\cdot q_2\; p_j\cdot q_1}\left[2-\frac{p_i\cdot q_1\; p_j\cdot q_2 + p_i\cdot q_2\; p_j\cdot q_1}{p_i\cdot(q_1+q_2)\; p_j\cdot(q_1+q_2)}\right]\\ &+\frac{p_i\cdot p_j}{2\; q_1\cdot q_2}\left[\frac{2}{p_i\cdot q_1\; p_j\cdot q_2}+\frac{2}{p_j\cdot q_1\; p_i\cdot q_2}-\frac{1}{p_i\cdot(q_1+q_2)\; p_j\cdot(q_1+q_2)}\right.\\ &\left.\times\left(4+\frac{(p_i\cdot q_1\; p_j\cdot q_2 + p_i\cdot q_2\; p_j\cdot q_1)^2}{p_i\cdot q_1\; p_j\cdot q_2\; p_i\cdot q_2\; p_j\cdot q_1}\right)\right]\,,\end{aligned} \tag{B.28}$$

and [20]

$$\begin{aligned}\mathcal{S}_{ij}^{m\neq 0}(q_1,q_2) = &-\frac{1}{4\; q_1\cdot q_2\; p_i\cdot q_1\; p_i\cdot q_2}+\frac{p_i\cdot p_j\; p_j\cdot(q_1+q_2)}{2\; p_i\cdot q_1\; p_j\cdot q_2\; p_i\cdot q_2\; p_j\cdot q_1\; p_i\cdot(q_1+q_2)}\\ &-\frac{1}{2\; q_1\cdot q_2\; p_i\cdot(q_1+q_2)\; p_j\cdot(q_1+q_2)}\left(\frac{(p_j\cdot q_1)^2}{p_i\cdot q_1\; p_j\cdot q_2}+\frac{(p_j\cdot q_2)^2}{p_i\cdot q_2\; p_j\cdot q_1}\right)\,.\end{aligned} \tag{B.29}$$

## B.3 Soft and collinear limits of one-loop matrix elements

The soft and collinear limits of the one-loop matrix elements are described in Eq. (3.58) and (3.59), where explicit formulas can be found in [1, 139–146]. However, for the construction of separately finite contributions in section 4.5 the one-loop matrix elements is split as

$$2\mathrm{Re}\,\langle\mathcal{M}_{n+1}^{(0)}|\mathcal{M}_{n+1}^{(1)}\rangle = 2\mathrm{Re}\,\langle\mathcal{M}_{n+1}^{(0)}|\mathbf{Z}^{(1)}|\mathcal{M}_{n+1}^{(0)}\rangle + 2\mathrm{Re}\,\langle\mathcal{M}_{n+1}^{(0)}|\mathcal{F}_{n+1}^{(1)}\rangle\,. \tag{B.30}$$

The collinear and soft limits for both contributions on the right hand side are needed.

### B.3.1 Limits of matrix elements of $\mathrm{Z}^{(1)}$

The matrix element of the $\mathbf{Z}^{(1)}$ operator can be obtained from Eq. (B.3)

$$\begin{aligned}
2\mathrm{Re}\,\langle\mathcal{M}^{(0)}_{n+1}|\mathbf{Z}^{(1)}|\mathcal{M}^{(0)}_{n+1}\rangle = \\
&\frac{\alpha_s}{4\pi}\,\frac{1}{\varepsilon}\left[\left(-\frac{2}{\varepsilon}\sum_{i_0}C_{i_0}+\sum_i\gamma_0^i\right)|\mathcal{M}^{(0)}_{n+1}|^2\right.\\
&\quad+2\sum_{(i_0,j_0)}\ln\left|\frac{\mu_R^2}{s_{i_0j_0}}\right|\,\langle\mathcal{M}^{(0)}_{n+1}|\mathbf{T}_{i_0}\cdot\mathbf{T}_{j_0}|\mathcal{M}^{(0)}_{n+1}\rangle\\
&\quad-\sum_{(I,J)}\frac{1}{v_{IJ}}\ln\left(\frac{1+v_{IJ}}{1-v_{IJ}}\right)\,\langle\mathcal{M}^{(0)}_{n+1}|\mathbf{T}_I\cdot\mathbf{T}_J|\mathcal{M}^{(0)}_{n+1}\rangle\\
&\quad\left.+4\sum_{I,j_0}\ln\left|\frac{m_I\mu_R}{s_{Ij_0}}\right|\,\langle\mathcal{M}^{(0)}_{n+1}|\mathbf{T}_I\cdot\mathbf{T}_{j_0}|\mathcal{M}^{(0)}_{n+1}\rangle\right].
\end{aligned}\tag{B.31}$$

The factorization of Eq. (B.31) in the collinear limit, Eq. (3.48), reads

$$\begin{aligned}
2\mathrm{Re}\,\langle\mathcal{M}^{(0)}_{a_1,a_2,\dots}(p_1,p_2,\dots)|\mathbf{Z}^{(1)}|\mathcal{M}^{(0)}_{a_1,a_2,\dots}(p_1,p_2,\dots)\rangle \simeq \\
&4\pi\alpha_s\frac{2}{s_{12}}\left\{2\mathrm{Re}\,\langle\mathcal{M}^{(0)}_{a,\dots}(p,\dots)|\hat{\mathbf{P}}^{(0)}_{a_1a_2}(z,k_\perp;\varepsilon)\,\mathbf{Z}^{(1)}|\mathcal{M}^{(0)}_{a,\dots}(p,\dots)\rangle\right.\\
&\quad+\frac{\alpha_s}{4\pi}\,\frac{1}{\varepsilon}\left[2\left(C_a-C_{a_1}-C_{a_2}\right)\left(\frac{1}{\varepsilon}+\ln\left|\frac{\mu_R^2}{s_{12}}\right|\right)\right.\\
&\quad-\left(\gamma_0^a-\gamma_0^{a_1}-\gamma_0^{a_2}\right)\\
&\qquad\left.+2C_a\ln\big|z(1-z)\big|+2\left(C_{a_1}-C_{a_2}\right)\ln\left|\frac{z}{1-z}\right|\right]\\
&\quad\left.\times\,\langle\mathcal{M}^{(0)}_{a,\dots}(p,\dots)|\hat{\mathbf{P}}^{(0)}_{a_1a_2}(z,k_\perp;\varepsilon)|\mathcal{M}^{(0)}_{a,\dots}(p,\dots)\rangle\right\}.
\end{aligned}\tag{B.32}$$

This expression is valid for both final- and initial state collinear limits, if the signflip by crossing of a fermion is taken into account. The factorization of Eq. (B.31) in the soft limit, $q \to 0$, reads

$$
\begin{aligned}
&2\mathrm{Re}\,\langle \mathcal{M}^{(0)}_{g,a_1,\dots}(q,p_1,\dots)|\mathbf{Z}^{(1)}|\mathcal{M}^{(0)}_{g,a_1,\dots}(q,p_1,\dots)\rangle \simeq \\
&\quad -4\pi\alpha_s\Bigg\{\sum_{(i,j)}\Big(\mathcal{S}_{ij}(q)-\mathcal{S}_{ii}(q)\Big)\,2\mathrm{Re}\,\langle \mathcal{M}^{(0)}_{a_1,\dots}(p_1,\dots)|\mathbf{T}_i\cdot\mathbf{T}_j\,\mathbf{Z}^{(1)}|\mathcal{M}^{(0)}_{a_1,\dots}(p_1,\dots)\rangle \\
&\qquad +\frac{\alpha_s}{4\pi}\,\frac{1}{\varepsilon}\Bigg[\sum_{(i,j)}\Big(\mathcal{S}_{ij}(q)-\mathcal{S}_{ii}(q)\Big)\left(-2C_A\left(\frac{1}{\varepsilon}+\ln\big(\tfrac{1}{2}\mu_R^2\mathcal{S}_{ij}(q)\big)\right)+\gamma_0^g\right) \\
&\qquad\qquad \times\,\langle \mathcal{M}^{(0)}_{a_1,\dots}(p_1,\dots)|\mathbf{T}_i\cdot\mathbf{T}_j|\mathcal{M}^{(0)}_{a_1,\dots}(p_1,\dots)\rangle \\
&\qquad\quad -C_A\sum_{(I,J)}\Big(\mathcal{S}_{IJ}(q)-\mathcal{S}_{II}(q)\Big)\left(\frac{1}{v_{IJ}}\ln\left(\frac{1+v_{IJ}}{1-v_{IJ}}\right)+2\ln\left(\frac{m_Im_J}{s_{IJ}}\right)\right) \\
&\qquad\qquad \times\,\langle \mathcal{M}^{(0)}_{a_1,\dots}(p_1,\dots)|\mathbf{T}_I\cdot\mathbf{T}_J|\mathcal{M}^{(0)}_{a_1,\dots}(p_1,\dots)\rangle \\
&\qquad\quad -4\pi\sum_{(i,j,k)}\mathcal{S}_{ik}(q)\left(\frac{1}{v_{ij}}\theta(\sigma_{ij})-\theta(\sigma_{iq})-\theta(\sigma_{jq})\right) \\
&\qquad\qquad \times\,\langle \mathcal{M}^{(0)}_{a_1,\dots}(p_1,\dots)|f^{abc}T_i^aT_j^bT_k^c|\mathcal{M}^{(0)}_{a_1,\dots}(p_1,\dots)\rangle\Bigg]\Bigg\}\,.
\end{aligned}
\tag{B.33}
$$

### B.3.2 Limits of the one-loop finite remainder

The factorization of the finite remainder in the collinear limit, 3.48, reads

$$
\begin{aligned}
&2\mathrm{Re}\,\langle \mathcal{M}^{(0)}_{a_1,a_2,\dots}(p_1,p_2,\dots)|\mathcal{F}^{(1)}_{a_1,a_2,\dots}(p_1,p_2,\dots)\rangle \simeq \\
&\quad 4\pi\alpha_s\frac{2}{s_{12}}\Bigg[2\mathrm{Re}\,\langle \mathcal{M}^{(0)}_{a,\dots}(p,\dots)|\hat{\mathbf{P}}^{(0)}_{a_1a_2}(z,k_\perp;\varepsilon=0)|\mathcal{F}^{(1)}_{a,\dots}(p,\dots)\rangle \\
&\qquad\qquad +\frac{\alpha_s}{4\pi}\langle \mathcal{M}^{(0)}_{a,\dots}(p,\dots)|\hat{\mathbf{P}}^{(1)}_{Fa_1a_2}(z,k_\perp)|\mathcal{M}^{(0)}_{a,\dots}(p,\dots)\rangle\Bigg]\,.
\end{aligned}
\tag{B.34}
$$

The finite one-loop splitting functions, $\hat{\mathbf{P}}^{(1)}_{Fa_1a_2}(z,k_\perp)$, are operators in spin space

$$
\langle s|\hat{\mathbf{P}}^{(1)}_{Fa_1a_2}(z,k_\perp)|s'\rangle = \hat{P}^{(1),\,ss'}_{Fa_1a_2}(z,k_\perp)\,,
\tag{B.35}
$$

with

$$
\begin{aligned}
\hat{P}^{(1),\,\mu\nu}_{Fgg}(z,k_\perp) &= r^{gg}_{SF}(z)\,\hat{P}^{(0),\mu\nu}_{gg}(z,k_\perp;\varepsilon=0)-\frac{4}{3}C_A\big(C_A-2T_Fn_l\big)\frac{k_\perp^\mu k_\perp^\nu}{k_\perp^2}\,, \\
\hat{P}^{(1),\,\mu\nu}_{Fq\bar{q}}(z,k_\perp) &= \hat{P}^{(1),\,\mu\nu}_{F\bar{q}q}(z,k_\perp) = r^{\bar{q}q}_{SF}(z)\,\hat{P}^{(0),\mu\nu}_{q\bar{q}}(z,k_\perp;\varepsilon=0)\,, \\
\hat{P}^{(1),\,ss'}_{Fqg}(z,k_\perp) &= \hat{P}^{(1),\,ss'}_{F\bar{q}g}(z,k_\perp) = r^{qg}_{SF}(z)\,\hat{P}^{(0),ss'}_{qg}(z,k_\perp;\varepsilon=0)+2C_F\big(C_A-C_F\big)\,\delta^{ss'}\,, \\
\hat{P}^{(1),\,ss'}_{Fgq}(z,k_\perp) &= \hat{P}^{(1),\,ss'}_{Fg\bar{q}}(z,k_\perp) = \hat{P}^{(1),\,ss'}_{Fqg}(1-z,k_\perp)\,.
\end{aligned}
\tag{B.36}
$$

The finite coefficients $r_{SF}^{a_1 a_2}(z)$ are given by

$$r_{SF}^{gg}(z) = C_A \left( \frac{5\pi^2}{6} - \ln^2\left|\frac{z}{1-z}\right| + 2\ln\left|z(1-z)\right| \ln\left|\frac{\mu_R^2}{s_{12}}\right| - \ln^2\left|\frac{\mu_R^2}{s_{12}}\right| \right) , \tag{B.37}$$

$$\begin{aligned} r_{SF}^{\bar{q}q}(z) = {} & C_A \left( \frac{152}{9} - \frac{3\pi^2}{2} \right) + C_F \left( \frac{7\pi^2}{3} - 16 \right) - \frac{40}{9} T_F n_l - C_A \ln^2\left|\frac{z}{1-z}\right| \\ & + 2\left( \beta_0 - 3C_F + C_A \ln\left|z(1-z)\right| \right) \ln\left|\frac{\mu_R^2}{s_{12}}\right| + \left(C_A - 2C_F\right) \ln^2\left|\frac{\mu_R^2}{s_{12}}\right| \qquad \text{(B.38)} \\ & + 2\left(C_A - C_F\right) \pi^2 \, \theta(-s_{12}) , \qquad \text{(B.39)} \end{aligned}$$

$$\begin{aligned} r_{SF}^{qg}(z) = {} & \frac{5\pi^2}{6} C_A + 4 C_F \ln|z| \ln\left|\frac{\mu_R^2}{s_{12}}\right| - C_A \left( \ln\left|\frac{z}{1-z}\right| + \ln\left|\frac{\mu_R^2}{s_{12}}\right| \right)^2 \qquad \text{(B.40)} \\ & + 4\left(C_F - C_A\right) \mathrm{Re}\,\mathrm{Li}_2\left(-\frac{1-z}{z}\right) . \qquad \text{(B.41)} \end{aligned}$$

These expressions are valid for both final- and initial state collinear limits, if the crossing relation is taken into account in the initial state case.

The factorization of the finite remainder in the soft limit, $q \to 0$, reads

$$\begin{aligned} & 2\mathrm{Re}\,\langle \mathcal{M}^{(0)}_{g,a_1,\ldots}(q,p_1,\ldots) | \mathcal{F}^{(1)}_{g,a_1,\ldots}(q,p_1,\ldots) \rangle \simeq \\ & \quad -4\pi\alpha_s \left\{ \sum_{(i,j)} \Big( \mathcal{S}_{ij}(q) - \mathcal{S}_{ii}(q) \Big) \, 2\mathrm{Re}\,\langle \mathcal{M}^{(0)}_{a_1,\ldots}(p_1,\ldots) | \mathbf{T}_i \cdot \mathbf{T}_j | \mathcal{F}^{(1)}_{a_1,\ldots}(p_1,\ldots) \rangle \right. \\ & \qquad + \frac{\alpha_s}{4\pi} \left[ \sum_{(i,j)} \left( \mathcal{S}_{ij}(q) - \mathcal{S}_{ii}(q) \right) \, R_{ij}^F \, \langle \mathcal{M}^{(0)}_{a_1,\ldots}(p_1,\ldots) | \mathbf{T}_i \cdot \mathbf{T}_j | \mathcal{M}^{(0)}_{a_1,\ldots}(p_1,\ldots) \rangle \right. \\ & \qquad\quad \left. \left. -4\pi \sum_{(i,j,k)} \mathcal{S}_{ik}(q) \, I_{ij}^F \, \langle \mathcal{M}^{(0)}_{a_1,\ldots}(p_1,\ldots) | f^{abc} T_i^a T_j^b T_k^c | \mathcal{M}^{(0)}_{a_1,\ldots}(p_1,\ldots) \rangle \right] \right\} , \end{aligned} \tag{B.42}$$

where the functions $R_{ij}^F$ and $I_{ij}^F$ are the $\mathcal{O}(\varepsilon^0)$ coefficients of the one-loop soft functions given in [146] after expanding in $\varepsilon$.

$$\begin{aligned} R_{ij}^F &= 4C_A \left( R_{ij}^{(0)} + R_{ij}^{(-1)} \ln\left( \tfrac{1}{2}\mu_R^2 \mathcal{S}_{ij}(q) \right) + \tfrac{1}{2} R_{ij}^{(-2)} \ln^2\left( \tfrac{1}{2}\mu_R^2 \mathcal{S}_{ij}(q) \right) \right) , \\ I_{ij}^F &= 2 \left( I_{ij}^{(0)} + I_{ij}^{(-1)} \ln\left( \tfrac{1}{2}\mu_R^2 \mathcal{S}_{ij}(q) \right) \right) . \end{aligned} \tag{B.43}$$

## B.4 Helicity splitting functions

The limit of matrix elements as external polarized partons become collinear is described by the function $\mathrm{Split}_\lambda^{a\to a_1 a_2}(p_1^{\lambda_1}, p_2^{\lambda_2})$ in Eq. (5.40) and by $\mathrm{Split}_\lambda^{a\to a_1 a_2 a_3}(p_1^{\lambda_1}, p_2^{\lambda_2}, p_3^{\lambda_3})$ in Eq. (5.44). The explicit form for all possible flavor assignments has been given in [224]. However, they have been rederived for the Implementation of Stripper, due to some inconsistencies in the formulas in the literature. For completeness all formulas for the triple splitting functions are listed in the following.

In contrast to [224] the helicity of the splitting particle is treated, as if it is outgoing. The purely gluonic case is considered first

$$\mathrm{Split}_{\lambda}^{g\to ggg}(p_1^{\lambda_1},p_2^{\lambda_2},p_3^{\lambda_3}) = (4\pi\alpha_s)\sum_{\sigma\in S_2}\left(-f^{cc_{\sigma_1}\bar{c}}f^{\bar{c}c_{\sigma_1}c_3}\right)\mathrm{split}_{\lambda}^{g\to ggg}(p_{\sigma_1}^{\lambda_{\sigma_1}},p_{\sigma_2}^{\lambda_{\sigma_2}},p_3^{\lambda_3})\,, \tag{B.44}$$

where the sum over repeated color indices is always understood. The summation runs over the two permutations $S_2$ of $\{1,2\}$. The color stripped functions read

$$\begin{aligned}
\mathrm{split}_{+}^{g\to ggg}(p_1^{+},p_2^{+},p_3^{+}) &= 2\frac{1}{\sqrt{z_1z_3}}\frac{1}{\langle p_1p_2\rangle\langle p_2p_3\rangle}\,,\\
\mathrm{split}_{-}^{g\to ggg}(p_1^{-},p_2^{+},p_3^{+}) &= 2\frac{z_1^2}{\sqrt{z_1z_3}}\frac{1}{\langle p_1p_2\rangle\langle p_2p_3\rangle}\,,\\
\mathrm{split}_{-}^{g\to ggg}(p_1^{+},p_2^{-},p_3^{+}) &= 2\frac{z_2^2}{\sqrt{z_1z_3}}\frac{1}{\langle p_1p_2\rangle\langle p_2p_3\rangle}\,,\\
\mathrm{split}_{-}^{g\to ggg}(p_1^{+},p_2^{+},p_3^{-}) &= 2\frac{z_3^2}{\sqrt{z_1z_3}}\frac{1}{\langle p_1p_2\rangle\langle p_2p_3\rangle}\,,\\
\mathrm{split}_{+}^{g\to ggg}(p_1^{+},p_2^{+},p_3^{-}) &= \frac{2}{s_{12}s_{23}}\left[\frac{s_{12}z_2}{(1-z_1)}+\frac{\delta^2(p_1,p_2,p_3)}{s_{123}}+\sqrt{\frac{z_2}{z_1z_3}}(1-z_3)\delta(p_1,p_2,p_3)\right]\,,\\
\mathrm{split}_{+}^{g\to ggg}(p_1^{-},p_2^{+},p_3^{+}) &= \mathrm{split}_{+}^{g\to ggg}(p_3^{+},p_2^{+},p_1^{-})\,,\\
\mathrm{split}_{+}^{g\to ggg}(p_1^{+},p_2^{-},p_3^{+}) &= -\mathrm{split}_{+}^{g\to ggg}(p_2^{-},p_1^{+},p_3^{+})-\mathrm{split}_{+}^{g\to ggg}(p_1^{+},p_3^{+},p_2^{-})\,,
\end{aligned} \tag{B.45}$$

where

$$\delta(p_1,p_2,p_3) = [p_1p_2]\left(\sqrt{z_1}\langle p_1p_3\rangle+\sqrt{z_2}\langle p_2p_3\rangle\right)\,. \tag{B.46}$$

The splitting of a gluon into a gluon and a $q\bar{q}$ pair can be expanded in its color structures

$$\begin{aligned}
&\mathrm{Split}_{\lambda}^{g\to g\bar{q}q}(p_1^{\lambda_1},p_2^{\lambda_2},p_3^{-\lambda_2}) =\\
&\qquad(4\pi\alpha_s)\left[(t^ct^{c_1})_{c_3c_2}\,\mathrm{split}_{\lambda}^{g\to g\bar{q}q}(p_1^{\lambda_1},p_2^{\lambda_2},p_3^{-\lambda_2})+(t^{c_1}t^{c})_{c_3c_2}\,\mathrm{split}_{\lambda}^{g\to g\bar{q}q}(p_1^{\lambda_1},p_3^{-\lambda_2},p_2^{\lambda_2})\right]\,.
\end{aligned} \tag{B.47}$$

The color stripped functions read

$$\begin{aligned}
\mathrm{split}_{-}^{g\to g\bar{q}q}(p_1^{+},p_2^{-},p_3^{+}) =& \frac{2}{\sqrt{z_1}s_{12}s_{23}s_{123}}z_2\Big(\sqrt{z_3}[p_1p_3][p_2p_3]s_{12}\\
&+[p_1p_2]\Big(\sqrt{z_1}[p_1p_3]s_{23}+\sqrt{z_2}[p_2p_3](s_{12}+s_{23})\Big)\Big)\,,\\
\mathrm{split}_{-}^{g\to g\bar{q}q}(p_1^{+},p_2^{+},p_3^{-}) =& -\frac{2}{\sqrt{z_1}s_{12}s_{23}s_{123}}z_3\Big(\sqrt{z_3}[p_1p_3][p_2p_3]s_{12}\\
&+[p_1p_2]\Big(\sqrt{z_1}[p_1p_3]s_{23}+\sqrt{z_2}[p_2p_3](s_{12}+s_{23})\Big)\Big)\,,\\
\mathrm{split}_{+}^{g\to g\bar{q}q}(p_1^{+},p_2^{-},p_3^{+}) =& -\frac{2}{\sqrt{z_1}(z_2+z_3)s_{12}s_{23}s_{123}}\Big(-[p_1p_2](s_{12}+s_{23})\Big(\sqrt{z_2}z_3(z_2+z_3)\langle p_2p_3\rangle\\
&-\Big(\sqrt{z_1z_2^3z_3}+\sqrt{z_1z_2z_3^3}\Big)\langle p_1p_2\rangle\Big)
\end{aligned}$$

$$
\begin{aligned}
&+ [p_1p_3]s_{12}\Big((z_2+z_3)\Big(\sqrt{z_1}(z_1+2z_3)\langle p_1p_2\rangle - z_3^{3/2}\langle p_2p_3\rangle\Big)\\
&- \Big(\sqrt{z_1z_2^3z_3}+\sqrt{z_1z_2z_3^3}\Big)\langle p_1p_3\rangle\Big)\\
&+ \Big(\sqrt{z_1^3z_2z_3}+\sqrt{z_1z_2^3z_3}+\sqrt{z_1z_2z_3^3}\Big)s_{12}(s_{12}+s_{13}+s_{23})\Big)\,,\\
\mathrm{split}_+^{g\to g\bar{q}q}(p_1^+,p_2^+,p_3^-) =& -\frac{2}{\sqrt{z_1}(z_2+z_3)s_{12}s_{23}s_{123}}\Big([p_1p_2]\Big(\sqrt{z_2}(z_2+z_3)\langle p_2p_3\rangle(z_2s_{12}+(z_1+z_2)s_{23})\\
&+ \sqrt{z_1}(z_2+z_3)\langle p_1p_3\rangle((z_1+z_2)s_{23}+(z_1+2z_2)s_{12})\\
&- \Big(\sqrt{z_1z_2^3z_3}+\sqrt{z_1z_2z_3^3}\Big)\langle p_1p_2\rangle s_{12}\Big)\\
&+ s_{12}\Big([p_1p_3]\Big(\sqrt{z_2}\sqrt{z_2z_3}(z_2+z_3)\langle p_2p_3\rangle + \Big(\sqrt{z_1z_2^3z_3}+\sqrt{z_1z_2z_3^3}\Big)\langle p_1p_3\rangle\Big)\\
&+ \Big(\sqrt{z_1^3z_2z_3}+\sqrt{z_1z_2^3z_3}+\sqrt{z_1z_2z_3^3}\Big)(s_{12}+s_{13}+s_{23})\Big)\Big)\,. \qquad \text{(B.48)}
\end{aligned}
$$

The splitting for $q\to qgg$ can be decomposed according to its color structures as

$$
\mathrm{Split}_{\lambda_1}^{q\to qgg}(p_1^{\lambda_1},p_2^{\lambda_2},p_3^{\lambda_3}) = (4\pi\alpha_s)\sum_{\sigma\in S_2}\left(t^{c_{\sigma_2}}t^{c_{\sigma_3}}\right)_{c_1c}\mathrm{split}_{\lambda_1}^{q\to qgg}(p_1^{\lambda_1},p_{\sigma_2}^{\lambda_{\sigma_2}},p_{\sigma_3}^{\lambda_{\sigma_3}})\,, \qquad \text{(B.49)}
$$

where $S_2$ denotes the permutations of $\{2,3\}$. The color stripped functions read

$$
\begin{aligned}
\mathrm{split}_+^{q\to qgg}(p_1^+,p_2^+,p_3^+) =& -\frac{2i}{\sqrt{z_2}\sqrt{z_3}s_{12}s_{23}s_{123}}\Big(\sqrt{z_3}[p_1p_3][p_2p_3]s_{12}\\
&+ [p_1p_2]\Big(\sqrt{z_1}[p_1p_3]s_{23}+\sqrt{z_2}[p_2p_3](s_{12}+s_{23})\Big)\Big)\,,\\
\mathrm{split}_-^{q\to qgg}(p_1^-,p_2^+,p_3^+) =& -\frac{2i}{\sqrt{z_2}\sqrt{z_3}s_{12}s_{23}s_{123}}z_1\Big(\sqrt{z_3}[p_1p_3][p_2p_3]s_{12}\\
&+ [p_1p_2]\Big(\sqrt{z_1}[p_1p_3]s_{23}+\sqrt{z_2}[p_2p_3](s_{12}+s_{23})\Big)\Big)\,,\\
\mathrm{split}_-^{q\to qgg}(p_1^+,p_2^-,p_3^+) =& \frac{2i}{\sqrt{z_2}\sqrt{z_3}(z_2+z_3)s_{12}s_{23}s_{123}}\Big(\sqrt{z_2}\Big(z_1(z_2+z_3)[p_2p_3]\langle p_1p_2\rangle s_{12}\\
&+ \sqrt{z_3}\Big(z_3^{3/2}(-[p_1p_2])\langle p_2p_3\rangle s_{12}-\sqrt{z_1}z_3\Big(s_{12}^2-s_{23}s_{12}+s_{13}s_{23}\Big)\\
&+ \sqrt{z_1}z_2(s_{12}(s_{13}+s_{23})-s_{13}s_{23})\Big)\Big)\\
&+ [p_1p_3]\Big(\sqrt{z_1}(z_1+z_2)(z_2+z_3)\langle p_1p_2\rangle s_{23}+\sqrt{z_3}\langle p_2p_3\rangle((z_1(z_2+z_3)\\
&+ z_3(2z_2+z_3))s_{12}-z_1(z_2+z_3)s_{23})\Big)\Big)\,,\\
\mathrm{split}_+^{q\to qgg}(p_1^+,p_2^+,p_3^-) =& \frac{2i}{\sqrt{z_2}\sqrt{z_3}(z_2+z_3)s_{12}s_{23}s_{123}}\Big([p_1p_2]\Big(\sqrt{z_1}(z_1+z_2)(z_2+z_3)\langle p_1p_3\rangle s_{23}\\
&+ \sqrt{z_2}\langle p_2p_3\rangle((z_1+z_2)(z_2+z_3)s_{23}+(z_2(z_1+z_2)+(z_1+2z_2)z_3)s_{12})\Big)\\
&- \sqrt{z_3}s_{12}\Big(\sqrt{z_2}\Big(z_2^{3/2}[p_1p_3]\langle p_2p_3\rangle+\sqrt{z_1}z_2(s_{23}-s_{13})+\sqrt{z_1}z_3(s_{12}+s_{23})\Big)\\
&- z_1(z_2+z_3)[p_2p_3]\langle p_1p_3\rangle\Big)\Big)\,.
\end{aligned}
$$

Finally, the splitting for the purely quark case reads

$$\begin{aligned}\mathrm{Split}_{\lambda_1}^{q\to q\bar{q}'q'}(p_1^{\lambda_1},p_2^{\lambda_2},p_3^{\lambda_3}) = (8\pi\alpha_s)\Big[t^{\bar{c}}_{c_1c}t^{\bar{c}}_{c_3c_2}\,\mathrm{split}_{\lambda_1}^{q\to q\bar{q}'q'}(p_1^{\lambda_1},p_2^{\lambda_2},p_3^{\lambda_3}) \\ - \delta_{qq'}t^{\bar{c}}_{c_3c}t^{\bar{c}}_{c_1c_2}\,\mathrm{split}_{\lambda_1}^{q\to q\bar{q}'q'}(p_3^{\lambda_3},p_2^{\lambda_2},p_1^{\lambda_1})\Big]\,,\end{aligned} \tag{B.50}$$

where the color stripped functions read

$$\begin{aligned}\mathrm{split}_{+}^{q\to q\bar{q}'q'}(p_1^{+},p_2^{-},p_3^{+}) &= \frac{i}{s_{23}}\left(\frac{\sqrt{z_1z_2z_3}}{1-z_1}+\frac{\delta(p_1,p_2,p_3)}{s_{123}}\right)\,,\\ \mathrm{split}_{-}^{q\to q\bar{q}'q'}(p_1^{-},p_2^{-},p_3^{+}) &= \mathrm{split}_{+}^{q\to q\bar{q}'q'}(p_1^{+},p_3^{-},p_2^{+})\,.\end{aligned} \tag{B.51}$$

The remaining splitting functions, $\mathrm{Split}_{-\lambda}^{a\to a_1a_2a_3}(p_1^{-\lambda_1},p_2^{-\lambda_2},p_3^{-\lambda_3})$, are obtained from $\mathrm{Split}_{\lambda}^{a\to a_1a_2a_3}(p_1^{\lambda_1},p_2^{\lambda_2},p_3^{\lambda_3})$ by replacing $\langle p_ip_j\rangle$ with $[p_jp_i]$ and vice versa. A factor $(-1)$ has to be multiplied, if the splitting function contains a $q\bar{q}$-pair in the final state.

## B.5 Crossing

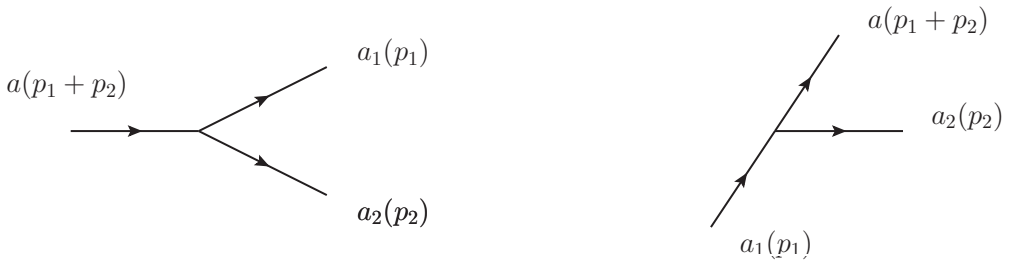


**Figure B.1:** Final state collinear splitting configuration (left) and initial state collinear splitting configuration (right).

All formulas presented in the previous sections have been given for final state collinear particles. If however, one of the particle is in the initial state the correct formulas are obtained by crossing. If the particle with momentum $p_1$ and flavour $a_1$ is crossed to the initial state,as depicted in Fig. B.1, the splitting functions obtain a sign for each fermion that is crossed

$$\hat{\mathbf{P}} \quad\longrightarrow\quad \big(-\big)^{2s_a+2s_{a_1}}\hat{\mathbf{P}}\,, \tag{B.52}$$

where $s_a$ and $s_{a_1}$ are the spins of partons $a$ and $a_1$ respectively. The splitting variable $z$ can be obtained in the collinear limit from the energies of the involved partons. The crossing amounts to the replacement

$$z=\frac{p_1^0}{p_1^0+p_2^0}\in[0,1] \quad\longrightarrow\quad z=\frac{p_1^0}{p_1^0-p_2^0}\in[1,+\infty[\,, \tag{B.53}$$

and similarly for the triple splitting functions

$$z=\frac{p_1^0}{p_1^0+p_2^0+p_3^0}\in[0,1] \quad\longrightarrow\quad z=\frac{p_1^0}{p_1^0-p_2^0-p_3^0}\in[1,+\infty[\,. \tag{B.54}$$

# List of Figures

# List of Tables

# Bibliography


1. Czakon, M. and D. Heymes: 'Four-dimensional formulation of the sector-improved residue subtraction scheme'. *Nucl.Phys.* (2014), volume B890: pages 152–227. doi: 10.1016/j.nuclphysb.2014.11.006. arXiv: 1408.2500 [hep-ph].
2. Heymes, David: 'General formulation of the sector-improved residue subtraction'. *J.Phys.Conf.Ser.* (2015), volume 608(1): page 012073. doi: 10.1088/1742-6596/608/1/012073. arXiv: 1410.2696 [hep-ph].
3. Heymes, David: 'Four-dimensional formulation of the sector improved residue subtraction'. *PoS* (2014), volume LL2014: page 004. arXiv: 1408.2679 [hep-ph].
4. Aad, Georges et al.: 'Observation of a new particle in the search for the Standard Model Higgs boson with the ATLAS detector at the LHC'. *Phys.Lett.* (2012), volume B716: pages 1–29. doi: 10.1016/j.physletb.2012.08.020. arXiv: 1207.7214 [hep-ex].
5. Chatrchyan, Serguei et al.: 'Observation of a new boson at a mass of 125 GeV with the CMS experiment at the LHC'. *Phys.Lett.* (2012), volume B716: pages 30–61. doi: 10.1016/j.physletb.2012.08.021. arXiv: 1207.7235 [hep-ex].
6. 'Projected Performance of an Upgraded CMS Detector at the LHC and HL-LHC: Contribution to the Snowmass Process'. (2013), volume. arXiv: 1307.7135.
7. 'Physics at a High-Luminosity LHC with ATLAS'. (2013), volume. arXiv: 1307.7292 [hep-ex].
8. Schael, S. et al.: 'Precision electroweak measurements on the $Z$ resonance'. *Phys.Rept.* (2006), volume 427: pages 257–454. doi: 10.1016/j.physrep.2005.12.006. arXiv: hep-ex/0509008 [hep-ex].
9. Czakon, Michal, Alexander Mitov, Michele Papucci, Joshua T. Ruderman, and Andreas Weiler: 'Closing the stop gap'. *Phys.Rev.Lett.* (2014), volume 113(20): page 201803. doi: 10.1103/PhysRevLett.113.201803. arXiv: 1407.1043 [hep-ph].
10. Ball, Richard D. et al.: 'Parton distributions for the LHC Run II'. *JHEP* (2015), volume 1504: page 040. doi: 10.1007/JHEP04(2015)040. arXiv: 1410.8849 [hep-ph].
11. Martin, A.D., W.J. Stirling, R.S. Thorne, and G. Watt: 'Parton distributions for the LHC'. *Eur.Phys.J.* (2009), volume C63: pages 189–285. doi: 10.1140/epjc/s10052-009-1072-5. arXiv: 0901.0002 [hep-ph].
12. Lai, Hung-Liang, Marco Guzzi, Joey Huston, Zhao Li, Pavel M. Nadolsky, et al.: 'New parton distributions for collider physics'. *Phys.Rev.* (2010), volume D82: page 074024. doi: 10.1103/PhysRevD.82.074024. arXiv: 1007.2241 [hep-ph].

13. Dulat, Sayipjamal, Tie Jiun Hou, Jun Gao, Marco Guzzi, Joey Huston, et al.: 'The CT14 Global Analysis of Quantum Chromodynamics'. (2015), volume. arXiv: 1506.07443 [hep-ph].
14. Alwall, J., R. Frederix, S. Frixione, V. Hirschi, F. Maltoni, et al.: 'The automated computation of tree-level and next-to-leading order differential cross sections, and their matching to parton shower simulations'. *JHEP* (2014), volume 1407: page 079. doi: 10.1007/JHEP07(2014)079. arXiv: 1405.0301 [hep-ph].
15. Cafarella, Alessandro, Costas G. Papadopoulos, and Malgorzata Worek: 'Helac-Phegas: A Generator for all parton level processes'. *Comput.Phys.Commun.* (2009), volume 180: pages 1941–1955. doi: 10.1016/j.cpc.2009.04.023. arXiv: 0710.2427 [hep-ph].
16. Catani, S. and M.H. Seymour: 'A General algorithm for calculating jet cross-sections in NLO QCD'. *Nucl.Phys.* (1997), volume B485: pages 291–419. doi: 10.1016/S0550-3213(96)00589-5. arXiv: hep-ph/9605323 [hep-ph].
17. Frixione, S., Z. Kunszt, and A. Signer: 'Three jet cross-sections to next-to-leading order'. *Nucl.Phys.* (1996), volume B467: pages 399–442. doi: 10.1016/0550-3213(96)00110-1. arXiv: hep-ph/9512328 [hep-ph].
18. Bevilacqua, G., M. Czakon, M.V. Garzelli, A. van Hameren, A. Kardos, et al.: 'HELAC-NLO'. *Comput.Phys.Commun.* (2013), volume 184: pages 986–997. doi: 10.1016/j.cpc.2012.10.033. arXiv: 1110.1499 [hep-ph].
19. Czakon, M.: 'A novel subtraction scheme for double-real radiation at NNLO'. *Phys.Lett.* (2010), volume B693: pages 259–268. doi: 10.1016/j.physletb.2010.08.036. arXiv: 1005.0274 [hep-ph].
20. Czakon, M.: 'Double-real radiation in hadronic top quark pair production as a proof of a certain concept'. *Nucl.Phys.* (2011), volume B849: pages 250–295. doi: 10.1016/j.nuclphysb.2011.03.020. arXiv: 1101.0642 [hep-ph].
21. Denner, Ansgar, Stefan Dittmaier, Markus Hecht, and Christian Pasold: 'NLO QCD and electroweak corrections to $W + \gamma$ production with leptonic W-boson decays'. *JHEP* (2015), volume 1504: page 018. doi: 10.1007/JHEP04(2015)018. arXiv: 1412.7421 [hep-ph].
22. Stirling, W.J.: *private communication.*
23. Anastasiou, Charalampos, Claude Duhr, Falko Dulat, Franz Herzog, and Bernhard Mistlberger: 'Higgs Boson Gluon-Fusion Production in QCD at Three Loops'. *Phys.Rev.Lett.* (2015), volume 114(21): page 212001. doi: 10.1103/PhysRevLett.114.212001. arXiv: 1503.06056 [hep-ph].
24. CMS-Collaboration: *Summary of CMS cross section measurements.* 2015. url: http://cern.ch/go/pNj7.
25. Gehrmann, T., M. Grazzini, S. Kallweit, P. Maierhöfer, A. von Manteuffel, et al.: '$W^+W^-$ Production at Hadron Colliders in Next to Next to Leading Order QCD'. *Phys.Rev.Lett.* (2014), volume 113(21): page 212001. doi: 10.1103/PhysRevLett.113.212001. arXiv: 1408.5243 [hep-ph].
26. Chatrchyan, Serguei et al.: 'Measurement of the $W^+W^-$ Cross section in $pp$ Collisions at $\sqrt{s} = 7$ TeV and Limits on Anomalous $WW\gamma$ and $WWZ$ couplings'. *Eur.Phys.J.* (2013), volume C73(10): page 2610. doi: 10.1140/epjc/s10052-013-2610-8. arXiv: 1306.1126 [hep-ex].

27. Collaboration, CMS: 'Measurement of the $W^+W^-$ cross section in pp collisions at sqrt(s) = 8 TeV and limits on anomalous gauge couplings'. (2015), volume.

28. ATLAS: *Summary plots from the ATLAS Top physics group*. May 2015. URL: https://atlas.web.cern.ch/Atlas/GROUPS/PHYSICS/CombinedSummaryPlots/TOP/.

29. Czakon, Michal, Paul Fiedler, Alexander Mitov, and Juan Rojo: 'Further exploration of top pair hadroproduction at NNLO'. (2013), volume. arXiv: 1305.3892 [hep-ph].

30. Aad, Georges et al.: 'Measurement of the top pair production cross-section in 8 TeV proton-proton collisions using kinematic information in the lepton+jets final state with ATLAS'. (2015), volume. arXiv: 1504.04251 [hep-ex].

31. Khachatryan, Vardan et al.: 'Measurement of the $t\bar{t}$ production cross section in $pp$ collisions at $\sqrt{s} = 8$ TeV in dilepton final states containing one $\tau$ lepton'. *Phys.Lett.* (2014), volume B739: pages 23–43. DOI: 10.1016/j.physletb.2014.10.032. arXiv: 1407.6643 [hep-ex].

32. Aad, Georges et al.: 'Measurement of the $t\bar{t}$ production cross-section using $e\mu$ events with $b$ -tagged jets in $pp$ collisions at $\sqrt{s} = 7$ and 8 TeV with the ATLAS detector'. *Eur.Phys.J.* (2014), volume C74(10): page 3109. DOI: 10.1140/epjc/s10052-014-3109-7. arXiv: 1406.5375 [hep-ex].

33. Chatrchyan, Serguei et al.: 'Measurement of the $t\bar{t}$ production cross section in the dilepton channel in pp collisions at $\sqrt{s} = 8$ TeV'. *JHEP* (2014), volume 1402: page 024. DOI: 10.1007/JHEP02(2014)024,10.1007/JHEP02(2014)102. arXiv: 1312.7582 [hep-ex].

34. Czakon, Michał, Paul Fiedler, and Alexander Mitov: 'Total Top-Quark Pair-Production Cross Section at Hadron Colliders Through $O(\alpha_S^4)$'. *Phys.Rev.Lett.* (2013), volume 110: page 252004. DOI: 10.1103/PhysRevLett.110.252004. arXiv: 1303.6254 [hep-ph].

35. Aad, Georges et al.: 'Measurement of the low-mass Drell-Yan differential cross section at $\sqrt{s} = 7$ TeV using the ATLAS detector'. *JHEP* (2014), volume 1406: page 112. DOI: 10.1007/JHEP06(2014)112. arXiv: 1404.1212 [hep-ex].

36. Gavin, Ryan, Ye Li, Frank Petriello, and Seth Quackenbush: 'FEWZ 2.0: A code for hadronic Z production at next-to-next-to-leading order'. *Comput.Phys.Commun.* (2011), volume 182: pages 2388–2403. DOI: 10.1016/j.cpc.2011.06.008. arXiv: 1011.3540 [hep-ph].

37. Frixione, Stefano and Bryan R. Webber: 'Matching NLO QCD computations and parton shower simulations'. *JHEP* (2002), volume 0206: page 029. DOI: 10.1088/1126-6708/2002/06/029. arXiv: hep-ph/0204244 [hep-ph].

38. Alioli, Simone, Paolo Nason, Carlo Oleari, and Emanuele Re: 'NLO vector-boson production matched with shower in POWHEG'. *JHEP* (2008), volume 0807: page 060. DOI: 10.1088/1126-6708/2008/07/060. arXiv: 0805.4802 [hep-ph].

39. Hamberg, R., W.L. van Neerven, and T. Matsuura: 'A Complete calculation of the order $\alpha - s^2$ correction to the Drell-Yan $K$ factor'. *Nucl.Phys.* (1991), volume B359: pages 343–405. DOI: 10.1016/0550-3213(91)90064-5.

40. Catani, Stefano, Leandro Cieri, Giancarlo Ferrera, Daniel de Florian, and Massimiliano Grazzini: 'Vector boson production at hadron colliders: a fully exclusive QCD calculation at NNLO'. *Phys.Rev.Lett.* (2009), volume 103: page 082001. DOI: 10.1103/PhysRevLett.103.082001. arXiv: 0903.2120 [hep-ph].

41. Catani, Stefano and Massimiliano Grazzini: 'An NNLO subtraction formalism in hadron collisions and its application to Higgs boson production at the LHC'. *Phys.Rev.Lett.* (2007), volume 98: page 222002. DOI: 10.1103/PhysRevLett.98.222002. arXiv: hep-ph/0703012 [hep-ph].

42. Melnikov, Kirill and Frank Petriello: 'Electroweak gauge boson production at hadron colliders through O(alpha(s)**2)'. *Phys.Rev.* (2006), volume D74: page 114017. DOI: 10.1103/PhysRevD.74.114017. arXiv: hep-ph/0609070 [hep-ph].

43. Anastasiou, Charalampos, Kirill Melnikov, and Frank Petriello: 'Higgs boson production at hadron colliders: Differential cross sections through next-to-next-to-leading order'. *Phys.Rev.Lett.* (2004), volume 93: page 262002. DOI: 10.1103/PhysRevLett.93.262002. arXiv: hep-ph/0409088 [hep-ph].

44. Anastasiou, Charalampos, Kirill Melnikov, and Frank Petriello: 'Fully differential Higgs boson production and the di-photon signal through next-to-next-to-leading order'. *Nucl.Phys.* (2005), volume B724: pages 197–246. DOI: 10.1016/j.nuclphysb.2005.06.036. arXiv: hep-ph/0501130 [hep-ph].

45. Grazzini, Massimiliano: 'NNLO predictions for the Higgs boson signal in the H —> WW —> lnu lnu and H —> ZZ —> 4l decay channels'. *JHEP* (2008), volume 0802: page 043. DOI: 10.1088/1126-6708/2008/02/043. arXiv: 0801.3232 [hep-ph].

46. Grazzini, Massimiliano and Hayk Sargsyan: 'Heavy-quark mass effects in Higgs boson production at the LHC'. *JHEP* (2013), volume 1309: page 129. DOI: 10.1007/JHEP09(2013)129. arXiv: 1306.4581 [hep-ph].

47. Gavin, Ryan, Ye Li, Frank Petriello, and Seth Quackenbush: 'W Physics at the LHC with FEWZ 2.1'. *Comput.Phys.Commun.* (2013), volume 184: pages 208–214. DOI: 10.1016/j.cpc.2012.09.005. arXiv: 1201.5896 [hep-ph].

48. Czakon, Michal, Paul Fiedler, and Alexander Mitov: 'Resolving the Tevatron top quark forward-backward asymmetry puzzle'. (2014), volume. arXiv: 1411.3007 [hep-ph].

49. Currie, James, Aude Gehrmann-De Ridder, E.W.N. Glover, and Joao Pires: 'NNLO QCD corrections to jet production at hadron colliders from gluon scattering'. *JHEP* (2014), volume 1401: page 110. DOI: 10.1007/JHEP01(2014)110. arXiv: 1310.3993 [hep-ph].

50. Gehrmann-De Ridder, Aude, Thomas Gehrmann, E.W.N. Glover, and Joao Pires: 'Second order QCD corrections to jet production at hadron colliders: the all-gluon contribution'. *Phys.Rev.Lett.* (2013), volume 110(16): page 162003. DOI: 10.1103/PhysRevLett.110.162003. arXiv: 1301.7310 [hep-ph].

51. Grazzini, Massimiliano, Stefan Kallweit, Dirk Rathlev, and Alessandro Torre: '$Z\gamma$ production at hadron colliders in NNLO QCD'. *Phys.Lett.* (2014), volume B731: pages 204–207. DOI: 10.1016/j.physletb.2014.02.037. arXiv: 1309.7000 [hep-ph].

52. Grazzini, Massimiliano, Stefan Kallweit, and Dirk Rathlev: '$W\gamma$ and $Z\gamma$ production at the LHC in NNLO QCD'. (2015), volume. arXiv: 1504.01330 [hep-ph].

53. Cascioli, F., T. Gehrmann, M. Grazzini, S. Kallweit, P. Maierhöfer, et al.: 'ZZ production at hadron colliders in NNLO QCD'. *Phys.Lett.* (2014), volume B735: pages 311–313. DOI: 10.1016/j.physletb.2014.06.056. arXiv: 1405.2219 [hep-ph].

54. Boughezal, Radja, Fabrizio Caola, Kirill Melnikov, Frank Petriello, and Markus Schulze: 'Higgs Boson Production in Association with a Jet at Next-to-Next-to-Leading Order'. (2015), volume. arXiv: 1504.07922 [hep-ph].

55. Boughezal, Radja, Fabrizio Caola, Kirill Melnikov, Frank Petriello, and Markus Schulze: 'Higgs boson production in association with a jet at next-to-next-to-leading order in perturbative QCD'. *JHEP* (2013), volume 1306: page 072. doi: 10.1007/JHEP06(2013)072. arXiv: 1302.6216 [hep-ph].

56. Boughezal, Radja, Christfried Focke, Xiaohui Liu, and Frank Petriello: '$W$-boson production in association with a jet at next-to-next-to-leading order in perturbative QCD'. (2015), volume. arXiv: 1504.02131 [hep-ph].

57. Faddeev, L.D. and V.N. Popov: 'Feynman Diagrams for the Yang-Mills Field'. *Phys.Lett.* (1967), volume B25: pages 29–30. doi: 10.1016/0370-2693(67)90067-6.

58. 't Hooft, Gerard and M.J.G. Veltman: 'Regularization and Renormalization of Gauge Fields'. *Nucl.Phys.* (1972), volume B44: pages 189–213. doi: 10.1016/0550-3213(72)90279-9.

59. Gross, D.J. and Frank Wilczek: 'Asymptotically Free Gauge Theories. 1'. *Phys.Rev.* (1973), volume D8: pages 3633–3652. doi: 10.1103/PhysRevD.8.3633.

60. Gross, D.J. and Frank Wilczek: 'ASYMPTOTICALLY FREE GAUGE THEORIES. 2.' *Phys.Rev.* (1974), volume D9: pages 980–993. doi: 10.1103/PhysRevD.9.980.

61. Politzer, H. David: 'Reliable Perturbative Results for Strong Interactions?' *Phys.Rev.Lett.* (1973), volume 30: pages 1346–1349. doi: 10.1103/PhysRevLett.30.1346.

62. Ritbergen, T. van, J.A.M. Vermaseren, and S.A. Larin: 'The Four loop beta function in quantum chromodynamics'. *Phys.Lett.* (1997), volume B400: pages 379–384. doi: 10.1016/S0370-2693(97)00370-5. arXiv: hep-ph/9701390 [hep-ph].

63. Czakon, M.: 'The Four-loop QCD beta-function and anomalous dimensions'. *Nucl.Phys.* (2005), volume B710: pages 485–498. doi: 10.1016/j.nuclphysb.2005.01.012. arXiv: hep-ph/0411261 [hep-ph].

64. Olive, K.A. et al.: 'Review of Particle Physics'. *Chin.Phys.* (2014), volume C38: page 090001. doi: 10.1088/1674-1137/38/9/090001.

65. Bernreuther, Werner and Werner Wetzel: 'Decoupling of Heavy Quarks in the Minimal Subtraction Scheme'. *Nucl.Phys.* (1982), volume B197: page 228. doi: 10.1016/0550-3213(82)90288-7.

66. Chetyrkin, K.G., Bernd A. Kniehl, and M. Steinhauser: 'Decoupling relations to O (alpha-s**3) and their connection to low-energy theorems'. *Nucl.Phys.* (1998), volume B510: pages 61–87. doi: 10.1016/S0550-3213(97)00649-4. arXiv: hep-ph/9708255 [hep-ph].

67. Chetyrkin, K.G., Johann H. Kuhn, and Christian Sturm: 'QCD decoupling at four loops'. *Nucl.Phys.* (2006), volume B744: pages 121–135. doi: 10.1016/j.nuclphysb.2006.03.020. arXiv: hep-ph/0512060 [hep-ph].

68. Collins, John C., Davison E. Soper, and George F. Sterman: 'Factorization of Hard Processes in QCD'. *Adv.Ser.Direct.High Energy Phys.* (1988), volume 5: pages 1–91. arXiv: hep-ph/0409313 [hep-ph].

69. Lee, T.D. and M. Nauenberg: 'Degenerate Systems and Mass Singularities'. *Phys.Rev.* (1964), volume 133: B1549–B1562. doi: 10.1103/PhysRev.133.B1549.

70. Kinoshita, T.: 'Mass singularities of Feynman amplitudes'. *J.Math.Phys.* (1962), volume 3: pages 650–677. doi: 10.1063/1.1724268.

71. Ellis, R.K., W.J. Stirling, and B.R. Webber: *QCD and Collider Physics*. Cambridge University Press, 1996.

72. Ellis, R. Keith, Zoltan Kunszt, Kirill Melnikov, and Giulia Zanderighi: 'One-loop calculations in quantum field theory: from Feynman diagrams to unitarity cuts'. *Phys.Rept.* (2012), volume 518: pages 141–250. doi: 10.1016/j.physrep.2012.01.008. arXiv: 1105.4319 [hep-ph].

73. Neerven, W.L. van and J.A.M. Vermaseren: 'LARGE LOOP INTEGRALS'. *Phys.Lett.* (1984), volume B137: page 241. doi: 10.1016/0370-2693(84)90237-5.

74. Melrose, D.B.: 'Reduction of Feynman diagrams'. *Nuovo Cim.* (1965), volume 40: pages 181–213. doi: 10.1007/BF02832919.

75. Denner, Ansgar, S. Dittmaier, and M. Roth: 'Nonfactorizable photonic corrections to e+ e- W W four fermions'. *Nucl.Phys.* (1998), volume B519: pages 39–84. doi: 10.1016/S0550-3213(98)00046-7. arXiv: hep-ph/9710521 [hep-ph].

76. Passarino, G. and M.J.G. Veltman: 'One Loop Corrections for e+ e- Annihilation Into mu+ mu- in the Weinberg Model'. *Nucl.Phys.* (1979), volume B160: page 151. doi: 10.1016/0550-3213(79)90234-7.

77. Denner, Ansgar and S. Dittmaier: 'Reduction of one loop tensor five point integrals'. *Nucl.Phys.* (2003), volume B658: pages 175–202. doi: 10.1016/S0550-3213(03)00184-6. arXiv: hep-ph/0212259 [hep-ph].

78. Denner, Ansgar and S. Dittmaier: 'Reduction schemes for one-loop tensor integrals'. *Nucl.Phys.* (2006), volume B734: pages 62–115. doi: 10.1016/j.nuclphysb.2005.11.007. arXiv: hep-ph/0509141 [hep-ph].

79. Bredenstein, A., A. Denner, S. Dittmaier, and S. Pozzorini: 'NLO QCD corrections to pp -> t anti-t b anti-b + X at the LHC'. *Phys.Rev.Lett.* (2009), volume 103: page 012002. doi: 10.1103/PhysRevLett.103.012002. arXiv: 0905.0110 [hep-ph].

80. Denner, A., S. Dittmaier, S. Kallweit, and S. Pozzorini: 'NLO QCD corrections to WWbb production at hadron colliders'. *Phys.Rev.Lett.* (2011), volume 106: page 052001. doi: 10.1103/PhysRevLett.106.052001. arXiv: 1012.3975 [hep-ph].

81. Ossola, Giovanni, Costas G. Papadopoulos, and Roberto Pittau: 'Reducing full one-loop amplitudes to scalar integrals at the integrand level'. *Nucl.Phys.* (2007), volume B763: pages 147–169. doi: 10.1016/j.nuclphysb.2006.11.012. arXiv: hep-ph/0609007 [hep-ph].

82. Ossola, Giovanni, Costas G. Papadopoulos, and Roberto Pittau: 'On the Rational Terms of the one-loop amplitudes'. *JHEP* (2008), volume 0805: page 004. doi: 10.1088/1126-6708/2008/05/004. arXiv: 0802.1876 [hep-ph].

83. Cutkosky, R.E.: 'Singularities and discontinuities of Feynman amplitudes'. *J.Math.Phys.* (1960), volume 1: pages 429–433. doi: 10.1063/1.1703676.

84. Bern, Zvi, Lance J. Dixon, David C. Dunbar, and David A. Kosower: 'Fusing gauge theory tree amplitudes into loop amplitudes'. *Nucl.Phys.* (1995), volume B435: pages 59–101. DOI: 10.1016/0550-3213(94)00488-Z. arXiv: hep-ph/9409265 [hep-ph].

85. Berends, Frits A. and W.T. Giele: 'Recursive Calculations for Processes with n Gluons'. *Nucl.Phys.* (1988), volume B306: page 759. DOI: 10.1016/0550-3213(88)90442-7.

86. Binoth, T., J.-Ph. Guillet, G. Heinrich, E. Pilon, and T. Reiter: 'Golem95: A Numerical program to calculate one-loop tensor integrals with up to six external legs'. *Comput.Phys.Commun.* (2009), volume 180: pages 2317–2330. DOI: 10.1016/j.cpc.2009.06.024. arXiv: 0810.0992 [hep-ph].

87. Cullen, G., J. Ph. Guillet, G. Heinrich, T. Kleinschmidt, E. Pilon, et al.: 'Golem95C: A library for one-loop integrals with complex masses'. *Comput.Phys.Commun.* (2011), volume 182: pages 2276–2284. DOI: 10.1016/j.cpc.2011.05.015. arXiv: 1101.5595 [hep-ph].

88. Guillet, J. Ph., G. Heinrich, and J.F. von Soden-Fraunhofen: 'Tools for NLO automation: extension of the golem95C integral library'. *Comput.Phys.Commun.* (2014), volume 185: pages 1828–1834. DOI: 10.1016/j.cpc.2014.03.009. arXiv: 1312.3887 [hep-ph].

89. Cascioli, Fabio, Philipp Maierhofer, and Stefano Pozzorini: 'Scattering Amplitudes with Open Loops'. *Phys.Rev.Lett.* (2012), volume 108: page 111601. DOI: 10.1103/PhysRevLett.108.111601. arXiv: 1111.5206 [hep-ph].

90. Berger, C.F., Z. Bern, L.J. Dixon, F. Febres Cordero, D. Forde, et al.: 'An Automated Implementation of On-Shell Methods for One-Loop Amplitudes'. *Phys.Rev.* (2008), volume D78: page 036003. DOI: 10.1103/PhysRevD.78.036003. arXiv: 0803.4180 [hep-ph].

91. Cullen, Gavin, Hans van Deurzen, Nicolas Greiner, Gudrun Heinrich, Gionata Luisoni, et al.: 'G*OSAM*-2.0: a tool for automated one-loop calculations within the Standard Model and beyond'. *Eur.Phys.J.* (2014), volume C74(8): page 3001. DOI: 10.1140/epjc/s10052-014-3001-5. arXiv: 1404.7096 [hep-ph].

92. Cullen, Gavin, Nicolas Greiner, Gudrun Heinrich, Gionata Luisoni, Pierpaolo Mastrolia, et al.: 'Automated One-Loop Calculations with GoSam'. *Eur.Phys.J.* (2012), volume C72: page 1889. DOI: 10.1140/epjc/s10052-012-1889-1. arXiv: 1111.2034 [hep-ph].

93. Hirschi, Valentin, Rikkert Frederix, Stefano Frixione, Maria Vittoria Garzelli, Fabio Maltoni, et al.: 'Automation of one-loop QCD corrections'. *JHEP* (2011), volume 1105: page 044. DOI: 10.1007/JHEP05(2011)044. arXiv: 1103.0621 [hep-ph].

94. Badger, Simon, Benedikt Biedermann, Peter Uwer, and Valery Yundin: 'Numerical evaluation of virtual corrections to multi-jet production in massless QCD'. *Comput.Phys.Commun.* (2013), volume 184: pages 1981–1998. DOI: 10.1016/j.cpc.2013.03.018. arXiv: 1209.0100 [hep-ph].

95. Becker, Sebastian, Daniel Goetz, Christian Reuschle, Christopher Schwan, and Stefan Weinzierl: 'NLO results for five, six and seven jets in electron-positron annihilation'. *Phys.Rev.Lett.* (2012), volume 108: page 032005. DOI: 10.1103/PhysRevLett.108.032005. arXiv: 1111.1733 [hep-ph].

96. Borowka, S., G. Heinrich, S.P. Jones, M. Kerner, J. Schlenk, et al.: 'SecDec-3.0: numerical evaluation of multi-scale integrals beyond one loop'. (2015), volume. arXiv: 1502.06595 [hep-ph].

97. Mastrolia, Pierpaolo, Edoardo Mirabella, Giovanni Ossola, and Tiziano Peraro: 'Multiloop Integrand Reduction for Dimensionally Regulated Amplitudes'. *Phys.Lett.* (2013), volume B727: pages 532–535. doi: 10.1016/j.physletb.2013.10.066. arXiv: 1307.5832 [hep-ph].

98. Feng, Bo and Rijun Huang: 'The classification of two-loop integrand basis in pure four-dimension'. *JHEP* (2013), volume 1302: page 117. doi: 10.1007/JHEP02(2013)117. arXiv: 1209.3747 [hep-ph].

99. Glover, E.W. Nigel, C. Oleari, and M.E. Tejeda-Yeomans: 'Two loop QCD corrections to gluon-gluon scattering'. *Nucl.Phys.* (2001), volume B605: pages 467–485. doi: 10.1016/S0550-3213(01)00210-3. arXiv: hep-ph/0102201 [hep-ph].

100. Anastasiou, C., E.W. Nigel Glover, C. Oleari, and M.E. Tejeda-Yeomans: 'Two-loop QCD corrections to the scattering of massless distinct quarks'. *Nucl.Phys.* (2001), volume B601: pages 318–340. doi: 10.1016/S0550-3213(01)00079-7. arXiv: hep-ph/0010212 [hep-ph].

101. Anastasiou, C., E.W. Nigel Glover, C. Oleari, and M.E. Tejeda-Yeomans: 'Two loop QCD corrections to massless quark gluon scattering'. *Nucl.Phys.* (2001), volume B605: pages 486–516. doi: 10.1016/S0550-3213(01)00195-X. arXiv: hep-ph/0101304 [hep-ph].

102. Anastasiou, C., E.W. Nigel Glover, C. Oleari, and M.E. Tejeda-Yeomans: 'Two loop QCD corrections to massless identical quark scattering'. *Nucl.Phys.* (2001), volume B601: pages 341–360. doi: 10.1016/S0550-3213(01)00080-3. arXiv: hep-ph/0011094 [hep-ph].

103. Czakon, M.: 'Tops from Light Quarks: Full Mass Dependence at Two-Loops in QCD'. *Phys.Lett.* (2008), volume B664: pages 307–314. doi: 10.1016/j.physletb.2008.05.028. arXiv: 0803.1400 [hep-ph].

104. Bärnreuther, P., M. Czakon, and P. Fiedler: 'Virtual amplitudes and threshold behaviour of hadronic top-quark pair-production cross sections'. *JHEP* (2014), volume 1402: page 078. doi: 10.1007/JHEP02(2014)078. arXiv: 1312.6279 [hep-ph].

105. Manteuffel, Andreas von and Lorenzo Tancredi: 'The two-loop helicity amplitudes for $gg \to V_1V_2 \to 4$ leptons'. (2015), volume. arXiv: 1503.08835 [hep-ph].

106. Bern, Zvi, Abilio De Freitas, and Lance J. Dixon: 'Two loop helicity amplitudes for gluon-gluon scattering in QCD and supersymmetric Yang-Mills theory'. *JHEP* (2002), volume 0203: page 018. doi: 10.1088/1126-6708/2002/03/018. arXiv: hep-ph/0201161 [hep-ph].

107. Bern, Zvi, Abilio De Freitas, and Lance J. Dixon: 'Two loop helicity amplitudes for quark gluon scattering in QCD and gluino gluon scattering in supersymmetric Yang-Mills theory'. *JHEP* (2003), volume 0306: page 028. doi: 10.1007/JHEP04(2014)112,10.1088/1126-6708/2003/06/028. arXiv: hep-ph/0304168 [hep-ph].

108. Chetyrkin, K.G. and F.V. Tkachov: 'Integration by Parts: The Algorithm to Calculate beta Functions in 4 Loops'. *Nucl.Phys.* (1981), volume B192: pages 159–204. doi: 10.1016/0550-3213(81)90199-1.

109. Gehrmann, T. and E. Remiddi: 'Differential equations for two loop four point functions'. *Nucl.Phys.* (2000), volume B580: pages 485–518. doi: 10.1016/S0550-3213(00)00223-6. arXiv: hep-ph/9912329 [hep-ph].

110. Laporta, S.: 'High precision calculation of multiloop Feynman integrals by difference equations'. *Int.J.Mod.Phys.* (2000), volume A15: pages 5087–5159. DOI: 10.1016/S0217-751X(00)00215-7. arXiv: hep-ph/0102033 [hep-ph].

111. Manteuffel, A. von and C. Studerus: 'Reduze 2 - Distributed Feynman Integral Reduction'. (2012), volume. arXiv: 1201.4330 [hep-ph].

112. Smirnov, A.V.: 'Algorithm FIRE – Feynman Integral REduction'. *JHEP* (2008), volume 0810: page 107. DOI: 10.1088/1126-6708/2008/10/107. arXiv: 0807.3243 [hep-ph].

113. Smirnov, Vladimir: *Evaluating Feynman Integrals*. Springer Berlin Heidelberg, 2005.

114. Duhr, Claude: 'Mathematical aspects of scattering amplitudes'. (2014), volume. arXiv: 1411.7538 [hep-ph].

115. Kotikov, A.V.: 'Differential equations method: The Calculation of vertex type Feynman diagrams'. *Phys.Lett.* (1991), volume B259: pages 314–322. DOI: 10.1016/0370-2693(91)90834-D.

116. Remiddi, Ettore: 'Differential equations for Feynman graph amplitudes'. *Nuovo Cim.* (1997), volume A110: pages 1435–1452. arXiv: hep-th/9711188 [hep-th].

117. Caffo, Michele, H. Czyz, S. Laporta, and E. Remiddi: 'The Master differential equations for the two loop sunrise selfmass amplitudes'. *Nuovo Cim.* (1998), volume A111: pages 365–389. arXiv: hep-th/9805118 [hep-th].

118. Henn, Johannes M.: 'Multiloop integrals in dimensional regularization made simple'. *Phys.Rev.Lett.* (2013), volume 110(25): page 251601. DOI: 10.1103/PhysRevLett.110.251601. arXiv: 1304.1806 [hep-th].

119. Gehrmann, Thomas, Lorenzo Tancredi, and Erich Weihs: 'Two-loop master integrals for $q\bar{q} \to VV$: the planar topologies'. *JHEP* (2013), volume 1308: page 070. DOI: 10.1007/JHEP08(2013)070. arXiv: 1306.6344.

120. Gehrmann, Thomas, Andreas von Manteuffel, Lorenzo Tancredi, and Erich Weihs: 'The two-loop master integrals for $q\bar{q} \to VV$'. *JHEP* (2014), volume 1406: page 032. DOI: 10.1007/JHEP06(2014)032. arXiv: 1404.4853 [hep-ph].

121. Henn, Johannes M., Kirill Melnikov, and Vladimir A. Smirnov: 'Two-loop planar master integrals for the production of off-shell vector bosons in hadron collisions'. *JHEP* (2014), volume 1405: page 090. DOI: 10.1007/JHEP05(2014)090,10.1007/s13130-014-8200-x. arXiv: 1402.7078 [hep-ph].

122. Caola, Fabrizio, Johannes M. Henn, Kirill Melnikov, and Vladimir A. Smirnov: 'Non-planar master integrals for the production of two off-shell vector bosons in collisions of massless partons'. *JHEP* (2014), volume 1409: page 043. DOI: 10.1007/JHEP09(2014)043. arXiv: 1404.5590 [hep-ph].

123. Papadopoulos, Costas G., Damiano Tommasini, and Christopher Wever: 'Two-loop Master Integrals with the Simplified Differential Equations approach'. *JHEP* (2015), volume 1501: page 072. DOI: 10.1007/JHEP01(2015)072. arXiv: 1409.6114 [hep-ph].

124. Gehrmann, Thomas, Andreas von Manteuffel, and Lorenzo Tancredi: 'The two-loop helicity amplitudes for $q\bar{q}' \to V_1V_2 \to 4$ leptons'. (2015), volume. arXiv: 1503.04812 [hep-ph].

125. Caola, Fabrizio, Johannes M. Henn, Kirill Melnikov, Alexander V. Smirnov, and Vladimir A. Smirnov: 'Two-loop helicity amplitudes for the production of two off-shell electroweak bosons in quark-antiquark collisions'. *JHEP* (2014), volume 1411: page 041. DOI: 10.1007/JHEP11(2014)041. arXiv: 1408.6409 [hep-ph].

126. Bonciani, R., A. Ferroglia, T. Gehrmann, A. von Manteuffel, and C. Studerus: 'Light-quark two-loop corrections to heavy-quark pair production in the gluon fusion channel'. *JHEP* (2013), volume 1312: page 038. DOI: 10.1007/JHEP12(2013)038. arXiv: 1309.4450 [hep-ph].

127. Bonciani, R., A. Ferroglia, T. Gehrmann, A. von Manteuffel, and C. Studerus: 'Two-Loop Leading Color Corrections to Heavy-Quark Pair Production in the Gluon Fusion Channel'. *JHEP* (2011), volume 1101: page 102. DOI: 10.1007/JHEP01(2011)102. arXiv: 1011.6661 [hep-ph].

128. Bonciani, R., A. Ferroglia, T. Gehrmann, and C. Studerus: 'Two-Loop Planar Corrections to Heavy-Quark Pair Production in the Quark-Antiquark Channel'. *JHEP* (2009), volume 0908: page 067. DOI: 10.1088/1126-6708/2009/08/067. arXiv: 0906.3671 [hep-ph].

129. Bonciani, R., A. Ferroglia, T. Gehrmann, D. Maitre, and C. Studerus: 'Two-Loop Fermionic Corrections to Heavy-Quark Pair Production: The Quark-Antiquark Channel'. *JHEP* (2008), volume 0807: page 129. DOI: 10.1088/1126-6708/2008/07/129. arXiv: 0806.2301 [hep-ph].

130. Glover, E.W. Nigel and M.E. Tejeda-Yeomans: 'One loop QCD corrections to gluon-gluon scattering at NNLO'. *JHEP* (2001), volume 0105: page 010. DOI: 10.1088/1126-6708/2001/05/010. arXiv: hep-ph/0104178 [hep-ph].

131. Fabricius, K., I. Schmitt, G. Kramer, and G. Schierholz: 'Higher Order Perturbative QCD Calculation of Jet Cross-Sections in e+ e- Annihilation'. *Z.Phys.* (1981), volume C11: page 315. DOI: 10.1007/BF01578281.

132. Baer, H., J. Ohnemus, and J.F. Owens: 'A Next-To-Leading Logarithm Calculation of Jet Photoproduction'. *Phys.Rev.* (1989), volume D40: page 2844. DOI: 10.1103/PhysRevD.40.2844.

133. Giele, W.T. and E.W. Nigel Glover: 'Higher order corrections to jet cross-sections in e+ e- annihilation'. *Phys.Rev.* (1992), volume D46: pages 1980–2010. DOI: 10.1103/PhysRevD.46.1980.

134. Giele, W.T., E.W. Nigel Glover, and David A. Kosower: 'Higher order corrections to jet cross-sections in hadron colliders'. *Nucl.Phys.* (1993), volume B403: pages 633–670. DOI: 10.1016/0550-3213(93)90365-V. arXiv: hep-ph/9302225 [hep-ph].

135. Catani, Stefano, Stefan Dittmaier, Michael H. Seymour, and Zoltan Trocsanyi: 'The Dipole formalism for next-to-leading order QCD calculations with massive partons'. *Nucl.Phys.* (2002), volume B627: pages 189–265. DOI: 10.1016/S0550-3213(02)00098-6. arXiv: hep-ph/0201036 [hep-ph].

136. Dittmaier, Stefan: 'A General approach to photon radiation off fermions'. *Nucl.Phys.* (2000), volume B565: pages 69–122. DOI: 10.1016/S0550-3213(99)00563-5. arXiv: hep-ph/9904440 [hep-ph].

137. Eynck, Tim Oliver, Eric Laenen, Lukas Phaf, and Stefan Weinzierl: 'Comparison of phase space slicing and dipole subtraction methods for gamma* —> anti-Q'. *Eur.Phys.J.* (2002), volume C23: pages 259–266. DOI: 10.1007/s100520100868. arXiv: hep-ph/0109246 [hep-ph].

138. Catani, Stefano and Massimiliano Grazzini: 'Infrared factorization of tree level QCD amplitudes at the next-to-next-to-leading order and beyond'. *Nucl.Phys.* (2000), volume B570: pages 287–325. DOI: 10.1016/S0550-3213(99)00778-6. arXiv: hep-ph/9908523 [hep-ph].

139. Bern, Zvi, Lance J. Dixon, David C. Dunbar, and David A. Kosower: 'One loop n point gauge theory amplitudes, unitarity and collinear limits'. *Nucl.Phys.* (1994), volume B425: pages 217–260. DOI: 10.1016/0550-3213(94)90179-1. arXiv: hep-ph/9403226 [hep-ph].

140. Bern, Zvi, Vittorio Del Duca, and Carl R. Schmidt: 'The Infrared behavior of one loop gluon amplitudes at next-to-next-to-leading order'. *Phys.Lett.* (1998), volume B445: pages 168–177. DOI: 10.1016/S0370-2693(98)01495-6. arXiv: hep-ph/9810409 [hep-ph].

141. Kosower, David A.: 'All order collinear behavior in gauge theories'. *Nucl.Phys.* (1999), volume B552: pages 319–336. DOI: 10.1016/S0550-3213(99)00251-5. arXiv: hep-ph/9901201 [hep-ph].

142. Kosower, David A. and Peter Uwer: 'One loop splitting amplitudes in gauge theory'. *Nucl.Phys.* (1999), volume B563: pages 477–505. DOI: 10.1016/S0550-3213(99)00583-0. arXiv: hep-ph/9903515 [hep-ph].

143. Bern, Zvi, Vittorio Del Duca, William B. Kilgore, and Carl R. Schmidt: 'The infrared behavior of one loop QCD amplitudes at next-to-next-to leading order'. *Phys.Rev.* (1999), volume D60: page 116001. DOI: 10.1103/PhysRevD.60.116001. arXiv: hep-ph/9903516 [hep-ph].

144. Somogyi, Gabor and Zoltan Trocsanyi: 'A Subtraction scheme for computing QCD jet cross sections at NNLO: Regularization of real-virtual emission'. *JHEP* (2007), volume 0701: page 052. DOI: 10.1088/1126-6708/2007/01/052. arXiv: hep-ph/0609043 [hep-ph].

145. Catani, Stefano and Massimiliano Grazzini: 'The soft gluon current at one loop order'. *Nucl.Phys.* (2000), volume B591: pages 435–454. DOI: 10.1016/S0550-3213(00)00572-1. arXiv: hep-ph/0007142 [hep-ph].

146. Bierenbaum, Isabella, Michal Czakon, and Alexander Mitov: 'The singular behavior of one-loop massive QCD amplitudes with one external soft gluon'. *Nucl.Phys.* (2012), volume B856: pages 228–246. DOI: 10.1016/j.nuclphysb.2011.11.002. arXiv: 1107.4384 [hep-ph].

147. Kosower, David A.: 'Antenna factorization of gauge theory amplitudes'. *Phys.Rev.* (1998), volume D57: pages 5410–5416. DOI: 10.1103/PhysRevD.57.5410. arXiv: hep-ph/9710213 [hep-ph].

148. Kosower, David A.: 'Antenna factorization in strongly ordered limits'. *Phys.Rev.* (2005), volume D71: page 045016. DOI: 10.1103/PhysRevD.71.045016. arXiv: hep-ph/0311272 [hep-ph].

149. Gehrmann-De Ridder, A., T. Gehrmann, and E.W. Nigel Glover: 'Antenna subtraction at NNLO'. *JHEP* (2005), volume 0509: page 056. DOI: 10.1088/1126-6708/2005/09/056. arXiv: hep-ph/0505111 [hep-ph].

150. Currie, James: 'Colourful antenna subtraction for gluon scattering'. *PoS* (2013), volume RADCOR2013: page 001. arXiv: 1311.6113 [hep-ph].

151. Gehrmann-De Ridder, A., T. Gehrmann, and G. Heinrich: 'Four particle phase space integrals in massless QCD'. *Nucl.Phys.* (2004), volume B682: pages 265–288. doi: 10.1016/j.nuclphysb.2004.01.023. arXiv: hep-ph/0311276 [hep-ph].

152. Gehrmann-De Ridder, A., T. Gehrmann, E.W.N. Glover, and G. Heinrich: 'Infrared structure of e+ e- —> 3 jets at NNLO'. *JHEP* (2007), volume 0711: page 058. doi: 10.1088/1126-6708/2007/11/058. arXiv: 0710.0346 [hep-ph].

153. Gehrmann-De Ridder, A., T. Gehrmann, E.W.N. Glover, and G. Heinrich: 'Jet rates in electron-positron annihilation at O(alpha(s)**3) in QCD'. *Phys.Rev.Lett.* (2008), volume 100: page 172001. doi: 10.1103/PhysRevLett.100.172001. arXiv: 0802.0813 [hep-ph].

154. Gehrmann-De Ridder, A., T. Gehrmann, E.W.N. Glover, and G. Heinrich: 'Second-order QCD corrections to the thrust distribution'. *Phys.Rev.Lett.* (2007), volume 99: page 132002. doi: 10.1103/PhysRevLett.99.132002. arXiv: 0707.1285 [hep-ph].

155. Gehrmann-De Ridder, A., T. Gehrmann, E.W.N. Glover, and G. Heinrich: 'NNLO corrections to event shapes in e+ e- annihilation'. *JHEP* (2007), volume 0712: page 094. doi: 10.1088/1126-6708/2007/12/094. arXiv: 0711.4711 [hep-ph].

156. Gehrmann-De Ridder, A., T. Gehrmann, E.W.N. Glover, and G. Heinrich: 'NNLO moments of event shapes in e+e- annihilation'. *JHEP* (2009), volume 0905: page 106. doi: 10.1088/1126-6708/2009/05/106. arXiv: 0903.4658 [hep-ph].

157. Weinzierl, Stefan: 'NNLO corrections to 3-jet observables in electron-positron annihilation'. *Phys.Rev.Lett.* (2008), volume 101: page 162001. doi: 10.1103/PhysRevLett.101.162001. arXiv: 0807.3241 [hep-ph].

158. Weinzierl, Stefan: 'The infrared structure of $e^+e^- \to 3$ jets at NNLO reloaded'. *JHEP* (2009), volume 0907: page 009. doi: 10.1088/1126-6708/2009/07/009. arXiv: 0904.1145 [hep-ph].

159. Weinzierl, Stefan: 'Event shapes and jet rates in electron-positron annihilation at NNLO'. *JHEP* (2009), volume 0906: page 041. doi: 10.1088/1126-6708/2009/06/041. arXiv: 0904.1077 [hep-ph].

160. Weinzierl, Stefan: 'Moments of event shapes in electron-positron annihilation at NNLO'. *Phys.Rev.* (2009), volume D80: page 094018. doi: 10.1103/PhysRevD.80.094018. arXiv: 0909.5056 [hep-ph].

161. Daleo, A., T. Gehrmann, and D. Maitre: 'Antenna subtraction with hadronic initial states'. *JHEP* (2007), volume 0704: page 016. doi: 10.1088/1126-6708/2007/04/016. arXiv: hep-ph/0612257 [hep-ph].

162. Daleo, Alejandro, Aude Gehrmann-De Ridder, Thomas Gehrmann, and Gionata Luisoni: 'Antenna subtraction at NNLO with hadronic initial states: initial-final configurations'. *JHEP* (2010), volume 1001: page 118. doi: 10.1007/JHEP01(2010)118. arXiv: 0912.0374 [hep-ph].

163. Boughezal, Radja, Aude Gehrmann-De Ridder, and Mathias Ritzmann: 'Antenna subtraction at NNLO with hadronic initial states: double real radiation for initial-initial configurations with two quark flavours'. *JHEP* (2011), volume 1102: page 098. doi: 10.1007/JHEP02(2011)098. arXiv: 1011.6631 [hep-ph].

164. Gehrmann-De Ridder, Aude, Thomas Gehrmann, and Mathias Ritzmann: 'Antenna subtraction at NNLO with hadronic initial states: double real initial-initial configurations'. *JHEP* (2012), volume 1210: page 047. DOI: 10.1007/JHEP10(2012)047. arXiv: 1207.5779 [hep-ph].

165. Gehrmann, Thomas and Pier Francesco Monni: 'Antenna subtraction at NNLO with hadronic initial states: real-virtual initial-initial configurations'. *JHEP* (2011), volume 1112: page 049. DOI: 10.1007/JHEP12(2011)049. arXiv: 1107.4037 [hep-ph].

166. Currie, James, E.W.N. Glover, and Steven Wells: 'Infrared Structure at NNLO Using Antenna Subtraction'. *JHEP* (2013), volume 1304: page 066. DOI: 10.1007/JHEP04(2013)066. arXiv: 1301.4693 [hep-ph].

167. Bernreuther, Werner, Christian Bogner, and Oliver Dekkers: 'The real radiation antenna function for $S \to Q\bar{Q}q\bar{q}$ at NNLO QCD'. *JHEP* (2011), volume 1106: page 032. DOI: 10.1007/JHEP06(2011)032. arXiv: 1105.0530 [hep-ph].

168. Dekkers, Oliver and Werner Bernreuther: 'The real-virtual antenna functions for $S \to Q\bar{Q}X$ at NNLO QCD'. *Phys.Lett.* (2014), volume B738: pages 325–333. DOI: 10.1016/j.physletb.2014.09.060. arXiv: 1409.3124 [hep-ph].

169. Abelof, Gabriel, Oliver Dekkers, and Aude Gehrmann-De Ridder: 'Antenna subtraction with massive fermions at NNLO: Double real initial-final configurations'. *JHEP* (2012), volume 1212: page 107. DOI: 10.1007/JHEP12(2012)107. arXiv: 1210.5059 [hep-ph].

170. Abelof, G. and A. Gehrmann-De Ridder: 'Antenna subtraction for the production of heavy particles at hadron colliders'. *JHEP* (2011), volume 1104: page 063. DOI: 10.1007/JHEP04(2011)063. arXiv: 1102.2443 [hep-ph].

171. Abelof, Gabriel and Aude Gehrmann-De Ridder: 'Double real radiation corrections to $t\bar{t}$ production at the LHC: the $gg \to t\bar{t}q\bar{q}$ channel'. *JHEP* (2012), volume 1211: page 074. DOI: 10.1007/JHEP11(2012)074. arXiv: 1207.6546 [hep-ph].

172. Abelof, Gabriel, Aude Gehrmann-De Ridder, and Imre Majer: 'Top quark pair production at NNLO in the quark-antiquark channel'. (2015), volume. arXiv: 1506.04037 [hep-ph].

173. Abelof, Gabriel, Aude Gehrmann-De Ridder, Philipp Maierhofer, and Stefano Pozzorini: 'NNLO QCD subtraction for top-antitop production in the $q\bar{q}$ channel'. *JHEP* (2014), volume 1408: page 035. DOI: 10.1007/JHEP08(2014)035. arXiv: 1404.6493 [hep-ph].

174. Chen, X., T. Gehrmann, E.W.N. Glover, and M. Jaquier: 'Precise QCD predictions for the production of Higgs + jet final states'. *Phys.Lett.* (2015), volume B740: pages 147–150. DOI: 10.1016/j.physletb.2014.11.021. arXiv: 1408.5325 [hep-ph].

175. Somogyi, Gabor, Zoltan Trocsanyi, and Vittorio Del Duca: 'Matching of singly- and doubly-unresolved limits of tree-level QCD squared matrix elements'. *JHEP* (2005), volume 0506: page 024. DOI: 10.1088/1126-6708/2005/06/024. arXiv: hep-ph/0502226 [hep-ph].

176. Somogyi, Gabor and Zoltan Trocsanyi: 'A New subtraction scheme for computing QCD jet cross sections at next-to-leading order accuracy'. (2006), volume. arXiv: hep-ph/0609041 [hep-ph].

177. Somogyi, Gabor, Zoltan Trocsanyi, and Vittorio Del Duca: 'A Subtraction scheme for computing QCD jet cross sections at NNLO: Regularization of doubly-real emissions'. *JHEP* (2007), volume 0701: page 070. DOI: 10.1088/1126-6708/2007/01/070. arXiv: hep-ph/0609042 [hep-ph].

178. Somogyi, Gabor and Zoltan Trocsanyi: 'A Subtraction scheme for computing QCD jet cross sections at NNLO: Integrating the subtraction terms. I.' *JHEP* (2008), volume 0808: page 042. DOI: 10.1088/1126-6708/2008/08/042. arXiv: 0807.0509 [hep-ph].

179. Aglietti, Ugo, Vittorio Del Duca, Claude Duhr, Gabor Somogyi, and Zoltan Trocsanyi: 'Analytic integration of real-virtual counterterms in NNLO jet cross sections. I.' *JHEP* (2008), volume 0809: page 107. DOI: 10.1088/1126-6708/2008/09/107. arXiv: 0807.0514 [hep-ph].

180. Somogyi, Gabor: 'Subtraction with hadronic initial states at NLO: An NNLO-compatible scheme'. *JHEP* (2009), volume 0905: page 016. DOI: 10.1088/1126-6708/2009/05/016. arXiv: 0903.1218 [hep-ph].

181. Bolzoni, Paolo, Sven-Olaf Moch, Gabor Somogyi, and Zoltan Trocsanyi: 'Analytic integration of real-virtual counterterms in NNLO jet cross sections. II.' *JHEP* (2009), volume 0908: page 079. DOI: 10.1088/1126-6708/2009/08/079. arXiv: 0905.4390 [hep-ph].

182. Bolzoni, Paolo, Gabor Somogyi, and Zoltan Trocsanyi: 'A subtraction scheme for computing QCD jet cross sections at NNLO: integrating the iterated singly-unresolved subtraction terms'. *JHEP* (2011), volume 1101: page 059. DOI: 10.1007/JHEP01(2011)059. arXiv: 1011.1909 [hep-ph].

183. Del Duca, Vittorio, Gabor Somogyi, and Zoltan Trocsanyi: 'Integration of collinear-type doubly unresolved counterterms in NNLO jet cross sections'. *JHEP* (2013), volume 1306: page 079. DOI: 10.1007/JHEP06(2013)079. arXiv: 1301.3504 [hep-ph].

184. Somogyi, Gabor: 'A subtraction scheme for computing QCD jet cross sections at NNLO: integrating the doubly unresolved subtraction terms'. *JHEP* (2013), volume 1304: page 010. DOI: 10.1007/JHEP04(2013)010. arXiv: 1301.3919 [hep-ph].

185. Del Duca, Vittorio, Claude Duhr, Gábor Somogyi, Francesco Tramontano, and Zoltán Trócsányi: 'Higgs boson decay into b-quarks at NNLO accuracy'. *JHEP* (2015), volume 1504: page 036. DOI: 10.1007/JHEP04(2015)036. arXiv: 1501.07226 [hep-ph].

186. Bozzi, Giuseppe, Stefano Catani, Daniel de Florian, and Massimiliano Grazzini: 'Transverse-momentum resummation and the spectrum of the Higgs boson at the LHC'. *Nucl.Phys.* (2006), volume B737: pages 73–120. DOI: 10.1016/j.nuclphysb.2005.12.022. arXiv: hep-ph/0508068 [hep-ph].

187. Catani, Stefano, Leandro Cieri, Daniel de Florian, Giancarlo Ferrera, and Massimiliano Grazzini: 'Universality of transverse-momentum resummation and hard factors at the NNLO'. *Nucl.Phys.* (2014), volume B881: pages 414–443. DOI: 10.1016/j.nuclphysb.2014.02.011. arXiv: 1311.1654 [hep-ph].

188. Ferrera, Giancarlo, Massimiliano Grazzini, and Francesco Tramontano: 'Associated WH production at hadron colliders: a fully exclusive QCD calculation at NNLO'. *Phys.Rev.Lett.* (2011), volume 107: page 152003. DOI: 10.1103/PhysRevLett.107.152003. arXiv: 1107.1164 [hep-ph].

189. Catani, Stefano, Leandro Cieri, Daniel de Florian, Giancarlo Ferrera, and Massimiliano Grazzini: 'Diphoton production at hadron colliders: a fully-differential QCD calculation at NNLO'. *Phys.Rev.Lett.* (2012), volume 108: page 072001. doi: 10.1103/PhysRevLett.108.072001. arXiv: 1110.2375 [hep-ph].

190. Zhu, Hua Xing, Chong Sheng Li, Hai Tao Li, Ding Yu Shao, and Li Lin Yang: 'Transverse-momentum resummation for top-quark pairs at hadron colliders'. *Phys.Rev.Lett.* (2013), volume 110(8): page 082001. doi: 10.1103/PhysRevLett.110.082001. arXiv: 1208.5774 [hep-ph].

191. Li, Hai Tao, Chong Sheng Li, Ding Yu Shao, Li Lin Yang, and Hua Xing Zhu: 'Top quark pair production at small transverse momentum in hadronic collisions'. *Phys.Rev.* (2013), volume D88: page 074004. doi: 10.1103/PhysRevD.88.074004. arXiv: 1307.2464.

192. Catani, Stefano, Massimiliano Grazzini, and A. Torre: 'Transverse-momentum resummation for heavy-quark hadroproduction'. *Nucl.Phys.* (2014), volume B890: pages 518–538. doi: 10.1016/j.nuclphysb.2014.11.019. arXiv: 1408.4564 [hep-ph].

193. Stewart, Iain W., Frank J. Tackmann, and Wouter J. Waalewijn: 'N-Jettiness: An Inclusive Event Shape to Veto Jets'. *Phys.Rev.Lett.* (2010), volume 105: page 092002. doi: 10.1103/PhysRevLett.105.092002. arXiv: 1004.2489 [hep-ph].

194. Gaunt, Jonathan, Maximilian Stahlhofen, Frank J. Tackmann, and Jonathan R. Walsh: 'N-jettiness Subtractions for NNLO QCD Calculations'. (2015), volume. arXiv: 1505.04794 [hep-ph].

195. Boughezal, Radja, Christfried Focke, Walter Giele, Xiaohui Liu, and Frank Petriello: 'Higgs boson production in association with a jet using jettiness subtraction'. (2015), volume. arXiv: 1505.03893 [hep-ph].

196. Boughezal, Radja, Xiaohui Liu, and Frank Petriello: '$N$-jettiness soft function at next-to-next-to-leading order'. *Phys.Rev.* (2015), volume D91(9): page 094035. doi: 10.1103/PhysRevD.91.094035. arXiv: 1504.02540 [hep-ph].

197. Stewart, Iain W., Frank J. Tackmann, and Wouter J. Waalewijn: 'The Beam Thrust Cross Section for Drell-Yan at NNLL Order'. *Phys.Rev.Lett.* (2011), volume 106: page 032001. doi: 10.1103/PhysRevLett.106.032001. arXiv: 1005.4060 [hep-ph].

198. Gaunt, Jonathan R., Maximilian Stahlhofen, and Frank J. Tackmann: 'The Quark Beam Function at Two Loops'. *JHEP* (2014), volume 1404: page 113. doi: 10.1007/JHEP04(2014)113. arXiv: 1401.5478 [hep-ph].

199. Gaunt, Jonathan, Maximilian Stahlhofen, and Frank J. Tackmann: 'The Gluon Beam Function at Two Loops'. *JHEP* (2014), volume 1408: page 020. doi: 10.1007/JHEP08(2014)020. arXiv: 1405.1044 [hep-ph].

200. Becher, Thomas and Matthias Neubert: 'Toward a NNLO calculation of the anti-B —> X(s) gamma decay rate with a cut on photon energy. II. Two-loop result for the jet function'. *Phys.Lett.* (2006), volume B637: pages 251–259. doi: 10.1016/j.physletb.2006.04.046. arXiv: hep-ph/0603140 [hep-ph].

201. Becher, Thomas and Guido Bell: 'The gluon jet function at two-loop order'. *Phys.Lett.* (2011), volume B695: pages 252–258. doi: 10.1016/j.physletb.2010.11.036. arXiv: 1008.1936 [hep-ph].

202. Bärnreuther, Peter, Michal Czakon, and Alexander Mitov: 'Percent Level Precision Physics at the Tevatron: First Genuine NNLO QCD Corrections to $q\bar{q} \to t\bar{t}+X$'. *Phys.Rev.Lett.* (2012), volume 109: page 132001. DOI: 10.1103/PhysRevLett.109.132001. arXiv: 1204.5201 [hep-ph].

203. Czakon, Michal and Alexander Mitov: 'NNLO corrections to top-pair production at hadron colliders: the all-fermionic scattering channels'. *JHEP* (2012), volume 1212: page 054. DOI: 10.1007/JHEP12(2012)054. arXiv: 1207.0236 [hep-ph].

204. Czakon, Michal and Alexander Mitov: 'NNLO corrections to top pair production at hadron colliders: the quark-gluon reaction'. *JHEP* (2013), volume 1301: page 080. DOI: 10.1007/JHEP01(2013)080. arXiv: 1210.6832 [hep-ph].

205. Boughezal, Radja, Kirill Melnikov, and Frank Petriello: 'A subtraction scheme for NNLO computations'. *Phys.Rev.* (2012), volume D85: page 034025. DOI: 10.1103/PhysRevD.85.034025. arXiv: 1111.7041 [hep-ph].

206. Brucherseifer, Mathias, Fabrizio Caola, and Kirill Melnikov: '$\mathcal{O}(\alpha_s^2)$ corrections to fully-differential top quark decays'. *JHEP* (2013), volume 1304: page 059. DOI: 10.1007/JHEP04(2013)059. arXiv: 1301.7133 [hep-ph].

207. Brucherseifer, Mathias, Fabrizio Caola, and Kirill Melnikov: 'On the $O(\alpha_s^2)$ corrections to $b \to X_u e\bar{\nu}$ inclusive decays'. *Phys.Lett.* (2013), volume B721: pages 107–110. DOI: 10.1016/j.physletb.2013.03.006. arXiv: 1302.0444 [hep-ph].

208. Caola, Fabrizio, Andrzej Czarnecki, Yi Liang, Kirill Melnikov, and Robert Szafron: 'Muon decay spin asymmetry'. *Phys.Rev.* (2014), volume D90(5): page 053004. DOI: 10.1103/PhysRevD.90.053004. arXiv: 1403.3386 [hep-ph].

209. Brucherseifer, Mathias, Fabrizio Caola, and Kirill Melnikov: 'On the NNLO QCD corrections to single-top production at the LHC'. *Phys.Lett.* (2014), volume B736: pages 58–63. DOI: 10.1016/j.physletb.2014.06.075. arXiv: 1404.7116 [hep-ph].

210. Binoth, T. and G. Heinrich: 'An automatized algorithm to compute infrared divergent multiloop integrals'. *Nucl.Phys.* (2000), volume B585: pages 741–759. DOI: 10.1016/S0550-3213(00)00429-6. arXiv: hep-ph/0004013 [hep-ph].

211. Weinzierl, Stefan: 'Does one need the O(epsilon)- and O(epsilon2)-terms of one-loop amplitudes in an NNLO calculation ?' *Phys.Rev.* (2011), volume D84: page 074007. DOI: 10.1103/PhysRevD.84.074007. arXiv: 1107.5131 [hep-ph].

212. Frixione, Stefano, Paolo Nason, and Carlo Oleari: 'Matching NLO QCD computations with Parton Shower simulations: the POWHEG method'. *JHEP* (2007), volume 0711: page 070. DOI: 10.1088/1126-6708/2007/11/070. arXiv: 0709.2092 [hep-ph].

213. Heymes, David: 'Double-real radiation for dijet production'. *unpublished.* Master's thesis. RWTH Aachen, 2012.

214. Bury, M. and A. van Hameren: 'Numerical evaluation of multi-gluon amplitudes for High Energy Factorization'. (2015), volume. arXiv: 1503.08612 [hep-ph].

215. Hameren, Andre van: 'PARNI for importance sampling and density estimation'. *Acta Phys.Polon.* (2009), volume B40: pages 259–272. arXiv: 0710.2448 [hep-ph].

216. Salam, Gavin P.: 'Towards Jetography'. *Eur.Phys.J.* (2010), volume C67: pages 637–686. DOI: 10.1140/epjc/s10052-010-1314-6. arXiv: 0906.1833 [hep-ph].

217. Dittmaier, S., P. Uwer, and S. Weinzierl: 'NLO QCD corrections to t anti-t + jet production at hadron colliders'. *Phys.Rev.Lett.* (2007), volume 98: page 262002. DOI: 10.1103/PhysRevLett.98.262002. arXiv: hep-ph/0703120 [HEP-PH].

218. Dittmaier, S., P. Uwer, and S. Weinzierl: 'Hadronic top-quark pair production in association with a hard jet at next-to-leading order QCD: Phenomenological studies for the Tevatron and the LHC'. *Eur.Phys.J.* (2009), volume C59: pages 625–646. DOI: 10.1140/epjc/s10052-008-0816-y. arXiv: 0810.0452 [hep-ph].

219. Czakon, M. and P. Fiedler: 'The soft function for color octet production at threshold'. *Nucl.Phys.* (2014), volume B879: pages 236–255. DOI: 10.1016/j.nuclphysb.2013.12.008. arXiv: 1311.2541 [hep-ph].

220. Draggiotis, Petros, Ronald H.P. Kleiss, and Costas G. Papadopoulos: 'On the computation of multigluon amplitudes'. *Phys.Lett.* (1998), volume B439: pages 157–164. DOI: 10.1016/S0370-2693(98)01015-6. arXiv: hep-ph/9807207 [hep-ph].

221. Goetz, Daniel, Christopher Schwan, and Stefan Weinzierl: 'Random Polarisations of the Dipoles'. *Phys.Rev.* (2012), volume D85: page 116011. DOI: 10.1103/PhysRevD.85.116011. arXiv: 1205.4109 [hep-ph].

222. Czakon, M., C.G. Papadopoulos, and M. Worek: 'Polarizing the Dipoles'. *JHEP* (2009), volume 0908: page 085. DOI: 10.1088/1126-6708/2009/08/085. arXiv: 0905.0883 [hep-ph].

223. Mangano, Michelangelo L. and Stephen J. Parke: 'Multiparton amplitudes in gauge theories'. *Phys.Rept.* (1991), volume 200: pages 301–367. DOI: 10.1016/0370-1573(91)90091-Y. arXiv: hep-th/0509223 [hep-th].

224. Del Duca, Vittorio, Alberto Frizzo, and Fabio Maltoni: 'Factorization of tree QCD amplitudes in the high-energy limit and in the collinear limit'. *Nucl.Phys.* (2000), volume B568: pages 211–262. DOI: 10.1016/S0550-3213(99)00657-4. arXiv: hep-ph/9909464 [hep-ph].

225. Campbell, John M. and E.W. Nigel Glover: 'Double unresolved approximations to multiparton scattering amplitudes'. *Nucl.Phys.* (1998), volume B527: pages 264–288. DOI: 10.1016/S0550-3213(98)00295-8. arXiv: hep-ph/9710255 [hep-ph].

226. Hahn, Thomas: 'Generating Feynman diagrams and amplitudes with FeynArts 3'. *Comput.Phys.Commun.* (2001), volume 140: pages 418–431. DOI: 10.1016/S0010-4655(01)00290-9. arXiv: hep-ph/0012260 [hep-ph].

227. Hahn, T. and M. Perez-Victoria: 'Automatized one loop calculations in four-dimensions and D-dimensions'. *Comput.Phys.Commun.* (1999), volume 118: pages 153–165. DOI: 10.1016/S0010-4655(98)00173-8. arXiv: hep-ph/9807565 [hep-ph].

228. Gehrmann, T. and E. Remiddi: 'Numerical evaluation of harmonic polylogarithms'. *Comput.Phys.Commun.* (2001), volume 141: pages 296–312. DOI: 10.1016/S0010-4655(01)00411-8. arXiv: hep-ph/0107173 [hep-ph].

229. Maltoni, F., K. Paul, T. Stelzer, and S. Willenbrock: 'Color flow decomposition of QCD amplitudes'. *Phys.Rev.* (2003), volume D67: page 014026. DOI: 10.1103/PhysRevD.67.014026. arXiv: hep-ph/0209271 [hep-ph].

230. Papadopoulos, Costas G. and Malgorzata Worek: 'Multi-parton cross sections at hadron colliders'. *Eur.Phys.J.* (2007), volume C50: pages 843–856. DOI: 10.1140/epjc/s10052-007-0246-2. arXiv: hep-ph/0512150 [hep-ph].

231. Aybat, S. Mert, Lance J. Dixon, and George F. Sterman: 'The Two-loop soft anomalous dimension matrix and resummation at next-to-next-to leading pole'. *Phys.Rev.* (2006), volume D74: page 074004. DOI: 10.1103/PhysRevD.74.074004. arXiv: hep-ph/0607309 [hep-ph].

232. Becher, Thomas and Matthias Neubert: 'Infrared singularities of QCD amplitudes with massive partons'. *Phys.Rev.* (2009), volume D79: page 125004. DOI: 10.1103/PhysRevD.79.125004,10.1103/PhysRevD.80.109901. arXiv: 0904.1021 [hep-ph].

233. Czakon, Michal, Alexander Mitov, and George F. Sterman: 'Threshold Resummation for Top-Pair Hadroproduction to Next-to-Next-to-Leading Log'. *Phys.Rev.* (2009), volume D80: page 074017. DOI: 10.1103/PhysRevD.80.074017. arXiv: 0907.1790 [hep-ph].

234. Mitov, Alexander, George F. Sterman, and Ilmo Sung: 'The Massive Soft Anomalous Dimension Matrix at Two Loops'. *Phys.Rev.* (2009), volume D79: page 094015. DOI: 10.1103/PhysRevD.79.094015. arXiv: 0903.3241 [hep-ph].

235. Ferroglia, Andrea, Matthias Neubert, Ben D. Pecjak, and Li Lin Yang: 'Two-loop divergences of massive scattering amplitudes in non-abelian gauge theories'. *JHEP* (2009), volume 0911: page 062. DOI: 10.1088/1126-6708/2009/11/062. arXiv: 0908.3676 [hep-ph].

236. Mitov, Alexander, George F. Sterman, and Ilmo Sung: 'Computation of the Soft Anomalous Dimension Matrix in Coordinate Space'. *Phys.Rev.* (2010), volume D82: page 034020. DOI: 10.1103/PhysRevD.82.034020. arXiv: 1005.4646 [hep-ph].

237. Becher, Thomas and Matthias Neubert: 'Infrared singularities of scattering amplitudes in perturbative QCD'. *Phys.Rev.Lett.* (2009), volume 102(19): page 162001. DOI: 10.1103/PhysRevLett.102.162001,10.1103/PhysRevLett.111.199905. arXiv: 0901.0722 [hep-ph].